

Volume 97

Number 3

March 2016

BAMS

Bulletin of the American Meteorological Society

HURRICANE CAMILLE REANALYSIS

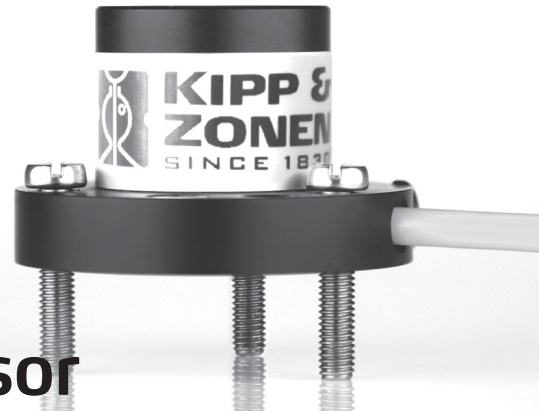
WOMEN'S MENTORING NETWORK

OCEAN WINDS SATELLITE



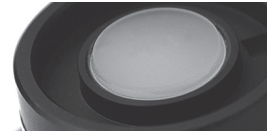
Alpha Jet

Observations with Get-Up-and-Go



PQS 1 PAR quantum sensor

for measuring Photosynthetic Active Radiation



For outdoor and indoor use
Excellent quantum response
Integrated leveling base

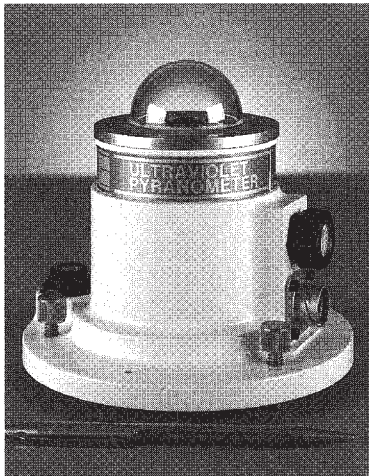
PQS 1 PAR Quantum sensor is developed for accurate measurement of PAR. It offers a response with an excellent match to the ideal PAR response. In addition the optical design of the diffuser offers optimized cosine correction. The instrument is designed for continuous outdoor or indoor installation. Perfect for studies of crop growth in green houses for example.

The sensitivity of the PQS 1 has been optimized to provide reliable and accurate measurements regardless of the PAR source.

ATMOSPHERIC RADIATION INSTRUMENTATION



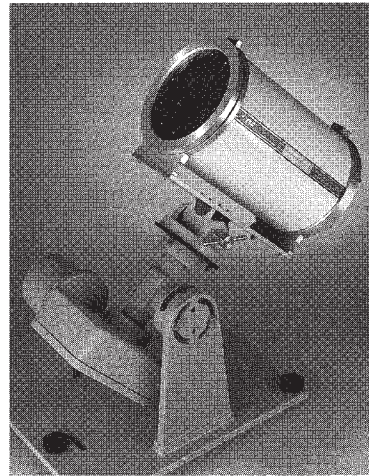
UV PYRANOMETERS



Thermally stabilized for long-term reference-grade measurements of global solar UV irradiance. Spectral sensitivity of 280 to 320 nm in the UVB and 320 to 400 nm in the UVA. High-level 0-5 VDC output signal. Hundreds in use in networks throughout the world.



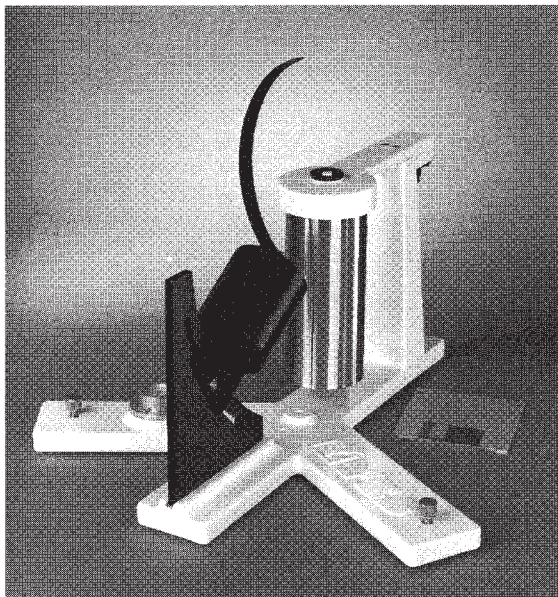
FILTER SPECTROMETERS



Measure direct normal solar irradiance at up to ten narrow-band wavelengths from 300 to 940 nm. Energy absorbing prefilters and state-of-the-art interference filters are environmentally sealed and thermally controlled to ensure long term stability. Mounts on most trackers.



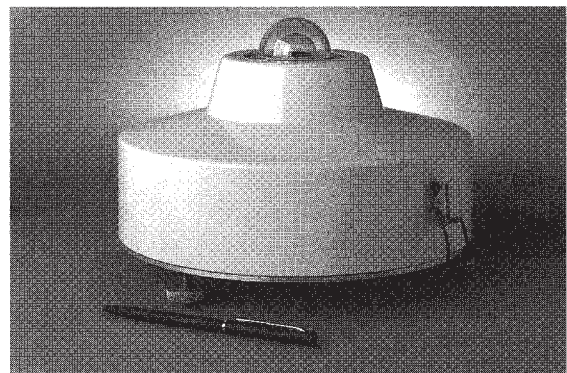
MULTIFILTER ROTATING SHADOWBAND RADIOMETERS



Simultaneously measure direct normal, total horizontal, and diffuse horizontal spectral irradiance using a unique algorithm and computer-controlled shadowband. Independent interference filter-diode detectors from 300 nm to 940 nm provide optical depth, aerosol, column ozone and water vapor data.



TOTAL SOLAR PYRANOMETERS



Ventilated and heated model meets WMO secondary standard pyranometer requirements. Platinum resistance thermometers replace older thermopile technology, resulting in an excellent cosine response and a high level output signal that is totally independent of ambient temperature changes.

YES produces an advanced line of atmospheric radiation instrumentation for reference-grade measurements in the UV through the visible and into the near-IR. Our instruments are field proven in networks throughout the world and form the core of the U.S. government's UVB monitoring network. All instruments are fully characterized in our state-of-the-art Optical Calibration laboratory.

E-mail, call, fax or write for detailed technical brochures on our products.



YANKEE ENVIRONMENTAL SYSTEMS, INC.

Airport Industrial Park
101 Industrial Blvd., Turners Falls, MA 01376 USA
Tel: (413) 863-0200 Fax: (413) 863-0255
E-mail: info@sunlight.yesinc.com <http://www.yesinc.com>

BAMS

Bulletin of the American Meteorological Society

VOLUME 97, NUMBER 3, MARCH 2016

IN BOX

- 329 **Mobile Radiosonde Deployments during the Mesoscale Predictability Experiment (MPEX)**
Rapid and Adaptive Sampling of Upscale Convective Feedbacks
R. J. TRAPP ET AL.
- 337 **An EF3 Multivortex Tornado over the Ionian Region**
Is It Time for a Dedicated Warning System over Italy?
M. M. MIGLIETTA AND R. ROTUNNO

ARTICLES

- 345 **The Earth Science Women's Network (ESWN)**
Community-Driven Mentoring for Women in the Atmospheric Sciences
A. S. ADAMS ET AL.
- 355 **Lessons from First-Generation Climate Science Integrators**
J. BRUGGER ET AL.
- 367 **A Reanalysis of Hurricane Camille** 
M. E. KIEPER ET AL.
- 385 **New Ocean Winds Satellite Mission to Probe Hurricanes and Tropical Convection** 
C. S. RUF ET AL.
- 397 **A New Instrumented Airborne Platform for Atmospheric Research**
P. HAMILL ET AL.
- 405 **Aircraft Observations of Dry Air, the ITCZ, Convective Cloud Systems, and Cold Pools in MJO during DYNAMO** 
S. S. CHEN ET AL.
- 425 **The Deep Propagating Gravity Wave Experiment (DEEPWAVE)**
An Airborne and Ground-Based Exploration of Gravity Wave Propagation and Effects from Their Sources throughout the Lower and Middle Atmosphere
D. C. FRITTS ET AL.

ON THE COVER

Once a subsonic attack jet, the Alpha Jet is now an instrument of atmospheric research. Able to record routine measurements of ozone, CO₂, and water vapor, for example, a notable feature of Alpha Jet is its ability to respond rapidly to unexpected atmospheric events such as forest fires or severe air quality events. For more information, see the article by Hamill et al. starting on p. 397. [Photo courtesy Matt Roby, Bay Area Environmental Research Institute, Petaluma, CA (now at Iowa State University)]

- 455 **The Causes of Foehn Warming in the Lee of Mountains**
A. D. ELVIDGE AND I. A. RENFREW

MEETING SUMMARIES

- online **Improving Rainfall Measurement in Gauge Poor Regions Thanks to Mobile Telecommunication Networks**
M. GOSSET ET AL.
- online **Sharing Experiences and Outlook on Coupling Technologies for Earth System Models**
S. VALCKE ET AL.
- online **Workshop on Climate Effects of Wind Turbines**
K. EMANUEL ET AL.

PUBLISHER

Keith L. Seitter

EDITOR-IN-CHIEF

Jeffrey Rosenfeld

SENIOR EDITOR

Christopher Cappella

BAMS EDITORIAL BOARD

Chair

Jeff Waldstreicher

Aerosol and Cloud Physics

Cynthia Twohy

Atmospheric Chemistry/Air

Quality

William R. Stockwell

Atmospheric Dynamics/

Tropical Meteorology

Chris Landsea

Brian Mapes

Ed Zipser

Biometeorology

Peter Blanken

Climate/Climate Variability

Art DeGaetano

Bjorn Stevens

Climate Analysis

Mike Alexander

Education

Gregory Byrd

History

James R. Fleming

Hydrology

Qingyun Duan

Numerical Analysis/

Mesoscale Modeling

Brian Etherton

Observing Systems

Tammy Weckwerth

Oceanography

Mike McPhaden

Operational Forecasting/

Services

Tom Fahey

Policy

Genevieve Fisher

Satellite Meteorology

Jeff Hawkins

Timothy J. Schmit

Society/Economic Impacts

Rebecca Morss

PRODUCTION STAFF

Managing Editor

Bryan Hanssen

News Editors

Rachel S. Thomas-Medwid

Matthew Gillespie

Production Editors

Denise M. Moy

Roger Wood

Meetings Editor

Claudia J. Gorski

Editorial Assistant

Melissa Fernau

Production Assistant

Jillian G. Neustel

Advertising

Kelly Garvey Savoie

DIRECTOR OF PUBLICATIONS

Kenneth F. Heideman

JOURNALS STAFF

Journals Production Manager

Michael Friedman

Managing Technical Editor

Mark E. Fernau

Managing Copy Editor

Jessica A. LaPointe

Copy Editors

Brandon M. Crose

Gary Gorski

Jordan Stillman

Lesley A. Williams

Publications Coordinator

Gwendolyn Whittaker

NOWCAST

325 NEWS AND NOTES

Glaciers and the Shaping of Mountains...How Volcanic Eruptions Could Lead to Polar Ice Melt...Ocean Warming and the Growing Number of Dead Zones... Climate Effects of the Tilting of the Earth

328 TECHNOLOGY

DEPARTMENTS

- 486 NEW MEMBERS
- 493 CALENDAR OF MEETINGS
- 498 CALL FOR PAPERS
- 500 NOMINATION SUBMISSIONS
- 503 CORPORATION AND INSTITUTIONAL MEMBERS
- 507 INDEX TO ADVERTISERS
- 508 PUBLICATION ORDER FORM

45 BEACON

471 LETTER FROM HEADQUARTERS

You Can Propose a Session for the Next Annual Meeting

472 LIVING ON THE REAL WORLD

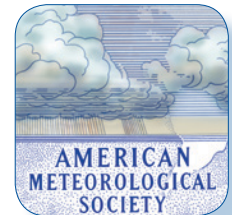
472 ON-AIR METEOROLOGY

475 ABOUT OUR MEMBERS

476 SCIENCE FAIRS

Read **BAMS** on your iPhone and iPad!

Download the **BAMS** app from the iOS App Store.



Supplements (📄) and online content are available online at <http://journals.ametsoc.org/toc/bams/9713>.

The *Bulletin of the American Meteorological Society* is the official organ of the Society, devoted to editorials, articles of interest to a large segment of the membership, professional and membership news, announcements, and Society activities. Editing and publishing are under the direction of Keith L. Seitter, executive director. Contributors are encouraged to send proposals to be considered for publication. For guidance on preparation and style, see the Authors' Resource Center online at www.ametsoc.org/pubs/arcindex.html.

AMS officers, councilors, and commissioners: president, Frederick H. Carr; president-elect, Matthew J. Parker, CCM; executive director, Keith L. Seitter; secretary-treasurer, Richard D. Rosen; past presidents, William B. Gail and Alexander MacDonald; councilors, Philip E. Ardanuy, Andrea J. Bleistein, Carol Anne Clayson, Heidi Cullen, William E. Easterling, Laura K. Furgione, Sue Ellen Haupt, Susan Jasko, James L. Kinter, Dennis Lettenmaier, Michael Morgan, Kevin R. Petty, Nicole Riemer, Wendy Schreiber-Abshire, and Alan R. Sealls, CBM; commissioners, William P. Mahoney, Maureen McCann, CBM, Robert M. Rauber, Rajul Pandya, Wendy Schreiber-Abshire, and David J. Stensrud.

The *Bulletin of the American Meteorological Society* (ISSN 0003-0007) is published monthly by the American Meteorological Society, 45 Beacon St., Boston, MA 02108-3693. Periodical postage paid at Boston, MA, and at additional mailing offices. Subscription price to members is included in annual dues. Subscription price to nonmembers is available on request; single issues are \$12.50 each for members, \$20 for nonmembers (prices incl. shipping and handling). Address all business communications to the Executive Director, AMS, 45 Beacon St., Boston, MA 02108-3693 (617-227-2425). POSTMASTER: Send address changes to *Bulletin of the American Meteorological Society*, 45 Beacon St., Boston, MA 02108-3693.

© Copyright 2016, American Meteorological Society (AMS). Permission to use figures, tables, and brief excerpts from this journal in scientific and educational work is hereby granted, provided source is acknowledged. Any use of the material in this journal that is considered to be "fair use" under Section 107 or that satisfies the conditions specified in Section 108 of the U.S. Copyright Law (17 USC, as revised by P.L. 94-553) does

not require the Society's permission. Items that do not bear their own separate copyright notices either are in the public domain or are U.S. Government works for which copyright protection is not available. Reproduction, systematic reproduction, and any other use of any material in this journal, unless exempted by the above statements, requires written permission or license from the AMS. Additional details are provided in the AMS Copyright Policies, available from the AMS at 617-227-2425 or amspubs@ametsoc.org. "American Meteorological Society," the Seal of the American Meteorological Society, and the AMS Seal of Approval are registered trademarks of the American Meteorological Society.

LETTER FROM THE EDITOR: COMMUNITY INFRASTRUCTURE

It's an election year, which means people are talking again about infrastructure—how to update it, how to pay for it. Inevitably discussion turns to massive projects—iconic initiatives like rebuilding highways, ensuring water supply, and updating communications grids.

The candidates disagree about priorities and approaches but the fact that they're all talking about infrastructure shows a general agreement that whatever happens, infrastructure is a common concern. I mean "common" in the sense of "communal." Whether private initiative or public works, infrastructure serves a community.

We see plenty about the communal value of infrastructure in this issue of BAMS. For example, Christopher Ruf and colleagues preview CYGNSS (p. 385), an exciting new constellation of satellites designed to measure ocean-surface winds. The ability to peer underneath the towering clouds of a hurricane and track the ferocious winds at ship's level will obviously be a valuable component of the infrastructure enabling warnings and forecasts.

Infrastructure doesn't just serve a community; it also improves a community. CYGNSS is all the more valuable because new and frequent wind measurements will be applied at a time when hurricane intensity forecasts have not improved as rapidly as track forecasts. Also, by penetrating the heavy rainfall at the base of convective systems, scientists will begin sorting out questions about the origin and propagation of the influential Madden–Julian Oscillation.

In future AMS meetings we may very well see whole sessions bringing scientists together to discuss new data from CYGNSS in order to answer questions that were once out of reach in tropical meteorology. Similarly, a whole new class of atmospheric studies might arise simply because of the capability to rapidly deploy Alpha Jet (p. 397) for fast sampling of low-level atmospheric chemistry. In short, infrastructure can both define a community and build one.

As influential as technology has become in our community, nothing builds up a community quite like a strong community. This is the realm not just of infrastructure but also of leadership—another theme of election years. Business executives are constantly talking about how their primary job is to groom new leaders for their companies. In the public realm, too, you hear similar sentiments from politicians, who are self-styled experts in community and leadership, if ever there were any. It's no longer enough to raise new generations of informed voters. Now politicians talk about raising the next wave of leadership.

It is a sad fact about our own community of science that we fail to retain many women: they enter atmospheric sciences, only to leave for other opportunities. Reading Adams et al. in this issue (p. 345), we see that, above all, to keep more enough women in the field they need to be able to see that a thriving community of women already exists in our field. Strong and numerous mentorships are a sign of a strong community—they are the thruways of comfort and high-voltage lines of advancement. Thanks to the leadership of the Earth Sciences Women's Network, perhaps that necessary infrastructure of people helping people will take hold—redefining, remaking, and improving our community.

—Jeff Rosenfeld, EDITOR-IN-CHIEF

MOBILE RADIOSONDE DEPLOYMENTS DURING THE MESOSCALE PREDICTABILITY EXPERIMENT (MPEX): RAPID AND ADAPTIVE SAMPLING OF UPSCALE CONVECTIVE FEEDBACKS

The Mesoscale Predictability Experiment (MPEX) was a field campaign conducted 15 May through 15 June 2013 within the Great Plains region of the United States. One of the research foci of MPEX regarded the upscaling effects of deep convective storms on their environment, and how these feed back to the convective-scale dynamics and predictability. Balloon-borne GPS radiosondes, or "upsondes," were used to sample such environmental feedbacks. Two of the upsonde teams employed dual-frequency sounding systems that allowed for upsonde observations at intervals as fast as 15 min. Because these dual-frequency systems also had the capacity for full mobility during sonde reception, highly adaptive and rapid storm-relative sampling of the convectively modified environment was possible. This article documents the mobile sounding capabilities and unique sampling strategies employed during MPEX. (Page 329)

AN EF3 MULTIVORTEX TORNADO OVER THE IONIAN REGION: IS IT TIME FOR A DEDICATED WARNING SYSTEM OVER ITALY?

The possibility offered by the Internet to share pictures of tornadoes, and the storm-report archiving in the European Storm Weather Database, have made it apparent that the occurrence of tornadoes over Europe has been underestimated. Together with weak waterspouts

ABSTRACTS

and tornadoes, large and intense vortices are occasionally observed. Among these, an EF3 multivortex tornado with a path width of some hundreds of meters affected southeastern Italy on 28 November 2012, causing one casualty and estimated damage of €60M to the largest steel plant in Europe. A tide gauge positioned near the location of tornado landfall and a vertical atmospheric profile available a few hours later near the affected region represent unique sources of information for these events in the Mediterranean. During its transit across the port of Taranto, a waterspout, which was to become the tornado, was observed to have induced a sea level rise of about 30 cm. The supercell responsible for the tornado developed from convective cells triggered by orographic uplift over the Apennines. The 0–1-km wind shear was exceptional in comparison with other Italian tornadoes, and was remarkable in comparison with U.S. events as well. Other indices for severe convection diagnosis also showed extremely high values. The occasional occurrence of events with similar or stronger intensities over Italy emphasizes the need for the Distributed National Weather Service—which will integrate Italian meteorological institutions under one agency and is currently under development—to devise a warning system dedicated to the monitoring and prediction of severe convective events. (Page 337)

THE EARTH SCIENCE WOMEN'S NETWORK (ESWN): COMMUNITY-DRIVEN MENTORING FOR WOMEN IN THE ATMOSPHERIC SCIENCES

Women are a growing percentage of undergraduate and graduate

students in the atmospheric sciences, yet they remain a minority in senior positions. One approach for the retention of women is increased mentoring, which is linked to successful promotions, higher incomes, and greater career satisfaction. Informal peer networking is a form of mentoring that may be effective for underrepresented groups. The Earth Science Women's Network (ESWN) was established in 2002 with the mission to promote career development, build community, provide informal mentoring and support, and facilitate professional collaborations for early career women in the Earth sciences. Over time, ESWN has developed a mentoring philosophy that has reduced some barriers and challenges that women face in traditional mentoring relationships. The five main

principles of the ESWN's mentoring philosophy have evolved to include community-driven mentoring, diverse mentoring approaches for diverse individuals, mentoring across career phases, combined personal and professional mentoring, and effective mentoring in a safe space. Surveys of ESWN members report gains in areas that are often considered barriers to career advancement, including recognition that they are not alone, new understanding of obstacles faced by women in science, and access to professional resources. These gains have been accomplished through online and in-person ESWN activities guided by the ESWN's mentoring philosophy. Understanding the success of the ESWN, as well as its limitations, has the potential to inform the larger atmospheric

www.distromet.com
 Your equipment to measure
 Rain Drop Size Distributions



JOSS - WALDVOGEL DISDROMETER
 by Distromet Ltd.
 Switzerland

science community of additional strategies to improve mentoring and retention of women in the atmospheric sciences. (Page 345)

LESSONS FROM FIRST-GENERATION CLIMATE SCIENCE INTEGRATORS

There is an increasing demand for climate science that decision-makers can readily use to address issues created by climate variability and climate change. To be usable, the science must be relevant to their context and the complex management challenges they face and credible and legitimate in their eyes. The literature on usable science provides guiding principles for its development, which indicate that climate scientists who want to participate in the process need skills in addition to their traditional disciplinary training to facilitate communicating, interacting, and developing and sustaining relationships with stakeholders outside their disciplines. However, the literature does not address questions about what specific skills are needed and how to provide climate scientists with these skills. To address these questions, this article presents insights from interviews with highly experienced and respected “first generation” climate science integrators from across the United States. The term “climate science integrator” is used to refer to climate scientists who specialize in helping decision-makers to integrate the best available climate science into their decision-making processes. The cadre of scientists who participated in the research has largely developed their methods for working successfully with stakeholders without formal training but often with the guidance of a mentor. Their collective wisdom

illuminates the kinds of skills needed to be a successful science integrator and provides mentoring for aspiring science integrators. It also suggests the types of training that would cultivate these skills and indicates ways to change academic training and institutions to better encourage the next generation and to support this kind of work. (Page 355)

A REANALYSIS OF HURRICANE CAMILLE

A reanalysis of 1969’s Hurricane Camille has been completed as part of the Atlantic Hurricane Database Reanalysis Project. The reanalysis of Hurricane Camille has been expedited to allow for a homogeneous comparison of all four of the U.S.-landfalling Saffir–Simpson hurricane wind-scale category 5 hurricanes since 1900. A review of the available ship, station, radar, aircraft, and satellite observations is presented, along with the reanalysis methodology. Highlights of the Best-Track Change Committee approved changes to Camille’s genesis, track, intensity, and dissipation are discussed. As part of the preparation for the reanalysis, research on Hurricane Camille uncovered new data useful to the reanalysis. Focus was placed on understanding the internal structure in a modern context, especially whether eye-wall replacement cycles occurred, including comparisons with a similar hurricane used as a proxy. A more detailed understanding was gained of the tropical wave and genesis phases. In addition, a 901-mb dropsonde reading that was later rejected was reanalyzed to find out why and to see if an accurate central pressure could be determined. New landfall surface pressures along the Mississippi

coast were discovered and a significant revision is made to the U.S.-landfall central pressure and intensity (maximum sustained surface winds). Additionally, a radar “loop” was constructed from archived Weather Surveillance Radar-1957 (WSR-57) film, including landfall, marking the very first time that this historic hurricane can be viewed in a time-lapse movie format. (Page 367)

NEW OCEAN WINDS SATELLITE MISSION TO PROBE HURRICANES AND TROPICAL CONVECTION

The Cyclone Global Navigation Satellite System (CYGNSS) is a new NASA earth science mission scheduled to be launched in 2016 that focuses on tropical cyclones (TCs) and tropical convection. The mission’s two primary objectives are the measurement of ocean surface wind speed with sufficient temporal resolution to resolve short-time-scale processes such as the rapid intensification phase of TC development and the ability of the surface measurements to penetrate through the extremely high precipitation rates typically encountered in the TC inner core. The mission’s goal is to support significant improvements in our ability to forecast TC track, intensity, and storm surge through better observations and, ultimately, better understanding of inner-core processes. CYGNSS meets its temporal sampling objective by deploying a constellation of eight satellites. Its ability to see through heavy precipitation is enabled by its operation as a bistatic radar using low-frequency GPS signals. The mission will deploy an eight-spacecraft constellation in a low-inclination (35°) circular orbit to maximize coverage and sampling

in the tropics. Each CYGNSS spacecraft carries a four-channel radar receiver that measures GPS navigation signals scattered by the ocean surface. The mission will measure inner-core surface winds with high temporal resolution and spatial coverage, under all precipitating conditions, and over the full dynamic range of TC wind speeds. (Page 385)

A NEW INSTRUMENTED AIRBORNE PLATFORM FOR ATMOSPHERIC RESEARCH

The NASA Ames Research Center operates a new research platform for atmospheric studies: an instrumented Alpha Jet. The present complement of instruments allows for the determination of carbon dioxide, ozone, water vapor, and methane concentrations as well as measurements of three-dimensional wind speeds, temperature, and pressure. Planned future instrumentation includes an Air-Core sampler and an instrument to measure formaldehyde. We give examples of measurements that have been made, including measurements carried out during a downward spiral over an expected methane source. An attractive property of this airborne system is its ability to respond rapidly to unexpected atmospheric events such as large forest fires or severe air quality events. (Page 397)

AIRCRAFT OBSERVATIONS OF DRY AIR, ITCZ, CONVECTIVE CLOUD SYSTEMS, AND COLD POOLS IN MJO DURING DYNAMO

One of the most challenging problems in predicting the Madden-Julian oscillation (MJO) is the initiation of large-scale convective activity associated with the MJO over the tropical Indian Ocean.

The lack of observations is a major obstacle. The Dynamics of the MJO (DYNAMO) field campaign collected unprecedented observations from air-, land-, and ship-based platforms from October 2011 to February 2012. Here we provide an overview of the aircraft observations in DYNAMO, which captured an MJO initiation event from November to December 2011. The National Oceanic and Atmospheric Administration (NOAA) WP-3D aircraft was stationed at Diego Garcia and the French Falcon 20 aircraft on Gan Island in the Maldives. Observations from the two aircraft provide a unique dataset of three-dimensional structure of convective cloud systems and their environment from the flight level, airborne Doppler radar, microphysics probes, ocean surface imaging, global positioning system (GPS) dropsonde, and airborne expendable bathythermograph (AXBT) data. The aircraft observations revealed interactions among dry air, the intertropical convergence zone (ITCZ), convective cloud systems, and air-sea interaction induced by convective cold pools, which may play important roles in the multi-scale processes of MJO initiation. This overview focuses on some key aspects of the aircraft observations that contribute directly to better understanding of the interactions among convective cloud systems, environmental moisture, and the upper ocean during the MJO initiation over the tropical Indian Ocean. Special emphasis is on the distinct characteristics of convective cloud systems, environmental moisture and winds, air-sea fluxes, and convective cold pools during the convectively suppressed, transition/onset, and active phases of the MJO. (Page 405)

THE DEEP PROPAGATING GRAVITY WAVE EXPERIMENT (DEEPWAVE): AN AIRBORNE AND GROUND-BASED EXPLORATION OF GRAVITY WAVE PROPAGATION AND EFFECTS FROM THEIR SOURCES THROUGHOUT THE LOWER AND MIDDLE ATMOSPHERE

The Deep Propagating Gravity Wave Experiment (DEEPWAVE) was designed to quantify gravity wave (GW) dynamics and effects from orographic and other sources to regions of dissipation at high altitudes. The core DEEPWAVE field phase took place from May through July 2014 using a comprehensive suite of airborne and ground-based instruments providing measurements from Earth's surface to ~100 km. Austral winter was chosen to observe deep GW propagation to high altitudes. DEEPWAVE was based on South Island, New Zealand, to provide access to the New Zealand and Tasmanian "hotspots" of GW activity and additional GW sources over the Southern Ocean and Tasman Sea. To observe GWs up to ~100 km, DEEPWAVE utilized three new instruments built specifically for the National Science Foundation (NSF)/National Center for Atmospheric Research (NCAR) Gulfstream V (GV): a Rayleigh lidar, a sodium resonance lidar, and an advanced mesosphere temperature mapper. These measurements were supplemented by in situ probes, dropsondes, and a microwave temperature profiler on the GV and by in situ probes and a Doppler lidar aboard the German DLR Falcon. Extensive ground-based instrumentation and radiosondes were deployed on South Island, Tasmania, and Southern Ocean islands. Deep

ABSTRACTS

orographic GWs were a primary target but multiple flights also observed deep GWs arising from deep convection, jet streams, and frontal systems. Highlights include the following: 1) strong orographic GW forcing accompanying strong cross-mountain flows, 2) strong high-altitude responses even when orographic forcing was weak, 3) large-scale GWs at high altitudes arising from jet stream sources, and 4) significant flight-level energy fluxes and often very large momentum fluxes at high altitudes. (Page 425)

THE CAUSES OF FOEHN WARMING IN THE LEE OF MOUNTAINS

The foehn effect is well known as the warming, drying, and cloud

clearance experienced on the lee side of mountain ranges during “flow over” conditions. Foehn flows were first described more than a century ago when two mechanisms for this warming effect were postulated: an *isentropic drawdown* mechanism, where potentially warmer air from aloft is brought down adiabatically, and a *latent heating and precipitation* mechanism, where air cools less on ascent—owing to condensation and latent heat release—than on its dry descent on the lee side. Here, for the first time, the direct quantitative contribution of these and other foehn warming mechanisms is shown. The results suggest a new paradigm is required after it is demonstrated that a third mechanism,

mechanical mixing of the foehn flow by turbulence, is significant. In fact, depending on the flow dynamics, any of the three warming mechanisms can dominate. A novel Lagrangian heat budget model, back trajectories, high-resolution numerical model output, and aircraft observations are all employed. The study focuses on a unique natural laboratory—one that allows unambiguous quantification of the leeside warming—namely, the Antarctic Peninsula and Larsen C Ice Shelf. The demonstration that three foehn warming mechanisms are important has ramifications for weather forecasting in mountainous areas and associated hazards such as ice shelf melt and wildfires. (Page 455)

NEW FROM AMS BOOKS!

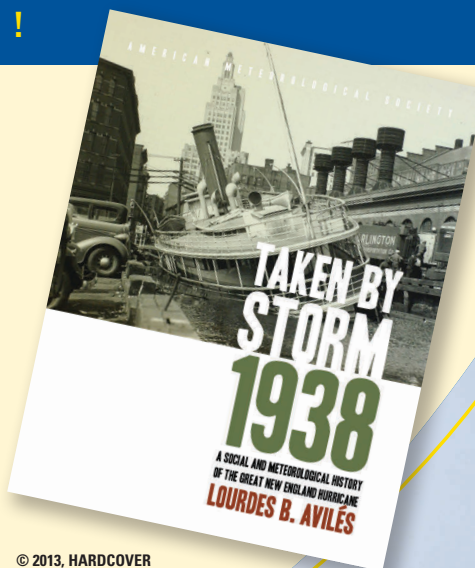
“An engrossing account of New England’s worst natural catastrophe.”

— KERRY EMANUEL, *Professor of Atmospheric Science, MIT*

Taken by Storm, 1938: *A Social and Meteorological History of the Great New England Hurricane*

LOURDES B. AVILÉS

When the Great New England Hurricane of 1938 hit the Northeast unannounced, it changed everything from the landscape, to Red Cross and Weather Bureau protocols, to the measure of Great Depression relief New Englanders would receive, and the resulting pace of regional economic recovery. The science behind this storm is presented here for the first time, with new data that sheds light on the motivations of the Weather Bureau forecasters. This compelling history successfully weaves science, historical accounts, and social analyses to create a comprehensive picture of the most powerful and devastating hurricane to hit New England to date.



© 2013, HARDCOVER
ISBN: 978-1-878220-37-0
LIST \$40 MEMBER \$30

AMS BOOKS

RESEARCH APPLICATIONS HISTORY

www.ametsoc.org/amsbookstore

NOWCAST

NEWS AND NOTES

GLACIERS HAVE IMPORTANT ROLE IN BUILDING MOUNTAINS

The seesaw competition between glacial erosion and plate tectonics in shaping mountains is—at least in some cases—being won by the glaciers, according to a new study published in the *Proceedings of the National Academy of Sciences*. The research, undertaken at the St. Elias Mountains on Alaska’s southeastern coast, highlights how changes in climate that lead to glacial activity can influence the shape of Earth’s mountains.

Scientists studied sediment cores taken from an underwater sediment fan in the Gulf of Alaska that comprised material eroded from the adjacent St. Elias range. They also looked at drill cores taken from the Gulf’s floor and from the Alaskan continental

shelf, which contained millions of years of geologic history in the area. They discovered that “the composition of the sediment gave clear evidence of when the glaciation started and then expanded, in sync with global climate trends,” explains study coauthor Alan Mix of Oregon State University, which allowed the researchers to accurately determine ages of the sediment sequences.

Their findings showed that “most sediments were younger than we anticipated, implying that erosion was higher than we expected,” explains the study’s lead author, Sean Gulick of the University of Texas. The mountain erosion increased approximately one million years ago, when 40,000-year climate oscillations turned into 100,000-year glacial periods

and “erosion of the mountains accelerated under attack from the ice,” says Gulick. “In fact, more rock was eroded than tectonics has replaced.” That trend has continued since the mid-Pleistocene, with erosion outpacing tectonic activity by rates of 50%–80% in the studied region.

“People often see mountain ranges as permanent, but they aren’t really,” notes coauthor John Jaeger of the University of Florida. “If more rock is pushed in, they grow, and if more rock is eroded away, they shrink.” [SOURCE: Oregon State University]

STUDY LINKS VOLCANIC ERUPTIONS, WEATHER PATTERNS, AND POLAR MELTING

A growing body of research has demonstrated that large volcanic eruptions lead to cooling across the world for several years due to the reflection of solar radiation by sulphate aerosols created from volcanic particles blasted into the atmosphere. But new research published in *Scientific Reports* “suggest[s] an extra layer of complexity” in the climatic impacts of eruptions, according to the lead author of the study, James Baldini of Durham University. The research reveals that very large eruptions could cause localized warming that has significant effects on ice sheets and sea levels.

Baldini and colleagues examined ice core, volcanological, and speleothem-based data from earlier

ECHOES

“ I want to walk in the woods. I’d like to be able to cut a Christmas tree when there’s snow on the ground, but I can’t do it this year.”

—VIRGINIA KUEBLER of the Buffalo, New York, suburb of East Aurora on the record-breaking lack of snow as of December 3. It had been a long time since the city had been without snow by that time of year—116 years to be exact, with the previous record for latest first measurable snowfall being December 3, 1899. The dry ground was quite a change from 2014, when Buffalo got hit in November with a historic storm that dropped up to seven feet of snow in some areas. The average temperature for this past November was 5.5°F above normal, making it Buffalo’s seventh warmest November on record. Temperatures were 4°–8°F above normal in almost all of the lake-effect snowbelt from Michigan to upstate New York, and the warm trend continued through most of December. The city finally received its first snowfall—albeit just a dusting—on December 18. In an average year, Buffalo would have had more than 20 inches of the white stuff by that date. [SOURCE: wivb.com]

studies that tracked temperature and rainfall changes over long time periods. The data suggested connections between eruptions and the location of each hemisphere's polar front that had far-ranging climatic consequences. For example, their findings indicated that all eight known volcanic eruptions in the Northern Hemisphere between 30,000 and 80,000 years ago that were as large or larger than the 1815 eruption of Mount Tambora—the largest volcanic eruption in recorded history—led to warm periods in the Antarctic region, as the cooling of the Northern Hemisphere due to the reflection of solar radiation by volcanic particles pushed the Southern Hemisphere polar front south. Similarly, the researchers found evidence of eruptions in the Southern Hemisphere during the last ice age that forced the

Northern Hemisphere polar front to retreat, producing warming in Greenland.

Although the overall global effect would still lead to lower average temperatures, it would occur “with warming in the polar regions in the hemisphere opposite the eruption, as well as a major disruption of low-latitude rainfall patterns,” explains Baldini. When applied to today's world, these localized polar impacts could cause destabilization of some of the world's largest ice sheets, with potentially significant implications for global sea levels. While Baldini points out that “there are no large Northern Hemisphere ice sheets to amplify the effects of the original eruption,” emissions of greenhouse gases and sulfates into the atmosphere since the Industrial Revolution “have already had an effect on

weather patterns,” and a large volcanic eruption “could add to this problem in an unexpected way.” He noted that a significant eruption in the Northern Hemisphere that produced moderate warming in the Antarctic would exacerbate the instability of the West Antarctic Ice Sheet and “could have very serious consequences.” [SOURCE: Durham University]

WARMING WATERS TRIGGER MORE DEAD ZONES

Oxygen Minimum Zones, also known as hypoxic zones or dead zones, can be devastating for marine life, either killing off species or forcing them to other locations. A study in 2008 found more than 400 dead zones throughout the world's oceans and large lakes, highlighting the importance of understanding what causes the in-

STRONG. SENSITIVE. SMART.

SENSORS FOR: WIND, TEMPERATURE, HUMIDITY, PRECIPITATION, SOLAR RADIATION, ATMOSPHERIC PRESSURE

50 YEARS

YOUNG
www.youngusa.com

creasingly common phenomenon. By looking back to the end of the last ice age, new research published in *Nature* has discovered a link between warming waters and the genesis of dead zones.

Researchers looked at marine sediment cores and plankton biomarkers collected from the North Pacific to put together a high-resolution record of climate there. The data indicated that about 14,700 years ago, and again about 11,500 years ago, rapidly occurring warming of about 4–5°C in the Gulf of Alaska spurred an increase in marine plankton known as diatoms settling to the ocean’s floor, which led to sudden oxygen loss in those locations. According to the study’s lead author, Summer Praetorius of the Carnegie Institution for Science, during both events, “the transition to hypoxia occurred abruptly and persisted for about 1,000 years, suggesting a feedback that sustained or amplified hypoxia.”

The researchers found that the feedback is connected to the lack of iron in the high latitudes of the North Pacific. When oxygen levels begin to decrease, a chemical reaction occurs, releasing iron that had been locked up in continental marine sediments. According to study coauthor Alan Mix of Oregon State University, “that iron then fuels diatoms, which bloom, die, and sink to the seafloor, consuming oxygen along the way.”

Praetorius noted that recent climate conditions, such as atypical warming of waters in the northeastern Pacific and the Bering Sea, “seem eerily reminiscent of past conditions that gave way to extended periods of hypoxia.” The new research indicates “that the ecological consequences of climate change can be massive and can

ECHOES

“ It’s a bad smog day, so people aren’t coming out.”
 —BILL ISLER, who owns a bar in Beijing, China, commenting on the effects the city’s extreme air pollution has on many businesses. After sales dropped by about one-third during a smoggy week, another Beijing bar introduced a beer called “Airpocalypse” that is priced on a sliding scale that depends on the air quality—when the air improves, the price goes down. In early December, the city announced its first-ever “red alert,” the country’s highest air pollution warning, which puts restrictions on automobile use, advises school closures, and shuts down outdoor construction sites and some industrial plants. Just two weeks later, a second red alert was issued. The pollution has hindered many businesses around the country, especially those related to tourism. However, some companies benefitted from the conditions, such as delivery services, which often see an uptick because residents tend to avoid going outside when the smog is severe. [SOURCE: Greenwire]



Smog seen from a hotel in Tianjin, China, about 75 miles southeast of Beijing. [Photo Credit: Mike Friedman, AMS]

occur pretty fast with little warning,” says Mix. [SOURCE: National Science Foundation]

NEW DISCOVERY ON HOW EARTH’S SLANT AFFECTS EQUATORIAL CLIMATE

Gravitational dynamics cause periodic variations in Earth’s movement on its axis and its orbit around the sun, and the well-known Milankovitch cycles describe the climatic effects

caused by these changes. A recent study in *Nature Communications* has made a surprising new breakthrough in this area by connecting a particular periodic tilt of the Earth to changes in the world’s heaviest rain belt and largest source of heat and moisture—the Intertropical Convergence Zone (ITCZ).

By comparing sediment cores dating back 282,000 years taken from the coast of Papua New

Guinea and stalagmite samples from ancient caves in China, researchers found a previously unknown effect in the western Pacific Ocean from obliquity, which is the angle between the plane of the equator and the plane of Earth's orbit around the Sun. As Milankovitch learned, Earth's obliquity fluctuates every 41,000 years between 22.1° and 24.5° due to the gravitational pull of the moon and planets.

The new study's coauthor, Kristine DeLong of Louisiana State University, "took the data and put it through a mathematical prism so I could look at the patterns, and that's where we see the obliquity cycle, that 41,000-year cycle." The analysis showed the obliquity in both the paleontological record and in computer model data, but the surprise was that in the computer spectral analysis ("prism"), the 41,000-year tilt appeared in the Tropics, and "that's not supposed to be there," explains DeLong.

"That's not what the textbooks tell us."

The research indicates a much more significant impact of obliquity on ITCZ migration than had previously been known, which subsequently indicates an in-

fluence on global hydroclimate cycles, as the ITCZ can have a major impact on rainfall in many equatorial areas, and over longer time periods can lead to intense droughts or flooding. [SOURCE: Louisiana State University]



THE UNIVERSAL SOUNDING DECODE & ANALYSIS PROGRAM

Customers say it best...

"Love what you have done with this program, GREAT WORK! You should be proud of this great piece of software for all of us in all sectors of Meteorology. It has come a long way and keeps getting better and better for students, operational Mets in government, private and academia sectors. Nice work!"

- R. Bianchi

RAOB...for the most versatile and accurate sounding analyses available!
Environmental Research Services, LLC • 570-491-4689 • www.raob.com

TECHNOLOGY

MINI-SATELLITES TO MONITOR WILDFIRES

NASA is currently developing a network of small sensors that can piggyback on satellites and monitor wildfires throughout the world. Researchers hope the FireSat program will help fire managers get potentially life-saving information more quickly.

The project would place approximately 200 thermal infrared imaging sensors—each about half the size of a shoebox—onto private-sector communication satellites. The sensors will be able to recognize fires as small as 35 feet wide as rapidly as 15 minutes

after they first ignite and send communications to emergency responders within 3 minutes of detection. They will then continuously supply fire activity updates in near-real time.

"While many wildfires are reported by 911 calls soon after ignition, some are not, and delays in detection can lead to rapid escalation of a fire and dramatic growth of the cost of suppression," notes the lead designer of FireSat, Robert Staehle of NASA's Jet Propulsion Laboratory. "The system we envision will work day and night for fires anywhere in the world."

Currently, satellite-based wildfire sensors can only identify blazes about two times per day and send out large images, but FireSat will be able to transmit low-resolution images every minute, and also identify the longitude and latitude of the fire, allowing for nearly constant communication to those on the ground. The system will also be useful for monitoring oil spills, explosions, and other high-heat events.

The first array of FireSat sensors is scheduled to launch in late 2017, with full implementation to be completed in 2018. [SOURCE: Jet Propulsion Laboratory]

Mobile Radiosonde Deployments During the Mesoscale Predictability Experiment (MPEX)

Rapid and Adaptive Sampling of Upscale Convective Feedbacks

BY ROBERT J. TRAPP, DAVID J. STENSRUD, MICHAEL C. CONIGLIO, RUSS S. SCHUMACHER,
MICHAEL E. BALDWIN, SEAN WAUGH, AND DON T. CONLEE

The Mesoscale Predictability Experiment (MPEX) was a field campaign conducted 15 May through 15 June 2013 within the Great Plains region of the United States. MPEX had two complementary research foci:

- *Focus 1:* The effects of upstream, prestorm mesoscale and subsynoptic-scale environmental features on regional-scale numerical weather prediction (NWP) of convective storms.
- *Focus 2:* The upscaling effects of isolated deep-convective storms on their environment, and the feedback of these effects to the convective-scale dynamics and predictability.

An overview of these foci and the multiple facets of the MPEX operations can be found in Weisman et al. (2015). The purpose of this brief but complementary article is to highlight Focus 2 activities. In particular, we describe both the feasibility and limitations of launching

balloon-borne GPS radiosondes from ground-based mobile platforms, in ways meant to mimic airborne dropsonde deployments. Documentation of our experiences is provided here for the benefit of future field experiments that need, as we did, an alternative to dropsondes over land and in the vicinity of active convection.

A BRIEF BACKGROUND. Within unstable, unsaturated layers, vertical circulations associated with the resultant convection mix high (low) virtual potential temperature air upward (downward), and thereby adjust the lapse rate of the convecting layer of air back toward a more statically stable state. Indeed, this idea of convective adjustment forms the basis for convective parameterization schemes in NWP models. But other processes besides vertical mixing are also at play in deep cumulus convection. For example, deep convective clouds diabatically heat the atmosphere when water vapor condenses into cloud droplets, and diabatically cool the atmosphere when subsequent precipitation falls out of the cloud and evaporates. Such diabatic heating, especially when sustained through mesoscale convective systems (MCSs), can lead to long-lasting modifications of the larger-scale geopotential height and wind field in the middle- and upper-troposphere. Diabatic cooling associated with precipitating downdrafts can result in a pool of cool air at the ground that spreads laterally away from the precipitating cloud. Both are forms of upscale feedbacks that have local as well as remote effects on the atmosphere and its ability to support subsequent cumulus convection. And, as supported by previous work, these effects are realized as measurable perturbations to the vertical distributions of atmospheric temperature, humidity, and wind.

Misrepresentation of, for example, the depth or areal extent of a surface cold pool in NWP models will

AFFILIATIONS: TRAPP—University of Illinois at Urbana-Champaign, Urbana, Illinois; STENSRUD—The Pennsylvania State University, University Park, Pennsylvania; CONIGLIO AND WAUGH—NOAA/National Severe Storms Laboratory, Norman, Oklahoma; SCHUMACHER—Colorado State University, Ft. Collins, Colorado; BALDWIN—Purdue University, West Lafayette, Indiana; CONLEE—Texas A&M University, College Station, Texas

CORRESPONDING AUTHOR: Robert J. Trapp, Department of Atmospheric Sciences, University of Illinois at Urbana-Champaign, 105 S. Gregory Street, Urbana, IL 61801

E-mail: jtrapp@illinois.edu

DOI:10.1175/BAMS-D-14-00258.1

© 2016 American Meteorological Society

necessarily induce some error in subsequent predictions of temperature, cloud coverage, precipitation, etc., at and beyond the scales commensurate with the several-kilometer grid lengths now used in high-resolution convection-permitting models. It is unclear, however, how the magnitudes of this and the other feedbacks, and the ultimate larger-scale and longer-term consequence of their misrepresentation, vary with the convective intensity and morphology. Consider that relative to ordinary convective storms, supercell thunderstorms possess large, intense, and long-lived updrafts and downdrafts owing to their unique dynamics. The implication is that an outbreak of supercell thunderstorms, and perhaps even an isolated supercell, should have comparatively large upscale feedbacks. Accordingly, supercells were specifically targeted during MPEX.

Attempts to quantify and otherwise characterize the 3D atmosphere near supercells are not unique to MPEX. Large field campaigns [such as the Verification of the Origins of Rotation (VORTEX) and VORTEX2] and even smaller-scale projects have included efforts to collect radiosonde observations within supercells and in their environments. But in contrast to the upscale focus of MPEX, the prior field studies were focused primarily on quantifying the environmental characteristics that beget the convective storms, which essentially is a downscaling perspective. Thus, even though VORTEX2 upsonde operations were, for example, mobile

and storm-following, they were designed to examine the variability of the mesoscale environment and how this may impact tornado formation (e.g., Parker 2014).

UPSONDE SYSTEMS. Teams from Purdue University (PU), the National Severe Storms Laboratory (NSSL), Colorado State University (CSU), and Texas A&M University (TAMU) fielded mobile radiosonde systems during MPEX (Fig. 1). As detailed in Table 1, PU, NSSL, and TAMU used systems manufactured by International Met Systems (iMet), and CSU employed a Vaisala system. The iMet sondes were preconfigured with four frequency options, and iMet provided MPEX investigators with a separate batch of sondes with four

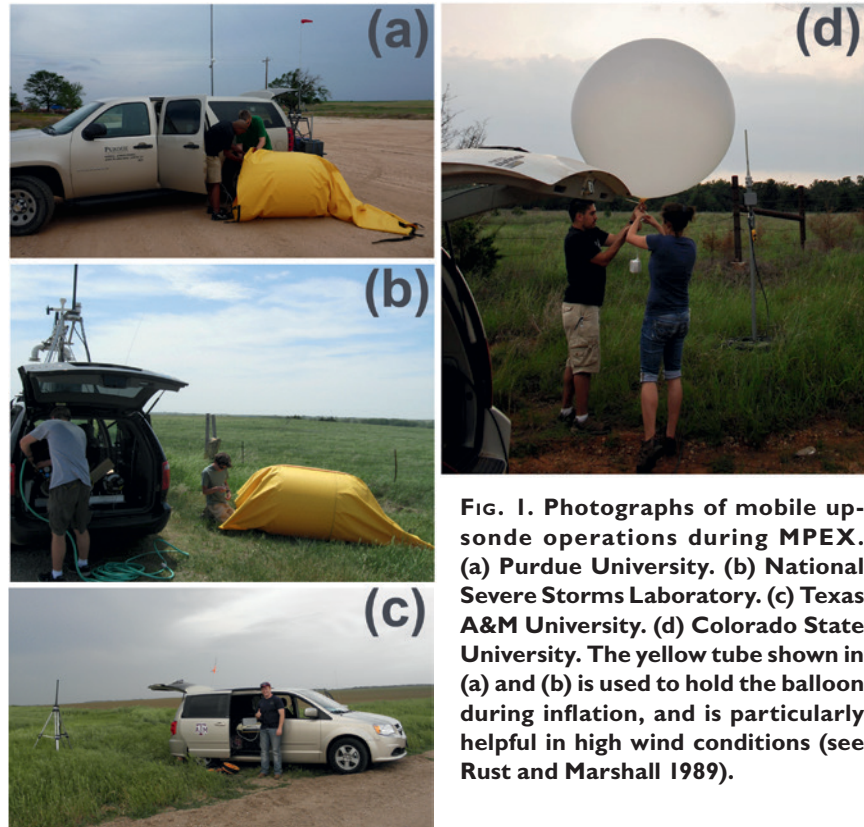


FIG. 1. Photographs of mobile upsonde operations during MPEX. (a) Purdue University. (b) National Severe Storms Laboratory. (c) Texas A&M University. (d) Colorado State University. The yellow tube shown in (a) and (b) is used to hold the balloon during inflation, and is particularly helpful in high wind conditions (see Rust and Marshall 1989).

TABLE 1. Details of radiosonde systems employed during MPEX.

Team	Model	Sonde types	Balloon
PU	iMet 3050 (2)	iMet-I-AB 403 MHz GPS radiosondes	200-g latex
NSSL	iMet 3050, and iMet 3150	iMet-I-AB 403 MHz GPS radiosondes	200-g latex
CSU	Vaisala Digicora MW2I	Vaisala RS92 radiosondes	200-g latex
TAMU	iMet 3050 (and iMet 3150 for redundancy)	iMet-I-AB, and iMet-I-AA 403 MHz GPS radiosondes	200-g latex

additional frequencies. These eight frequency options combined with the narrow transmission band of the iMet sondes allowed the teams to conduct operations without being concerned with frequency overlap.

In fact, PU and NSSL both had the capability to simultaneously receive signals from two separate sondes that were transmitting at different frequencies. When combined with the single frequency systems of CSU and TAMU (whose participation was limited to 23–31 May 2013),¹ simultaneous sampling with six sondes was afforded. Moreover, because of vehicle-mounted antennas and a mobile power source (via an inverter) in the PU, NSSL, and TAMU systems, signal reception while mobile was fully enabled and generally without issue.

The use of 200-g balloons allowed the sondes to ascend well above the tropopause within 45 to 60 min after launch, after which time the data collection usually was terminated owing to a typically weak sonde signal or balloon burst. At this time, CSU and TAMU could launch a new sonde using a different frequency. PU and NSSL could, on the other hand, launch a new sonde at any time, and on occasion did so at approximately 15-min intervals; in practice, and given acceptable and safe launch conditions, PU and NSSL typically staggered their individual launches by 30 min, so that they each could keep two sondes in the air continuously. It is noteworthy to mention here that the time to configure the sonde, enter needed data into the receiving system, and inflate the balloon varied depending upon operator experience and weather conditions, but typically took only 5–10 min.

Laptop computers were used to process the radio-sonde data in real time. These data were often used by the in-field Upsonde Director (UD) to make deployment decisions, especially during preconvective periods. Pre- and active-convective deployment decisions made by the UD were also facilitated by the in-field availability of real-time radar and other meteorological data. In fact, knowledge of team location relative to observed storm structure and other mesoscale features was paramount to the successful execution of the types of sampling strategies described in the sections that follow.

DATA QUALITY CONTROL AND SONDE INTERCOMPARISON. Although the iMet and Vaisala systems both offered data quality control (QC) during initial processing, additional QC was

performed by the individual teams and by NCAR EOL personnel at the completion of the field campaign. For example, sonde data collected after balloon burst were manually removed, as were spurious data that were recorded following, say, an unintended sonde passage through a downdraft. Intercomparisons of soundings were used to check for any obvious inconsistencies in observed GPS altitude, pressure, and other variables.

To examine the viability of intermixing the two different sondes for environmental sampling, a comprehensive intercomparison between the iMet and Vaisala sondes was made prior to the field campaign. On 14 days during May 2012, an iMet-1 AB sonde and a Vaisala RS92 sonde were suspended from the same 200-g balloon and launched from the same location in Norman, Oklahoma, in the daytime (between 1400 UTC and 2000 UTC). The measurements made by the two sondes had very small differences in temperature, with the median difference less than 0.5 K everywhere below 200 hPa (Fig. 2a). The iMet sonde relative humidity was slightly lower in the boundary layer (median values ~ -2%) and slightly higher in the 500–300 hPa layer (median values ~ +2%) (Fig. 2a), but overall the differences were small everywhere in the troposphere.

ENVIRONMENTAL SAMPLING STRATEGIES.

The two basic objectives of the upsonde teams were to sample the mesoscale environment over regions of anticipated convection initiation (CI), and then to sample the mesoscale environment that had been disturbed by subsequent convective storms. These objectives were accomplished through preconvective environment (PCE) strategies and convectively disturbed environment (CDE) strategies, respectively.

PCE Sampling. The full tropospheric structure of the mesoscale environment, prior to and in the region of anticipated CI, was sampled with a PCE strategy. During a typical PCE deployment, the upsonde teams were positioned relative to the time and location of expected CI, with the first upsonde observations made upstream of the expected CI location, and the last observations made downstream of and near the time of CI occurrence. This strategy allowed for data collection on the presumed contributor to CI (e.g., a mesoscale boundary), and then concluded with favorable positioning of the teams for CDE deployment. Most importantly, it allowed for samples of the preconvective environment (and its mesoscale

¹ TAMU periodically collected upsonde observations at College Station, Texas, at other times during the field campaign.

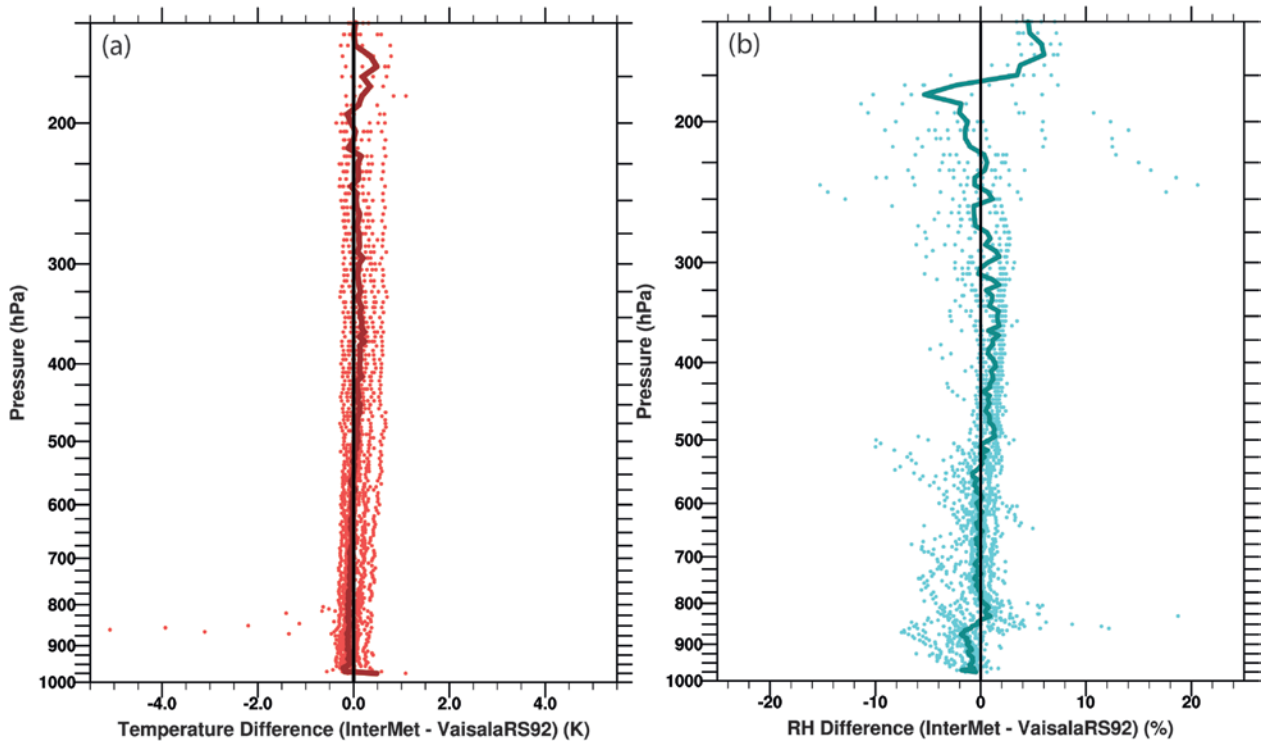


FIG. 2. Difference in (a) temperature (K) and (b) relative humidity (%) between InterMet and Vaisala RS92 sondes from 14 intercomparison flights. Dots are the differences for each flight and the solid line is the median difference.

variability) that could later be compared to samples of the convectively disturbed environment.

The range of PCE deployments during the project depended mostly on the expected CI mechanism and location, and surprisingly little on identification of suitable observation sites. Indeed, the teams quickly became adept at site identification and rapid deployment. Guided by an experimental ensemble of convection-permitting NWP models and by operational meteorological information, an initial target domain was typically identified by 1500 UTC, with data collection beginning between 1800 and 2000 UTC, but was delayed to as late as 2100 UTC. Given a choice of more than one domain, preference was often given to the one that showed more uncertainty in storm occurrence within the model ensemble, to accommodate later studies on the impact of the assimilation of the PCE soundings on model forecasts of the event.

The preconvective operations on 20 May 2013 exemplify the type of PCE sampling that was envisioned in the experimental plan. At ~1715 UTC, the PU, CSU, and NSSL teams sampled the preconvective environment west of a zone of enhanced mesoscale convergence in central Oklahoma, and east of a more extensive quasistationary boundary; these

launches were also coordinated in time with the National Weather Service radiosonde launch at Norman, Oklahoma (Fig. 3). Thereafter, PU redeployed to the east-northeast of its initial position, to facilitate PCE sampling in the vicinity and east of the convergence zone at ~1815 UTC. Local CI occurred west of the array at approximately this same time, albeit in association with the quasistationary boundary rather than the more subtle convergence zone. By 2000 UTC, one of the convective cells had matured into a tornadic supercell near Marlow, Oklahoma, and within the next two hours would move through the region that had been sampled previously (and also sampled subsequently, using the CDE strategies).

Although analysis of the upsonde data from this case is ongoing, the PCE (and CDE) samples have already revealed interesting contrasts in boundary layer evolution that depend on storm-relative launch locations. For example, the CSU soundings at 1714 UTC (not shown), 1827 UTC, and 2030 UTC (Fig. 4a), which were collected in the preconvective environment and then inflow of the supercell, show a gradual *deepening* in the height of the capping inversion and thus increase in the convective boundary layer depth, presumably owing to large-scale ascent.

The PU soundings at 1815 UTC (Fig. 3b), 1958 UTC (not shown), and 2045 UTC (Fig. 4b), which were collected in the preconvective environment and then downwind of the supercell, show a gradual *lowering* of the inversion and boundary layer depth; note that the launch locations of CSU and PU prior to 2000 UTC were separated by only 22 km (Fig. 3). Accounting for the sonde drift during data collection (see Fig. 3), this contrasting evolution in the PU-sampled boundary layer could have resulted from low-level (~850 hPa) adiabatic descent and warming (and drying) in proximate subsidence, and from midlevel (~750 hPa) diabatic cooling in a weak unsaturated downdraft farther downwind underneath the anvil of the approaching supercell. Numerical model simulations of this and other cases are being used to help provide further insight into these possible upscale effects.

CDE Sampling. CDE strategies were used to sample the full tropospheric structure of the mesoscale environment in close proximity to intense convective storms. During typical CDE deployments, the upsonde teams

executed time-coordinated sonde launches at 30-min intervals (60-min intervals for CSU and TAMU) at locations relative to the convective-storm motion

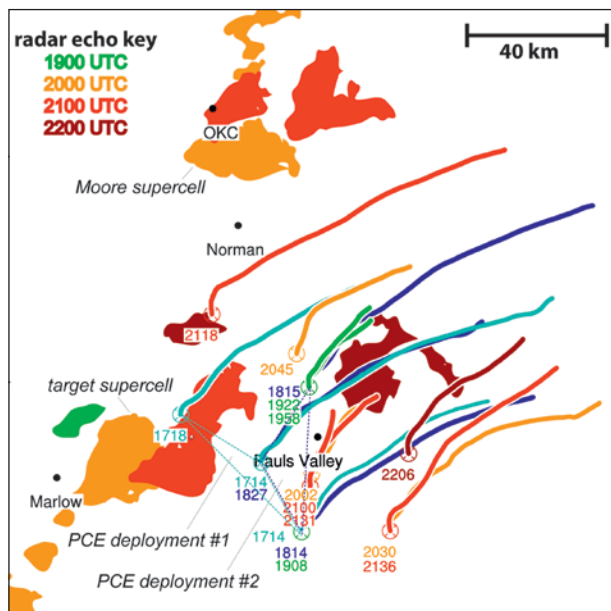


FIG. 3. PCE sampling on 20 May 2013. Hybrid-scan radar reflectivity factor ≥ 45 dBZ from the NSSL multiradar, multisensor analysis is shown by the filled contours, which are color coded by time (UTC) to match the color of the lines depicting the trajectory of the radiosonde flights within that hour. Thin dashed lines serve to highlight select coordinated radiosonde observations. To enhance clarity of the presentation, some radar echoes outside the immediate sampling area have been removed.

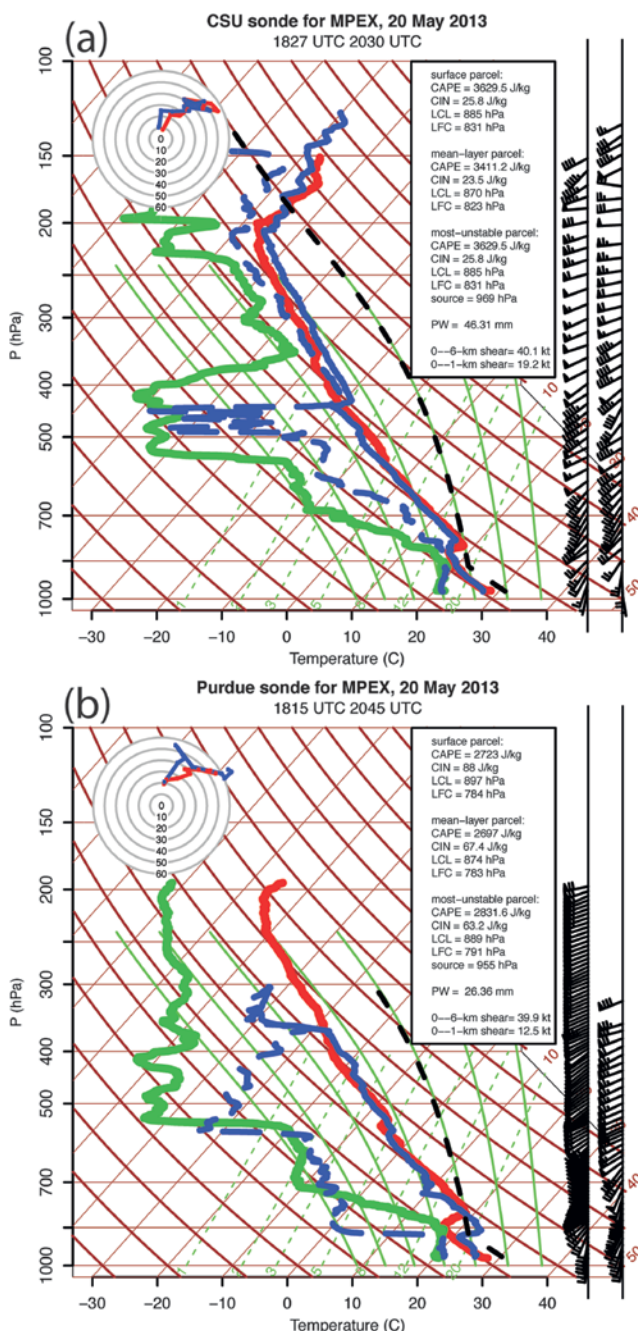


FIG. 4. Boundary layer evolution on 20 May 2013, as revealed through MPEX upsonde operations. (a) CSU soundings in a skew T -log p diagram at 1827 UTC (red/green) and 2030 UTC (blue/blue dashed). (b) PU soundings in a skew T -log p diagram at 1815 UTC (red/green) and 2045 UTC (blue/blue dashed). See Fig. 3 for sounding locations.

vector. Such storm-relative sampling was facilitated by the use of a combination of mobile communications (an MPEX chatroom, text messages, and cellular phone calls) and weather radar displays with real-time overlays of vehicle positions. The launch positions and launch times were determined by the UD and were based upon the evolving storm characteristics, our general operating plan, and the road network. Lapses in communication often forced the teams to operate autonomously, but nonetheless the teams were often still able to time-coordinate their respective launches in their designated storm-relative locations. The PU and NSSL teams would then immediately go mobile to get into position for the next launch.

The CDE operations on 19 May 2013 illustrate the adaptive and innovative strategies employed during MPEX. After the PCE sampling at 1900 UTC, the upsonde teams targeted a rapidly intensifying cell located upstream from their north-central Oklahoma locations. Accounting for the storm-motion vector, the teams redeployed east and south, such that NSSL and CSU (PU) would be north (south) of the cell that would ultimately spawn a tornado near Edmond, Oklahoma (Fig. 5). Environmental soundings were collected as the now tornadic supercell moved through this north-south array. Subsequently, the teams redeployed farther south and east to target the supercell that produced a tornado near Shawnee, Oklahoma. The environment disturbed by this supercell was nominally sampled at 0045 UTC using a triangular array that yielded a wake sounding, an inflow sounding, and a downstream sounding (Fig. 5). These soundings are shown in Weisman et al. (2015), who note that other than the (temperature, moisture, and wind) changes induced at low levels by the cold pool, the environmental structure in the immediate wake of the Shawnee supercell was relatively unmodified.

Note that in this case and others, an offset distance between the launch location and the edge of the convective echo was chosen to be ~10–20 km, but ultimately depended on suitable roads and the storm motion. Also in this case, east-west staggering was introduced to the launch locations when possible, to result in observation “triangles.” These will facilitate the calculation of kinematic quantities (vorticity, divergence) using the triangle method.

Although operations preference was given to slow-moving supercellular convection (see Table 2), other modes of convection were also targeted. For example, consider the CDE operations on 29 May 2013. Upon completion of PCE soundings in the northwest

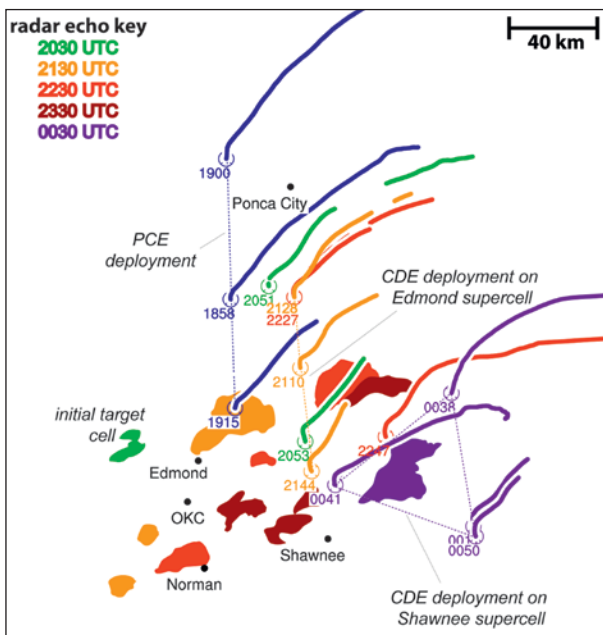


FIG. 5. As in Fig. 3, except on 19–20 May 2013.

Oklahoma/northeast Texas Panhandle at 1800 UTC, the four teams rotated their “box” pattern counterclockwise into a “diamond” pattern to better surround an approaching target cell that had developed well southwest of Canadian, Texas (Fig. 6). The expectation was that this cell would transition into a supercell by

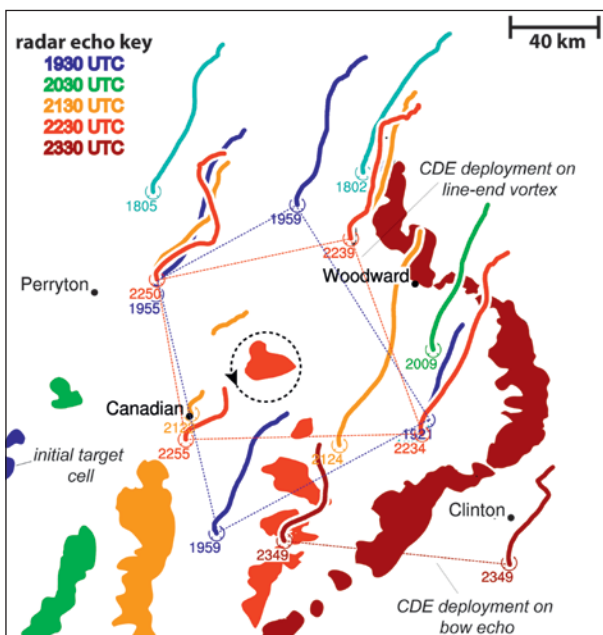


FIG. 6. As in Fig. 3, except on 29–30 May 2013 and reflectivity ≥ 40 dBZ.

the time it reached the upsonde array, so coordinated soundings were taken at ~2000 UTC. After 2000 UTC, however, the target cell began to dissipate, so a decision was made to consider the convective line that was developing southwest of the array. As the convective line evolved into a squall-line bow echo, the teams were able to reorient their array and at ~2240 UTC successfully sample the environment disturbed by the northern line-end vortex and associated deep convection (Fig. 6). A final set of soundings was collected at 2349 UTC by two teams, who were able to rapidly redeploy to the south and simultaneously sample the inflow and outflow of the squall-line bow echo.

CONCLUDING REMARKS. The improvements in the cost, reliability, and usability of radiosonde

systems and mobile communications led to a unique application of these observing systems during MPEX. What was initially envisioned as an aircraft-only data collection experiment evolved into one that included mobile ground-based operations, wherein upsondes were launched at high rates in locations around moving convective storms throughout their life cycles. In fact, ground-based operations had the distinct advantage of being free from air-traffic control and other aircraft logistics, which thus allowed for relatively more flexibility in targets and strategy. Given the use of graduate and undergraduate students to assist in the field deployments, and an availability of relatively low-cost yet high-quality radiosonde systems, the cost of the ground-based operations was also comparatively lower. Of course, (storm-following)

TABLE 2. Summary of upsonde deployments during MPEX.

Date	Brief description
15 May	Northern Texas, tornadic supercell (NSSL-only deployment)
16 May	Southwestern Kansas, convective cells; coordination test
18 May	West-central Kansas tornadic supercell
19 May	Central Oklahoma, two tornadic supercells
20 May	Central Oklahoma, tornadic supercell
23 May	Northwestern Texas, tornadic supercell, with wake/cold pool soundings, and some inflow soundings into developing MCS
27 May	Central Kansas, intense cell with some supercell characteristics
28 May	South-central Kansas, demise of intense cell
29 May	Western Oklahoma/eastern Texas Panhandle, developing bow echo, with surround sampling of the northern bookend vortex, and additional sampling of cold pool and inflow of QLCS
30 May	South-central Oklahoma, nontornadic supercell (all teams), and some Purdue-only sampling of wake of additional nontornadic supercell
31 May	Central Oklahoma, tornadic supercell
3 June	Oklahoma Panhandle, southwest Kansas, intense cells with some (HP) supercell characteristics, surround strategy, then additional sampling of developing bow echo
4 June	Eastern Texas Panhandle, mesoscale environment
8 June	Southwest Kansas, Oklahoma Panhandle, intense cell within line
11 June	Western Nebraska, weak convection and additional cell
12 June	Eastern Wyoming, mesoscale environment
14 June	Kansas–Colorado, weak convective line

GEONOR

**Geonor T-200B series
All-weather precipitation gauges
600 mm • 1000 mm • 1500 mm**



- More than 25 years of field use
- No moving parts
- Easy installation and maintenance
- No internal heating necessary
- Precipitation intensity can be calculated
- Interfaces to most data acquisition systems

Proven long term reliability

Manufacturer:
Geonor AS, Norway
www.geonor.no

US distributor:
Geonor Inc, USA
www.geonor.com

ground-based operations will always be limited by suitable road and deployment-site availability, and inherently by the storm movement relative to allowable driving speeds. Thus, one trade-off is a relatively reduced area of sounding coverage per time interval.

In future field campaigns, inclusion of additional upsonde teams would help ground-based upsonde operations approach parity with airborne dropsonde operations. This is most relevant when the logistics of the scientific problem and observational domain render airborne deployments infeasible. As one example, similar observation strategies with mobile upsondes were used to investigate nocturnal convective systems in the Plains Elevated Convection at Night (PECAN) experiment, held in 2015 within the Great Plains region of the United States.

FOR FURTHER READING

- Bluestein, H. B., 1999: A history of severe-storm-intercept field programs. *Wea. Forecasting*, **14**, 558–577, doi:10.1175/1520-0434(1999)014<0558:AHOSI>2.0.CO;2.
- Bretherton, C. S., 1993: The nature of adjustment in cumulus cloud fields. *The Representation of Cumulus Convection in Numerical Models*, Meteor. Monogr., No. 46, Amer. Meteor. Soc., 63–74.
- Parker, M. D., 2014: Composite VORTEX2 supercell environments from near-storm soundings. *Mon. Wea. Rev.*, **142**, 508–529, doi:10.1175/MWR-D-13-00167.1.
- Rust, W. D., and T. C. Marshall, 1989: Mobile, high-wind, balloon-launching apparatus. *J. Atmos. Oceanic Technol.*, **6**, 215–217, doi:10.1175/1520-0426(1989)006<0215:MHWBLA>2.0.CO;2.
- , D. W. Burgess, R. A. Maddox, L. C. Showell, T. C. Marshall, and D. K. Lauritsen, 1990: Testing a Mobile Version of a Cross-Chain Loran Atmospheric (M-CLASS) sounding system. *Bull. Amer. Meteor. Soc.*, **71**, 173–180, doi:10.1175/1520-0477(1990)071<0173:TAMVOA>2.0.CO;2.
- Spencer, P. L., D. J. Stensrud, and J. M. Fritsch, 2003: A method for improved analyses of scalars and their derivatives. *Mon. Wea. Rev.*, **131**, 2555–2576, doi:10.1175/1520-0493(2003)131<2555:AMFIAO>2.0.CO;2.
- Trapp, R. J., 2013: *Mesoscale-Convective Processes in the Atmosphere*. Cambridge University Press, 346 pp.
- Weisman, M. L., and Coauthors, 2015: The Mesoscale Predictability Experiment (MPEX). *Bull. Amer. Meteor. Soc.*, **96**, 2127–2149, doi:10.1175/BAMS-D-13-00281.1.

An EF3 Multivortex Tornado over the Ionian Region

Is It Time for a Dedicated Warning System over Italy?

BY MARIO MARCELLO MIGLIETTA AND RICHARD ROTUNNO

On 28 November 2012, an intense tornado affected southeastern Italy. At approximately 1050 LT (0950 UTC), this tornado, initially formed as a waterspout over the Ionian Sea, moved inland near the port city of Taranto, the third-largest in southern Italy, and hit the ILVA, the largest steel plant in Europe (Fig. 1). The tornado blew down the operator's cabin from a crane on which an employee was working in the harbor; his body was recovered some days later, 100 m farther out to sea. Fortunately, most of the ILVA workers were at home due to a temporary production stoppage, otherwise the outcome could have been far worse. The estimated damage to the

plant was €60M, of which €20M was reported in the port area first crossed by the vortex.

An early warning message was sent out by the Italian Civil Protection Department (DPC), which has been in charge of issuing warnings since 2004, at an ordinary criticality level. The message warned of gale-force winds and the possibility of occasional thunderstorms or showers. Unfortunately, as in the majority of European countries (Rauhala and Schultz 2009), in Italy there are no procedures to warn for tornadoes and severe thunderstorms, which in our opinion is rather inadequate considering their potential threat.



FIG. 1. Map of (left) the central Mediterranean, (middle) southeastern Italy, and (right) a detail of the Taranto area. The tornado track is shown with a thick red line, while the later supercell movement is shown with a dashed red line (Source: Google Earth). The names of the places and stations mentioned in the text are shown. The box in the left (central) panel identifies the area shown on the middle (right) panel.

AFFILIATIONS: MIGLIETTA—The Institute of Atmospheric Sciences and Climate-National Research Council (ISAC-CNR), Lecce, Italy; ROTUNNO—National Center for Atmospheric Research,* Boulder, Colorado

*The National Center for Atmospheric Research is sponsored by the National Science Foundation.

CORRESPONDING AUTHOR: Mario Marcello Miglietta, CNR-ISAC, strada provinciale Lecce-Monteroni, 73100 Lecce, Italy

E-mail: m.miglietta@isac.cnr.it

DOI:10.1175/BAMS-D-14-00227.1

© 2016 American Meteorological Society

TRACK AND CHARACTERISTICS.

Early in the morning of 28 November, several convective cells were generated along the west side of the Ionian Sea. After crossing the relatively warm sea (the sea surface temperature measured in Taranto was 18.6°C), one of the cells assumed supercellular characteristics, and a waterspout was generated. In this phase, a fairly unique measurement of sea level was made by a buoy located just a few hundred meters to the east of where the tornado made landfall at the port of Taranto

(Fig. 1): after a small decrease, the sea level increased rapidly by 30 cm, followed by a period of oscillations of decreasing intensity (Fig. 2).

After landfall, the vortex motion slightly deviated, moving from south to north for about 12 km, from west of Taranto to the small town of Statte (Fig. 1). When the supercell started crossing the Murge hills, it deviated northeastward; the funnel cloud lifted from the ground in this phase. After crossing the hills, significant damage was again caused to vegetation (hardwood trees were uprooted) and to a tourist village near the Adriatic Sea (as documented in Venerito et al. 2013), nearly 50 min after and about 50 km away from the location of the landfall. Unfortunately, no Doppler radar data are available in the area.

From the damage recorded at the ILVA, following the “Enhanced Fujita (EF) Scale Damage Indicators (DI) and Degrees of Damage (DOD)” (McDonald and Mehta, 2006), the event can be conservatively classified near the lower end of the category EF3,¹ with a maximum wind speed of approximately 230 km h⁻¹, which is the expected wind speed for the reported damages—collapsed rigid parts of metal structures (DI = 21, DOD = 7), significant damage to some external and internal building walls (DI = 17, DOD = 6), and removal of electricity pylons (DI = 24, DOD = 6). Also, in the area,

¹ Since the degree of damage measures is based on U.S.-specific construction practices, the wind speed may have been underestimated. The application of the International Fujita Scale, adopted at the European Severe Storms Laboratory, would suggest an estimated wind speed of 324 km h⁻¹ (weak brick structure with walls partly collapsed).

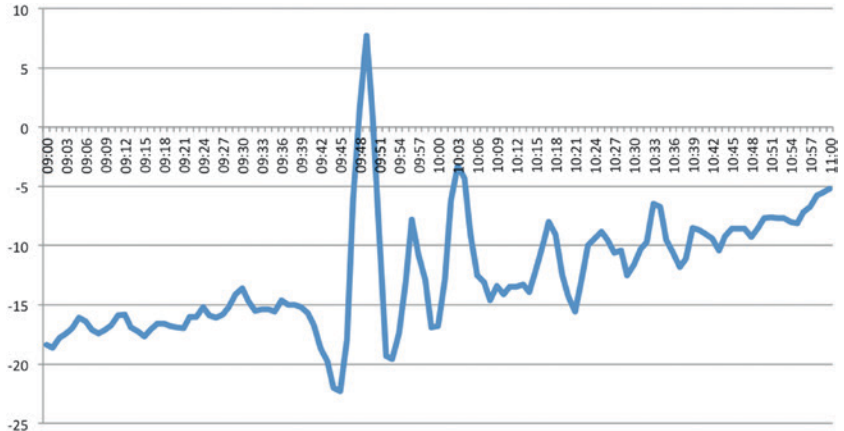


FIG. 2. Sea level height (cm) with respect to the mean value. Data are provided by the station of Taranto from the national tide gauge network belonging to Servizio Mareografico ISPRA.



FIG. 3. (top) Collapse of metal structures in the port area; (middle) a crane weighing several tons lifted; and (bottom) a concrete chimney completely destroyed (courtesy ILVA S.p.A.).



FIG. 4. Photograph taken near the tornado landfall, extracted from www.youtube.com/watch?v=9ZOaOHK10_A (courtesy Giovanni Viscardi).

cranes weighing several tons were lifted and a concrete chimney was completely destroyed (Fig. 3). The path width was estimated to be about 300 m just after landfall. Several photos and videos are available on the Internet (see, for example, Fig. 4). Some of them show the presence of a multivortex structure during this phase (www.youtube.com/watch?v=h7RbLqWt9Ns), with the presence of some minor vortices around the main structure, which in some cases were temporarily able to touch the ground, a typical behavior of such events (Bluestein 2013, p. 313).

Along the northern part of its track, near the city of Statte (Fig. 1), where the cyclonic circulation was still very intense and the canopy of a gas station was destroyed, the tornado of Taranto took extraordinary horizontal dimensions (among the largest ever photographed in Europe) similar to the so-called "wedge" tornadoes (Hill and Bronski 2009), since the diameter of its visual funnel² appears comparable to the lifting condensation level (LCL), which in the present case was about 700 m AGL (www.youtube.com/watch?v=NcL3LuAT1xE).

STORM ENVIRONMENT. The synoptic environment was characterized by a deep upper-level trough over the Tyrrhenian Sea, associated with a mean sea level pressure minimum over Corsica. An intense upper-level southwesterly flow of relatively cold and dry air affected the Ionian region, while at lower levels a warm tongue extended northward up to northern Europe, producing conditions of potential

² A path width of about 500 m was estimated in this phase using geomorphological methods (Venerito et al. 2013).

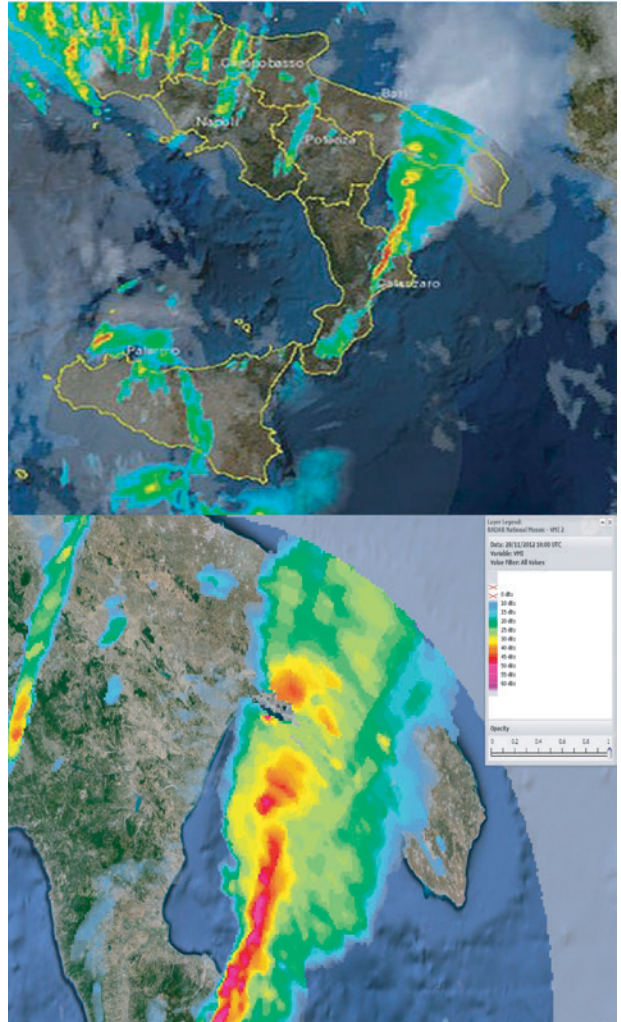


FIG. 5. (top) Radar reflectivity (Vertical maximum intensity) at 1100 LT (Source: website of the Italian Civil Protection Department–Presidency of the Council of Ministers) over southern Italy and (bottom) zoomed in on the Ionian regions. In the top panel, heavy rainfall is denoted by red, moderate/heavy by orange, moderate by yellow, moderate/weak by green, weak by cyan, and cloudy but with no precipitation by gray.

instability. Radar reflectivity maps (Source: Italian Civil Protection Agency) clarify the genesis of the event: the lifting induced by the Apennines appears to have triggered convection and generated a series of convective cells elongated in the direction of the upper-level wind, from south-southwest to north-northeast (Fig. 5). The same genesis mechanism was identified for other severe convective events in the region (e.g., Mastrangelo et al. 2011).

The vertical profile from Brindisi (the closest in time and space to the event) at 1200 UTC on 28

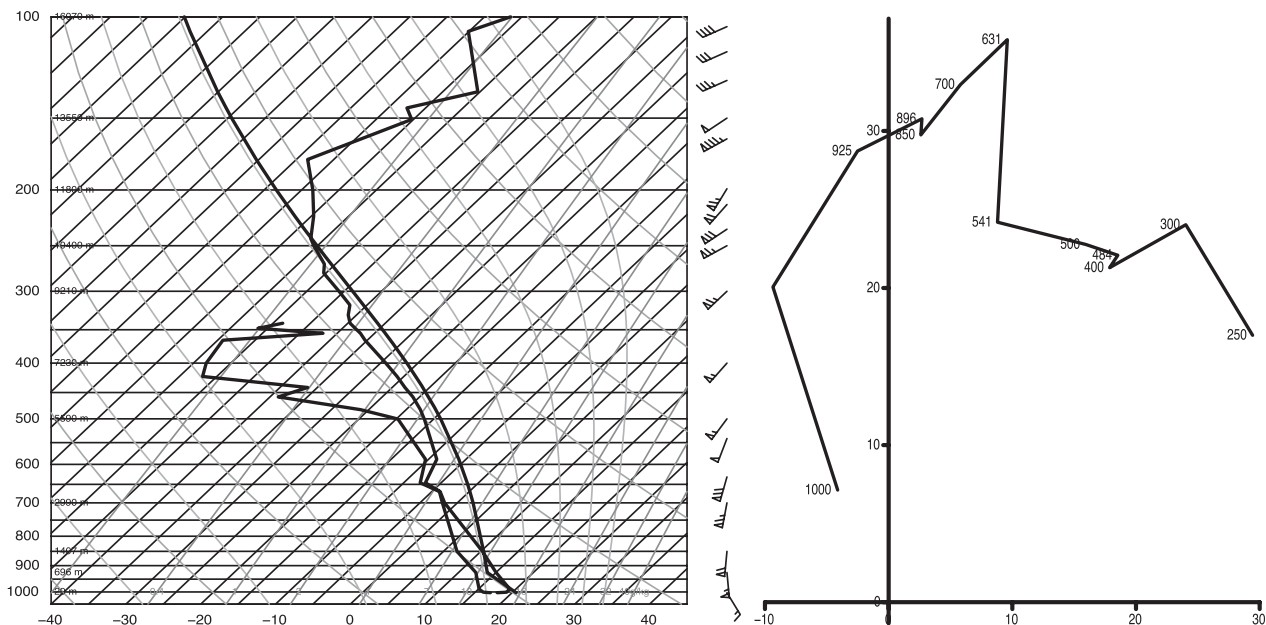


FIG. 6. (left) Skew-T diagram and (right) hodograph from Brindisi at 1200 UTC, 28 Nov 2012. In the Skew-T, wind units are in knots, temperature in °C, and pressure in hPa; in the hodograph, wind units are in m s⁻¹. (Source: University of Wyoming)

November 2012 (Fig. 6a) shows the presence of very moist air in the lower levels, advected by the southerly flow below 500 hPa, with the atmosphere close to saturation near the ground. A strong pressure gradient is consistent with the intense wind speed over the region, with the low-level wind reaching 56 kt at 686 m above sea level (57 kt at 606 m, 12 h later), an absolutely extraordinary value. As a consequence, a very large vertical wind shear was present in the lowest km of the atmosphere.

The hodograph shown in Fig. 6b indicates a sharp increase in wind speed with altitude and implies a flow with large values of horizontal vorticity; the curved hodograph is typical of tornadic supercells in the United States (Maddox 1976). The storm-relative helicity (SRH) was 686 m² s⁻² in the layer 0–3-km AGL (553 m² s⁻² in the lowest km) in the Brindisi sounding (Source: Plymouth State Weather Center). The 0–3- (0–1)-km Energy-Helicity Index (EHI) reached the high value of 3.4 (2.7), although only moderate instability was present [the surface-based convective available potential energy (CAPE), obtained by lifting a parcel from 2-m height and including the virtual temperature correction, was 970 J kg⁻¹].

COMPARISON WITH CLIMATOLOGY. Comparing these values with the only existing climatology of tornadoes in Italy extracted from 10 years of data

(Gaiotti et al. 2007), it is found that the low-level vertical wind shear for this event was more than twice the climatological mean for F3 tornadoes. Also, the values of 0–3-km SRH and EHI turned out to be the largest.

Even compared with U.S. tornadoes, the tornado of Taranto shows some unique characteristics. Considering the 0–1-km wind difference of 24.8 m s⁻¹ and the mixed-layer LCL of about 700 m shown in the Brindisi sounding, the environment of this tornado fell into the high end of the two-dimensional distribution associated with U.S. tornadoes (cf. Fig. 7.4 in Bluestein 2013, and Fig. 10.13 in Markowski and Richardson 2010). The storm motion, estimated from the nearby hodograph, was from the south-southwest with a speed of 45 kt.³ Considering this value as a proxy for the translation velocity, the tornado would fall above the 75th percentile of the Alexander and Wurman (2008, their Fig. 3) distribution.⁴

³ The storm motion was calculated using the scheme proposed in Bunkers et al. (2000), but changing the layer for the calculation of mean wind from 0–6 km to 0–8 km, as discussed in Ramsay and Doswell (2005).

⁴ However, this distribution is biased toward the U.S. Great Plains states, a region where typically, relatively slow right-moving supercells are favored.

Together with the favorable wind profile, other local factors may have favored the development of the tornado. The Taranto bay called Mar Grande (Fig. 1) may have locally enhanced the instability shown in the Brindisi sounding, behaving as a source of high equivalent potential temperature, due to its low bathymetry. Also, the high surface temperature of the Ionian Sea (about 2°C higher than the climatology) may have played an important role in producing intense sensible and latent heat fluxes and in providing energy to convection. This would also explain the occurrence of the tornado late in the season, compared to the peak in tornado activity, which is generally observed over Italy in late summer and early fall.

The possibilities offered by the Internet to post and share images and videos of tornadoes and waterspouts and the storm report archiving in the European Storm Weather Database have made it apparent that the frequency of their occurrence over the Mediterranean has been largely underestimated. Together with a large number of weak events, large and moderate-to-intense vortices are regularly observed. From Giaiotti et al. 2007, it appears that at least 3 F2 tornadoes occur per year, with an F3 event every 1.5 years. A significant fraction of Europe's deadliest recorded tornadoes occurred in Italy [see Groenemeijer and Kühne (2014)'s Table 1]. Although the information is increasingly fragmented when going back in time, three events of intensity greater than F3 are estimated to have affected Italy in the last century, the strongest one (F4/F5) occurring in northeastern Italy (Montello) in 1930, while 36 casualties were reported in an F3/F4 tornado near Venice in 1970.

The distribution of past events suggests that their occurrence is concentrated in some specific areas [see Groenemeijer and Kühne (2014)'s Figs. 1 and 2b], and Salento (Fig. 1) appears to be one of these. In particular, in the last few years, several weak and small waterspouts, which remained mostly confined over the sea, have been photographed offshore of the port of Taranto. A detailed study of historical chronicles and newspapers has been carried out in Gianfreda et al. (2005), showing that the earliest documented tornado in Salento dates back to 1546. Most of the historical events appear to have a similar propagation from the Ionian Sea inland, in a few cases producing severe damage and casualties. In particular, the tornado affecting the region in September 1897 killed at least 55 people, which is among the highest number of fatalities caused by a tornado ever documented in Europe.

OPPORTUNITY FOR A DEDICATED TORNADO WARNING SYSTEM.

From the evidence presented here, it is clear that, although rare, tornadoes having EF2 or stronger intensity can occasionally affect the Italian territory, while weaker events are more frequent. Just as an example, according to the European Severe Weather Database (ESWD; Dotzek et al. 2009), from the beginning of October to mid-November 2014, 25 tornadoes were identified over Italy, one being classified as F2 and four as F1. The detection and prediction well in advance of the possible occurrence of these events appears to be a necessary task for civil protection purposes, which, we believe, cannot be further postponed.

Following the complex evolution of the Italian National Weather Service discussed in Visconti and Marzano (2008), the institution by law of the National Distributed Weather Service in 2012 (although its organization and implementation is still a work in progress⁵) is the result of a long discussion started in the early 1990s. The new service will merge together the activity of the DPC, the Air Force Weather Service (until now the Italian National Service “de facto”), and the Regional Hydrometeorological Services, and should allow for a more rational organization of a system where, until now, competencies and tasks have often overlapped. The situation is critical mainly in southern Italy, where the Civil Protection Agency regional offices are still under development, and observational sites are distributed among a plethora of different institutions, often with no specific competency in meteorology.

However, the new organization is not expected to issue alerts for the prediction of localized severe thunderstorms, and we believe that several obstacles need to be overcome in order to establish a dedicated warning system.

First, detailed and accurate statistics of the intensity and distribution of these events is still lacking over Italy. The only climatological study for tornadoes specific for Italy is incomplete and not up to date, and only a few case studies (mainly affecting northeastern Italy) have been the subject of a detailed analysis and have been published in the scientific literature (e.g., Alberoni et al. 2000; Bechini et al. 2001). Also, very few studies are

⁵ The Presidential Decree that would establish the organization of the National Distributed Weather Service has been submitted to the Italian government (Davolio et al. 2015).

available dealing with the climatology of thunderstorms (Cacciamani et al. 1995), hail (Morgan 1973), and lightning (Feudale and Manzato 2014), and are limited to the Po Valley.

The ability to predict a tornado's precise path and intensity is an extremely complex process, requiring years of experimentation. Even if such a long-term goal is still very far off, at least some initial steps should be taken toward the identification of possible risk scenarios. The conditions associated with tornadoes have been extensively studied and include contributions from an environment conducive to deep moist convection and a source of easily stretched low-level vertical vorticity (Doswell et al. 2012), either vertically advected from a strongly sheared environment or converged from preexisting fields of vertical vorticity. Considering the morphology of the Italian territory, where complex circulations induced and/or modulated by the presence of the sea and of the orography may especially affect the meso-gamma scale, it appears that the conceptual models developed for the U.S. Midwest should be modified or adapted to the peculiar Mediterranean environment. In particular, the role of the warm Mediterranean sea surface and the presence of a very long and complex coastline should be properly investigated and analyzed.

In the United States, watches and warnings are issued mainly based on observed data; as discussed in Brotzge and Donner (2013), weather radar is the primary tool for the detection of supercell thunderstorms, allowing the identification of the rotation that precedes tornadogenesis. It is clear that in areas with limited Doppler radar coverage, as in Italy, the detection and forecasting of tornadoes is severely hampered. The radar reflectivity mosaic recently (finally!) made available in real time over Italy can help detect dangerous situations. Some regional operational Doppler and a few polarimetric radars can be very helpful, where available, to discover tornado signatures and to represent the wind field correctly, although these provide only limited coverage.

Finally, the chains of limited-area models (deterministic or ensemble) operationally implemented over Italy do not include sufficient guidance to assist in forecasting localized severe convection among the output fields. This limitation precludes the possibility of forecasting the presence of dangerous conditions well in advance.

The recent cooperative effort during the Hydrological Cycle in Mediterranean Experiment

(HyMeX; Ducrocq et al. 2014) has made clear that, even without dedicated funding and without the official support of the Air Force Weather Service, it is possible to share resources and expertise from the different regional services and the scientific community (Ferretti et al. 2014; Davolio et al. 2015) and overcome—at least temporarily—the traditional fragmentation of the Italian system. The institution of the National Distributed Weather Service should accelerate this process and give new impetus to the research, which has often been neglected in the scarcity or even absence of specific funding from the operational centers and from the central government, and to the academic education in the field. Currently, Italian universities do not offer any five-year educational training specific to atmospheric physics and meteorology.

The new organization should plan to establish an office dedicated to the diagnosis, monitoring, and forecasting of severe thunderstorms and tornadoes. A potential model for this organization could be the Storm Prediction Center (SPC; www.spc.noaa.gov) in the United States, a forecast center that issues convective outlooks, mesoscale discussions, and watches. The European Storm Forecast Experiment (www.estofex.org; Brooks et al. 2011) is experimenting with producing a European-centric version of SPC's convective outlooks. However, to properly satisfy the needs of a warning system at the national level, information at finer horizontal and temporal scales is needed, possibly issuing high-resolution warnings for selected regions that can take into account the inhomogeneity of the Italian territory—similar to the practice of the Bureau of Meteorology in Australia. This would represent a relevant improvement in a country where, until now, the meteorological information provided—but also that required by the final users—has often been of low quality (Tibaldi 2014).

Finally, the population should be educated to deal with alerts. The recurring floods over Italy in the last few years have surely increased the awareness of the risks associated with severe weather and made clear the need to adopt more precautionary behavior. However, there is still a long way to go to reach an acceptable level. An increased consciousness regarding tornadoes and severe localized convection is a necessary objective. This task requires some substantial background research, not just in meteorology but in social science (see for example, Simmons and Sutter 2011), identifying whether a hazard-information flow

substantially different from the U.S. system would be more appropriate.

ACKNOWLEDGMENTS. Comments by two anonymous reviewers, Jeff Waldstreicher, Andrea Buzzi, Silvio Davolio, Vincenzo Levizzani, and Agostino Manzato on the first draft are gratefully acknowledged. We are indebted to ILVA S.p.A. for the permission to publish Fig. 3 and to Giovanni Viscardi for Fig. 4.

FOR FURTHER READING

- Alberoni, P. P., V. Levizzani, R. Watson, A. Holt, S. Costa, P. Mezzasalma, and S. Nanni, 2000: The 18 June 1997 companion supercells: Multiparametric Doppler radar analysis. *Meteor. Atmos. Phys.*, **75**, 101–120, doi:10.1007/s007030070018.
- Alexander, C. R., and J. Wurman, 2008: Updated mobile radar climatology of supercell tornado structures and dynamics. *24th Conf. on Severe Local Storms*, Savannah, GA, AMS. [Available online at <https://ams.confex.com/ams/pdfpapers/141821.pdf>.]
- Bechini, R., D. Giaioti, A. Manzato, F. Stel, and S. Micheletti, 2001: The June 4th 1999 severe weather episode in San Quirino: A tornado event? *Atmos. Res.*, **56**, 213–232, doi:10.1016/S0169-8095(00)00074-0.
- Bluestein, H. B., 2013: *Severe Convective Storms and Tornadoes: Observations and Dynamics*. Springer-Verlag, 456 pp.
- Brooks, H. E., and Coauthors, 2011: Evaluation of European Storm Forecast Experiment (ESTOFEX) forecasts. *Atmos. Res.*, **100**, 538–546, doi:10.1016/j.atmosres.2010.09.004.
- Brotzge, J., and W. Donner, 2013: The tornado warning process: A review of current research, challenges, and opportunities. *Bull. Amer. Meteor. Soc.*, **94**, 1715–1733, doi:10.1175/BAMS-D-12-00147.1.
- Bunkers, M. J., B. A. Klimowski, J. W. Zeitler, R. L. Thompson, and M. L. Weisman, 2000: Predicting supercell motion using a new hodograph technique. *Wea. Forecasting*, **15**, 61–79, doi:10.1175/1520-0434(2000)015<0061:PSMUAN>2.0.CO;2.
- Cacciamani, C., F. Battaglia, P. Patrino, L. Pomi, A. Selvini, and S. Tibaldi, 1995: A climatological study of thunderstorm activity in the Po Valley. *Theor. Appl. Climatol.*, **50**, 185–203, doi:10.1007/BF00866116.
- Davolio, S., and Coauthors, 2015: The role of the Italian scientific community in the first HyMeX SOP: An outstanding multidisciplinary experience. *Met. Zeit.*, **24**, 261–267, doi:10.1127/metz/2014/0624.
- Doswell III, C. A., G. W. Carbin, and H. E. Brooks, 2012: The tornadoes of spring 2011 in the USA: An historical perspective. *Weather*, **67**, 88–94, doi:10.1002/wea.1902.
- Dotzek, N., P. Groenemeijer, B. Feuerstein, and A. M. Holzer, 2009: Overview of ESSL's severe convective storms research using the European Severe Weather Database ESWD. *Atmos. Res.*, **93**, 575–586, doi:10.1016/j.atmosres.2008.10.020.
- Ducrocq, V., and Coauthors, 2014: HyMeX-SOP1: The field campaign dedicated to heavy precipitation and flash flooding in the northwestern Mediterranean. *Bull. Amer. Meteor. Soc.*, **95**, 1083–1100, doi:10.1175/BAMS-D-12-00244.1.
- Ferretti, R., and Coauthors, 2014: Overview of the first HyMeX Special Observation Period over Italy: Observations and model results. *Hydrol. Earth Syst. Sci.*, **18**, 1953–1977, doi:10.5194/hess-18-1953-2014.
- Feudale, L., and A. Manzato, 2014: Cloud-to-ground lightning distribution and its relationship with orography and anthropogenic emissions in the Po Valley. *J. Appl. Meteor. Climatol.*, **53**, 2651–2670, doi:10.1175/JAMC-D-14-0037.1.
- Giaioti, D. B., M. Giovannoni, A. Pucillo, and F. Stel, 2007: The climatology of tornadoes and waterspouts in Italy. *Atmos. Res.*, **83**, 534–541, doi:10.1016/j.atmosres.2005.10.020.
- Gianfreda, F., M. M. Miglietta, and P. Sansò, 2005: Tornadoes in Southern Apulia (Italy). *Nat. Hazards*, **34**, 71–89, doi:10.1007/s11069-004-1966-3.
- Groenemeijer, P., and T. Kühne, 2014: A climatology of tornadoes in Europe: Results from the European Severe Weather Database. *Mon. Wea. Rev.*, **142**, 4775–4790, doi:10.1175/MWR-D-14-00107.1.
- Hill, R., and P. Bronski, 2009: *Hunting Nature's Fury: A Storm Chaser's Obsession with Tornadoes, Hurricanes, and Other Natural Disasters*. Wilderness Press, 206 pp.
- Maddox, R. A., 1976: An evaluation of tornado proximity wind and stability data. *Mon. Wea. Rev.*, **104**, 133–142, doi:10.1175/1520-0493(1976)104<0133:AEOTPW>2.0.CO;2.
- Markowski, P., and Y. Richardson, 2010: *Mesoscale Meteorology in Midlatitudes*. John Wiley & Sons, 407 pp.
- Mastrangelo, D., A. Riccio, K. Horvath, and M. M. Miglietta, 2011: Mechanisms for convection development in a long-lasting heavy precipitation event over southeastern Italy. *Atmos. Res.*, **100**, 586–602, doi:10.1016/j.atmosres.2010.10.010.

- McDonald, J., and K. C. Mehta, 2006: A recommendation for an Enhanced Fujita Scale (EF-Scale), Revision 2. Wind Science and Engineering Research Center, Texas Tech University, 111 pp.
- Morgan, G. M., 1973: A general description of the hail problem in the Po Valley of northern Italy. *J. Appl. Meteor.*, **12**, 338–353, doi:10.1175/1520-0450(1973)012<0338:AGDOTH>2.0.CO;2.
- Ramsay, H. A., and C. A. Doswell III, 2005: A sensitivity study of hodograph-based methods for estimating supercell motion. *Wea. Forecasting*, **20**, 954–970, doi:10.1175/WAF889.1.
- Rauhala, J., and D. M. Schultz, 2009: Severe thunderstorm and tornado warnings in Europe. *Atmos. Res.*, **93**, 369–380, doi:10.1016/j.atmosres.2008.09.026.
- Simmons, K. M., and D. Sutter, 2011: *Economic and Societal Impact of Tornadoes*. American Meteorological Society Press, 282 pp.
- Tibaldi, S., 2014: Meteorologia operativa: l'Italia arranca. *Ecoscienza*, **4**, 56–58.
- Venerito, M., P. Fago, C. Colella, R. Laviano, F. Montanaro, P. Sansò, and G. Mastronuzzi, 2013: Il tornado di Taranto del 28 novembre 2012: Percorso, orografia e vulnerabilità. *Geologia dell'Ambiente*, **4/2013**, 2–9.
- Visconti, G., and F. S. Marzano, 2008: An independent overview of the National Weather Service in Italy. *Bull. Amer. Meteor. Soc.*, **89**, 1279–1284, doi:10.1175/2008BAMS2372.1.

NEW FROM AMS BOOKS!

“A thoughtful analysis of actions that we need to take to reduce the impacts of extreme weather... a must-read for everyone with an interest in the weather and climate.”

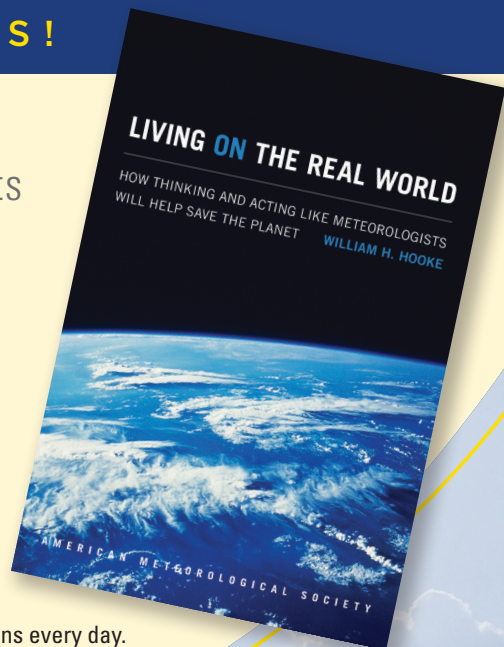
— FRANKLIN W. NUTTER,
President, Reinsurance Association of America

Living on the Real World: How Thinking and Acting Like Meteorologists Will Help Save the Planet

WILLIAM H. HOOKE

Meteorologists sift through a deluge of information to make predictions every day. Instead of being overwhelmed by the data and possibilities, they focus on small bits of information while using frequent collaboration to make decisions. With climate change a reality, William H. Hooke suggests we look to the way meteorologists operate as a model for how we can solve the twenty-first century's most urgent environmental problems.

© 2014, PAPERBACK 978-1-935704-56-0
LIST \$30 MEMBER \$22



AMS BOOKS

RESEARCH APPLICATIONS HISTORY

www.ametsoc.org/amsbookstore

THE EARTH SCIENCE WOMEN'S NETWORK (ESWN)

Community-Driven Mentoring for Women in the Atmospheric Sciences

BY AMANDA S. ADAMS, ALLISON L. STEINER, AND CHRISTINE WIEDINMYER

The mentoring philosophy and activities of the Earth Science Women's Network's (ESWN) have reduced some barriers that female atmospheric scientists may face in career advancement.

Membership surveys of the American Meteorological Society (AMS) indicate that women remain a minority in the atmospheric science community (LeMone and Waukau 1982; Hartten and LeMone 2010; MacPhee and Canetto 2015). The greatest gender disparity occurs in senior positions, with the percentage of women in tenure-track faculty positions in atmospheric science departments decreasing significantly with

rank, from 30% of assistant professors to 12% of full professors (MacPhee and Canetto 2015). The shortage of senior female faculty and the lack of retention along the career trajectory is not unique to the atmospheric sciences and is observed in many science, technology, engineering, and mathematics (STEM) fields. A report by the National Research Council (2006) found that the number of women in science and engineering decreases at every educational transition, and the consequences of inaction will be detrimental to the nation's competitiveness. Within the geosciences, the atmospheric science and meteorological community has the lowest percentage of female faculty at doctorate-granting institutions (Holmes and O'Connell 2008). The observed gender disparity in STEM fields is not fully understood but has been attributed to gender bias, harassment, marginalization and isolation, attitudes about career choice, work-life balance challenges, and lack of role models (National Research Council 2006).

To increase the representation of women in STEM and specifically the atmospheric sciences, the community needs to achieve an array of challenging goals, including improving work climates, removing gender biases, increasing role models, and offering more mentoring to women. Mentoring is a mechanism that can potentially overcome some of the gender disparity

AFFILIATIONS: ADAMS—University of North Carolina at Charlotte, Charlotte, North Carolina; STEINER—Department of Atmospheric, Oceanic and Space Sciences, University of Michigan, Ann Arbor, Michigan; WIEDINMYER—National Center for Atmospheric Research,* Boulder, Colorado

* The National Center for Atmospheric Research is sponsored by the National Science Foundation

CORRESPONDING AUTHOR: Allison L. Steiner, Department of Atmospheric, Oceanic and Space Sciences, University of Michigan, 2455 Hayward St., Ann Arbor, MI 48109-2143
E-mail: alsteiner@umich.edu

The abstract for this article can be found in this issue, following the table of contents.

DOI:10.1175/BAMS-D-15-00040.1

In final form 6 May 2015
©2016 American Meteorological Society

in STEM and may serve to increase the number of women at higher ranks. Here we define a mentor as one who actively engages with mentees to provide guidance and support for their professional development. We distinguish this from a role model, whose career serves as an example or blueprint that others wish to emulate in their own careers. While a number of role models and mentors may have some overlap in responsibility, they each serve unique functions.

The paucity of women in senior positions leads to a shortage of female mentors and role models, which may influence the retention of women in the STEM fields. One of the roles of a mentor is to help the mentee fit into the institution, and being the “only one” can be viewed as not fitting the norm. Thus, senior minorities in a department are often perceived as unable to help potential mentees even when the potential mentee is also a minority (Chesler and Chesler 2002). Holmes et al. (2008) suggest women need to compose 15%–30% of a department or organization before they start having institutional effects, thus implying that adding a few representatives will not be sufficient. Avallone et al. (2013) point out that in atmospheric science, all but one department at U.S. schools and universities have less than 25% women faculty, and the majority have below 15%. As of 2009, 53% of atmospheric science departments had two or fewer female tenure-track or tenured faculty (MacPhee and Canetto 2015). In departments lacking female faculty, female students have a harder time believing that their presence in the major is “normal” (Seymour and Hewitt 1997). MacPhee and Canetto (2015) found a higher percentage of female graduate students in atmospheric science departments that had a higher percentage of female faculty, yet this correlation was not statistically significant. While cross-gender mentoring is an important component of mentoring and can be very successful, Kram (1985) points out that these relationships are more complex because of the potential for the adoption of stereotypical gender roles.

Formal discussions within the atmospheric science community about the representation of women have occurred for decades. The creation of the AMS Committee on the Status of Women and the AMS Committee on the Status of Minorities in 1974 grew into the formation of the AMS Board on Women and Minorities in 1975. AMS currently hosts an annual women’s luncheon at the AMS annual meeting. Within the atmospheric science community, mentoring has been established in several programs, including the Significant Opportunities in Atmospheric Research and Science (SOARS) program, the AMS Enterprise Commission mentoring program, and

Atmospheric Science Collaborations and Enriching Networks (ASCENT). While SOARS is focused on all underrepresented groups [women; racial minorities; lesbian, gay, bisexual, transgender, and queer (LGBTQ) community; among others] at the undergraduate to graduate level and the AMS Private Sector Mentorship Program is industry focused, these programs show the growing momentum within the atmospheric science community to include mentoring as a component of career development. Despite these efforts, resources for women navigating their careers in the atmospheric sciences remain limited.

A grassroots organization, the Earth Science Women’s Network (ESWN), has contributed to the mentoring of women in the atmospheric sciences over the past decade. The ESWN, established in 2002 by six early career atmospheric chemists, has increased to an international membership of over 2000 women in the Earth sciences spanning a geographical extent of more than 50 countries. In 2014, ESWN was formally established as a nonprofit organization. While atmospheric scientists are the largest group in the ESWN membership, women from many disciplines in the Earth sciences are members (Fig. 1). The mission of the ESWN is to promote career development, build community, provide opportunities for informal mentoring and support, and facilitate professional collaborations. ESWN has traditionally focused on providing support for early career women scientists; however, the membership includes women at all career stages. Results from a 2013 membership survey showed that respondents comprise 31% graduate students, 19% postdoctoral researchers, 25% in higher education instructional positions (defined as postsecondary education), and 17% in research positions. Respondents under the age of 40 totaled 85%. At the time of this survey (2013), 45% of respondents reported that the most important type of professional growth needed to advance their careers was to build more extensive networks with others in their field, which is the primary goal of ESWN.

ESWN’s growth is in large part due to its activities, which are guided by a self-defined mentoring philosophy that has developed over the past decade. The following section of this paper will provide background on different types of mentoring and the obstacles that women can face under different mentoring strategies. A description of the ESWN’s mentoring philosophy and its techniques for addressing the challenges women face in traditional mentoring structures is presented, followed by specific examples of how ESWN’s mentoring philosophy is executed and how those activities relate to member gains reported

ESWN Membership by Discipline

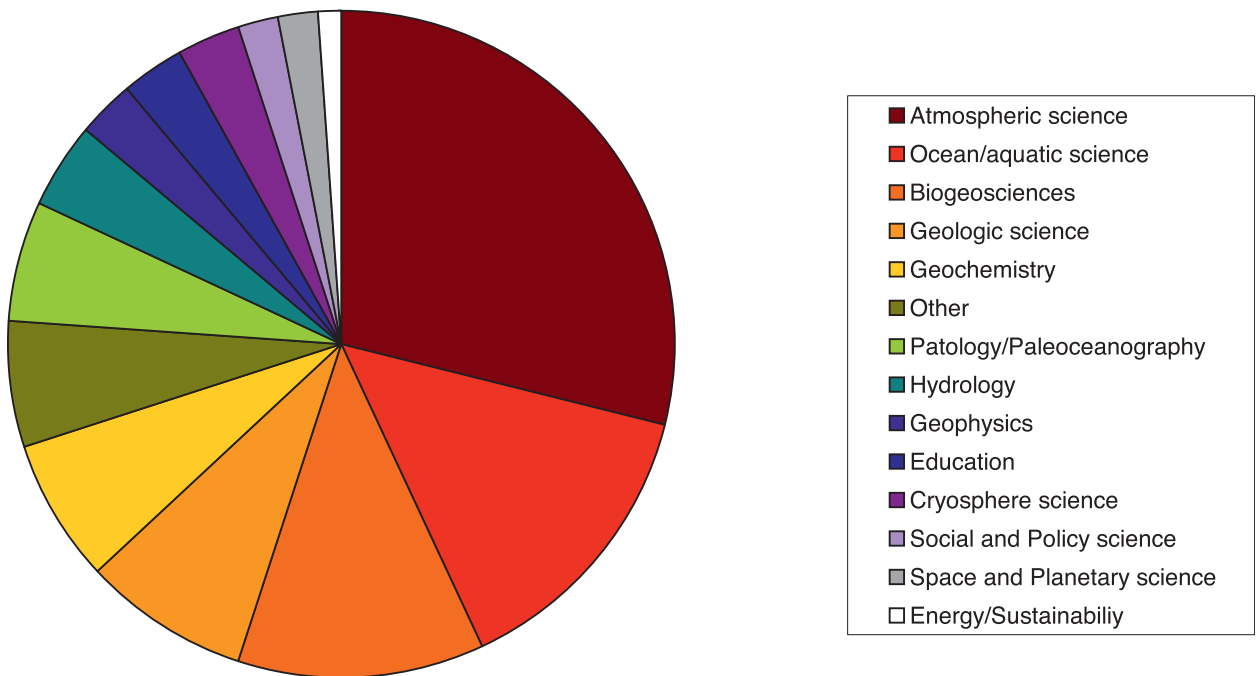


FIG. 1. ESWN membership by discipline, adapted from Archie and Laursen (2013b) based on 2013 member survey.

in a survey of the ESWN. The final section of this paper offers suggestions for the broader atmospheric science community to meet the mentoring needs of women based on the lessons learned from the ESWN.

UNDERSTANDING TYPES OF MENTORING. Mentoring seeks to provide the protégé, or mentee, with career development and psychosocial development (Ragins and Cotton 1999), both of which are important for building a successful career. Mentors can provide a mentee with coaching, professional exposure, protection, and sponsorship (Kram 1985). Additionally, the interpersonal nature of mentoring relationships provides mentees with psychosocial development, which helps mentees develop the personal skills necessary to navigate the social interactions in their careers and increases their sense of competence, self-efficacy, and personal development (Ragins and Cotton 1999).

Mentoring has tangible and intangible benefits for both mentors and mentees, even though the mentoring process is often focused on the needs of the mentee. Mentoring has been linked to positive metrics for mentees, such as increased promotions (Scandura 1992), higher incomes (Chao et al. 1992; Dreher and Ash 1990), and more mobility (Scandura 1992). Intangible benefits to mentees include increased

self-confidence (Eby et al. 2007) and greater career satisfaction (Fagenson 1989). Mentors often report benefits, such as psychological gratification and gaining a sense of guiding the next generation through mentoring (Levinson et al. 1978; Ragins and Scandura 1994). Hansford et al. (2004) found that the most commonly reported outcomes from educational mentoring studies by mentees were related to support, empathy, encouragement, counseling, and friendship. The positive consequences of mentoring, especially promotion and higher income, align with results needed to help women in STEM attain high-level positions and begin to close the wage gap between genders. Additionally, if more women were engaged in positive mentoring relationships, then greater career satisfaction, combined with support, empathy, and encouragement, may help more women remain in the science “pipeline.”

Mentoring can take on many different forms: formal mentoring (set program with defined roles), informal mentoring (mutually selected relationship outside of a formal program), one-on-one mentoring, multiple mentoring (single mentee benefits from multiple mentors), peer mentoring (individuals at the same career stage mentor each other), or collective mentoring [mentor(s) accepts responsibility to mentor a collection of mentees together]. Mentoring

commonly includes one-on-one informal relationships and relies on a mutual self-selection of the mentor and mentee to enter into a mentoring relationship. With that self-selection comes a level of trust that is necessary for the relationship to provide gains. For the mentors, this is often based on a view of their mentees as younger versions of themselves (Ragins and Cotton 1999), which can pose a challenge for young women in a male-dominated field. The issue of gender is further complicated for women because mentees will often look for mentors that have faced similar challenges, and the lack of women in senior positions makes it more difficult for junior women to find and identify mentors with the relevant experience (Holmes and O'Connell 2003).

Many institutions have implemented formal mentoring programs as one strategy to complement informal mentoring and provide equal mentoring opportunities. While formal mentoring programs offer many benefits (Murray and Owen 1991), they may create additional challenges. For example, formal relationships often have a shorter time frame (e.g., one to several years), while informal mentoring relationships may span the mentee's career (Ragins and Cotton 1999). As a result, informal relationships can bridge career transitions, whereas formal relationships are often tied to an institution and thus do not help the mentees as their careers progress. Formal mentors may view their mentees as at-risk performers who need the mentoring because they underperform, which is in stark contrast to development in informal mentoring relationships based on the mentee's potential (Ragins 1997). This perception may occur because of the opt-in nature of many formal mentoring programs, which may self-select from underrepresented groups who may lack informal mentoring opportunities. Finally, formal mentors may not participate in mentoring activities, such as sponsorship, for fear that it may be construed as favoritism (Ragins and Cotton 1999). Hansford et al. (2004) pointed out the most common problems reported by formal mentees include 1) lack of mentor time; 2) professional expertise or personality mismatch; and 3) mentors being critical, out of touch, defensive, and/or untrusting. The professional expertise/personality mismatch is more common in formal mentoring relationships than informal because the pairs are often assigned rather than self-selected. Mentors' lack of time can also be more problematic in formal mentoring relationships, as the mentors can be entering the relationships out of obligation rather than a sense of mutual benefits. Additionally, many formal mentoring programs target a specific career stage (i.e., graduate student, postdoctoral researcher,

new faculty), but those mentoring programs can then fail to help mentees transition career stages in the way informal mentoring does.

In light of the challenges of the formal mentoring model, new mentoring models have been developed to provide career support to women and underrepresented minorities. Chesler and Chesler (2002) cite new techniques, such as 1) multiple mentoring, 2) peer mentoring, and 3) collective mentoring. Multiple mentoring is an approach where mentees contact several different mentors for specific aspects of their careers. In this approach, individual mentors take responsibility for a specific component of mentoring and thus may have no knowledge of any other mentors working with the same mentee. Peer mentoring relies on the mentees to receive and simultaneously provide career support and advice to their peers. In this method, there may be no distinction in professional level or field, and the focus may be on overcoming psychosocial issues. A benefit of peer mentoring is that it allows women to reject outdated ideas of what a successful culture of science entails (Ginorio 1996). Collective mentoring is institutional in nature, with a collective group of mentors accepting responsibility to mentor a mentee or group of mentees. This type of mentoring does not rely on the one-on-one relationship but still utilizes formal relationships. For example, an academic department may mentor an incoming class of graduate students as a whole, where multiple faculty members work together to mentor students and take collective responsibility for the mentoring. Within the atmospheric science community, several of these mentoring models have started to appear. For example, SOARS utilizes multiple mentoring, where the protégés in the SOARS program are assigned a writing mentor, a science mentor, and a community mentor. The SOARS program also enables informal peer mentoring between the program participants.

To address mentoring gaps for women in the Earth sciences, the ESWN has taken aspects of peer mentoring, multiple mentoring, and collective mentoring to create a network that aims to address some of the mentoring gaps for women in the Earth sciences. Here we call this multipronged approach "community-driven mentoring." Research indicates that that early inclusion into a peer network provides a jump start to a scientific career (Etzkowitz et al. 1994; Ginorio 1996). Cain and Leahey (2014) found that women had higher levels of career success and greater career retention as a result of informal relationships with colleagues. The flexibility and informality of network-based mentoring allows for women to engage in the mentoring in a way that best fits with their personal

needs at varying career and life stages (Sorcinelli and Yun 2007; Rockquemore 2013). In the following section, we describe this approach in greater detail.

MENTORING PHILOSOPHY OF THE ESWN. Over the past decade, the ESWN has initiated, promoted, and organized various activities to provide members with a multipronged approach to mentoring. As a result of these activities, we have developed a mentoring philosophy based on the following five principles:

- 1) Support community-driven mentoring
- 2) Encourage diverse mentoring approaches for diverse individuals
- 3) Facilitate mentoring across career phases
- 4) Promote combined personal and professional mentoring
- 5) Champion effective mentoring in a safe space

Here, these five principles are described, followed with specific examples of implementation.

Support community-driven mentoring. The ESWN organization has adopted a grassroots, member-driven approach that evolves to respond to the ESWN community needs. Specifically, the ESWN has taken a nontraditional method to mentoring by intentionally *not* providing structured mentoring partnerships or groups. Instead, the ESWN enables informal interactions among members to develop a broader, meaningful professional network for each individual. The mentoring within ESWN includes peer-to-peer mentoring for women at all levels of careers and positions, hence using portions of the peer mentoring approach. An online network provides access to advice, feedback, and career-relevant information from any member, regardless of career level, who would like to contribute to the online conversation. This follows the “multiple mentor” system and allows women to tap into a range of advice from peers. Finally, collective mentoring occurs through small, informal groups that discuss specific topics and issues. In the collective mentoring that occurs online, interactions between members range from passive (e.g., observing conversations of others) to active, including the development of more robust personal and professional relationships. Overall, this community-driven approach overcomes several issues with formal mentoring programs, as it allows members of the community to respond to questions and concerns from other network members on their own time, thereby eliminating problems with finding time from mentors as well as scheduling in-person

meetings. Further, this technique works to eliminate professional and personal mismatches between mentors and mentees, as the large community provides a range of professional and personality types.

Encourage diverse mentoring approaches for diverse individuals. ESWN offers different mechanisms to develop potential mentoring relationships. Our primary approach is an online forum, previously in the form of an e-mail listserv (2005–13) and more recently in a social networking platform (<http://eswnonline.org>) launched in February 2013. The online network provides a place for women to post questions, concerns, solicitations for advice, and successes to all members. There are several advantages to this approach. Women who feel isolated at their institutions have a virtual support group they can turn to for advice. Further, women who respond best to passive mentoring can read advice and use the network to inform their own career decisions. While passive mentoring is difficult to quantify, it can be very powerful, as it identifies women’s unique career challenges and develops solution strategies in a safe, nonconfrontational setting. By allowing our members to self-select their participations in online discussions, they can choose the level of contact that best works for them.

Another mechanism of the ESWN to enhance mentoring within its membership is in-person meetings. To date, this includes receptions at professional society meetings, informal meetings at smaller conferences and workshops, regular get-togethers in cities with large ESWN membership, small on-site writing groups, workshops at academic institutions and professional meetings, and multiday professional development workshops funded by the National Science Foundation (NSF). These in-person meetings are essential for building relationships for those in specific geographical regions or in small subdisciplines. Face-to-face connections also enable members to solidify the relationships they establish online. Receptions, such as the one hosted at the annual fall meeting of the American Geophysical Union, allow our members to network with a large number of women and provide an opportunity to be the gender majority in the room. Additionally, ESWN members have hosted discussion forums at the American Meteorological Society’s women’s luncheon to raise awareness of ESWN in the AMS community and discuss relevant issues.

By allowing members to opt in for the resources and support that they need, either online or in person, ESWN offers an alternative to more rigid, formal mentoring structures. Further, it allows members of the community to develop resources for peers.

Facilitate mentoring across career phases. ESWN recognizes that a mentor's effectiveness is not necessarily based on career rank but rather life experience. Knowing that women at all career stages have valuable insight into various issues, our approach to mentoring allows all members to have an equal voice. One of the unique aspects of our membership is that the ESWN attracts members who self-identify as "nontraditional" for the Earth sciences; this may be due to members' age relative to their career stage, sexual orientation, or chosen career and life paths. As a result, our online discussions are open to a wide range of voices, which leads to diverse feedback and a greater likelihood of mentoring effectiveness. Our open philosophy empowers our members by helping them realize that their voices and experiences offer value to other women, regardless of where they are in their career. This also enables members to act in the capacity of a mentor for some occasions and a mentee for others. Additionally, mentoring across career phases and Earth science disciplines builds members' professional networks by opening up opportunities for new collaborations, research ideas, and experiences.

Promote combined personal and professional mentoring. The ESWN recognizes that career mentoring of women in the Earth sciences should not be separate from mentoring on personal issues (e.g., work-life balance). Women in the Earth sciences face all of the typical problems of women in academia, such as the juxtaposition of graduate school and the tenure clock with the biological clock. Family and career balance is viewed as the major career challenge by female graduate students in the atmospheric sciences (Canetto et al. 2012). Further, the importance of fieldwork in the Earth sciences adds complexity to this balance. For women with high demands at home, it is particularly challenging to spend weeks or months in remote locations collecting data that are crucial for their career success. The ESWN recognizes that career advice alone is not sufficient, and that this should be accompanied by advice and support for the balance between personal life and work, which is done continuously through the online and in-person resources that ESWN provides. While some formal mentoring relationships may be able to provide this balance, it is contingent upon the availability of mentors who have had similar work-life balance challenges.

Champion effective mentoring in a safe space. Surveys of the ESWN membership suggest that members find the ESWN forums to be safe places to discuss challenges and successes of their careers without

judgment or repercussions. To date, the membership of ESWN has grown almost exclusively by word of mouth. The personal connection that occurs when joining ESWN creates a safe space for career and personal discussions. By refraining from formal, structured roles of mentor and mentee, the feeling of equality and of every member being valued is emphasized. The undefined power differential helps our members to feel that the environment is secure, reliable, and protected.

EXECUTION OF THE MENTORING PHILOSOPHY. Here, three examples of the execution of the ESWN mentoring philosophy are discussed and results from membership surveys are presented. Several surveys of the ESWN and affiliates have been conducted over the past several years, including 1) the full membership in 2010 and 2013 (Kogan and Laursen 2010; Archie and Laursen 2013b); 2) ESWN workshop attendees before and after 2-day workshops (Archie and Laursen 2013a; Archie et al. 2012; Kogan and Laursen 2011a); and 3) the ES_JOBS e-mail list in 2010, which also included ESWN members, men, and non-ESWN-member women (Kogan and Laursen 2011b; Archie and Laursen 2013b). The surveys requested information about the level of participation in the ESWN as well as gains on a variety of career-development-related skills. Results from these surveys provide insight into the contribution of the ESWN to the professional development of women in the Earth sciences.

Online forum discussions. The online network is at the core of the ESWN membership and addresses all aspects of the ESWN mentoring philosophy. It is built on a community model that includes women across career phases and diverse backgrounds, addresses both personal and professional issues, and provides a safe space for women to discuss their discipline-specific concerns and share career resources. The ESWN originally began as an online discussion in 2005 through a listserv hosted by the National Center for Atmospheric Research (NCAR). In 2013, with support from the National Science Foundation's Increasing the Participation and Advancement of Women in Academic Science and Engineering Careers (ADVANCE) program and the American Geophysical Union, the ESWN migrated to a new, online social networking platform built to enhance online interactions and discussions. With the new platform, members can develop and manage individual profiles, create and join subgroups that are professional and/or personal in nature, and follow

discussions among the ESWN membership. Overall, the high level of trust among the group and presence of a “safe” space remains important to our members. Archie and Laursen (2013b) found the online forum to be an important component of member involvement and member-reported career gains.

Most importantly, the online forum allows members to receive informal mentoring on an array of professional and personal questions. Between September 2009 and December 2012, the most active threads each month on the ESWN e-mail list have included general career topics (30% of months), female-specific topics (33% of months), and maternity and child care topics (15% of months; Archie and Laursen 2013b), highlighting the fact that women seek and require mentoring on both professional and personal matters. General career topics include funding opportunities, job opportunities, and other career resources (e.g., books, webpages, discussion articles). Archie and Laursen (2013b) defined female-specific topics as those that refer to career topics specific to women, such as gender discrimination, underrepresentation of women, sexual harassment, and name changes as a result of marriage. While gender certainly plays a role in the discussion, a large fraction of the active threads categorized were focused on nongender-specific issues.

This analysis of top threads from online discussion shows that members are using the ESWN for both gender-specific topics and general career advice. We infer that the prevalence of nongender specific topics suggests that the ESWN’s community-driven mentoring provides an alternative mechanism for women to engage in mentoring and receive career advice that supplements current mentoring or compensates for a lack of formal mentoring. Many women in atmospheric science feel isolated across career phases (Avallone et al. 2013), and the online discussion forums may circumvent the perception of isolation and provide the psychosocial skills that were previously shared in other mentoring forms. In fact, Archie and Laursen (2013b) found that the largest gain reported by ESWN members in both 2010 and 2013 surveys is the “recognition that you are not alone,” and these respondents ranked the online network as the most helpful activity in making these and other gains. While members reported gains through a variety of involvement in the ESWN, members who participated more online and attended in-person events reported higher gains. Results of the 2013 member survey reported that the sense of community provided by the ESWN was appreciated across career stages, which suggests that our mentoring philosophy and framework can support women across career transitions.

In-person networking events at national meetings and workshops. In addition to the online activities, the ESWN has supported in-person networking events that reinforce online mentoring and bring new members to the ESWN. An in-person networking event at the fall American Geophysical Union (AGU) meeting has occurred over the history of the organization, first in 2003 and has continued with support from NCAR, the journal *Environmental Research Letters*, the U.S. NSF, the Association for Women Geoscientists (AWG), and AGU. This annual event allows long-term members to reconnect as well as bring first-time AGU attendees into the peer network. At other professional workshops and meetings, member-led get-togethers develop discipline-specific connections and peer support. At AMS meetings, ESWN in-person opportunities have occurred at the annual meeting, at smaller discipline-specific conferences, and at a promotional booth at the AMS Graduate and Career Fair.

As noted above, ESWN membership evaluation surveys showed that members who had attended in-person ESWN events showed higher gains from the network than members who only participated online (Archie and Laursen 2013b). This suggests that personal relationships and connections are strengthened by face-to-face contact and can lead to more worthwhile and meaningful experiences for members. Additionally, members who participated in any sort of in-person activity reported a better sense of community within the ESWN than members who only interacted online.

Professional development workshops. Through funding from the National Oceanic and Atmospheric Administration (NOAA), the NSF ADVANCE program and the NSF Geosciences Directorate, and the University of Bergen (Norway), the ESWN has developed a series of professional development workshops that identify and develop specific skills necessary for career success. While the workshop topics are not gender specific, the ESWN aims to provide a series of specific resources to its members that they may otherwise not receive as part of their academic training. These annual events have targeted different skills for a variety of career levels (see Table 1). For example, at the 2013 management skills workshop, content was developed for all attendees and included breakout sessions with specific discussions by career level (e.g., graduate students, research scientists, and professors). The ESWN has also focused on including women from outside traditional academic careers and ensuring workshops are applicable to all women Earth scientists.

TABLE 1. List of professional development training developed by ESWN. Intensive workshops are focused 1- to 2½-day meetings and have traditionally been held for women only. Workshops at professional meetings are short (1–3 h) workshops held for attendees at the AGU and the Association of Polar Early Career Scientists (APECS) and have been open to all genders and career stages.

Workshop title	Year	Sponsorship
Intensive workshops		
Building Leadership Skills for Success in Scientific Organizations	2008	NOAA
Developing Your Research Identity	2011	NSF
Skills for Networking and Communication	2012	NSF
Building Leadership and Management Skills for Success	2013	NSF
Writing an Op-Ed	2013	University of Bergen
Workshops at professional meetings		
Navigating the National Science Foundation	2009–14	NSF/AGU
Publishing Tips	2010	NSF/AGU
Getting Out in the Field	2013	NSF/AGU/ APECS
Success on the Tenure Track	2012–14	NSF/AGU
Careers beyond Academia	2014	AGU

Surveys of workshop participants confirm that the workshops are a positive experience. Participants reported gains in areas specific to each workshop topic (Archie and Laursen 2013a; Archie et al. 2012; Kogan and Laursen 2011a). Additionally, participants also reported gains in more general areas, including reductions of feelings of isolation, development of new career knowledge, and acquisition of new resources that will support their careers (Archie and Laursen 2013b). Some postworkshop gains are similar to benefits that result from traditional one-on-one mentoring relationships, such as preparedness to navigate a path to their career goals and psychosocial improvements, such as confidence in professional identity and confidence in building professional relationships. This suggests that despite their short duration, these focused workshops can provide members an alternative mechanism to gain the skills normally obtained through traditional mentoring.

FINAL THOUGHTS AND SUGGESTIONS FOR THE BROADER COMMUNITY. As ESWN continues to grow in its second decade, its history, accomplishments, and member base suggest that it is making a positive contribution to mentoring women in the atmospheric and Earth sciences. The ESWN provides a unique way to supplement existing mentoring programs and relationships. There are several lessons that can be learned from

our framework and mentoring philosophy, including the following:

- Connecting women can reduce feelings of isolation.
- Capitalizing on social networking technology allows women to opt in to mentoring on their own terms.
- Creating a safe space provides opportunities to discuss issues of importance and relevance to women.
- Participation, either online or in person, is key toward seeing the benefits of the network.

Many aspects of the ESWN can be carried over to individual academic departments and governmental institutions. Based on the ESWN experience, recommendations to other organizations include the following:

- Encourage women and minorities to seek out multiple avenues of mentoring early in their careers and at new career stages. Immediate encouragement to find mentoring resources will avoid giving the impression that mentoring is being suggested because the individual is perceived as failing to succeed.
- Recognize and acknowledge that some issues may be gender specific, and encourage peer mentoring when possible.
- Recognize that the perception of viable role models and mentors for women and other minorities can differ.

- A diverse group of mentors can be valuable, and both men and women have a critical role to play in mentoring the next generation of atmospheric scientists.
- Provide links to resources, connections to other women, and exposure to potential role models/mentors across campus or the organization.
- Recognize that individuals can mentor on certain aspects of their careers without having to take responsibility for mentoring *all* aspects of their careers.

Overall, these strategies can improve the climate for women in the atmospheric and Earth sciences and work to change the face of the atmospheric science workforce.

ACKNOWLEDGMENTS. ESWN was supported by the National Oceanic and Atmospheric Administration and the National Science Foundation under Grants HRD 0929782, 0929839, 0929509, 0930118, and 0929828. The authors wish to thank Peggy LeMone, Gannet Hallar, and Sue Weiler for their helpful reviews on this manuscript. Additionally, we thank our evaluators, Tim Archie, Marina Kogan, and Sandra Laursen of Ethnography and Evaluation Research, University of Colorado Boulder, who conducted, analyzed, and provided survey results and essential comments on this manuscript.

REFERENCES

Archie, T., and S. Laursen, 2013a: Evaluation report: 2013 career development workshop from the Earth Science Women's Network "Building Leadership and Management Skills for Success." Ethnography and Evaluation Research, University of Colorado Boulder, 19 pp. [Available online at www.colorado.edu/eer/research/documents/ESWN_2013_workshop_report_final.pdf.]

—, and —, 2013b: Summative report on the Earth Science Women's Network (ESWN) NSF ADVANCE PAID Collaborative Award (2009-2013). Ethnography and Evaluation Research, University of Colorado Boulder, 149 pp. [Available online at www.colorado.edu/eer/research/documents/ESWNfinalReportALL_2013.pdf.]

—, M. Kogan, and S. Laursen, 2012: Evaluation report: 2012 career development workshop from the Earth Science Women's Network "Skills for Networking and Communication." Ethnography and Evaluation Research, University of Colorado Boulder, 20 pp. [Available online at www.colorado.edu/eer/research/documents/ESWN_2012_workshop_report_0712_final.pdf.]

Avallone, L. M., A. G. Hallar, H. Thiry, and L. M. Edwards, 2013: Supporting the retention and advancement of women in the atmospheric sciences: What women are saying. *Bull. Amer. Meteor. Soc.*, **94**, 1313–1316, doi:10.1175/BAMS-D-12-00078.1.

Cain, C. L., and E. Leahey, 2014: Cultural correlates of gender integration in science. *Gender Work Organ.*, **21**, 516–530, doi:10.1111/gwao.12052.

Canetto, S. S., C. D. Trott, J. J. Thomas, and C. A. Wynstra, 2012: Making sense of the atmospheric science gender gap: Do female and male graduate students have different career motives, goals and challenges? *J. Geosci. Educ.*, **60**, 408–416, doi:10.5408/12-296.1.

Chao, G. T., P. M. Waltz, and P. D. Gardner, 1992: Formal and informal mentorships: A comparison on mentoring functions and contrast with non-mentored counterparts. *Pers. Psychol.*, **45**, 619–636, doi:10.1111/j.1744-6570.1992.tb00863.x.

Chesler N. C., and M. A. Chesler, 2002: Gender-informed mentoring strategies for women engineering scholars: On establishing a caring community. *J. Eng. Educ.*, **91**, 49–55, doi:10.1002/j.2168-9830.2002.tb00672.x.

Dreher, G. F., and R. A. Ash, 1990: A comparative study of mentoring among men and women in managerial, professional, and technical positions. *J. Appl. Psychol.*, **75**, 538–546.

Eby, L. T., J. E. Rhodes, and T. D. Allen, 2007: Definition and evolution of mentoring. *The Blackwell Handbook of Mentoring: A Multiple Perspectives Approach*, T. D. Allen and L. T. Eby, Eds., Blackwell, 7–20.

Etzkowitz, H., C. Kemelgor, M. Neuschatz, B. Uzzi, and J. Alonzo, 1994: The paradox of critical mass for women in science. *Science*, **266**, 51–54, doi:10.1126/science.7939644.

Fagenson, E. A., 1989: The mentor advantage: Perceived career/job experiences of proteges versus non-proteges. *J. Organ. Behav.*, **10**, 309–320, doi:10.1002/job.4030100403.

Genorio, A., 1996: A culture of meaningful community. *Bridging the Gender Gap in Engineering and Science: The Challenge of Institutional Transformation*, Carnegie Mellon University, 28–32.

Hall, R., and B. Sandler, 1983: Academic mentoring for women students and faculty: A new look at the old ways to get ahead. Project on the Status and Education of Women, Association of American Colleges, 16 pp.

Hansford, B. C., L. C. Ehrich, and L. Tennent, 2004: Formal mentoring programs in education and other professions: A review of the literature. *Educ. Adm. Quart.*, **40**, 518–540, doi:10.1177/0013161X04267118.

Hartten, L. M., and M. A. LeMone, 2010: The evolution and current state of the atmospheric sciences

- “pipeline.” *Bull. Amer. Meteor. Soc.*, **91**, 942–956, doi:10.1175/2010BAMS2537.1.
- Holmes, M. A., and S. O’Connell, 2003: Where are the women geoscience professors?: Report on the workshop Where are the Women Geoscience Professors? National Science Foundation, 41 pp.
- , —, 2008. Gender parity in the geosciences: Data and geoscientists’ perceptions. *Nat. Geosci.*, **1**, 79–82, doi:10.1038/ngeo113.
- , —, C. Frey, and L. Ongley, 2008: Gender imbalance in US geoscience academia. *Nat. Geosci.*, **1**, 79–82, doi:10.1038/ngeo113.
- Kogan, M., and S. L. Laursen, 2010: Evaluating career development resources: Lessons from the Earth Science Women’s Network (ESWN). *2010 Fall Meeting*, San Francisco, CA, Amer. Geophys. Union, Abstract ED13A-0600.
- , and —, 2011a: Collaborative research: Facilitating career advancement for women in the geosciences through the Earth Science Women’s Network (ESWN); Evaluation report: 2011 professional development workshop. *Ethnography and Evaluation Research*, University of Colorado Boulder, 14 pp. [Available online at www.colorado.edu/eer/research/documents/ESWN_2011workshopReportFinal.pdf.]
- , and —, 2011b: Obstacles in advancement of young female geoscientists: Research results from the Earth Science Women’s Network (ESWN). *2011 Fall Meeting*, San Francisco, CA, Amer. Geophys. Union, Abstract ED23B-0617.
- Kram, K. E., 1985: Improving the mentoring process. *Train. Dev. J.*, **39**, 40–43.
- LeMone, M. A., and P. L. Waukau, 1982: Women in meteorology. *Bull. Amer. Meteor. Soc.*, **63**, 1266–1276, doi:10.1175/1520-0477(1982)063<1266:WIM>2.0.CO;2.
- Levinson, D. J., D. Darrow, M. Levinson, E. B. Klein, and B. McKee, 1978: *Seasons of a Man’s Life*. Academic Press, 384 pp.
- MacPhee, D., and S. S. Canetto, 2015: Women in academic atmospheric sciences. *Bull. Amer. Meteor. Soc.*, **96**, 59–67, doi:10.1175/BAMS-D-12-00215.1.
- Muller, C. B., 1997: The potential of industrial “E-mentoring” as a retention strategy for women in science and engineering. *Proceedings: Frontiers in Education 1997; 27th Annual Conference*, EP Innovations, Ed., Vol. 2, IEEE, 622–626.
- Murray, M., and M. A. Owen, 1991: *Beyond the Myth and Magic of Mentoring: How to Facilitate an Effective Mentoring Program*. Jossey Bass, 240 pp.
- National Research Council, 2006: *To Recruit and Advance: Women Students and Faculty in Science and Engineering*. National Academies Press, 148 pp.
- Ragins, B. R., 1997: Diversified mentoring relationships in organizations: A power perspective. *Acad. Manage. Rev.*, **22**, 482–521, doi:10.5465/AMR.1997.9707154067.
- , and T. A. Scandura, 1994: Gender differences in expected outcomes of mentoring relationships. *Acad. Manage. J.*, **37**, 957–971, doi:10.2307/256606.
- , and J. L. Cotton, 1999: Mentoring functions and outcomes: A comparison of men and women in formal and informal mentoring relationships. *J. Appl. Psychol.*, **84**, 529–550, doi:10.1037/0021-9010.84.4.529.
- Rockquemore, K. A., 2013: A new model of mentoring. *Inside Higher Ed*. [Available online at www.insidehighered.com/advice/2013/07/22/essay-calling-senior-faculty-embrace-new-style-mentoring.]
- Scandura, T. A., 1992: Mentorship and career mobility: An empirical investigation. *J. Organ. Behav.*, **13**, 169–174, doi:10.1002/job.4030130206.
- Seymour, E., and N. M. Hewitt, 1997: *Talking about Leaving: Why Undergraduates Leave the Sciences*. Westview Press, 429 pp.
- Sorcinelli, M. D., and J. Yun, 2007: From mentor to mentoring networks: Mentoring in the new academy. *Change*, **39**, 58–61, doi:10.3200/CHNG.39.6.58-C4.

LESSONS FROM FIRST-GENERATION CLIMATE SCIENCE INTEGRATORS

BY JULIE BRUGGER, ALISON MEADOW, AND ALEXANDRA HORANGIC

Climate science integrators use specific skill sets to further the development of usable climate science.

Decision-makers at scales ranging from agricultural producers making decisions for individual enterprises to public land managers concerned about massive tracts of publicly owned land are increasingly finding it necessary to address impacts created by both climate variability and climate change. To do this, they will need the best available climate science in a form they can readily use. To be usable, the science must be relevant to their context and the complex management challenges they face and credible and legitimate in their eyes (Cash et al. 2003). In recognition of this growing need, the federal government has recently created several networks of regionally based organizations that share an overarching goal of facilitating connections between scientists and decision-makers in order to promote

the development of usable science. These networks include the Department of the Interior (DOI) Climate Science Centers (CSCs) and Landscape Conservation Cooperatives (LCCs) and the U.S. Department of Agriculture (USDA) Climate Hubs. These new organizations follow the example provided by the USDA Cooperative Extension System (CES), state climatology offices, and the National Oceanic and Atmospheric Administration's (NOAA) Sea Grant and Regional Integrated and Sciences and Assessments (RISA) Programs, which have been involved in the effort to develop usable science for decades and, in the case of the CES, for over a hundred years.

Accompanying this growing demand is a growing literature that seeks to increase the supply of usable climate science by identifying guiding principles for its development (Dilling and Lemos 2011; McNie 2007), often through the process of coproduction of knowledge (Lemos and Morehouse 2005) or provision of decision support (NRC 2009). However, this literature does not address questions about how to increase the supply of climate scientists who want to participate in the process of developing usable science, what specific skills are needed to put these guidelines into practice, and how to provide scientists with these skills. In this article we address these questions by presenting insights from highly respected "first generation" climate science integrators from

AFFILIATIONS: BRUGGER, MEADOW, AND HORANGIC—The University of Arizona, Tucson, Arizona

CORRESPONDING AUTHOR: Julie Brugger, The University of Arizona, 2714 E. 8th St., Tucson, AZ 85716
E-mail: julieb3@email.arizona.edu

The abstract for this article can be found in this issue, following the table of contents.

DOI:10.1175/BAMS-D-14-00289.1

In final form 26 May 2015
©2016 American Meteorological Society

across the United States, who collectively have more than 200 years of experience bridging the gap between scientists and decision-makers. We use the term “climate science integrator,” following Jacobs et al. (2005), to refer to climate scientists who specialize in helping decision-makers across a broad spectrum of sectors to integrate the best available climate science into their decision-making processes. There may be similar techniques used in fields such as translational medicine, but what we feel sets climate science integration apart is the emphasis on coproduction. In the medical field, translational research has been defined as bringing the results of research to the public (Woolf 2008), which implies a unidirectional model rather than the bidirectional model of coproduction. Science integration work encompasses a range of activities, from responding to individual inquiries over the telephone to collaborating with stakeholders over an extended period of time. The cadre of scientists who participated in our research has largely developed their methods for working successfully with stakeholders on their own, without formal training. The collective wisdom of this group illuminates the kinds of skills needed in order to be a successful science integrator, suggests the types of training that would cultivate these skills, and indicates ways to change academic training and institutions to better encourage aspiring climate science integrators and to support this kind of work. Their insights both supplement and reinforce the literature on developing usable science.

In this literature, the foremost principle is that efforts to develop usable science require two-way flows of information between and among scientists and diverse decision-makers (Hirsch Hadorn et al. 2006; Jahn et al. 2012; Lemos et al. 2012), rather than the one-way flow of information—from science to society—assumed in the traditional, “linear,” or “loading dock” model of science (Cash et al. 2006; McNie 2007). Another key principle is that scientists from a variety of physical, natural, and social sciences, as well as decision-makers from different sectors, will have to work together to address the complex social and ecological issues related to climate variability and change (Jacobs et al. 2005; Lemos and Morehouse 2005). Third, in order for science to be usable by decision-makers, they must perceive it as salient—relevant to their context and needs, credible—scientifically sound and accurate, and legitimate—unbiased, produced in a transparent manner, and respectful of their beliefs and values (Cash et al. 2003). Scientists must acquire a firm grasp of the context for decision-making in order to produce science that has these

characteristics (Dilling and Lemos 2011; Jacobs et al. 2005; Kirchhoff et al. 2013; Lemos et al. 2012; McNie 2007). In addition, research shows that users’ perceptions of information are highly influenced by the quality of their interactions with information providers. Thus, a fourth principle is the need for relationships between scientists and decision-makers that are characterized by mutual understanding, respect, and trust (Cash et al. 2003; Dilling and Lemos 2011; Ferguson et al. 2014; Jacobs et al. 2005, 2010; Kirchhoff et al. 2013; Lemos and Morehouse 2005; Lemos et al. 2012; McNie 2007). Lemos and Morehouse (2005) suggest that the level of fit between the knowledge being produced and the information stakeholders believe they need is enhanced by relationships that are long term and iterative. The literature also notes that developing and maintaining these relationships is time and resource intensive and often not regarded as legitimate scientific activity (Dilling and Lemos 2011; Jacobs et al. 2010; Kirchhoff 2013; McNie 2007).

From this brief review of guiding principles for developing usable science, it becomes apparent that climate scientists who want to participate in the process of developing usable science need skills, in addition to their traditional disciplinary training, that facilitate communicating, interacting, and developing and sustaining relationships with scientists from other disciplines, practitioners, decision-makers, and technical experts. However, training in basic science approaches is still the norm for most scientists—education focuses on the methods, approaches, and tools necessary to succeed in a particular scientific field of inquiry, with little attention paid to how the knowledge might be used outside of academia (Shanley and López 2009). Stokes (1997) traces the split between basic and applied research as far back as the Greek natural philosophers, who consciously separated inquiry from use. When technological innovation outpaced basic science inquiry, basic research became the domain of universities, leaving industry to pursue usable technology. In the United States the split was codified after World War II by President Roosevelt’s science advisor, Vannevar Bush, who formalized the distinction between basic and applied research and separated their federal funding mechanisms (Stokes 1997). With the external boundaries in place, they are often reinforced from within scientific communities through a process Gieryn (1983) refers to as “boundary work,” in which scientists seek to separate themselves from society in order to protect the perception of their purity of purpose and action—they are not influenced by or seek to influence society. Universities remain the home of basic research, which is reflected

in their reward systems, such as the prioritization of peer-reviewed journal articles over work that is used by people outside of the research community (NRC 2004; Shanley and López 2009; Dilling and Lemos 2011). Given the need to encourage, support, and train the next generation of climate science integrators, the goal of this article is to contribute to ongoing efforts to develop guidance and training resources for scientists interested in working with stakeholders to develop usable science and to improve institutional support for this type of work.

METHODS. The results presented in this paper are from two separate research projects that both seek to understand how scientists work with stakeholders, their methods for doing so, and challenges they have faced doing this type of work. One project focused on understanding the challenges that novice climate science integrators face and how to overcome them. The other focused on how experienced climate science integrators evaluate their own work and their recommendations for developing evaluative metrics for the field of climate science integration and coproduction of climate science more broadly. While the interview guides were different, there was a significant amount of overlap. Together, the two research teams conducted 15 in-depth semistructured interviews with experienced climate science integrators (defined as at least five years of experience). Most of these researchers are, or were, in the NOAA RISA system, but the group also includes researchers in DOI CSCs, current or former state climatologists, and extension faculty. The sample is not intended to be representative of all science integrators; rather, participants were selected based on years of experience and positive reputation in the field. Interviews took place in 2014, either in person or over the telephone, and lasted approximately 60–90 minutes each. Interview questions were designed to elicit information about 1) the types of science integration activities in which interviewees engage, 2) their background and the career path that led them to their current position, 3) what they see as the challenges of doing science integration and how to address them, and 4) what advice they would give to aspiring science integrators. The interviews were transcribed and were analyzed using a mixed inductive/deductive grounded theory approach (Bernard and Ryan 2010; Strauss and Corbin 1998) to identify key themes and emerging trends both within and across datasets. In this article we also use preliminary results from interviews with four stakeholders who work with an early career climate science integrator to triangulate our results. Because the sample size

is small, we discuss the results qualitatively. We use quotes from the interviews to illustrate themes and to better convey interviewees' meanings. In what follows, quoted phrases and extended indented passages are excerpts from these interviews.

FINDINGS. *How do the scientists interact with decision-makers?* The scientists in this study described a wide spectrum of ways in which they interact with decision-makers, from answering individual telephone inquiries to working collaboratively with small, interdisciplinary groups over an extended period of time to develop information or decision support tools specific to decision-makers' needs. Several used the metaphor of "matchmaker" to describe the work they do. The job of a matchmaker is to understand what types of data are available; to understand the context, the needs, and the values of the stakeholder; and then to make a match between them. We found that the ways of interacting that the scientists described fit into a model developed by Ferguson et al. (2016) to conceptualize the ways in which stakeholders interact with the NOAA RISA for the Southwest. The four primary ways are 1) as an information broker communicating climate information, 2) as an informal consultant, 3) as a short-term partner, and 4) as a collaborator. Ferguson et al. found that most interactions were in the first category with percentages decreasing in each succeeding category. Our study participants also described a potential fifth category: as a liaison or networker, someone who makes connections among individuals or organizations with common needs and facilitates cooperation among them.

Some examples of information broker interactions from our interviews include providing information over the phone on a one-time basis or in newsletters, websites, podcasts, and conference presentations and giving public talks in which they are "translating and synthesizing, or value-adding to climate information." Interactions in the informal consultant category include providing expert advice on project development or data interpretation. For example: "It's not at all unusual to get calls from agency partners related to something: they want to do a new project, or where we are on a project, or what do you think about this. So basically I will get used as a subject matter expert." This category was the most frequently mentioned in our research. Examples of short-term partnerships include helping to organize and/or participating in workshops and webinars to address a specific weather-/climate-related issue. Interviewees also described being involved in long-term collaborations with stakeholders: for example,

working with tribes to develop a drought plan for a reservation or using climate projections to help city planners understand the city's vulnerabilities. Finally, the types of interactions that fall into the networker category include those of an investigator with one of the CSCs who was connecting with other agencies in the region that worked with stakeholders to learn about and provide for their climate science needs. For all of these types of interactions, the scientists felt that certain skills and attributes, described below, were key to successful engagement with individuals, groups, and organizations.

What motivates them to do this kind of work? Despite increasing emphasis on funding research that benefits society and contributes to the achievement of desired societal outcomes (e.g., NSF 2013), as well as the efforts of the boundary-spanning organizations mentioned at the beginning of this paper, the scientists in our study note that in academia incentives for engaging directly with stakeholders are still limited, even in applied research projects. Many of them perceive significant challenges for science integrators working in the academic system, which we discuss in greater detail below. They are motivated to do engaged work in spite of these challenges by personal incentives: a desire to do scientific work that is useful, helps someone, or helps society. Many interviewees expressed a sense of deep satisfaction in producing research that responded to a specific problem or issue and “had an impact.” Just publishing papers was not nearly motivation enough for them—they wanted to see their research “out there” in the world, potentially “having something to do with maybe a paradigm shift for management” and “making the world a better place.”

The scientists we interviewed were also motivated by the diversity of opportunities for different types of research that their work offered. They were intrigued by the type of creativity and ingenuity required to respond to a stakeholder's question or need, which differed from the problem-solving skills ordinarily applied in their discipline. Several noted that working with stakeholders allowed them to look at a problem in new ways, leading to novel insights. For example, some water managers working with a climate scientist to understand streamflow reconstructions from tree-ring data reported that the process opened their eyes to a range of variability, and a level of vulnerability, far greater than what the historical data they based their planning on revealed. Finally, one of the scientists we interviewed enthused that he had “a job that I look forward to coming to each day.” The personal satisfaction these scientists derive from doing

this type of work seems to far outweigh the lack of external incentives.

How did they learn their craft? The scientists we interviewed were trained in meteorology, atmospheric science, climatology, or another physical science. Some also had social science training in undergraduate or graduate school. However, when the majority of them began their careers, there was little informal or formal interdisciplinary training or training in science integration available. Most just “fell into” working with stakeholders while in graduate school or in an early job and discovered they liked it. They described their learning process as “learning by doing,” “trial and error,” or “sink or swim.” For example, “It really was just trial and error. Just going out with the information you had and, for me, really being as good a listener and watcher of people's expressions and body language.” One scientist compared learning how to provide climate services to learning a craft: “It's like any trade; you have to learn it by doing it. And you discover whether you have a facility for it along the way.”

Many of our interviewees mentioned that they had informal mentors, such as academic advisors, job supervisors, or coworkers who were doing applied climatology or translational science work and who encouraged and supported them or served as role models. One scientist recalled that “So much of what I learned I learned by quietly working behind the scenes under the guidance of an excellent mentor, the former State Climatologist, who let me learn slowly without throwing me in the deep end of the pool too early.” Although no one reported that their first introduction to science integration work came from the nascent literature on the subject, several people reported that finding the literature later in their careers elucidated and reaffirmed what they were doing.

Many also cited experiences in their personal backgrounds that they felt helped prepare them for doing science integration work: for example, growing up in a farming community prepared them to be able to communicate with growers; being a union steward or a lay congregation leader prepared them for organizing meetings, speaking to large groups, and developing programs; congressional fellowships prepared them for working with policymakers. Overall, their learning process was experiential and their suggestions for training the next generation of climate science integrators, which we discuss below, also focus on providing experiential learning opportunities.

What are the key lessons they have learned about working with decision-makers? Many of the interviewees felt that being a good science integrator was not something that everyone could learn, that it takes a certain kind of personality, or that some people just have a “knack” for it. For example,

Partly we’re talking about personality. And I don’t know if it’s fair to say that there’s something genetic, you know, it’s that old saying, “You either have it or you don’t.” [Laughs] And to me it’s a really good question, is that really the case, or can a person really change something so that they do have it?...I do not know if you can be trained for this. I know a lot of people that there’s just no way they could do this and some will openly admit it, they’re not comfortable going out and talking to people.

However, when asked about the most important things they have learned about doing science integration work or about the advice they would give to aspiring science integrators, their responses revealed some specific personal characteristics and practices that they felt made them successful. Whether acquired by nature or nurture, the experienced integrators articulated specific guidance for the next generation. We discuss nine practices, beginning with the most commonly mentioned. Although we discuss them separately, they tend to be interrelated and to build on and reinforce one another.

BE A GOOD LISTENER. The most prominent characteristic that emerged is the need to be a good listener and to ask questions. According to one interviewee,

One of the things that I learned, or I guess just maybe picked up early on...just kind of to let them talk. They may call up asking for, you know, “I need this rainfall data from this place”...So I’d ask them, “What do you need this for? Can you describe the kind of project?” Because oftentimes there’d be other data that might be more appropriate for their study that they didn’t know existed...I learned to listen, to get them to tell their stories.

By responding initially in this way, the scientist initiates two-way communication and sets the tone of the relationship. He signals that it is one of mutual respect and understanding between peers who are experts in different fields and that he is “*genuinely* there to learn.” By engaging decision-makers in conversation, the scientist also begins to learn about the decision-making context. In addition, two

interviewees pointed out that “what [users initially] asked was usually not what they needed,” so that engaging them in conversation made it possible to identify their actual needs.

UNDERSTAND AND RESPECT THE PEOPLE YOU WORK WITH. Scientists in the study emphasized that it is also essential to understand decision-makers’ perspectives and what they value. This makes it possible to couch communications and to interact with them in ways sensitive to their perspectives and respectful of their values, which gives you “credibility” and makes you trustworthy in their eyes. This interviewee emphasizes the importance of sincerity in this endeavor:

When you are working with users, you gain a lot more traction with them if you are viewed as credible in their camp. And this takes some extra work on the part of the translators: you can’t just sit in your office and kind of come at it from one way; you’ve got to put yourself in other people’s minds. This is the whole issue of empathy. It’s the primary way you can work with people is by being empathetic, and by that I don’t mean painted on, but you actually really understand their situation.

The scientists also found that when stakeholders and scientists can make a personal connection, such as sharing a similar upbringing, hobby, or interest, it enhances this type of credibility. Our interviewees mentioned specific commonalities like being raised in a farming community or on a military base as good foundations for a relationship.

Using the same language as stakeholders and speaking conversationally rather than “coming across as an academic” or lecturing has a similar effect. One scientist related an experience he had after giving a talk to wildfire managers that illustrates this: “At the end of [the talk], one of them comes up to me and asks, ‘You have a Ph.D., right?’ And I go, ‘Yes.’ And she goes, ‘Well, that’s so odd. Because you were actually talking *to* us, not at us. So you’re using our language.’ And that’s the day that I knew what I was trying to do was working.”

UNDERSTAND THE DECISION-MAKING CONTEXT. Listening begins to set the tone of the relationship and to bring the decision-making context into focus, but for deeper understanding the scientist may undertake activities that resemble the participant observation of anthropological fieldwork: for example, shadowing a stakeholder, which one interviewee described as the “terribly fascinating job of driving around with

somebody, and doing their job. And then having discussions about weather and climate and those kinds of things, with them” at their workplace. Gaining experiential understanding of the context can shortcut a lengthy question-and-answer process in which the scientist may not yet have enough grasp of the context to ask the right questions. Another interviewee who is working with government agencies that manage wildfire went “through the training that firefighters go through so I could see how that worked. And then I embedded myself with as many managers as would put up with me so I could understand their decision-making process.” This made it possible to coproduce fire-climate, fire-weather, and operational products that have become essential to agency decision-making processes.

Coming to understand the decision-maker’s context is a prerequisite for the scientist to be able to develop science that is salient to that context, but the process also contributes to decision-makers’ trust in the scientist and their perceptions that the science is legitimate—two characteristics of usable science that Cash et al. (2003) identified. A thorough understanding of the context for decision-making also makes it possible for the scientist to recognize that science sometimes plays a very small role in the decision-making process because decision-makers have many other factors to consider, including policy, politics, economics, and resource availability. Even the best available, most actionable science does not guarantee its eventual use in decision-making, as several of our interviewees noted.

BE HUMBLE. A science integrator needs to have humility. Aspects of humility are illustrated by the preceding three characteristics: the humility to realize that she needs to listen rather than talk; to learn from stakeholders about their context, needs, and values; and to respect their perspectives and values, rather than to try to change them. This can be challenging for scientists who sincerely believe in the value of science, as this scientist explains:

I think with scientists...finding out that what they know how to do is not actually what people need has been a real challenge. I think for the climate science community as a whole we do...science that, it’s clearly important, but it doesn’t often fit as largely in people’s portfolios as we’d like it to. And so, you have to just sort of accept that. And you can’t cram into their worldview and sort of lever it open and make it bigger, even though maybe it should be. Maybe the risk is huge and maybe you do need to

worry about it, but you’ve got to sort of meet people where they’re at.

In addition, interviewees pointed out the need to have “the right amount of humility about how much we think we know about this stuff, and not coming off as too cocksure about anything,” the humility “not to be defensive when someone questions some aspect of your science,” and “being humble enough to know that you may not be able to give them anything.” Being humble, as well as the three preceding characteristics and practices, contribute to earning the trust of the decision-makers the scientist is working with.

MAINTAIN CREDIBILITY IN BOTH THE SCIENTIFIC AND STAKEHOLDER COMMUNITIES. Interviewees pointed out that the science integrator must maintain credibility in both the scientific and stakeholder communities, which one scientist described as a “tough trick,” which “if you take it seriously, puts a lot of onus on you to go the extra mile to try to be good in both arenas.” To maintain credibility in the scientific community, she needs to be well-grounded in a climate science-related discipline, as this interviewee emphasizes:

I always encourage people to at least get through their Masters, get a degree in a discipline, maybe some interdisciplinary work but make sure that you’re well-grounded in the discipline...So have something that gives you the credentials, it gives you the depth of knowledge in that field, and then try to weave in the interdisciplinary from there.

To maintain credibility in the scientific community, she also needs to remain unbiased, to “offer an independent opinion on things,” and not become an advocate for a particular stakeholder group or solution, or a “stoolie for some agency.”

We have already discussed how understanding and respecting the people you work with gives you credibility in the user community. To maintain credibility in that community, the science integrator needs to be seen as unbiased by that community as well. She should not try to “advocate any one thing,” because “people are always on the lookout for hidden agendas,” and she would lose the trust she has built up in the user community by coming across as “just another vested interest.” At the same time, she would reflect poorly on “the [scientific] enterprise by having the spokesman for it come out as being seen as having a hidden agenda.” When the climate scientist herself has credibility with the user community, its members are more likely to perceive the science as credible and legitimate (Lemos et al. 2012).

ENJOY INTERACTING WITH PEOPLE. In general, the scientists described themselves as people who enjoyed interacting with other people. However, they noted that one need not be an extrovert or gregarious to be successful at science integration work; in fact, several described themselves as introverts. But these scientists also found it “difficult and isolating [to work alone for] hours on end.” They welcomed the opportunity for interaction and they really enjoyed “the one-on-one stuff.”

BE CURIOUS/INTERESTED IN A VARIETY OF THINGS. Because learning about the context and understanding other people’s perspectives takes time and effort, it helps to be the type of person who likes to learn about new and different things. Many of the interviewees described themselves in this way. For example, one scientist described himself as a “generalist” and found it “rewarding...learning about another world.” When he worked with the National Aeronautics and Space Administration (NASA) on climate adaptation, he talked with “the people who work on the launches of the space shuttle” and “the people who work on making flushing the toilets work,” and “learned all these things about infrastructure that [he] never would have learned otherwise.”

BE PATIENT. The scientist needs to be patient because the processes of listening, learning, and developing trustful relationships takes time. The scientist needs to be patient with stakeholders as they learn more about his domain and with himself as he learns more about theirs. Here, an interviewee describes the patience it takes to make the “match” between what he knows and what stakeholders need:

For the most part when it is about information use and applications, it’s trying to find that little nugget of intersection between something that you know is out there or something that you can do and a need that they have, and sort of being very patient about finding that. And not overwhelming the person with a thousand different potential things they could do. But sort of trying to figure out where they’re at and then making that match.

REFLECT ON WHAT YOU ARE DOING. To be able to learn from experience and to put all of the pieces we have discussed so far together, the scientist needs to take time to reflect on what he is doing. One interviewee explained that when he was trying to figure out how to work with stakeholders, he found “just reflecting and trying to study the immersion process” and all the things he was “learning about people and what

they do and how they do it” helped him to know when he was “really sort of hitting the mark on meeting a potential user need.” In contrast, another scientist felt that his lack of time to reflect negatively affected his work. He felt that he and his colleagues were often “flying by the seat of our pants” and doing things “ad hoc all the time. And you know there’s a certain amount of that that has to be because the situations are unique.” But he felt that it would be beneficial to reflect on their experience in order to develop a more systematic approach to working with stakeholders and to developing and managing science integration projects.

Preliminary analysis of interviews with stakeholders working with a climate science integrator reinforced the importance of some of the personal characteristics and practices listed here. For example, what one stakeholder found most helpful in interacting with the science integrator is that “He has always been very interested in joining meetings that talk about the specifics of the project, whether it’s ecological response models or the social science part of it... He’s easy to talk to, he’s interested, he has the validity to actually talk at a level that we can understand, but he’s a very good listener.”

Challenges of pursuing science translation as a career. Interviewees identified several challenges associated with doing science integration work. The most prominent among them were time, academic culture, and the lack of well-defined career paths.

TIME. The biggest challenge for the scientists in our study is the time it takes to develop and maintain relationships with stakeholders and to understand their decision-making context, which echoes previous findings (see, e.g., Dilling and Lemos 2011; Jacobs et al. 2010; Kirchoff et al. 2013; McNie 2007; Shanley and López 2009). In the words of one interviewee,

Each one of these relationships with stakeholders is like a marriage, especially if you’re going to do a multiyear process with them. And, you know, a marriage requires a whole lot of relationship building and care and feeding, and the relationship evolves and you have to be sensitive to that too, and needs change, and understanding of the science changes, understanding of the relationship changes, the state of the science changes, the events come and go.

The time demand is compounded for science integrators who have faculty positions and the time-intensive activities associated with them. One scientist brought

up the “burnout factor”: “I’m publishing papers, trying to be an administrator, and then also running [an organization] and maintaining the current connections with stakeholders: it is a lot of time, a lot of work, and a lot of travel. And it takes its toll.” In addition, as science integrators advance in their careers they tend to take on more project management duties, which are also time intensive, and for which they often have little training.

ACADEMIC CULTURE. A second challenge for science integrators is an academic culture that does not value the type of work that they do. Some of those we interviewed had experienced this challenge in their own careers; others identified it as a challenge for aspiring science integrators. In the following quote, the interviewee reflects the contention that many scientists may see participating in this type of research as “at best uncomfortable and at worst inconsistent with real scholarship” (Cash et al. 2003, p. 8090):

[In academia] it’s about research. So especially in the earlier years, and there’s still a fair amount of this now, there is not as much receptivity—in some people’s minds this is doing sort of second-rate stuff, you’re dealing with the unwashed, and you’re not using the most of your talent because you’re out talking to all these folks—and it is really hard to fund it...Some colleagues might view you as being second-tier because you’re not out in the forefront of the science side...Especially with the funding atmosphere and so forth, people are so preoccupied with “Where’s my next grant going to come from. How am I going to keep myself going?” that this kind of stuff we’re talking about here is viewed as kind of a luxury.

Others noted that the reward system in academia, which is based primarily on the peer-reviewed journal article (McNie 2007; Shanley and López 2009), is not a good metric for the success of science integrator stakeholder engagement. For example, “If you are rated based on your number of peer-reviewed publications then that is a very different outcome than if you are allowed to be rated in part with your interactions with the community.” Because of the mismatch between academic and engagement metrics, some interviewees had struggled with the tenure process, even at institutions where they had achieved recognition as successful science integrators. Others expressed concern about how the predominant academic culture will impact the ability to train and employ the next generation of science integrators:

I’m not saying everybody has to fill this role, but I feel like there really needs to be more value in the academic system for people that want to engage in this kind of work.... And so for the few people that want to engage in it, it’s like there’s no opportunity to learn the skills, number one, you have to do it on your own, and number two, once you emerge there might not be a job for you.

LACK OF WELL-DEFINED CAREER PATHS. Interviewees pointed out that while recognition of the importance of the role of science integrators and demand for their services are growing, as well as interest in doing this type of work among undergraduate and graduate students, there is a lack of awareness in academia of job opportunities and of a career path to follow. For example, an interviewee who is a university professor felt that

There’s still a problem, or challenge out there with jobs. If you want to go into this field...there are limited opportunities that really do this bridging. I think over time people will create more private sector engagement, some of the things, especially engineering firms are doing with climate change now, and adaptation. There it’s starting to open up...But sometimes students will come by and ask, “What is out there?” And to be honest it’s not clear right now. It’s a transitional kind of thing.

On the other hand, a state climatologist pointed out that

There are quite a few applied climate jobs in private industry, but they’re not widely promoted. You have to go search them out, anywhere from the climatologist working behind the scenes at the Chicago Stock Exchange, to the folks that do reinsurance and, there’s quite a batch of climate work that goes on behind the scenes in the insurance and reinsurance businesses, I mean there’s a lot of places and there aren’t very many universities teaching how to do this.

And within the federal organizations designed to facilitate science-stakeholder interactions, such as the NOAA RISA system, there is limited funding for integrator positions, as this RISA scientist pointed out:

I think that there’s a need for more jobs like this, there’s clearly the demand from the stakeholder community for more people doing RISA-like work, but where do we employ those people? [It’s not

possible] with the base funding available [in the RISA system] that's been flat for 15 years.

Thus, scientists introduced to science integration work through graduate assistantships or postdocs in these organizations often have to look elsewhere to pursue this type of work.

Recommendations for developing and supporting the next generation of science integrators. The scientists we interviewed offered a number of suggestions for overcoming these challenges and for developing and supporting the next generation of science integrators. They see the next generation as the key to overcoming the time challenge because increasing the supply of science translators to meet the increasing demand for this kind of work will reduce the burden on those who are already engaged in it. One scientist put it this way: “That’s why we need new college graduates to be hired all of the time. They’ve got more time on their hands in terms of the ability to go out and really spend time

talking to the stakeholders. And they’re young and enthusiastic; they multitask [laughs] better than those of us who are getting older do.” And even though interviewees indicated overwhelmingly that the best way to learn science integration work is to “just do it,” they provided insights into appropriate training for the next generation—particularly involving experiential learning opportunities similar to those from which they learned the “craft” of science integration. Their suggestions are summarized in Table 1.

Regarding the challenges posed by academic culture, the science integrators we interviewed saw it changing already, albeit slowly. One example of changes they were seeing is that there is more interest in interdisciplinary applications among students and more interdisciplinary courses being offered in meteorology departments. A second example is the attainment of upper-level administrative positions in academia by proponents of this type of work where they can “nurture” programs that support the types of bridging activities needed to connect climate science and decision-makers. A third

TABLE 1. Suggestions for training climate science integrators.

Type of training	Example
Job shadowing or apprenticing experienced science integrators	A graduate student who is shadowing the regional climatologist at a regional climate center
Internships with climate service providers	Internships for high-school, undergraduate, and graduate students at state climatology offices
Exchange programs with stakeholders	A climatologist who “embedded” in land management agencies and took firefighter training to learn about fire management; at the same time, an agency person embedded in his group
Working with extension faculty	Working with extension faculty as a graduate student; learning from their experience working with clientele; benefiting from extension’s social capital for building relationships and trust
Support or professional networks of science integrators	From extension: Association of Natural Resource Extension Professionals; National Association of Community Development Extension Professionals
Service learning components in academic courses	Applied Climatology course (University of Oklahoma)
Postdoctoral fellowships that encourage work with stakeholders	American Association for the Advancement of Science (AAAS) policy fellowship; NOAA Postdocs Applying Climate Expertise (PACE) program; Sea Grant Knauss fellowship
Science integrator training programs	Certificate for Science and Decision Making (The University of Arizona); Graduate Certificate in Science and Technology Policy (University of Colorado Boulder)
Training in social science research methods	Social science methods for nonsocial scientists: to raise understanding of methods, ethics, and cultural differences
Training in science communication	A series of workshops on science communication through the Cooperative Institute for Research in Environmental Sciences (University of Colorado Boulder)

example is increased interest in supporting these activities by university administrators when they are seen to be able to bring in large grants, such as those for NOAA RISAs and the DOI CSCs. These scientists also see the proliferation of federal initiatives to connect scientists and decision-makers as an indication that prospects for employment are improving and career paths are beginning to emerge. They also anticipate that more employment will become available in the private sector as the need for adaptation to climate change becomes more widely recognized.

CONCLUSIONS. In this article we have called on some of the most respected first-generation climate science integrators to provide insights about how to train the next generations. Their pioneering efforts have demonstrated the value of science integration work, as we have seen, in improved drought planning for tribes, and risk assessment and planning for city planners, water managers, and government land management agencies, and contributed to the rapid increase in demand for usable climate science. Their enthusiasm for their work demonstrates that they have found it personally rewarding. Some of those we interviewed are now retired or about to retire. Before this generation leaves the work force, we need to draw on their collective wisdom to ensure that their shoes will be filled and the ranks of science integrators expanded.

Many of their suggestions concur with those of proponents of science integration work who have suggested principles for developing usable science and have been calling for training programs for science integrators, changes in academic culture to encourage and support science integration work, and incentives from funding agencies for including science integrators in research projects for some time (e.g., Averyt 2010; Jacobs 2002; Jacobs et al. 2005; McNeeley et al. 2012; NRC 2009). The voice of experience should lend weight to these appeals and momentum to the changes in science policy and academic culture beginning to take place.

However, our interviewees have also provided details and put a human face on the general principles for developing usable science through their practical guidance on the personal characteristics and practices that aspiring integrators should cultivate in order to work successfully with decision-makers. They have offered tangible ideas for the types of training that will help cultivate new climate science integrators. They have described the rewards of this type of work, as well as the demands and the challenges, and their personal stories are stories of overcoming those challenges to find personal growth in their work. We hope

these stories will provide mentorship and inspiration to future generations of climate science integrators.

Acknowledgments. We thank the scientists who participated in the interviews for sharing their time and insights and for providing role models for aspiring climate science integrators. This work was supported by NOAA's Climate Program Office through Award NA12OAR4310136 to the RISAs Climate Assessment for the Southwest and Western Water Assessment and Department of the Interior Southwest Climate Science Center Award G13AC00326.

REFERENCES

- Averyt, K., 2010: Are we successfully adapting science to climate change? *Bull. Amer. Meteor. Soc.*, **91**, 723–726, doi:10.1175/2010BAMS2906.1.
- Bernard, H. R., and G. W. Ryan, 2010: *Analyzing Qualitative Data: Systematic Approaches*. Sage Publications, 480 pp.
- Cash, D. W., W. C. Clark, F. Alcock, N. M. Dickson, N. Eckley, D. H. Guston, and J. Jäger, 2003: Knowledge systems for sustainable development. *Proc. Natl. Acad. Sci. USA*, **100**, 8086–8091, doi:10.1073/pnas.1231332100.
- , J. C. Borck, and A. C. Patt, 2006: Countering the loading-dock approach to linking science and decision making: Comparative analysis of El Niño/Southern Oscillation forecasting systems. *Sci. Technol. Hum. Values*, **31**, 465–494, doi:10.1177/0162243906287547.
- Dilling, L., and M. C. Lemos, 2011: Creating usable science: Opportunities and constraints for climate knowledge use and their implications for policy. *Global Environ. Change*, **21**, 680–689, doi:10.1016/j.gloenvcha.2010.11.006.
- Ferguson, D. B., J. L. Rice, and C. A. Woodhouse, 2014: Linking environmental research and practice: Lessons from the integration of climate science and water management in the western United States. Climate Assessment for the Southwest, University of Arizona Tech. Rep., 18 pp. [Available online at www.climas.arizona.edu/publication/report/linking-environmental-research-and-practice.]
- , M. L. Finucane, V. W. Keener, and G. Owen, 2016: Evaluation to advance science policy: Lessons from Pacific RISA and CLIMAS. *Climate in Context: Science and Society Partnering for Adaptation*, A. Parris and G. Garfin, Eds., Wiley-Blackwell, 215–233.
- Gieryn, T. F., 1983: Boundary-work and the demarcation of science from non-science: Strains and interests in professional ideologies of scientists. *Amer. Sociol. Rev.*, **48**, 781–795, doi:10.2307/2095325.

- Hirsch Hadorn, G., D. Bradley, C. Pohl, S. Rist, and U. Wiesmann, 2006: Implications of transdisciplinarity for sustainability research. *Ecol. Econ.*, **60**, 119–128, doi:10.1016/j.ecolecon.2005.12.002.
- Jacobs, K. L., 2002: Connecting science, policy, and decision-making: A handbook for researchers and science agencies. NOAA Office of Global Programs Rep., 25 pp.
- , G. Garfin, and M. Lenart, 2005: More than just talk. *Environment*, **47** (9), 6–21, doi:10.3200/ENVT.47.9.6-21.
- , and Coauthors, 2010: Linking knowledge with action in the pursuit of sustainable water-resources management. *Proc. Natl. Acad. Sci. USA*, doi:10.1073/pnas.0813125107.
- Jahn, T., M. Bergmann, and F. Keil, 2012: Transdisciplinarity: Between mainstreaming and marginalization. *Ecol. Econ.*, **79**, 1–10, doi:10.1016/j.ecolecon.2012.04.017.
- Kirchhoff, C. J., 2013: Understanding and enhancing climate information use in water management. *Climatic Change*, **119**, 495–509, doi:10.1007/s10584-013-0703-x.
- , M. C. Lemos, and S. Dessai, 2013: Actionable knowledge for environmental decision making: Broadening the usability of climate science. *Annu. Rev. Environ. Resour.*, **38**, 393–414, doi:10.1146/annurev-environ-022112-112828.
- Lemos, M. C., and B. J. Morehouse, 2005: The co-production of science and policy in integrated climate assessments. *Global Environ. Change*, **15**, 57–68, doi:10.1016/j.gloenvcha.2004.09.004.
- , C. J. Kirchhoff, and V. Ramprasad, 2012: Narrowing the climate information usability gap. *Nat. Climate Change*, **2**, 789–794, doi:10.1038/nclimate1614.
- McNeeley, S. M., and Coauthors, 2012: Catalyzing frontiers in water–climate–society research: A view from early career scientists and junior faculty. *Bull. Amer. Meteor. Soc.*, **93**, 477–484, doi:10.1175/BAMS-D-11-00221.1.
- McNie, E. C., 2007: Reconciling the supply of scientific information with user demands: An analysis of the problem and review of the literature. *Environ. Sci. Policy*, **10**, 17–38, doi:10.1016/j.envsci.2006.10.004.
- NRC, 2004: *Facilitating Interdisciplinary Research*. The National Academies Press, 332 pp.
- , 2009: *Informing Decisions in a Changing Climate*. The National Academies Press, 200 pp.
- , 2013: Proposal and award policies and procedures guide. Part I—Grant proposal guide. The National Science Foundation NSF 14-1, OMB Control Number 3145-0058, 76 pp. [Available online at www.nsf.gov/pubs/policydocs/pappguide/nsf13001/gpgprint.pdf.]
- Shanley, P., and C. López, 2009: Out of the loop: Why research rarely reaches policy makers and the public and what can be done. *Biotropica*, **41**, 535–544, doi:10.1111/j.1744-7429.2009.00561.x.
- Stokes, D. E., 1997: *Pasteur's Quadrant: Basic Science and Technological Innovation*. Brookings Institution Press, 180 pp.
- Strauss, A., and J. Corbin, 1998: *Basics of Qualitative Research: Techniques and Procedures for Developing Grounded Theory*. 2nd ed. Sage Publications, 336 pp.
- Wolf, S. A., 2008: The meaning of translational research and why it matters. *J. Amer. Med. Soc.*, **299**, 211–213, doi:10.1001/jama.2007.26.

AMS titles now available as eBooks at **springer.com**

AMS BOOKS

RESEARCH APPLICATIONS HISTORY

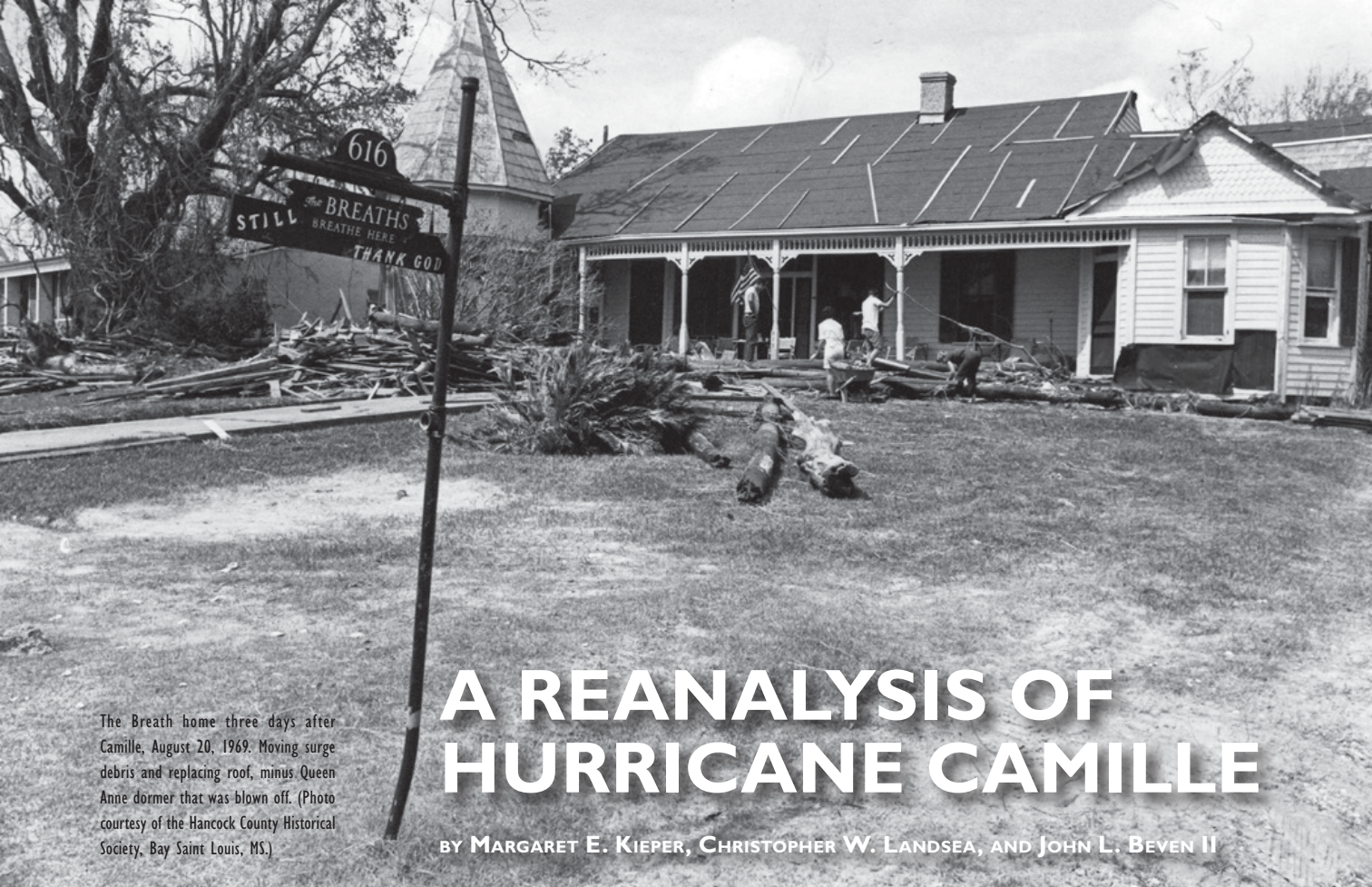
www.ametsoc.org/amsbookstore



Scan to see
AMS eBook titles
at springer.com



AMERICAN METEOROLOGICAL SOCIETY



The Breath home three days after Camille, August 20, 1969. Moving surge debris and replacing roof, minus Queen Anne dormer that was blown off. (Photo courtesy of the Hancock County Historical Society, Bay Saint Louis, MS.)

A REANALYSIS OF HURRICANE CAMILLE

BY MARGARET E. KIEPER, CHRISTOPHER W. LANDSEA, AND JOHN L. BEVEN II

A modern look at one of the United States' most destructive hurricanes indicates that it was deeper than, but not quite as intense as, originally estimated.

The pressure gradient must have been tremendously steep. Because of this...I think of Camille as a giant, well-organized tornado rather than as a small, very intense hurricane.

—Dr. Luis R. Rivas in a letter to Leonard G. Pardue of the National Hurricane Center

With the passage of almost 50 years and the recent memory of a number of major hurricane landfalls along the northern Gulf Coast of Louisiana, Mississippi, Alabama, and the Florida Panhandle, including Dennis and Ivan in 2004, and Katrina and Rita in 2005, and, further back, Andrew in 1992, Elena in 1985, and Frederick in 1979, Hurricane Camille in 1969 may not come readily to mind, except for those who lived through it. But for tropical meteorologists, Hurricane Camille holds a continuing fascination as one of the most intense U.S.-landfalling hurricanes on record and for a number of mysteries associated with its meteorological statistics and best-track record.

The African easterly wave that spawned Hurricane Camille traveled across the Atlantic main development region with very little associated convection or organization. However, after entering the Caribbean, the wave amplified and split into two areas of disturbed weather, one in the Bahamas and another near the Cayman Islands. The National Hurricane Center (NHC) sent weather reconnaissance flights to both areas on 14 August 1969, expecting the northern area would be the one to develop but finding that the area in the Caribbean had already developed into a tropical storm. Camille continued to develop rapidly before making landfall at 2200 UTC 15 August over the extreme western edge of Cuba at just under major hurricane strength. A few hours later, Camille moved into the Gulf of Mexico at the onset of the diurnal convective maximum and began rapidly intensifying, achieving category 5 status at 150 knots (kt; $1 \text{ kt} = 0.51 \text{ m s}^{-1}$) and a pressure reading of 908 mb ($1 \text{ mb} = 1 \text{ hPa}$) by 1800 UTC 16 August. Six hours later, the pressure had dropped to 905 mb. At this time, early Saturday evening local

time, Camille was about 290 n mi (1 n mi = 1.852 km) south-southwest of the mouth of the Mississippi River. The hurricane began to significantly affect the Mississippi Gulf Coast on Sunday evening, with the eye making landfall near midnight Sunday local time (0400 UTC 18 August). The bathymetry of the coastline enabled the hurricane to generate a tremendous storm surge that devastated the coastal communities on and near the western Mississippi coast and that would not be approached or eclipsed until Hurricane Katrina in 2005. Camille then moved northward through the Tennessee Valley and eastward through the mid-Atlantic states, where it produced record rainfall over the Appalachians. It subsequently redeveloped into a tropical storm in the Atlantic, after which it underwent extratropical transition and dissipated.

A reanalysis of the NHC's second-generation North Atlantic hurricane database (HURDAT2; Landsea and Franklin 2013) now covers the period from 1851 to the mid-twentieth century (e.g., Hagen et al. 2012). The reassessment of the existing database is necessary to correct random and systematic errors; to incorporate current understanding of tropical cyclones (TCs) upon previously collected raw observations; to include explicit analyses of the time, position, and intensity at landfall; and to add previously unrecognized TCs. Because previous reanalysis results had already addressed the three other category 5 hurricanes on the Saffir–Simpson hurricane wind scale to have impacted the United States during the twentieth century, NHC management requested an expedited reanalysis of Camille because of the need to answer a simple question: which is the strongest hurricane to have struck the United States?

In the context of modern understanding of TC intensity, tropical meteorologists have long held

some skepticism about Camille's landfall intensity, for several reasons. An extraordinary wind speed of 180 kt was reported by the last reconnaissance flight into Camille near 1800 UTC 17 August based on visual estimation of surface wind speeds observed from the surface sea state and an observed dropsonde 901-mb surface pressure. This resulted in a forecast intensity and accepted landfall intensity (10 h later) of 1-min winds of 165 kt, which is near the upper bound for globally known TC intensity in the combined NHC and Joint Typhoon Warning Center best-track data. The 901-mb mean sea level pressure (MSLP) that was noted in real time and in earlier reports (e.g., NHC *Preliminary Report, Climatological Data* monthly summary) disappeared from later reports (e.g., *Monthly Weather Review's* Atlantic hurricane season summary, *Climatological Data* yearly summary), and the earlier 905-mb pressure was identified as the lowest measured pressure (Simpson et al. 1970). In addition, Camille's MSLP and intensity at landfall were at odds with the two other category 5 mainland-U.S.-landfalling hurricanes—the 1935 Labor Day hurricane and Andrew in 1992. Particularly when compared to the Labor Day hurricane, Camille's landfall intensity appeared too high in relation to the MSLP (interestingly, MSLP readings in all three of these category 5 landfalls were taken by private individuals and the barometers were confirmed for accuracy). In addition, the original best track shows Camille gradually strengthening as a category 5 hurricane for more than 24 h before landfall—that contrasts with many other major hurricanes that have made landfall along the northern Gulf Coast, which weakened prior to landfall. All 11 hurricanes—most notably Hurricane Katrina in 2005—during the period from 1985 to 2005 having a central pressure less than 973 mb 12 h before landfall in the northern Gulf of Mexico weakened during these last 12 h (Rappaport et al. 2010).

After almost 50 years, can we answer these questions: During the Gulf of Mexico transit, did any weakening occur? How strong was Camille at landfall in Mississippi? A reanalysis of Hurricane Camille has enabled us to answer these questions to the extent the data will allow.

The official revisions for Hurricane Camille, which have been approved by the Best-Track Change Committee, are summarized below:

Generally, very small (0.3° latitude–longitude or less) changes were introduced to the center positions of Camille throughout its lifetime based upon a combination of ship, station, aircraft penetration, aircraft radar, land-based radar, and satellite observations

AFFILIATIONS: KIEPER—Florida International University, Miami, Florida; LANDSEA and BEVEN—NOAA/NWS/NCEP/National Hurricane Center, Miami, Florida

CORRESPONDING AUTHOR: Christopher W. Landsea, NOAA/NWS/NCEP/National Hurricane Center, 11691 SW 17th Street, Miami, FL 33165

E-mail: chris.landsea@noaa.gov

The abstract for this article can be found in this issue, following the table of contents.

DOI:10.1175/BAMS-D-14-00137.1

A supplement to this article is available online (10.1175/BAMS-D-14-00137.2)

In final form 30 March 2015

©2016 American Meteorological Society

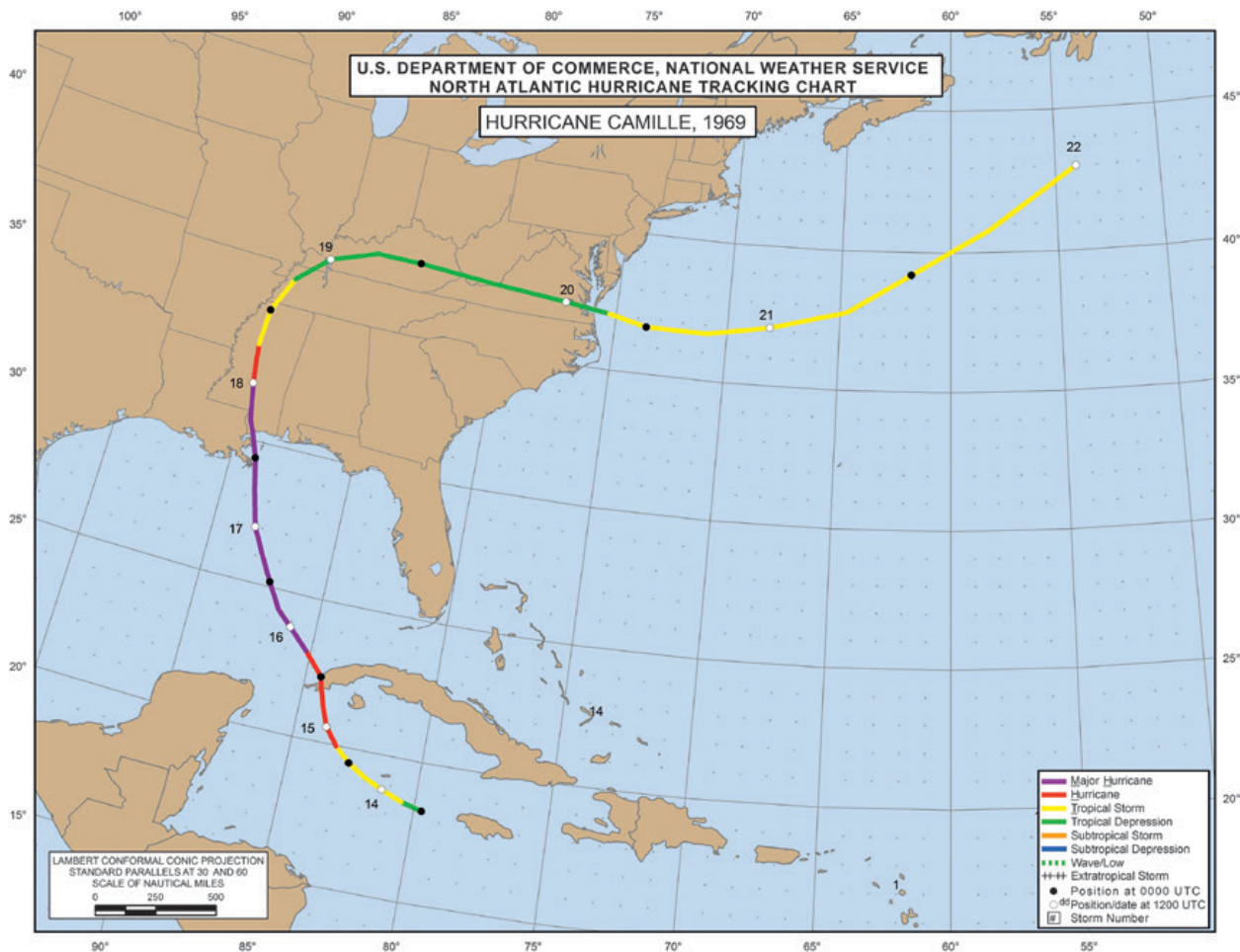


FIG. 1. Track map of Hurricane Camille, 14–22 Aug 1969.

(Fig. 1). Such relatively minor changes in the track are typical of systems in this era, as aircraft reconnaissance allowed for fairly accurate determination of the location of the center. The largest alteration to the positions was early on 20 August by about 50 n mi to the east-southeast when Camille was inland as a tropical depression over Kentucky. This adjustment was made to smooth out changes in forward speed as Camille accelerated eastward.

Minor intensity changes were analyzed for the periods around the Cuban landfall and at the end of the life cycle while the cyclone was moving over the mid-Atlantic states into the Atlantic Ocean. Major changes were made to the period Camille transited the northern portion of the Gulf of Mexico from the completion of the period of rapid intensification through an eyewall replacement to the Mississippi landfall, which resulted in modifications to the peak intensity and the timing of the peak intensity. These more substantial changes will be described in detail.

DATASETS AND METHODOLOGY.

Observational capabilities of Atlantic basin TCs in 1969 continued to evolve from those available earlier in the twentieth century. Through the early 1940s, the only measurements available of these primarily oceanic mesoscale cyclones were from unfortunately placed ships at sea and from coastal weather stations (Landsea et al. 2004b, 2008, 2012). These surface observations continued to play a crucial role in the reanalysis of Camille, from measurements obtained via the Comprehensive Ocean–Atmosphere Data Set (Woodruff et al. 1987), original U.S. station observations obtained from the National Climatic Data Center’s EV2 website (www.ncdc.noaa.gov/EdadsV2/), original Cuban station observations provided by the Cuban Meteorological Service, summaries of observations in *Monthly Weather Review* and other articles, microfilmed hand-drawn synoptic maps by the NHC analysts and forecasters in 1969, and the “storm wallet” of observations/analyses made available in real time and postanalysis to the NHC forecasters.



FIG. 2. Aircraft reconnaissance available in Hurricane Camille. (left) Image from ESSA (1969) provides the individual center fixes (small circles and triangles) and the original 6-hourly best-track positions (large circles). (right) Types of aircraft used to provide aircraft reconnaissance into Hurricane Camille.

For this particular reanalysis of Hurricane Camille, special observations and eyewitness accounts were also used, including Hamilton and Steere (1969, oil platform measurements), Breath (2007, personal communication, interviews of survivors), Mississippi Test Facility (1969, MTF observations), and N. C. Roberts Jr. (1969, unpublished manuscript, collection of unofficial observations).

Beginning in the mid-1940s, rudimentary aircraft reconnaissance missions were conducted for TCs (Hagen et al. 2012). These platforms were quite adept at providing center fixes, either by directly penetrating the eye of the storm, by locating the center from the plane's nose radar, or by circumnavigating the cyclone. The aircraft, however, were not able to accurately measure flight-level winds in hurricane conditions, though they were able to provide visual estimates of the surface winds. If the aircraft did obtain a penetration center fix, then they could also provide a central pressure, either via extrapolating the

flight-level pressure to the surface or by dropping a sonde into the eye. These capabilities and limitations continued into the 1969 hurricane season, with a mix of aircraft: the Navy's WC-121s, the Air Force's C-130s, and the Environmental Science Services Administration's [ESSA; the predecessor to the National Oceanic and Atmospheric Administration (NOAA)] DC-6s (Fig. 2).

In addition, the coastal array of Weather Surveillance Radar-57 (WSR-57) radars had been fully deployed during the 1960s and was available to monitor the position of Camille as it made landfall in the United States (Fig. 3). These radars provided a plethora of center fixes from a few locations every 30 min within a couple hundred miles from the coast.

Finally, an emerging capability available operationally at NHC in the 1960s was satellite imagery (Fig. 4). These were visible images from the polar-orbiting ESSA-8, ESSA-9, and *Nimbus-3* satellites, which each provided a snapshot of Camille about once per day.

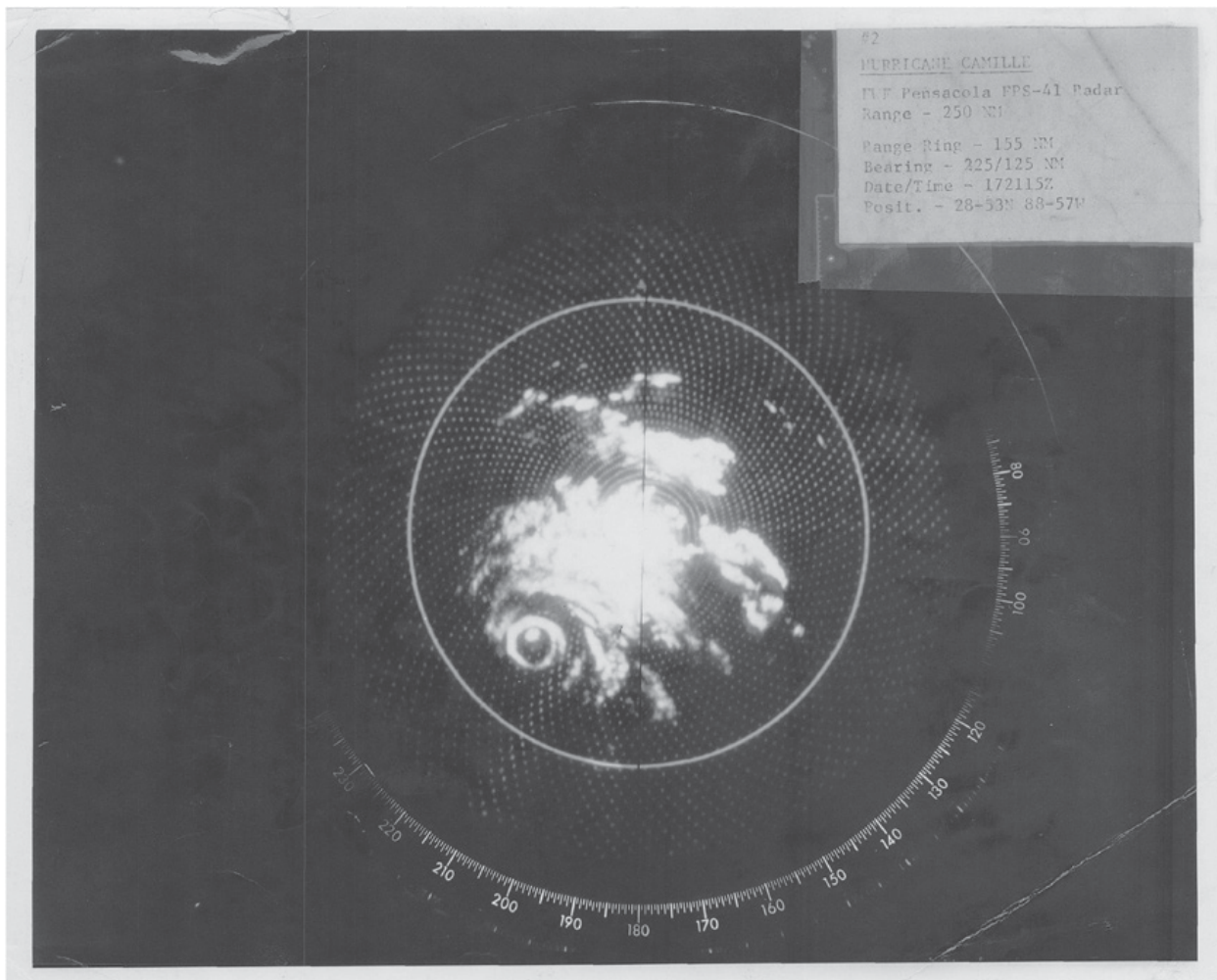


FIG. 3. WSR-57 image of Hurricane Camille at 2115 UTC 17 Aug 1969 from the Fleet Weather Facility Pensacola FPS-41 radar (NHC 1969).

The *Nimbus-3* satellite also had an infrared sensor, which while not available operationally, did show poststorm potential for providing imagery day or night (Allison et al. 1971). The National Aeronautics and Space Administration (NASA) also had an experimental geostationary satellite, the Applications Technology Satellite (ATS), which also provided after-the-fact visible imagery of Camille (Parmenter 1969). These images allowed for some qualitative assessment of Camille, but because of poor navigation, coarse resolution, and spotty temporal coverage, the satellite imagery of 1969 is only marginally of use for knowing Camille's exact position and intensity. For example, the aforementioned issues make it difficult at best to use the Dvorak (1984) technique for estimating TC intensity from satellite imagery. Almost a decade after Camille, *Nimbus* infrared and water vapor imagery and ATS visible imagery were analyzed (Shenk and Rogers 1978).

The methodology for the reanalysis of Camille follows similar steps established in earlier reanalysis efforts: 1) obtain all available raw observational data into a single database, 2) conduct synoptic analysis four times daily, 3) determine genesis changes, 4) determine track changes, 5) determine intensity (maximum sustained surface wind) changes, 6) determine status/dissipation changes, and 7) document all revisions in a metadata file. The track revisions primarily relied on aircraft and radar fixes. The intensity revisions primarily relied on aircraft and coastal central pressure measurements converted to maximum winds via the Brown et al. (2006) and Landsea et al. (2004b) pressure–wind relationships. These intensity values could then be adjusted based on the observed radius of maximum wind (RMW; a measure of inner-core size), radius of the outermost closed isobar (ROCI; a measure of TC size), pressure of the outermost closed isobar (POCI; a measure of

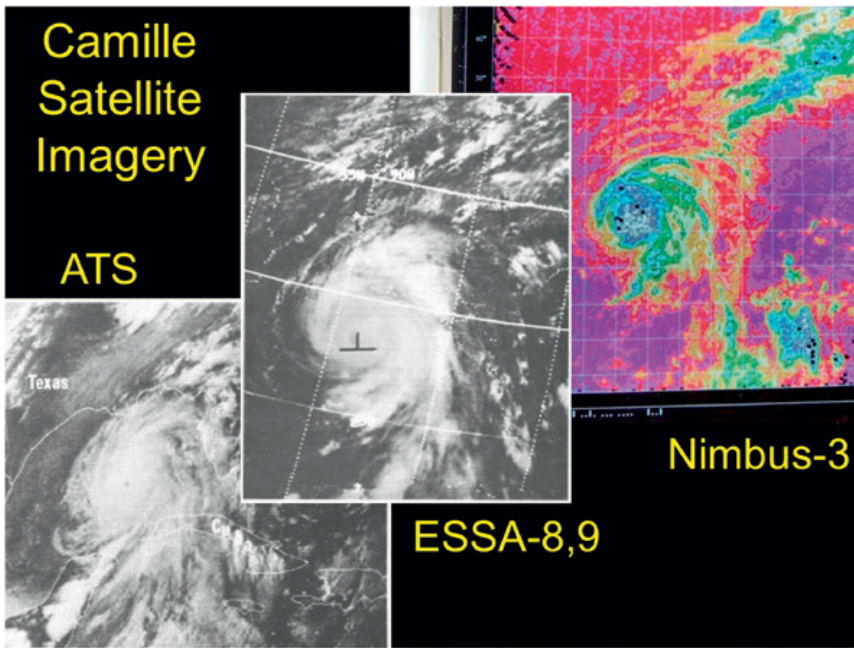


FIG. 4. Satellite imagery of Hurricane Camille. (bottom left) Visible image is from the experimental NASA ATS geostationary satellite at 2340 UTC 16 Aug 1969 (Parmenter 1969). (middle) Visible image is from the ESSA-8 polar-orbiting satellite at 1957 UTC 16 Aug 1969 (ESSA 1969). (top right) Infrared image is from the Nimbus-3 polar-orbiting satellite at 0500 UTC 16 Aug 1969 (Allison et al. 1971).

the environmental pressure), and TC forward motion varied from the climatology of Vickery et al. (2000).

The reanalysis methods documented in Landsea et al. (2004a) have been established in an attempt to provide consistency in the reanalyzed data. Since there is an inherent uncertainty in the wind–pressure

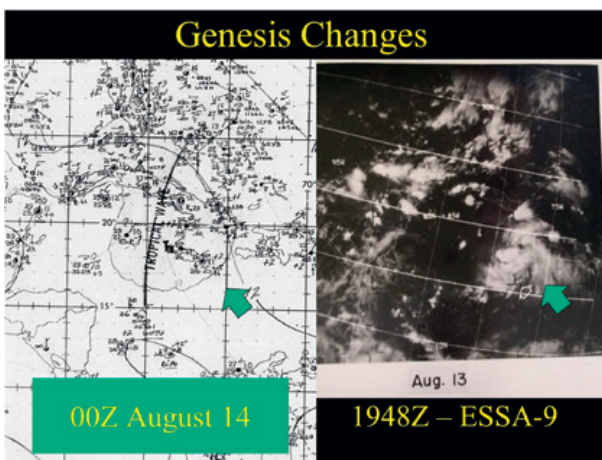


FIG. 5. Observations (0000 UTC 14 Aug 1969; microfilm archives at the NHC library) and satellite imagery (1948 UTC 13 Aug 1969; Weather Bureau 1969) providing evidence for an earlier genesis of Camille than originally indicated.

relationships used in the reanalysis, this translates into uncertainties in the reanalyzed best track intensities. Even using today’s data, the NHC considers their best-track intensities accurate to within about $\pm 10\%$ (Landsea and Franklin 2013). The uncertainty would be higher for storms of the Camille era.

More details on the reanalysis of Hurricane Camille, including data, files, and imagery, are available online. The full metadata, consisting of highlights of daily observations and descriptions about the changes to genesis, track, intensity, landfall, and dissipation, is available on the Atlantic Hurricane Database Reanalysis Project website (www.aoml.noaa.gov/hrd/data_sub/re_anal.html). This also includes the most recent HURDAT2

file, a database of all relevant raw observations, all of the NHC microfilm imagery, and comments from and responses to the Best-Track Change Committee. Additionally, comprehensive “storm wallet” archives maintained at NHC from the late 1950s onward (www.nhc.noaa.gov/archive/storm_wallets/cdmp/) also provide a large source of observations, which have been thoroughly mined for the reanalysis of Camille and other TCs.

GENESIS OF CAMILLE. Camille began as a tropical wave that emerged from the coast of West Africa on 5 August, which did not develop until it reached the western Caribbean Sea. Surface observations in the vicinity of the wave during genesis (Fig. 5) are somewhat sparse and are ambiguous as to when the system had a closed circulation. HURDAT2 originally indicated an “instant” 50-kt TC beginning at 1800 UTC 14 August. A closed circulation was not observed at 1200 UTC 13 August when the system passed over Jamaica; however, a closed circulation of tropical storm strength had developed by 1500 UTC 14 August. Satellite imagery late on 13 August (Fig. 5) indicated the deep convection associated with the wave had organized banding. Given the improved structure seen in the satellite imagery at that time, the

ambiguous surface observations, and the subsequent observations of the system being a moderate tropical storm around midday on 14 August, the best estimate of when genesis occurred is now 0000 UTC 14 August. While this is 18 h earlier than originally indicated, the exact time of genesis is uncertain to ± 6 h.

PEAK INTENSITY IN THE GULF OF MEXICO. Near the end of 3 days of rapid intensification, resulting in an intensity increase of 120 kt from its inception as a tropical depression, Camille reached its initial peak intensity of 150 kt from 1800 UTC 16 August to 0000 UTC 17 August. At 1835 UTC 16 August, an Air Force reconnaissance aircraft measured 908-mb central pressures from two separate dropwindsondes inside a circular eye of 10 n mi diameter. This eye size yields an approximate 8 n mi RMW using Kimball and Mulekar (2004). This pressure suggests maximum winds of 151 kt based on the Brown et al. (2006) pressure–wind relationship for intensifying storms south of 25°N latitude. Given a near-average environmental pressure from the 1010-mb outer closed isobar, a slow forward speed of 9 kt, and a tiny RMW of 8 n mi versus the 12 n mi climatology for this latitude and central pressure (Vickery et al. 2000), the intensity is analyzed at 150 kt. This is a 20-kt major increase from the previous best track value for 1800 UTC 16 August.

A similar methodology is used at the subsequent 0000 UTC 17 August best-track time. The same aircraft sortie observed a 905-mb central pressure at 0016 UTC 17 August with no change in eye size. As the cyclone was now straddling the 25°N latitude line, the 905-mb pressure suggests an intensity of 151 and 154 kt based on the Brown et al. (2006)

pressure–wind relationships for intensifying storms both north and south of 25°N latitude, respectively. An intensity of 150 kt at 0000 UTC 17 August is analyzed from these values, an increase of 10 kt from the previous best-track value.

INTERNAL STORM STRUCTURE OF CAMILLE IN THE GULF OF MEXICO. When environmental conditions are very favorable for TC development (low shear, warm SSTs, and deep warm water of the northwestern Caribbean and the Gulf of Mexico Loop Current) and the intensity has reached major hurricane status, hurricanes are likely to begin an eyewall replacement cycle (ERC),

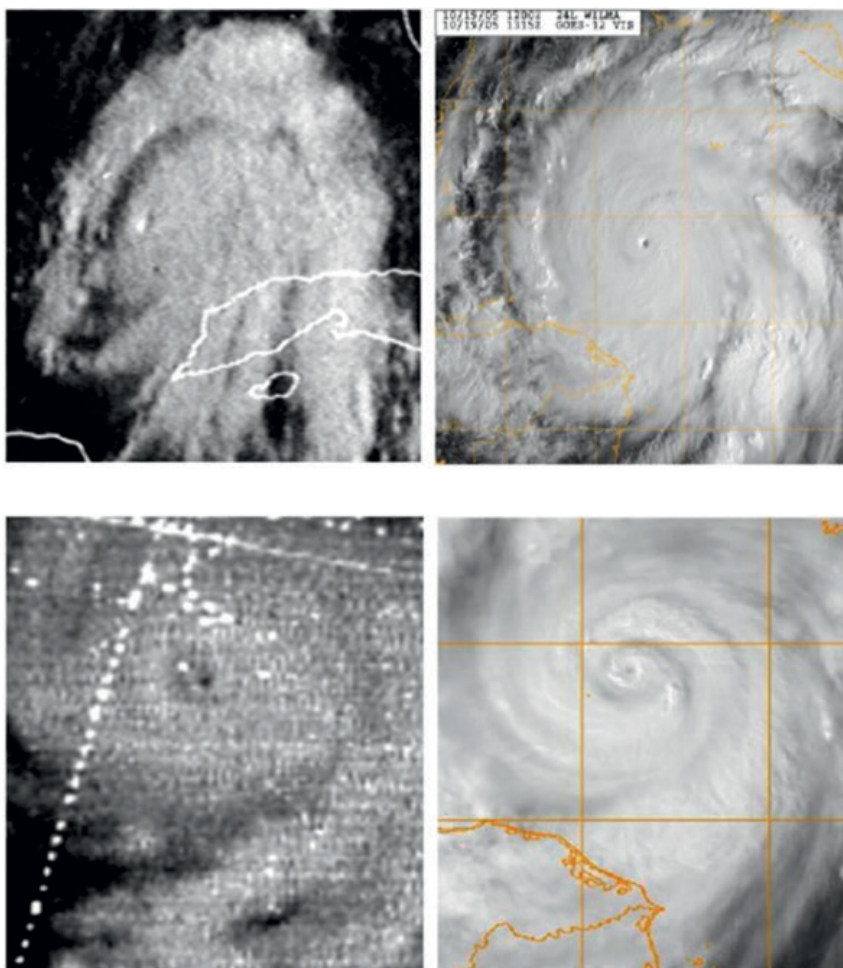


FIG. 6. (top left) Visible satellite image of Hurricane Camille at 1311 UTC 16 Aug 1969 near initial peak intensity and 5 h before 1800 UTC 908-mb pressure and 150-kt intensity. (top right) Visible satellite image of Hurricane Wilma at 1315 UTC 19 Oct 2005 near peak intensity of 882 mb and 160 kt. (bottom left) Visible satellite image of Hurricane Camille suggestive of a double eyewall at 1953 UTC 17 Aug 1969 at 919-mb pressure and 135-kt intensity. (bottom right) Visible satellite image of Hurricane Wilma showing the double eyewall confirmed by aircraft data at 1915 UTC 19 Oct 2005 at 892-mb pressure and 140-kt intensity.

CAMILLE'S 901-MB DROPSONDE

During the penetration of the eye of Camille near 1815 UTC 17 August, an Air Force dropsonde in the eye recorded a 901-mb pressure. For a short time, this was documented in the operational advisories, the *Preliminary Report* (Weather Bureau 1969), the *Climatological Data* (DeAngelis and Nelson 1969), and the *Mariners Weather Log* (DeAngelis 1970) to be Camille's deepest sea level pressure as well as the lowest pressure of record ever recorded by aircraft reconnaissance. Some months later in the *Monthly Weather Review* article on the 1969 hurricane season (Simpson et al. 1970), the 905-mb figure from an earlier drop was identified as the lowest sea level pressure for Camille. A footnote in Simpson et al. (1970, p. 295) said only, "Preliminary reports and other publications indicated a lowest pressure of 901 mb. Recently, a check of the raw data indicates this should be corrected to the 905-mb value given here." This footnote was ambiguous and could have meant two things: either that the earlier drop yielding a 905-mb pressure became the lowest pressure when the 901-mb reading was thrown out, or that the 901-mb reading was recalibrated to achieve a 905-mb reading. It appears that the decision was the former one, to use the 905-mb pressure from the aircraft reconnaissance flight 20 h earlier. There is no documentation on why the 901-mb sea

level pressure was rejected, nor was the decision clarified after contacting the surviving NHC hurricane forecasters from the 1969 hurricane season.

A review of the sonde data (Fig. SBI) indicates that the 850-mb geopotential height was 692 m. This is inconsistent with a 901-mb surface pressure based on comparison to other aircraft data and dropsondes. For example, an aircraft in the eye of 2005's Hurricane Wilma extrapolated a sea level pressure of 901 mb from an 850-mb height of 516 m—176 m lower than the height on the Camille sonde. Two other eye sondes from Camille reported 905- and 908-mb central pressures along with 850-mb heights of 551 and 586 m, respectively. The 850-mb heights from the Camille 905- and 908-mb sondes and the Wilma 901-mb extrapolation are all consistent, while the 850-mb height on the Camille "901-mb" sonde is an outlier.

Several methods were tried to better estimate the central pressure at the time of the 1815 UTC 17 Aug fix. These methods are summarized here.

Method 1.

A rule of thumb used at the NHC is that a 10-m change in the aircraft-reported 850-mb height roughly corresponds to a 1-mb change in the surface pressure. The 692-m height

of the "901-mb" dropsonde is 141 m higher than that of the 905-mb sonde and 106 m higher than that of the 908-mb sonde. This suggests a pressure of 918–919 mb as a first rough estimate.

Method 2.

Inside the eye, the aircraft reported a 700-mb geopotential height of 2390 m and a temperature of 16.6°C. Using standardized tables previously employed at NHC (OFCM 1997) for extrapolating the sea level pressure from these data using the standard environmental lapse rate yield an estimated minimum sea level pressure of 920 mb. It is notable that at the time of the 905-mb sonde, the aircraft reported a 700-mb height of 2240 m and a temperature of 22°C. Using the tables, these numbers yield an extrapolated pressure near 902 mb.

Method 3.

The sonde data (decoded in Table SBI, along with the calculated water vapor mixing ratio and equivalent temperature) were also used to determine sea level pressure using the hydrostatic equation. The mean equivalent temperature of the layer was taken from a skew *T* analysis to be about 27.0°C, or 300.2 K. The data were entered into the hydrostatic equation below:

$$\begin{aligned} \text{Pressure (sea level)} &= \text{Pressure} \times \exp[(\text{Gravity} \times \text{Geopotential height})/(\text{Gas constant for dry air} \times \text{Mean equivalent temperature})] \\ &= 700 \times \exp[(9.81 \text{ m s}^{-2} \times 2390 \text{ m})/287 \text{ K}^{-1} \times 300.2 \text{ K}] \\ &= 919 \text{ mb} \end{aligned}$$

TABLE SBI. Decoded Camille eye dropsonde data at 2125 UTC 17 Aug 1969.

Pressure (mb)	Temp (°C)	Dewpoint (°C)	Geopotential height (m)	Water vapor mixing ratio (g kg ⁻¹)	Equivalent temp (°C)
700	16.6	16.6	2390	14.3	19.0
732	19.4	18.4	—	17.5	22.3
850	28.0	26.7	692	27.0	32.5
874	29.4	27.8	—	27.0	33.9
901	30.8	28.3	—	28.0	35.9

Based upon the three methods, a central pressure of about 919 mb is estimated for 1800 UTC 17 August for Camille, with a derived intensity of 135 kt.

There are two questions about the "901-mb" sonde that are likely

unanswerable. First, E. Uhlhorn (2015, personal communication) indicates that a combination of a surface pressure of 919 mb, and surface temperature of 30.8°C, and a 28.0 g kg⁻¹ surface mixing ratio yields a surface θ_e of 382 K, which is 8 K warmer than other such

values in recent dropsondes. Was there an instrumentation error, or were these data representative of extreme conditions in Camille's eye? Second, did the sonde actually reach the surface?

```

NNNN+MEMUUV
URX KCHS 172125Z
GULL THREE CAMILLE THREE
97779 71717 TT 1742/ 99282 70188 08188 99901 30825 00///
///// 85692 28013 70390 166// 88999 77999
VV 1742/ 99282 70188 08188 00901 30825 11874 29413 22732
19410 33700 16600 51515 10168 07370

URXX KCHS 172140ZPOST FLIGHT SUMMARY
CAPT ZUBER AND CAPT WADAGNOLO
FIXED EYE 1815Z AT CORDINATES 28 DEGREES 12 MIN N 88 DEGREES 46 MIN W
WELL DEFINED EYE CLOSED WITH FEEDER BAND IN ALL QUADRANTS MAX SFC WINDS
OBSERVED IN SE QUADRANT OF 180 KTS PLUS MAX FL WND OBS SE QUAD AT
95 KTS MISSION ABORT 0000Z FIX DUE TO SHUTDOWN NO. FOUR ENGINE

```

FIG. SBI. (top) Dropsonde coded message at 2125 UTC 17 Aug 1969 for the sonde released into the eye of Camille near 1815 UTC that day. (bottom) Postflight summary from the Air Force aircraft reconnaissance mission that launched this dropsonde. Images were obtained from the microfilm archives at the NHC library.

where a new eyewall forms outside the original small eyewall. This new eyewall then contracts as the old inner eyewall dissipates. Satellite imagery near the time of peak intensity on 16 August showed a remarkably distinct pinhole eye, which is often seen in an intense hurricane. However, Camille was still 28 h from landfall on the northern Gulf Coast and climatologically, if the environment remained favorable, an eyewall replacement would likely have occurred during that time. The existence of double/concentric eyewalls was known in 1969, as there is one documented radar fix report of a double eyewall for Camille, in reviewing all hourly radar fixes. However, the importance of the ERC—the cycle of temporary weakening followed by reintensification as the ERC completes and the new outer eyewall contracts—would not be fully understood until Willoughby et al. (1982).

The next and last reconnaissance flight into Camille occurred 18 h after 905 mb was measured. It is unknown if Camille intensified further during that time, which would have included the overnight diurnal convective maximum. It is also unknown when an ERC may have started. But 18 h later, there

was evidence of an ongoing ERC from four different sources: radar, reconnaissance, satellite imagery, and ground observations. In a serendipitous coincidence, on 17 August there are radar images from both Naval Air Station (NAS) Pensacola (2115 UTC) and NWS New Orleans (1732 UTC); a visible satellite image from 1953 UTC; and an aircraft penetration near 1815 UTC. Both radar images show a well-formed symmetric double eyewall (Figs. 3 and SB2a). In the description from the aircraft, “‘Just as we were near the [eye] wall cloud we suddenly broke into a clear area and could see the sea surface below,’ the copilot, Robert Lee Clark, wrote in 1982” (Sheets and Williams 2001, p. 152). The clear area was possibly a moat that separated the inner and outer eyewalls. In addition, although faint, the visible satellite image shows what appears to be a moat (Fig. 6, bottom). Finally, observations from Freeport Sulphur Company at Garden Island Bay, Louisiana (near the mouth of the Mississippi River), at 2255 UTC 17 August noted, “the western eye would have been some ten miles distant [to the east]. However a brief lull was observed, with wind velocities dropping to 30–35 mph” (N. C. Roberts Jr. 1969, unpublished manuscript).

CAMILLE LANDFALL PRESSURES

A key parameter in analyzing tropical cyclones is the central pressure. Unfortunately, for Hurricane Camille, no aircraft reconnaissance flights were in the storm during the last several hours before it made landfall. Several pressure measurements obtained along the Mississippi coast were examined to determine which, if any, could provide a central pressure value for Camille.

Two pressures were measured at or near the time of eye passage in Bay St. Louis, 909 and 904 mb (26.85 and 26.70 in. Hg, respectively), and a pressure in the eyewall was measured in Pass Christian, Mississippi, 919 mb (27.15 in. Hg). The estimated distance between the 909- and 904-mb readings and the center of the eye is 3–4 n mi; that is to say, it was on the eastern edge of the small eye (which had a 10 n mi diameter, suggesting a radius of maximum wind of 6–8 n mi). The estimated distance between the Pass Christian eyewall pressure reading and the center of the eye is 7 n mi.

From NHC (1969) a letter detailing the 919-mb eyewall pressure reading in Pass Christian:

Mr. James Cagle, one of my co-workers here, took barometric readings at his home in Pass Christian during the passage of Camille. His lowest reading was 27.05 at 2330, August 17. I checked his aneroid barometer and found it to have a +0.10 error. Therefore the corrected reading should be 27.15. He also reports that there was no “lull” in his area... my own lowest reading of 29.28, [was]...30 miles east of the eye....

The two documented pressure readings in the eye were taken by Charles Breath, a boat dealer and mariner, who had a marine barometer in his home as well as a wall barometer. He logged pressure readings starting a couple days prior to the arrival of Camille and increased the frequency of the readings to hourly and then to half hourly as the hurricane approached landfall. The first low reading, the 909 mb, was taken just as the roof had partially come off and the family was

awaiting the arrival of the eye in order to evacuate to one of their other (rental) homes on their property farther back from the river bluff. He took the marine barometer with him, and once they had walked back to the rental property, took another reading, which was lower—the 904 mb. He provided the 904-mb reading to the MTF (today it is Stennis Space Center) meteorologists and to Nash and Ep Roberts.

Nash Roberts, a local New Orleans meteorologist, put out a request on-air for weather data, and there was a record that he was contacted by phone by Mr. Breath regarding the 904-mb reading (Loyola University 2001). The barometer and possibly the log were provided to Ep Roberts, Nash’s brother, a meteorologist as well, who had a store that sold meteorological instruments. The barometer was checked and found to be accurate. It is not known how NHC came to obtain the 909-mb measurement and why they did not use the 904 mb, but it could be that they went by the log, which had the 909 mb as the last entry.

A week after the storm, two MTF employees, meteorologists at the weather station there, talked to Mr. Breath while driving around the area observing damage and trying to determine the extent of the eye passage. At that time, he told them of the 904-mb reading and they documented it in their report (Mississippi Test Facility 1969):

Mr. Breath...always religiously kept up with the weather. His home was over 100 years old, but sturdily built of wood. Although most of the roof was blown off, the studs of the roof still stood...During the brief time they had in the “eye,” not more than 10 minutes, they evacuated to a home on higher ground.

He first observed his Aneroid type wall decorative barometer, scaled to 28 inches pressure when the pressure began plunging. He stated the needle just fell off rapidly beyond the 28 inch limit. In the turmoil, he remembered his Marine type barometer and went into another

room and observed it. During some time period when he knew he was in the “eye,” he read 26 point something, and later recalled that it was probably 26.7 inches pressure. He stated that this was a reading in the “eye” but possibly was not the lowest he observed.

An interview was conducted with Mr. Breath in 1979 (Pyle 1984) as part of the University of Southern Mississippi oral history program.

Mr. Pyle: As Hurricane Camille started to come up in the gulf that Sunday afternoon, your wife here has got a panoramic view of the gulf right out in front of you, what did you see? What did it look like, the atmosphere?

Mr. Breath: I have had through the years a habit of watching the barometer. I go more by the barometer than anything else. And I started taking hourly checks on it. And then when the barometer really started to fall, regardless of what we saw out in the gulf or whatever, we started really getting ready to leave. We knew something bad was coming up.

...

Mr. Pyle: How aware were you of the time you were in the house before you left?

Mr. Breath: Oh, I was watching closely because I was keeping this log, see. I was watching it close. I had a log in the beginning at every hour. And then as it would start falling more, I’d have it every half hour and make a recording of it.

...

Mr. Pyle: When you saw the barometer, when you could actually see it dropping, what were your thoughts? It might be hard to recall. I was just wondering if you were thinking about your family, your house—

Mr. Breath: Well, I just couldn't believe what I was seeing. Actually, I just [couldn't believe it].

Mr. Pyle: Did you ever question if your barometer was right?

Mr. Breath: Nash Roberts, who is a weather report man, had one of his men come over and interview me. He asked permission to take the barometer to have it checked in New Orleans to see if they were actually accurate, or whether I had made a mistake, or what. And I certainly agreed to it. They brought it back in a couple of weeks, and said that it was within a tenth of a point of being right, and that could be the difference between the sea level here and the sea level in New Orleans.

...

Mr. Pyle: And then, you took your last reading and left about what time?

Mr. Breath: Oh, probably about eleven-fifteen.

Mr. Pyle: And the reading then, for the record, was how low?

Mr. Breath: 26.85!

Mr. Pyle: Inches of mercury, that's terrifically [low]! [laughter]

Mr. Breath: And I feel sure that it dropped a little bit more than that, but that's what I actually have a record of.

In the University of Southern Mississippi interview, Mr. Breath states again that he obtained a lower reading but that he was not able to document it (probably not having brought the log back with him to the other property). It sounds like he meant the 26.70 in. Hg reading, as he says he "felt sure" the barometer fell lower than 26.85 in. Hg.

These 904-, 909-, and 919-mb pressure measurements are crucial for the assessment of a 900-mb central pressure analysis for Camille's landfall as described in the main text. They do highlight the importance of unofficial meteorological observations, even for a hurricane like Camille in a relatively recent era.

An ERC was in progress, but what could this mean for Camille's intensity at this time? Because the plane had radar and their observations focused on the inner eye, this suggests that radar reflectivity of the outer eye was weaker compared to the inner eye and that the inner eye was still the prominent feature. This suggests that the ERC was not complete.

A comparison of Camille to 2005's Hurricane Wilma (Pasch et al. 2006) is instructive, as it appears that the central pressures and inner-core structures may be quite similar. Figure 6 (top) shows Camille's and Wilma's satellite appearance when both storms were near peak intensity. The similarities between the satellite images of the two hurricanes include a very well-defined pinhole eye, smooth central dense overcast (CDO) with subsidence around the CDO, and similar CDO size. Figure 6 (bottom) shows both Camille and Wilma undergoing an eyewall replacement, likely at a similar stage of an eyewall replacement cycle. Both images show a moat between an outer eyewall and the still-well-defined inner eyewall. Wilma's pressure between the peak and the ongoing ERC had increased 10 mb from 882 to 892 mb. Therefore, it is logical for Camille's pressure at this time to have risen about 10 mb from the minimum of 905 mb. An analysis of the "901"-mb dropsonde suggests a central pressure of about 919 mb (see the sidebar "Camille's 901-mb dropsonde"). This is a rise in pressure of about 14 mb and is close

to the expected 10-mb rise in the comparison with Wilma.

Wilma's intensity decreased modestly from 160 to 140 kt at this stage of the ERC. Thus, it is logical for Camille's intensity to also have weakened slightly from its estimated 150-kt peak intensity. The re-analyzed central pressure of 919 mb, which is newly added into the 1800 UTC 17 August best-track time, suggests an intensity of 133 kt. Because of the intensity decrease from the ERC followed by reintensification, both the normal and weakening subsets of the Brown et al. (2006) pressure-wind relationships for north of 25°N latitude were used, with values of 133 and 127 kt, respectively. With the concentric eyewall structure, a low environmental pressure of 1008 mb for the outer closed isobar, a somewhat faster forward speed of 12 kt, and a continued tiny inner RMW, the best-track intensities for Camille are reduced to 135 kt at 1800 UTC 17 August and 140 kt at 0000 UTC 18 August. These are major changes downward from the original 165 kt. Unfortunately, no further aircraft reconnaissance fixes were available before landfall in the United States.

LANDFALL OF CAMILLE IN MISSISSIPPI.

Camille made landfall near Waveland, Mississippi, at 30.3°N, 89.4°W at 0400 UTC 18 August, based on radar fixes and pressure measurements at the coast (Fig. 1). The hurricane displayed a concentric eyewall

CAMILLE RADAR ANIMATION

For the first time, a radar loop of Hurricane Camille was constructed from archived radar imagery.

In the 1960s, U.S. Weather Bureau radar imagery could only be viewed in real time by the on-site radar operators. A radar coded message containing a center fix and a rough description of precipitative features was transmitted hourly to the NHC. This meant that with the exception of hurricanes within range of the collocated local Miami, Florida, radar, no real-time radar imagery of hurricanes was available to the hurricane specialists. Also, there was no real-time animation of radar data available, even to the radar operators. This is much different from modern-day radar data availability.

The WSR-57 radar had an archive capability with a camera automatically recording the radar image once per minute onto 16-mm film, independent of operator-controlled gain and other radar controls, and not including the transparency overlay of the surface map that the radar operator would change when changing the range of the radar. In August 1969, Camille was at different times within the range of a number of radars at Key West, Florida; Pensacola, Florida; Mobile, Alabama; Jackson, Mississippi; New Orleans, Louisiana; Baton Rouge, Louisiana; and Lake Charles, Louisiana. The best available archive images were from New Orleans, which fortunately was in a position to record imagery of the approach to the coast and the Mississippi landfall. These images were obtained from the National Climate Data Center (NCDC). Sets of two consecutive images, every 10 min, were photocopied from the plan position indicator (PPI) scope image, from 1630 UTC 17 August 1969 through 0730 UTC 18 August (Fig. SB2, top).

To utilize the radar images, the 1969 radar location needed to be determined, and a surface map was created based on the 50 n mi range rings available in the radar data. This map was then precisely overlaid on each radar image (Fig. SB2, bottom), which were subsequently incorporated into a GIF animation.

The entire loop can be viewed in the provided supplemental material.

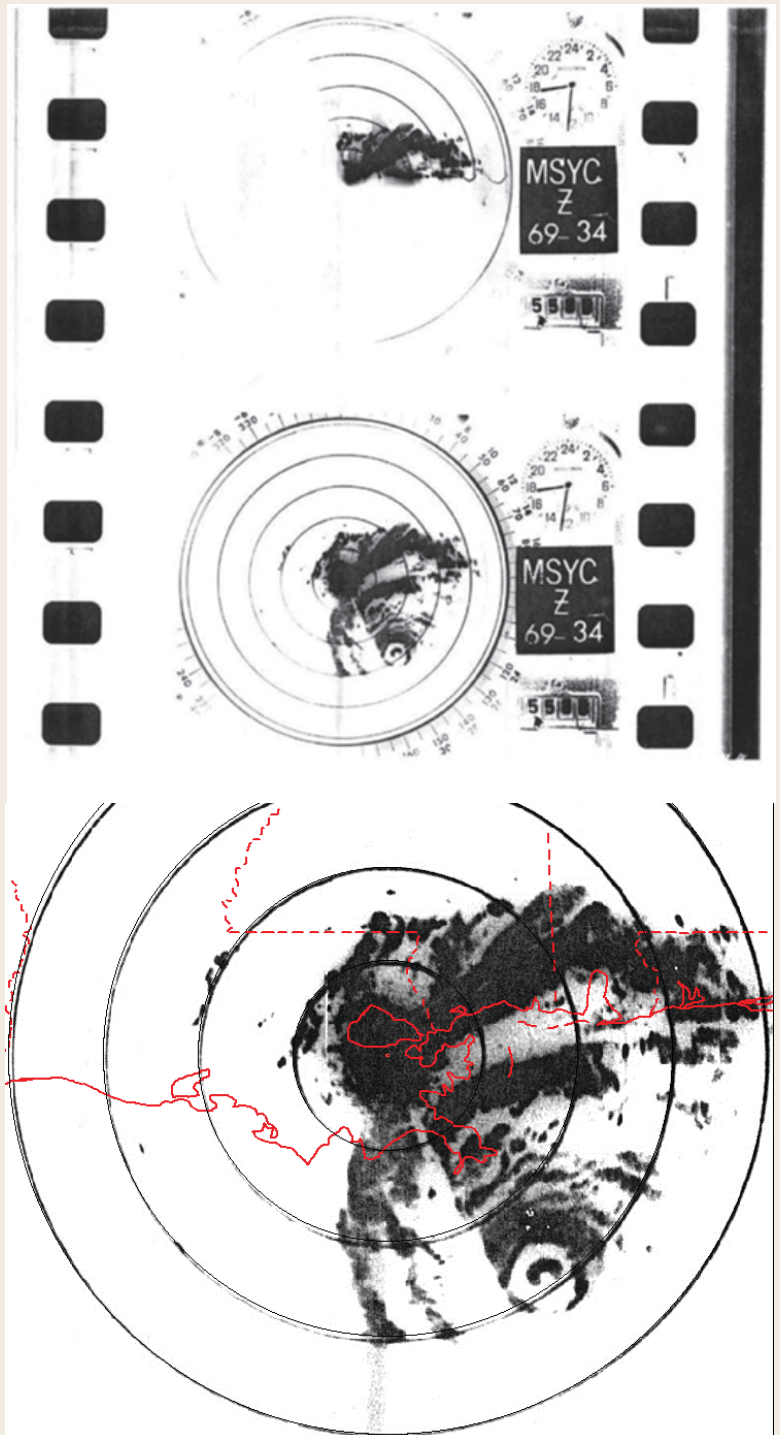


FIG. SB2. (top) Sample of the photocopy of the PPI scope WSR-57 radar from New Orleans of Hurricane Camille at 1732 UTC 17 Aug 1969. (bottom) Subsequent radar image with the map overlay and scaling.

structure with circular eyes with diameters of 10 and 30 n mi with some additional prominent banding at larger radii. The inner eye near the time of landfall could be considered elliptical with a major axis of 12 n mi oriented northwest–southeast and a minor axis of 8 n mi (N. C. Roberts Jr. 1969, unpublished manuscript). The POCI at landfall was a very low 1004 mb, but the hurricane was also quite tiny with an ROCI of 150 n mi. Camille’s forward speed had increased to about 15 kt at the time of landfall.

The discovery of additional landfall pressures and radar imagery from the New Orleans Weather Bureau Office aided analysis of the Mississippi landfall. There were three pressure values of interest near the point of landfall. A pressure of 909 mb was measured by Mr. Charles Breath at the onset of the eye in his home just west of the bridge in Bay St. Louis, Mississippi, which was about 3–4 n mi east of the landfall point. This marine aneroid barometer was subsequently tested and determined to be accurately calibrated. The 909-mb value had been the accepted central pressure value at landfall originally as shown in HURDAT2 and discussed in Simpson et al. (1970). However, Mr. Breath also measured a 904-mb pressure at a later point in the eye passage a short distance west of the first measurement (see the sidebar “Camille landfall pressures” for additional discussion about this 904-mb measurement), in one of his rental properties behind his damaged house, as reported by N. C. Roberts Jr. (1969, unpublished manuscript) and confirmed in interviews of the Breath family (Breath 2007). In addition, N. C. Roberts Jr. (1969, unpublished manuscript) documents an even lower value of 897-mb pressure reading, also in Bay St. Louis, with additional details on its location and time from the Loyola University archives of Roberts’s records. However, there is no documentation on the accuracy of the instrument and this barometer could not be located today. Moreover, the value provided in inches of mercury—26.50 in.—appears to be rounded to the nearest 0.5 in. Thus, this value cannot be assumed to be completely accurate. Given that the 904-mb pressure reading was taken near the eastern edge of the eye, a 900-mb central pressure is analyzed at landfall. It is of interest that this corresponds closely to the 901 mb that N. C. Roberts Jr. (1969, unpublished manuscript) analyzed as the central pressure, taking a mix of the Waveland–Lakeshore–Bay St. Louis observations.

This central pressure of 900 mb—a roughly 20-mb decrease in the 10 h since the last aircraft data—shows Camille was strengthening at landfall, possibly because of the end of the ERC. Brown et al. (2006) suggest maximum sustained winds at landfall

of 148 kt using the standard relationship or 155 kt using the intensifying subset north of 25°N. Given the competing factors of a tiny RMW of approximately 6–8 n mi and a moderate forward speed of 15 kt, but a very low pressure of the outer closed isobar of 1004 mb, an intensity of 150 kt is reanalyzed for the time of landfall (a graph of the previous and reanalyzed best-track intensities is provided in Fig. 7). The 150 kt at landfall show Camille as a category 5 hurricane at landfall in Mississippi. This intensity assessment confirms the original indication of Camille as a category 5 striking the United States (Hebert and Taylor 1978).

The intensity changes of Camille on 16 and 17 August appear similar to those of 1992’s Hurricane Andrew on 23 and 24 August. Andrew reached an initial peak intensity of 150 kt with a 922-mb central pressure near 1800 UTC 23 August (Landsea et al. 2004a). After this, an ERC commenced with the winds decreasing to 125 kt and the pressure rising to 941 mb early on 24 August.¹ As the ERC completed, Andrew rapidly reintensified to an intensity of 145 kt and a central pressure of 922 mb as it made landfall in southern Florida near 0900 UTC 24 August.

Additional indirect support for the landfall intensity comes from inland observations and use of

¹ Aircraft data documenting the ERC available online (http://verif.rap.ucar.edu/jntweb/tcdata/vortex/sources/raw_VDMs_v1.000/1992/vortex_AL041992_ANDREW.txt).

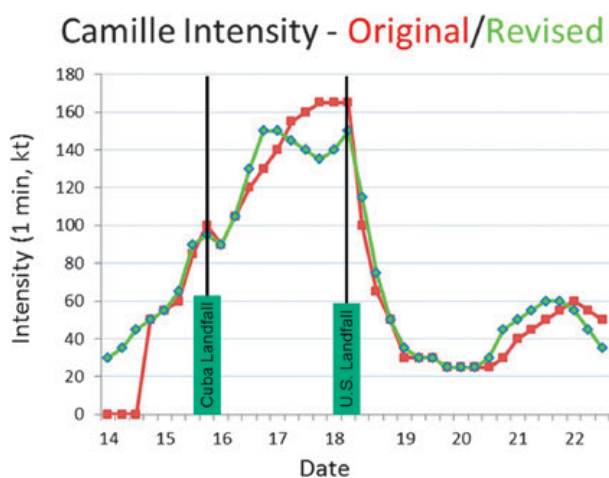


FIG. 7. Original (red) and revised (light green) intensity of Camille. Intensity is the analyzed maximum 1-min surface wind associated with the circulation of the TC. Camille’s landfalls in Cuba and in the United States are indicated with the black vertical lines.

TABLE 1. The official revisions for Hurricane Camille in the 6-hourly HURDAT2, 14–22 Aug 1969, which have been approved by the Best-Track Change Committee. Changes are listed in boldface with the original best-track value, if existing, in parentheses. Three new best-track entries were added at the beginning, and two new nonsynoptic-time landfall entries were added for the Cuba and Mississippi landfalls. There were no significant position changes.

Time and date	Lat (°N)	Lon (°W)	Max wind speed (kt)	Central pressure (mb)	Storm status
0000 UTC 14 Aug	18.3	79.7	30	—	Tropical depression
0600 UTC 14 Aug	18.5	80.5	35	—	Tropical storm
1200 UTC 14 Aug	18.8	81.3	45	—	Tropical storm
1800 UTC 14 Aug	19.1 (19.4)	82.0	50	991	Tropical storm
0000 UTC 15 Aug	19.5 (19.7)	82.7	55	991	Tropical storm
0600 UTC 15 Aug	20.0 (20.1)	83.3	65 (60)	—	Hurricane
1200 UTC 15 Aug	20.6 (20.7)	83.8	90 (85)	969 (970)	Hurricane
1800 UTC 15 Aug	21.3 (21.2)	84.1	95 (100)	966 (964)	Hurricane
2200 UTC 15 Aug	21.9	84.3	95	—	Landfall over western Cuba
0000 UTC 16 Aug	22.3	84.4	90	—	Hurricane
0600 UTC 16 Aug	23.1	85.2	105	—	Hurricane
1200 UTC 16 Aug	23.8 (23.7)	86.0 (85.9)	130 (120)	—	Hurricane
1800 UTC 16 Aug	24.3 (24.2)	86.6 (86.5)	150 (130)	908	Hurricane
0000 UTC 17 Aug	25.2	87.2	150 (140)	905	Hurricane
0600 UTC 17 Aug	26.0	87.7	145 (155)	—	Hurricane
1200 UTC 17 Aug	27.0	88.3 (88.2)	140 (160)	—	Hurricane
1800 UTC 17 Aug	28.2 (28.3)	88.7	135 (165)	919	Hurricane
0000 UTC 18 Aug	29.4	89.0 (89.1)	140 (165)	909	Hurricane
0400 UTC 18 Aug	30.3	89.4	150	900	Landfall near Waveland, MS
0600 UTC 18 Aug	30.7	89.6	115 (100)	—	Hurricane
1200 UTC 18 Aug	32.0 (32.2)	89.9 (90.0)	75 (65)	—	Hurricane
1800 UTC 18 Aug	33.4	90.1	50	—	Tropical storm
0000 UTC 19 Aug	34.7	90.0	35 (30)	—	Tropical storm
0600 UTC 19 Aug	36.0	89.3	30	—	Tropical depression
1200 UTC 19 Aug	37.0	88.0	30	—	Tropical depression
1800 UTC 19 Aug	37.6 (37.7)	86.0	25	—	Tropical depression
0000 UTC 20 Aug	37.6 (38.0)	84.0 (84.8)	25	—	Tropical depression

TABLE I. Continued.

Time and date	Lat (°N)	Lon (°W)	Max wind speed (kt)	Central pressure (mb)	Storm status
0600 UTC 20 Aug	37.4	80.6 (80.2)	25	—	Tropical depression
1200 UTC 20 Aug	37.2 (37.3)	77.3 (77.0)	30 (25)	—	Tropical depression
1800 UTC 20 Aug	37.0	75.3 (75.1)	45 (30)	1000	Tropical storm
0000 UTC 21 Aug	36.7 (36.6)	73.6 (73.4)	50 (40)	—	Tropical storm
0600 UTC 21 Aug	36.7	70.9	55 (45)	—	Tropical storm
1200 UTC 21 Aug	37.1 (37.3)	68.1 (68.4)	60 (50)	—	Tropical storm
1800 UTC 21 Aug	37.8 (38.0)	64.7 (64.9)	60 (55)	—	Tropical storm
0000 UTC 22 Aug	39.2	61.8 (61.4)	55 (60)	—	Tropical storm
0600 UTC 22 Aug	40.8	58.2	45 (55)	—	Tropical storm
1200 UTC 22 Aug	43.0	54.0	35 (50)	—	Extratropical storm

the Kaplan and DeMaria (1995) inland decay model for TCs. Columbia, Mississippi, reported a “fastest mile” sustained wind of 104 kt about 4 h after landfall in or near the RMW. This value adjusts to 99 kt in converting to a peak 1-min wind (Powell et al. 1996). Application of the Kaplan–DeMaria model with a landfall intensity of 150 kt yields a value of 101 kt, which is close to the Columbia observation.

Other than the observation in Columbia, no anemometer measurement recorded extreme winds near the RMW, mainly because of the lack of anemometers in the landfall area. The highest observed sustained (roughly 10 min) winds in Camille were 113 kt, at which point the anemometer failed, at the Transworld drilling rig block 92 about halfway between the mouth of the Mississippi River and the Mississippi coast, at some point during the eye passage to the east. This measurement was almost certainly higher than 10 m above the ocean, but its exact altitude is unknown.

With the movement of Camille across the marshlands of northeastern St. Bernard Parish, Louisiana, category 5 winds are assessed to have occurred in Louisiana as well as Mississippi. Runs of the Schwerdt et al. (1979) parametric hurricane wind model suggest maximum sustained winds of 75–80 kt in far southwestern Alabama. Category 1 winds for Alabama would be consistent with the impacts observed just west of there in Pascagoula, Mississippi.

The original best track showed a brief landfall in southeastern Louisiana near the mouth of the Mississippi River just before 0000 UTC 18 August (Table 1). However, the numerous radar fixes available indicated that the center of the hurricane remained just offshore, which is consistent with the radar-based track shown in the *Preliminary Report* (Weather Bureau 1969). Camille passed over the marshy regions of northeastern St. Bernard Parish around 0230–0330 UTC 18 August, but no landfall point is indicated here because of the lack of dry land in the vicinity.

It should be noted that the original HURDAT format did not allow for nonsynoptic best-track points. The new HURDAT2 format allows for this, so that position and intensity at landfall can be accurately documented.

EXTRATROPICAL TRANSITION AND DISSIPATION OF CAMILLE.

The original best track did not indicate an extratropical stage occurred in Camille; however, Simpson et al. (1970) stated that extratropical transition (ET) did occur. Data examined during the reanalysis show that Camille became embedded within a frontal boundary by 1200 UTC 22 August and ET occurred at that time. The best track has been updated to clarify this by indicating ET at 1200 UTC 22 August. No change was introduced to the timing of Camille’s dissipation, which occurred just after extratropical transition.

COMPARISONS OF CAMILLE WITH OTHER U.S. CATEGORY 5 HURRICANES.

Three other category 5 Atlantic basin hurricanes are known to have struck the United States: the 1928 “San Felipe” hurricane in Puerto Rico, the 1935 “Labor Day” hurricane in the Florida Keys, and 1992’s Hurricane Andrew in southeast Florida. This record of U.S. category 5 hurricanes is likely complete since 1900. However, before that time, coastal U.S. populations were quite sparse—especially in parts of Florida, Louisiana, and Texas—and a category 5 could have struck the coast but not been recognized as such, or may have even been missed completely as one goes farther back in time. In comparing the MSLP and landfall intensity of these category 5 hurricanes, Camille, at 900 mb and 150 kt, ranks in intensity for U.S. hurricanes just below the 1935 Labor Day hurricane, at 892 mb and 160 kt (Landsea et al. 2014); however, it is slightly stronger than Andrew in 1992, at 922 mb and 145 kt (Landsea et al. 2004a), and the 1928 San Felipe hurricane in Puerto Rico, at 931 mb and 140 kt (Landsea et al. 2012), for strongest hurricanes at landfall.

SUMMARY. A reassessment of Hurricane Camille has introduced a number of significant changes into the best-track database:

Genesis time changed to 18 h earlier than originally indicated, at 0000 UTC 14 August.

Major intensity changes of least 20 kt from the original best-track values were introduced for Camille’s intensity at these time periods:

- an increase from 130 to 150 kt at 1800 UTC 16 August;
- a decrease from 160 to 140 kt at 1200 UTC 17 August;
- a decrease from 165 to 135 kt at 1800 UTC 17 August; and
- a decrease from 165 to 140 kt at 0000 UTC 18 August.

Additional intensity changes include reductions in the peak intensity of Camille from 165 to 150 kt and the timing of the peak intensity:

- previous peak intensity of 165 kt was just prior to the Mississippi landfall, at best-track points 1800 UTC 17 August and 0000 UTC 18 August;
- new peak intensity of 150 kt in the Gulf of Mexico at the time of the 908- and 905-mb readings, at 1800 UTC 16 August and 0000 UTC 17 August; and

- the peak intensity of 150 kt was reached again at the time of the Mississippi landfall at 0400 UTC 18 August.

At U.S. landfall at Waveland, Mississippi, at 0400 UTC 18 August, Camille is assessed to have struck with a central pressure of around 900 mb and an intensity of 150 kt. This is deeper but slightly weaker than the original 909-mb and 165-kt landfall intensity implied by the last entry in HURDAT2 before landfall at 0000 UTC 18 August.

A brief extratropical cyclone stage was formally documented at the last point in Camille’s life cycle at 1200 UTC 22 August, but no change to the dissipation timing was indicated.

No major changes were introduced for the track of Camille.

The reanalysis of Camille reconfirms that the devastating hurricane came ashore as a category 5 on the Saffir–Simpson hurricane wind scale, but it is now considered to be the second-most-intense hurricane in the United States’ record. After Camille’s revision, it is not anticipated that any other single storm will be reassessed out of sequence, as this completes analysis of all category 5 U.S.-landfalling hurricanes. The Atlantic Hurricane Database Reanalysis Project will continue to revise the HURDAT2 database through the end of the twentieth century and provide official updates to the database’s roughly 10 hurricane seasons every calendar year.

ACKNOWLEDGMENTS. This work has been sponsored by a grant from the NOAA Climate Program Office on “Atlantic basin tropical cyclone database reanalysis and impact of incomplete sampling.” The authors wish to thank the remainder of the NHC Best-Track Change Committee (Eric Blake, Todd Kimberlain, Richard Pasch, Gladys Rubio, and Eric Uhlhorn) for their comments and detailed suggestions leading to the final revisions to Camille’s best track (the third author on this paper is the chair of the committee). Sandy Delgado provided the revised track map for Camille. Special thanks to Scott Stephens and Gregory Hammer of National Climate Data Center for providing copies of the original archived WSR-57 radar imagery for Camille. Special thanks also Trish Nugent, C. A., special collections and archives coordinator, Monroe Library, Loyola University, New Orleans, for providing access to the Nash Roberts Camille archive papers. Thanks to Hugh Willoughby for assisting with the 901-mb sonde analysis. Many thanks to Louis M. Kyriakouides, Ph.D., director of the Center for Oral History and Cultural Heritage at the University of Southern

Mississippi, for directly providing scans of the 1984 Camille interviews. Many thanks to William E. (Eddie) Coleman of the Hancock County Historical Society for providing the post-Camille photo of the Breath home. Thanks also are provided to Gloria Aversano, the NHC librarian, for tirelessly tracking down additional sources in support of this reanalysis. Alex Fierro, Dan Lindsey, Bobbi Schwarz-Biederman, Kevin Tyle, and Ryan Wade all provided a scanned version of Camille's infrared image that was on the front cover of the September 1971 *Bulletin of the American Meteorological Society*. Maritza Ballester graciously provided Cuban archive information from Camille, including scanned hand-drawn synoptic maps. Finally, Eric Blake, Sandy Delgado, and Eric Uhlhorn provided helpful reviews of an earlier version of this paper. The first author would also like to acknowledge her advisor, Prof. Haiyan Jiang.

REFERENCES

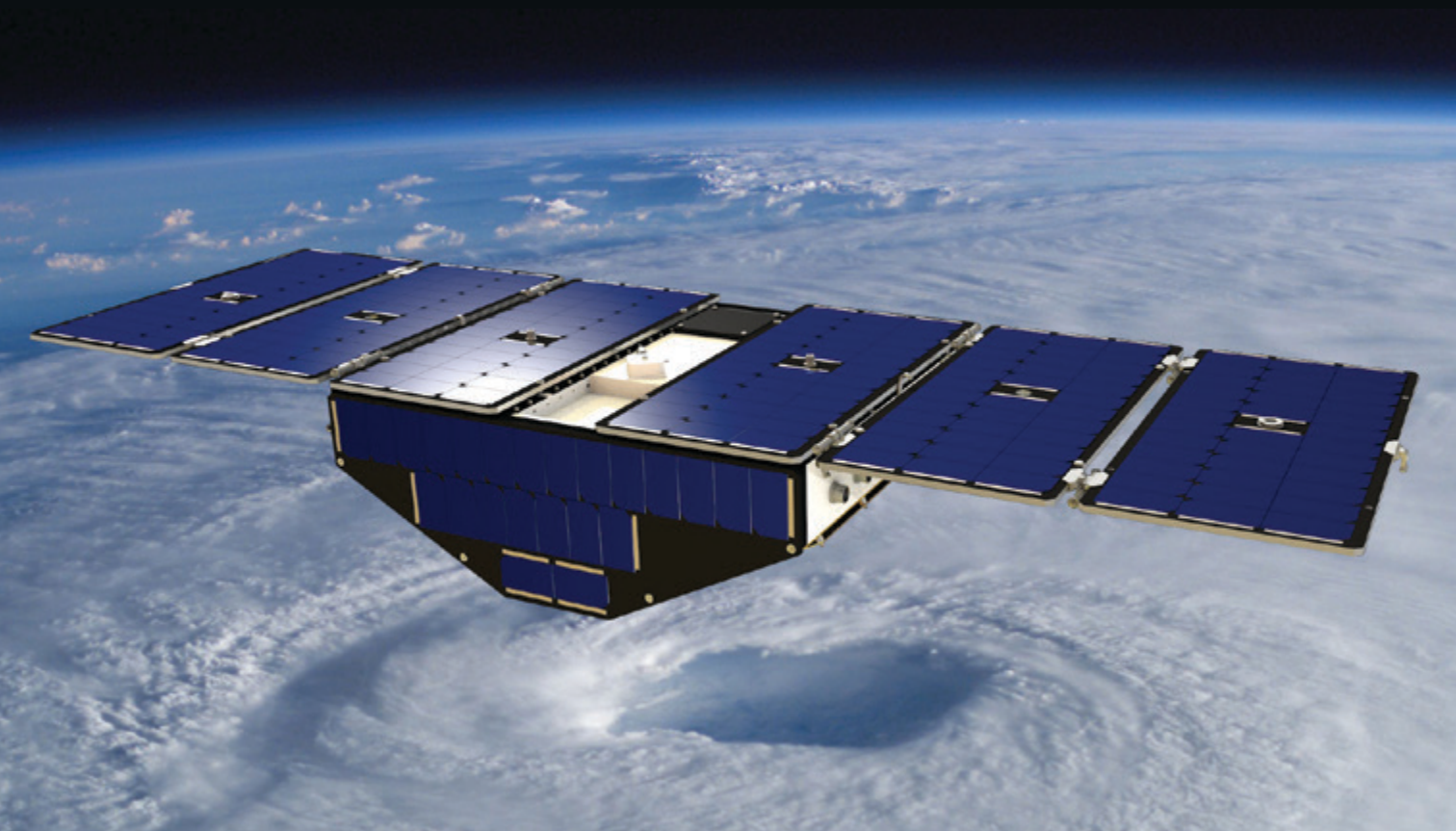
- Allison, L. J., G. T. Cherrix, and H. Ausfresser, 1971: Color analysis of Hurricane Camille, 1969, using Nimbus infrared radiation data. *Bull. Amer. Meteor. Soc.*, **52**, 862 and cover page.
- Brown, D. P., J. L. Franklin, and C. W. Landsea, 2006: A fresh look at tropical cyclone pressure–wind relationships using recent reconnaissance-based “best track” data (1998–2005). *27th Conf. on Hurricanes and Tropical Meteorology*, Monterey, CA, Amer. Meteor. Soc., 3B.5. [Available online at https://ams.confex.com/ams/27Hurricanes/techprogram/paper_107190.htm.]
- DeAngelis, R. M., 1970: North Atlantic tropical cyclones, 1969. *Mariners Wea. Log*, **14**, 1–11.
- , and E. R. Nelson, 1969: Hurricane Camille, August 5–22, 1969. *Climatological Data National Summary*, No. 8, U.S. Department of Commerce/NOAA/Environmental Data Service, Asheville, NC, 451–475.
- Dvorak, V. F., 1984: Tropical cyclone intensity analysis using satellite data. NOAA Tech. Rep. NESDIS 11, 47 pp.
- ESSA, 1969: Hurricane Camille—A report to the administrator. Department of Commerce Rep. ESSA/PI 690034, 30 pp.
- Hagen, A. B., D. Strahan-Sakoskie, and C. Lockett, 2012: A reanalysis of the 1944–53 Atlantic hurricane seasons—The first decade of aircraft reconnaissance. *J. Climate*, **25**, 4441–4460, doi:10.1175/JCLI-D-11-00419.1.
- Hamilton, R. C., and D. B. Steere, 1969: Covering Hurricane Camille, 17 August 1969. Ocean Data Gathering Program Rep. 2, Baylor Company, 136 pp.
- Hebert, P. J., and G. Taylor, 1978: The deadliest, costliest, and most intense United States hurricanes of this century (and other frequently requested hurricane facts). NOAA Tech. Memo. NWS NHC 7, 24 pp. [Available online at www.nhc.noaa.gov/pdf/NWS-NHC-1978-7.pdf.]
- Kaplan, J., and M. DeMaria, 1995: A simple empirical model for predicting the decay of tropical cyclone winds after landfall. *J. Appl. Meteor.*, **34**, 2499–2512, doi:10.1175/1520-0450(1995)034<2499:ASEMFP>2.0.CO;2.
- Kimball, S. K., and M. S. Mulekar, 2004: A 15-year climatology of North Atlantic tropical cyclones. Part I: Size parameters. *J. Climate*, **17**, 3555–3575, doi:10.1175/1520-0442(2004)017<3555:AYCONA>2.0.CO;2.
- Landsea, C. W., and J. L. Franklin, 2013: Atlantic hurricane database uncertainty and presentation of a new database format. *Mon. Wea. Rev.*, **141**, 3576–3592, doi:10.1175/MWR-D-12-00254.1.
- , and Coauthors, 2004a: A reanalysis of Hurricane Andrew's intensity. *Bull. Amer. Meteor. Soc.*, **85**, 1699–1712, doi:10.1175/BAMS-85-11-1699.
- , and Coauthors, 2004b: The Atlantic Hurricane Database Re-Analysis Project: Documentation for the 1851–1910 alterations and additions to the HURDAT database. *Hurricanes and Typhoons: Past, Present, and Future*, R. J. Murnane and K.-B. Liu, Eds., Columbia University Press, 177–221.
- , and Coauthors, 2008: A reanalysis of the 1911–20 Atlantic hurricane database. *J. Climate*, **21**, 2138–2168, doi:10.1175/2007JCLI1119.1.
- , S. Feuer, A. Hagen, D. A. Glenn, J. Sims, R. Perez, M. Chenoweth, and N. Anderson, 2012: A reanalysis of the 1921–30 Atlantic hurricane database. *J. Climate*, **25**, 865–885, doi:10.1175/JCLI-D-11-00026.1.
- , A. Hagen, W. Bredemeyer, C. Carrasco, D. A. Glenn, A. Santiago, D. Strahan-Sakoskie, M. Dickinson, 2014: A reanalysis of the 1931–43 Atlantic hurricane database. *J. Climate*, **27**, 6093–6118, doi:10.1175/JCLI-D-13-00503.1.
- Loyola University, 2001: Nash Roberts hurricane papers, 1948–2000. 57 Boxes, 7 Portfolios. [Available Monroe Library, Loyola University, 6368 St. Charles Avenue, Suite 198, New Orleans, LA 70118.]
- Mississippi Test Facility, 1969: Hurricane Camille enters Mississippi—August 17, 1969. [Available online at www.nhc.noaa.gov/archive/storm_wallets/cdmp/.]
- NHC, 1969: Tropical Cyclone Storm Wallet Electronic Archive: Camille. [Available online at www.nhc.noaa.gov/archive/storm_wallets/cdmp/.]
- OFCM, 1997: National hurricane operations plan. U.S. Department of Commerce/NOAA Rep. FCM-P12-1997, 150 pp.
- Parmenter, F. C., 1969: Picture of the month—Hurricane Camille. *Mon. Wea. Rev.*, **97**, 828–829, doi:10.1175/1520-0493(1969)097<0828:HC>2.3.CO;2.

- Pasch, R. J., E. S. Blake, H. D. Cobb III, and D. P. Roberts, 2006: Hurricane Wilma, 15–25 October 2005. National Hurricane Center Tropical Cyclone Rep., 27 pp. [Available online at www.nhc.noaa.gov/data/tcr/AL252005_Wilma.pdf.]
- Powell, M. D., S. H. Houston, and T. A. Reinhold, 1996: Hurricane Andrew's landfall in south Florida. Part I: Standardizing measurements for documentation of surface wind fields. *Wea. Forecasting*, **11**, 304–328, doi:10.1175/1520-0434(1996)011<0304:HALISF>2.0.CO;2.
- Pyle, R. W., 1984: An oral history with Charles and Mary Breath, Hurricane Camille survivors. Vol. 228. [Available from the Mississippi Oral History Project, Center for Oral History and Cultural Heritage, University of Southern Mississippi, 118 College Drive, Hattiesburg, MS 39406-0001.]
- Rappaport, E. N., J. L. Franklin, A. B. Schumacher, M. DeMaria, L. K. Shay, and E. J. Gibney, 2010: Tropical cyclone intensity change before U.S. Gulf Coast landfall. *Wea. Forecasting*, **25**, 1380–1396, doi:10.1175/2010WAF2222369.1.
- Schwerdt, R. W., F. P. Ho, and R. R. Watkins, 1979: Meteorological criteria for standard project hurricane and probable maximum hurricane wind fields, Gulf and East Coasts of the United States. NOAA Tech. Rep. NWS 23, 317 pp.
- Sheets, B., and J. Williams, 2001: *Hurricane Watch: Forecasting the Deadliest Storms on Earth*. Vintage Books, 331 pp.
- Shenk, W. E., and E. B. Rodgers, 1978: Nimbus 3/ATS 3 observations of the evolution of Hurricane Camille. *J. Appl. Meteor.*, **17**, 458–476, doi:10.1175/1520-0450(1978)017<0458:NOOTEO>2.0.CO;2.
- Simpson, R. H., and Coauthors, 1970: The Atlantic hurricane season of 1969. *Mon. Wea. Rev.*, **98**, 293–306, doi:10.1175/1520-0493-98.4.293.
- Vickery, P. J., P. F. Skerlj, and L. A. Twisdale, 2000: Simulation of hurricane risk in the U.S. using empirical track model. *J. Struct. Eng.*, **126**, 1222–1237, doi:10.1061/(ASCE)0733-9445(2000)126:10(1222).
- Weather Bureau, 1969: Hurricane Camille—August 14–22, 1969. Preliminary Rep., U.S. Department of Commerce, Environmental Science Services Administration, 58 pp.
- Willoughby, H. E., J. A. Clos, and M. B. Shoreibah, 1982: Concentric eyewalls, secondary wind maxima, and the development of the hurricane vortex. *J. Atmos. Sci.*, **39**, 395–411, doi:10.1175/1520-0469(1982)039<0395:CEWSWM>2.0.CO;2.
- Woodruff, S. D., R. J. Slutz, R. L. Jenne, and P. M. Steurer, 1987: A comprehensive ocean–atmosphere data set. *Bull. Amer. Meteor. Soc.*, **68**, 1239–1250, doi:10.1175/1520-0477(1987)068<1239:ACOADS>2.0.CO;2.

NEW OCEAN WINDS SATELLITE MISSION TO PROBE HURRICANES AND TROPICAL CONVECTION

BY CHRISTOPHER S. RUF, ROBERT ATLAS, PAUL S. CHANG, MARIA PAOLA CLARIZIA, JAMES L. GARRISON, SCOTT GLEASON, STEPHEN J. KATZBERG, ZORANA JELENAK, JOEL T. JOHNSON, SHARANYA J. MAJUMDAR, ANDREW O'BRIEN, DEREK J. POSSELT, AARON J. RIDLEY, RANDALL J. ROSE, AND VALERY U. ZAVOROTNY

The CYGNSS constellation of eight satellites, scheduled to launch in 2016, will measure hurricane-force ocean-surface wind speed in the presence of precipitation encountered in the inner core of hurricanes.



The Cyclone Global Navigation Satellite System (CYGNSS) is a constellation of eight small satellites designed to measure ocean surface wind speed with high temporal resolution, 25-km spatial resolution, and extensive spatial coverage, under all precipitating conditions and over the full dynamic range of wind speeds experienced in a tropical cyclone (TC). Near-surface winds over the ocean are major contributors to and indicators of momentum and energy fluxes at the air–sea interface. The mission’s goal is to better understand the coupling between surface winds and the moist atmosphere within a TC. CYGNSS will provide surface winds in the TC inner core, including regions beneath the eyewall and rainbands that could not previously be measured from space owing to attenuation and scattering by the rain and ice aloft. Mission simulation studies predict typical revisit times in hours, which is a dramatic improvement over multiple-day revisit times obtained with individual spaceborne scatterometers. The CYGNSS wind fields, when combined with precipitation fields sampled as frequently [e.g., as produced by the Global Precipitation Measurement (GPM) core satellite and its constellation of precipitation imagers], will map the evolution of both the precipitation and underlying wind fields throughout complete TC life cycles. Together, they will provide coupled observations of moist atmospheric thermodynamics and ocean surface response, enabling new insights into TC inner-core dynamics and energetics.

SCIENTIFIC MOTIVATION. TC track forecasts have improved in accuracy by approximately 50% since 1990, largely as a result of improved mesoscale and synoptic modeling and data assimilation. During the same period, improvements in intensity forecasting have been relatively modest, although recent advances in high-resolution modeling have shown promise (Gall et al. 2013). The lack of improvement in intensity forecast skill has, in part, resulted from inadequate observations and modeling of the inner core of the storm. Observations of the inner core by the current suite of spaceborne remote sensing instruments tend to be obscured by the intense precipitation found in the eyewall and inner rainbands. In addition, the current suite of polar-orbiting instruments tends to inadequately sample the shorter time-scale stages of the TC life cycle such as rapid intensification.

The value of wind observations in precipitating conditions. In addition to the rainbands and eyewall of tropical cyclones, precipitation-producing tropical deep convection exhibits organization on a wide range of spatial and temporal scales. In particular, mesoscale convective systems (MCSs) contribute more than half of the total rainfall in the tropics (Rickenbach and Rutledge 1998; Nesbitt et al. 2000) and serve as the precursors to TCs (Houze 2004, and references therein). MCSs are affected by feedback on the sensible and latent heat fluxes at the ocean surface, as well as on their structure and propagation velocity. Over the ocean, the organization of the fluxes depends on a complex interaction between surface-level winds and storm dynamics (Houze 2004). MCS development and characteristics depend critically on the interaction between ocean surface properties, moist atmospheric thermodynamics, radiation, and convective dynamics (Stephens et al. 2004). In addition to producing the bulk of the rainfall in the tropics, MCSs also play a key role in the formation and propagation of the Madden–Julian oscillation (MJO), which directly influences the genesis of tropical storms in the Pacific Ocean and Caribbean Sea.

Understanding MJO structure and improving its forecasting require detailed knowledge of the convective environment. Existing measurement systems are capable of characterizing the thermodynamic environment and rain rate associated with the MJO, but information about the surface winds has been limited. Conventional satellite scatterometer measurements are capable of observing the frequency and characteristics of the MJO, but their effectiveness is significantly reduced by their inability to observe surface-level winds in heavy precipitation (Arguez

AFFILIATIONS: RUF, CLARIZIA, POSSELT, AND RIDLEY—University of Michigan, Ann Arbor, Michigan; ATLAS—NOAA/AOML, Miami, Florida; CHANG AND JELENAK—NOAA/NESDIS/STAR, College Park, Maryland; GARRISON—Purdue University, West Lafayette, Indiana; GLEASON AND ROSE—Southwest Research Institute, Boulder, Colorado; KATZBERG*—NASA LaRC, Hampton, Virginia; JOHNSON AND O'BRIEN—The Ohio State University, Columbus, Ohio; MAJUMDAR—University of Miami, Coral Gables, Florida; ZAVOROTNY—NOAA/ESRL, Boulder, Colorado

* Retired

CORRESPONDING AUTHOR: Prof. Christopher Ruf, Dept. of Climate and Space, University of Michigan, 2455 Hayward St., Ann Arbor, MI 48109-2143

E-mail: cruf@umich.edu

The abstract for this article can be found in this issue, following the table of contents.

DOI:10.1175/BAMS-D-14-00218.1

A supplement to this article is available online (10.1175/BAMS-D-14-00218.2)

In final form 31 May 2015

©2016 American Meteorological Society

Prediction of Hurricane Cindy using QuikSCAT Data

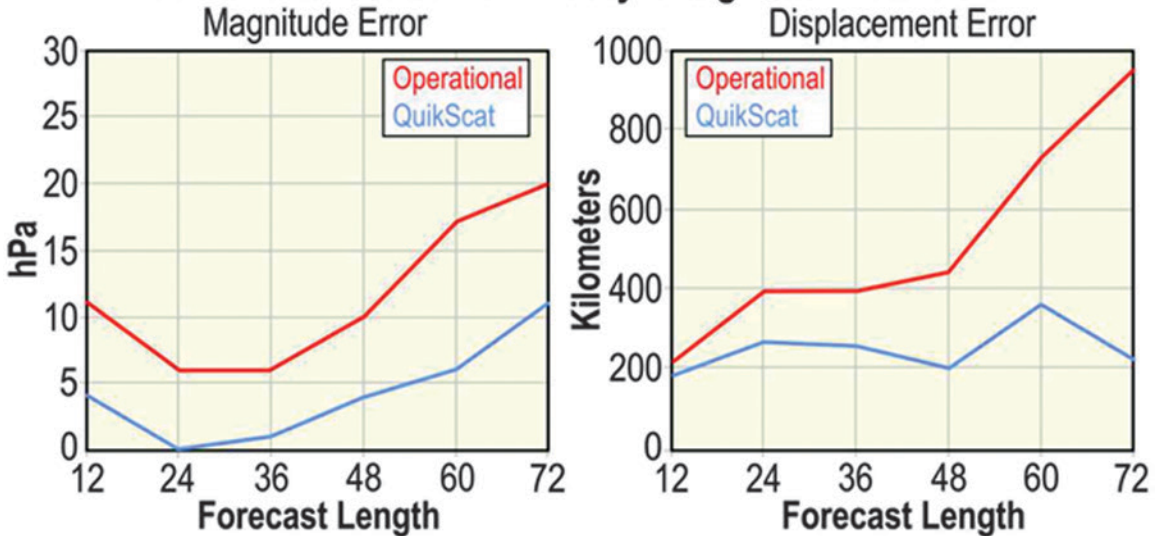


FIG. 1. Hurricane Cindy case study of the impact of satellite wind field observations on (left) intensity and (right) position forecast error (Atlas et al. 2005a). Both forecasts use the NCEP operational data assimilation system and forecast model in place at the time of the study. The “operational” run used all ground-based and satellite data that were assimilated operationally, including satellite atmospheric sounders but not QuikSCAT surface winds. The “QuikSCAT” run used all operational data plus the QuikSCAT surface winds. Neither run used any bogus data or vortex relocation. This case demonstrates the potential for satellite surface wind data to improve TC predictions, but it does not imply that this level of improvement would occur in all cases.

et al. 2005). The limitations of existing spaceborne measurements of ocean surface winds under precipitating conditions become even more severe in TCs. As a result, in the absence of reconnaissance aircraft, the availability and accuracy of wind speed estimates in the TC inner core are often highly compromised. For example, errors in operational estimates of intensity using the Dvorak technique are over 2.5 m s^{-1} in about half of all cases and over 6 m s^{-1} in a quarter of all cases. Large outliers in intensity estimation error also exist (Brown and Franklin 2004).

The value of frequent wind observations. Most current spaceborne active and passive microwave instruments are in polar low-Earth orbits (LEOs). The orbits maximize global coverage but can result in large gaps in the tropics. Schlax et al. (2001) present a comprehensive analysis of the sampling characteristics of conventional polar-orbiting swath-based imaging systems, including consideration of so-called tandem missions. The study demonstrates that a single broad-swath, high-resolution scatterometer system cannot resolve synoptic-scale spatial detail everywhere on the globe, and in particular not in the tropics. The irregular and infrequent revisit times (typically 11–35 h) are likewise not sufficient to resolve synoptic-scale temporal variability. Missed sampling of an organized

storm system can occur when it passes through an imager’s coverage gap or when its motion is offset from the motion of the imager’s swath.

The value of wind observations for tropical cyclone forecasting. Observations of sea surface winds, waves, and rain-rate conditions are among the most important factors in both improving our understanding of TCs and predicting them operationally. Climatologists, oceanographers, and operational forecasters use wind information principally in three ways: 1) to improve fundamental knowledge about atmospheric phenomena, such as El Niño, TCs, and large-scale tropical oscillations; 2) to provide input forcing for deterministic models of the coupled ocean–atmosphere system; and 3) to improve the accuracy and reliability of, and to extend the lead time for, forecasts of TCs (Atlas et al. 2001, 2005b).

A case of strong positive impact of satellite wind observations on TC forecast skill is illustrated by the 60-h forecast of Hurricane Cindy that had been performed with an earlier version of the National Centers for Environmental Prediction (NCEP) operational system, with and without QuikSCAT wind fields (Atlas et al. 2005a). Errors in the forecast of storm intensity and track are shown in Fig. 1. The intensity forecast error (error in forecasting the maximum air

pressure depression in the TC core) is reduced by approximately 50% or more with QuikSCAT for all forecast lengths. The track forecast error (error in forecasting the location of the TC eye) also grows much more slowly with forecast length when wind field data are included, reaching approximately 200-km error at 72 h as opposed to approximately 1000 km when no satellite data are included. This case is one example of the potential that satellite surface wind data have to improve tropical cyclone predictions, but this level of improvement does not occur in all cases.

GNSS BISTATIC SCATTEROMETRY. The CYGNSS mission uses a bistatic radar method (i.e., transmitter and receiver in different locations) for measuring winds, as opposed to the monostatic method (i.e., transmitter and receiver on the same satellite) used by traditional scatterometers. The use of satellite navigation signals as the transmitter half of a bistatic radar for Earth remote sensing is commonly referred to as Global Navigation Satellite System reflectometry (GNSS-R). There are a number

of navigation satellite systems currently in operation, the most common being the global positioning system (GPS). The GNSS-R technique benefits from significantly reduced sensor requirements as compared to traditional scatterometers, since no transmitter is required on the “receive only” spacecraft.

Airborne development of ocean surface wind retrieval by GNSS-R. The first GNSS-R sensor, based on a commercial GPS chipset, was field tested in 1997 over the Chesapeake Bay, collecting GPS signals scattered from the water surface (Garrison et al. 1998). One year later, the relationship between the ocean surface slope probability density and the modulation of the navigation signal caused by scattering from the rough ocean surface was identified, along with the relationship to surface wind speed (Lin et al. 1998). Shortly thereafter, a theoretical framework was developed to characterize the magnitude and spectral and temporal dependencies of the received GNSS signal as functions of the sea state, the measurement geometry, and the signal processing performed by the receiver (Zavorotny and Voronovich 2000). A number of airborne flight campaigns were conducted to continue the study of the sea state–GNSS signal relationship (Garrison et al. 2002).

GNSS-R receivers also began to be deployed on NOAA “hurricane hunter” aircraft to expand the study to very high wind speeds. In 2000, the first GPS-reflected data were acquired inside a TC (Katzberg et al. 2001). Since that time, penetration data inside TCs have been acquired during nearly every Atlantic hurricane season. Wind speed retrievals have been compared to a large set of dropwindsonde data and show the GPS method to be capable of responding well to wind speeds of 40 m s⁻¹ or less (Katzberg et al. 2006; Katzberg and Dunion 2009). It should be noted that a small wind direction dependence is likely also present in the data, but it has not yet been fully characterized or incorporated into a retrieval algorithm.

CYGNSS uses the GPS “L1” channel at 1575 MHz (19-cm wavelength), which suffers no appreciable attenuation at even severe rainfall rates. An example of wind speed retrieval in the presence of high rain rates is given in Fig. 2, which shows the wind speed retrieved by a GNSS-R instrument and by the Stepped Frequency Microwave Radiometer (SFMR) during a NOAA P-3 aircraft overpass of Hurricane Bill on 19 August 2009. The rain rate retrieved by SFMR is also shown. SFMR surface observations are directly below the aircraft, with passage through the hurricane eye occurring at elapsed times 6600–6700 s. GNSS-R surface observations are displaced away from

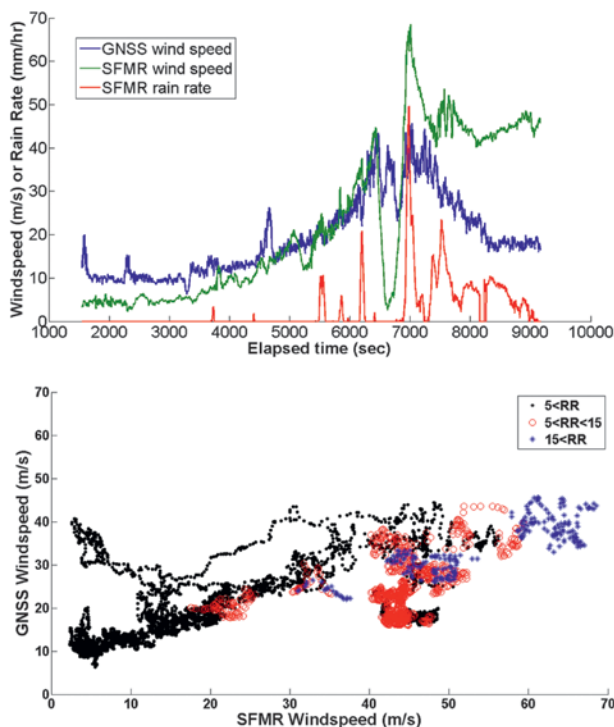


FIG. 2. (top) Time series of the wind speed retrieved by a GNSS-R instrument and by the SFMR during a NOAA P-3 aircraft overpass of Hurricane Bill on 19 Aug 2009. The rain rate retrieved by SFMR is also shown. (bottom) Scatterplot of the GNSS-R- and SFMR-retrieved winds, divided into low, moderate, and heavy rain conditions as determined by the SFMR rain-rate retrieval.

nadir by the specular scattering geometry between the GPS satellite transmitter and the receiver on the aircraft. As such, the two wind measurements are not collocated and a direct comparison between them should not be expected to result in a 1:1 agreement. For example, the transect of the GNSS-R measurements misses the eye during this overpass. A scatterplot of the SFMR and GNSS-R wind speeds is shown in the bottom panel of Fig. 2. It is divided into low, moderate, and heavy rain conditions, as determined by the SFMR rain-rate retrieval, to illustrate that there is no significant difference in the relationship between the two wind speeds as the rain rate varies.

Spaceborne demonstration of ocean surface wind retrieval by GNSS-R. The first successful detection of a GPS-reflected signal in space was reported by Lowe et al. (2002). Subsequently, data from the GPS experiment on the U.K. *Disaster Monitoring Constellation* (UK-DMC) satellite demonstrated that measurements of sufficient signal-to-noise ratio (SNR) could be used to perform successful ocean wave and wind estimation (Gleason et al. 2005, 2010; Clarizia et al. 2009, 2014). These results show that it is possible to detect reflected GPS signals from space across a range of surface wind and wave conditions using a relatively modest instrument configuration. Notably, the UK-DMC sensor had a lower receiver antenna gain (11.8 dBi) and is in a higher orbit (686 km) than the CYGNSS design (14 dBi and 510 km, respectively). Therefore, CYGNSS measurements are expected to have better sensitivity to changes in surface conditions.

The measurements made by a GNSS-R bistatic radar are referred to as delay Doppler maps (DDMs). These are maps of the power in the GNSS signal scattered by the ocean surface after the signals are selectively filtered by time delay and Doppler shift. The time delay is the difference in time of arrival between the direct signal (propagating directly from the transmitting to the receiving satellite) and the signal scattered by the ocean surface. The Doppler shift is the difference in frequency between the signal emitted by the transmitting satellite and the one received from the ocean surface. Both delay and Doppler are varied in the DDM across a range that includes the (delay, Doppler) coordinates of the nominal specular reflection point on the surface with respect to mean sea level. Shorter delays generally correspond to locations above the surface, from which there is no significant scattered signal. Longer delays correspond to isodelay contours on the surface that are centered on the specular point. Doppler values above and below that of the specular point correspond to iso-Doppler

contours on the surface to either side of it. The DDM is thus a map of the diffuse surface scattering in the vicinity of the nominal specular point. The transformation between spatial location on the sea surface and location in the DDM is one to one at the DDM specular location, but it can have ambiguities (i.e., multiple spatial locations mapped to the same DDM location) outside the specular region. Examples are shown in Fig. 3 of DDMs measured by the UK-DMC receiver at low, average, and higher wind speed conditions. In each case, the scattered power is highest near the specular point (the top of the “horseshoe” arc in the figure). However, the peak power decreases as the wind speed increases, owing to higher ocean roughness, and the diffuse scattering away from the specular point conversely increases with increasing wind speed and roughness.

Results from the UK-DMC experiment demonstrate a connection between the near-surface wind speed and the measured DDMs. The UK-DMC measurements were made when the specular reflection point passed within 50 km of an active National Data Buoy Center (NDBC) ocean buoy, which provides near-surface (10-m referenced) wind information (Gleason 2013). One example of wind retrieval performance using UK-DMC data is described by Clarizia et al. (2014), in which a minimum variance (MV) wind speed estimator is developed and tested. The estimator is a composite of winds retrieved using five different observables that are derived from the DDMs. Regression-based wind retrievals are developed for each individual observable using empirical geophysical model functions that are derived from NDBC buoy–wind matchups. The root-mean-square (RMS) error in the MV estimator, for wind speeds over the range 2–12 m s⁻¹, is 1.65 m s⁻¹.

CYGNSS MISSION DESCRIPTION. The CYGNSS constellation is composed of eight observatories, evenly spaced about a common orbit plane at 510-km altitude and 35° inclination angle. Each observatory contains a delay Doppler mapping instrument (DDMI) that consists of a multichannel GNSS-R receiver, a low-gain zenith antenna for reception of the direct signals, and two high-gain nadir antennas for reception of the surface scattered signals (Rose et al. 2012; Ruf et al. 2012). There are typically many specular reflections from the surface available at any given time because of the large number of GPS-transmitting satellites. Each DDMI selects the four specular reflections located in the highest sensitivity region of its nadir antenna pattern and simultaneously computes DDMs centered on each of

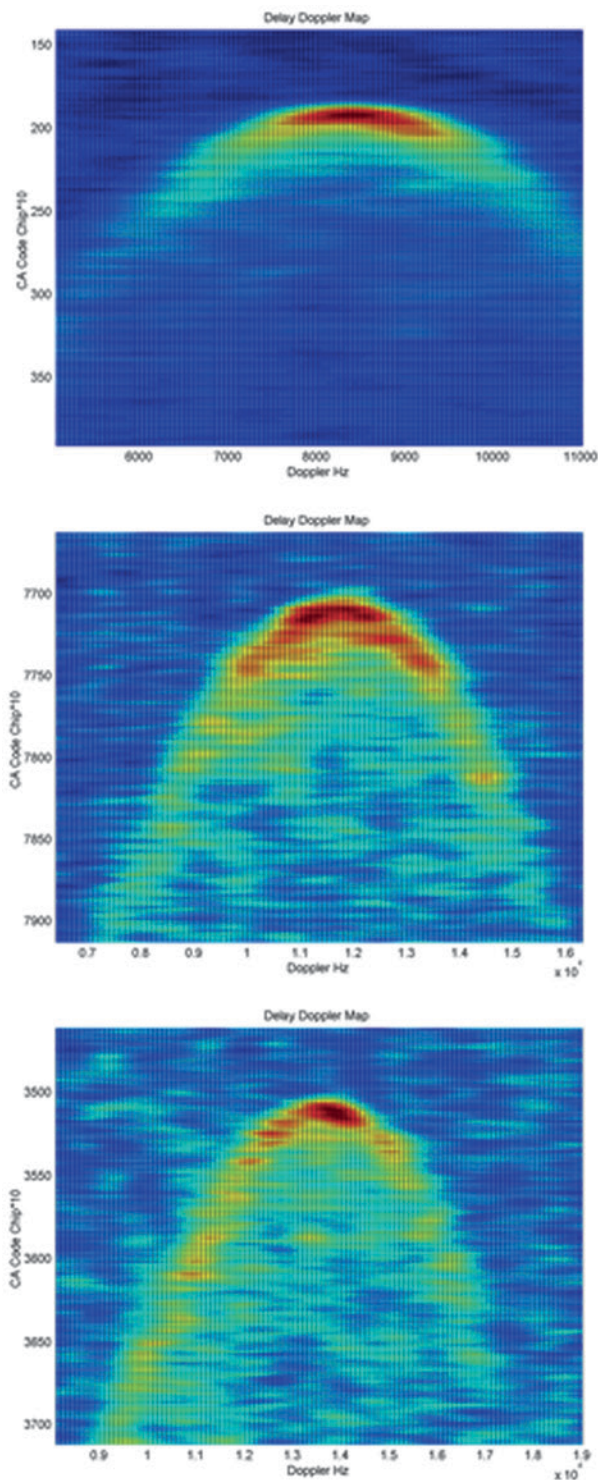


FIG. 3. DDMs of scattered power from the ocean surface as measured by the UK-DMC GNSS-R bistatic radar receiver during NDBC buoy overpasses for three wind speed conditions: (top) 2, (middle) 7, and (bottom) 10 m s⁻¹. The highest power occurs at the specular reflection point (the top of the horseshoe-shaped arc). Diffuse scattered power, away from the specular point, increases as the ocean surface roughness increases due to strengthening winds (Gleason 2006).

them. Individual DDM integration times last 1 s and wind speeds are derived from measurements over a 25×25 km² region centered on the specular point. This results in a total of 32 wind measurements per second by the full constellation. CYGNSS spatial sampling consists of 32 simultaneous single pixel “swaths” that are 25 km wide and, typically, hundreds of kilometers long, as the specular points move across the surface owing to orbital motion by CYGNSS and the GPS satellites. This sampling process is illustrated by an animation available online (<http://dx.doi.org/10.1175/BAMS-D-14-00218.2>). Examples of the spatial coverage obtained after 90 min (one orbit) and 24 h are shown in the top and middle panels of Fig. 4. Temporal sampling occurs randomly owing to the asynchronous nature of the CYGNSS and GPS satellite orbits. As a result, the CYGNSS revisit time is best described by its probability distribution. The distribution, shown in the bottom panel of Fig. 4, is derived empirically using a mission simulator to determine the time and location of each sample within the $\pm 38^\circ$ -latitude coverage zone and then examining the time difference between samples at the same location. The empirical distribution features a high probability of very short revisit times (e.g., resulting from sequential samples by trailing satellites spaced tens of minutes apart) and a long tapering “tail” at higher revisit times. Its median value is 2.8 h and the mean revisit time is 7.2 h.

Wind speed retrieval algorithm. The baseline wind speed retrieval algorithm planned for CYGNSS is an extension of one previously developed for the UK-DMC spaceborne mission, as described in Clarizia et al. (2014) and summarized in the section “Spaceborne demonstration of ocean surface wind retrieval by GNSS-R.” The algorithm uses an empirically derived geophysical model function to estimate the 10-m referenced wind speed from the measured DDM within a 25×25 km² region centered on the specular reflection point. The UK-DMC algorithm has been extended to higher wind speeds by applying a detailed end-to-end simulator of the CYGNSS measurements to a realistic nature run simulation of the full life cycle of a category-4 hurricane (Nolan et al. 2013). The end-to-end simulator models the complete bistatic radar measurement process, including electromagnetic propagation down from the GPS satellite to the ocean surface, rough surface scattering by the ocean, propagation back up to the CYGNSS satellite, and the engineering design of the CYGNSS GNSS-R receiver (O’Brien 2014). A large population of simulated DDMs, covering a wide dynamic range

of wind speeds, is generated and used to extend the geophysical model function from the lower wind speed regime experienced by UK-DMC to the much higher winds of interest to CYGNSS. The RMS wind speed retrieval error is expected to meet or exceed the mission requirement of 2 m s^{-1} or 10% of the wind speed, whichever is greater.

Postlaunch calibration and validation plans.

The primary objectives of the calibration and validation effort are to characterize the geophysical model function, evaluate the performance of each sensor, evaluate the retrieval algorithm, and evaluate the retrieved wind speeds. The first step in this process is collocating various “truth” data with the CYGNSS data. These truth data include numerical model output parameters, GPS dropsondes, other satellite data [e.g., Advanced Scatterometer (ASCAT), *Ocean Satellite (Oceansat)-2* Scatterometer (OSCAT), wind-measuring satellite system (WindSat), Advanced Microwave Scanning Radiometer-2 (AMSR2)], and aircraft-based measurements. The next steps involve statistical analyses of the collocation database. The geophysical model function is characterized and any unexpected artifacts or trends are analyzed. The collocation database is also used to evaluate measurement performance relative to the instrument characteristics and measurement geometry for each sensor. The wind speed retrieval algorithm is analyzed and its strengths and weaknesses

are characterized. Quality control flags are developed based on these analyses to be included with the final product files provided to the end users. Another facet of the wind speed retrieval validation will be in the

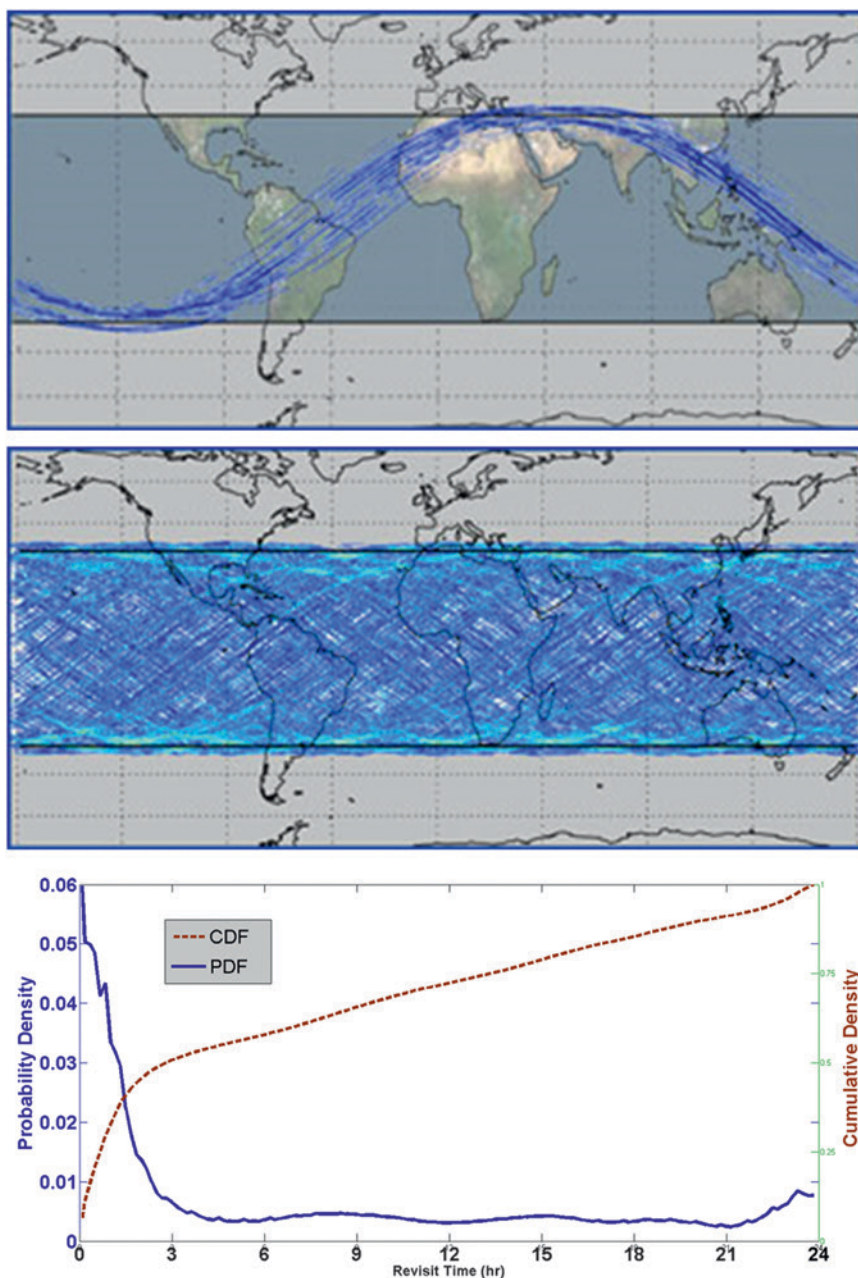


FIG. 4. Each LEO CYGNSS observatory will orbit at an inclination of 35° and be capable of measuring four simultaneous reflections, resulting in 32 wind measurements per second across the globe. The configuration is optimized allowing for high-temporal-resolution wind field imagery of TC genesis, intensification, and decay. Shown here are the CYGNSS spatial coverage tracks after (top) 90 min and (middle) 24 h. (bottom) Temporal sampling is characterized by the probability and cumulative density functions of revisit time. Sampling occurs randomly because of the asynchronous nature of the CYGNSS and GPS satellite orbits, and revisit time is best characterized via statistics of these distributions. The median and mean revisit times are 2.8 and 7.2 h, respectively.

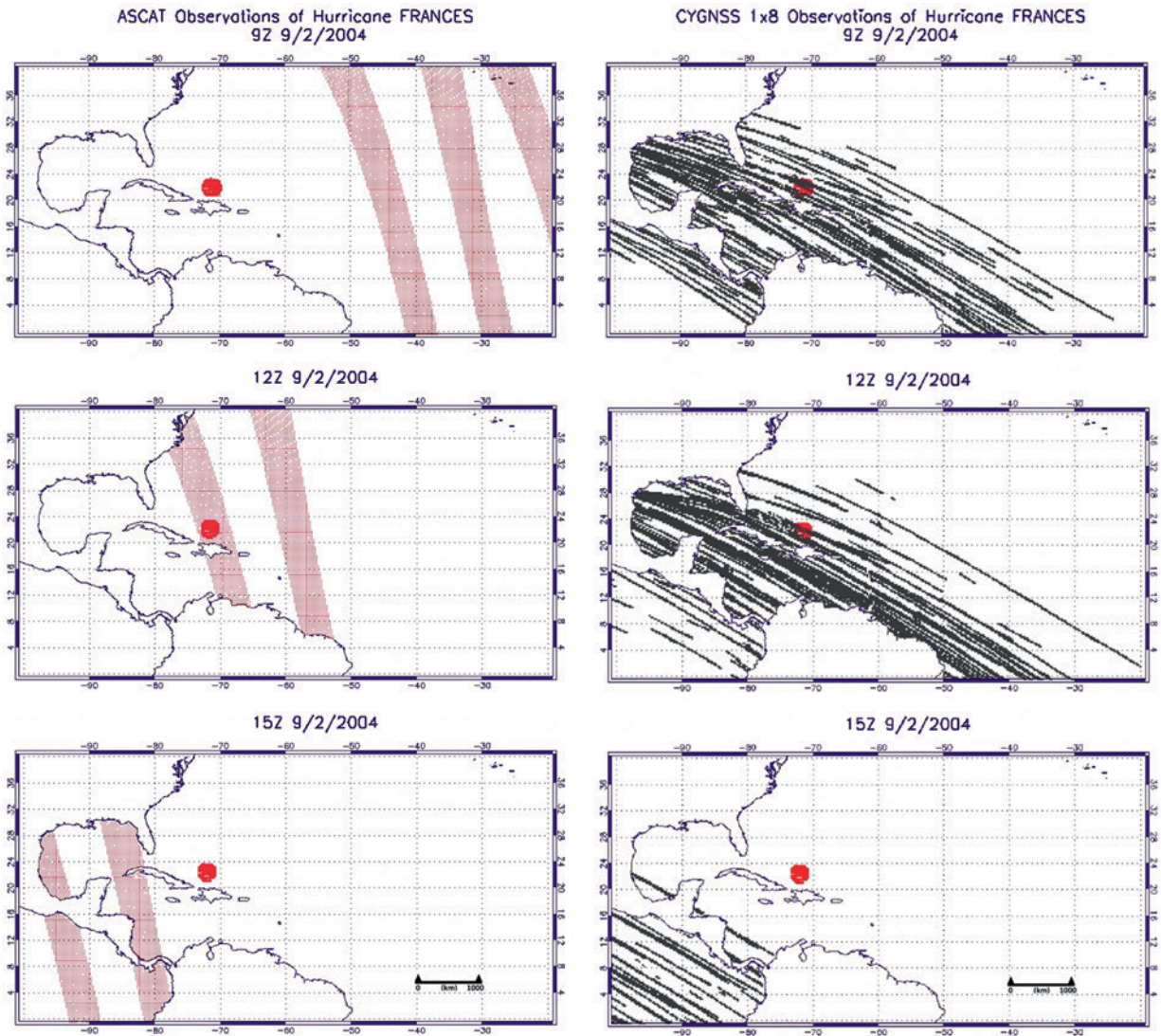


FIG. 5. Time-lapse simulation comparing the spatial and temporal sampling properties of CYGNSS and ASCAT if they had both been in orbit during the Hurricane Frances U.S. landfall on 2 Sep 2004 (Ruf et al. 2012). Each row shows all samples made over successive 3-h intervals and by (left) ASCAT and (right) CYGNSS. The red dot, centered on the storm center and with a 75-km radius, represents the inner-core region. ASCAT swaths are separated by about 1000 km and progress from east to west over time. Only one of the swaths passes over the inner core during the 9-h interval shown. CYGNSS transects are distributed more widely and thus sample in and near the inner core more often.

context of the operational forecasting environment and evaluation of the CYGNSS wind speed product performance by marine forecasters. This type of validation has proven to be invaluable for other satellite data in revealing performance characteristics that are not readily apparent from standard statistical analysis.

There also exists the possibility of directing some under flights of CYGNSS in hurricanes with the NOAA P-3 aircraft for some additional direct comparison datasets at high wind speeds and in limiting environmental conditions. Being the first

space-based GNSS-R constellation system that will systematically provide wind speed retrievals over much of the world's oceans, CYGNSS will provide a unique opportunity to characterize and understand the performance of the GNSS-R measurement technique for ocean surface wind speeds.

Another facet of the validation effort will include engaging the operational forecasters at the NOAA National Hurricane Center (NHC). Following each Atlantic hurricane season after launch, the CYGNSS wind retrievals, along with proper training data, will be provided to forecasters to utilize and

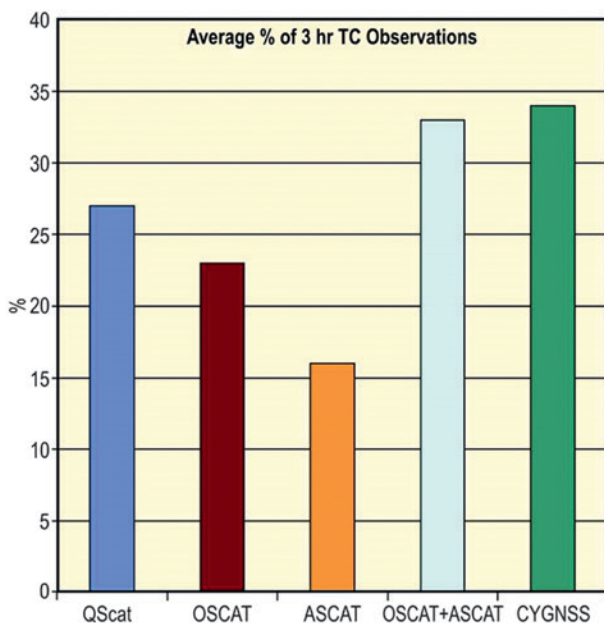


FIG. 6. TC sampling capability as percentage of 3-h intervals in which each sensor measures the TC inner core.

evaluate during their postseason storm analyses. Should CYGNSS data become available in near-real time, an effort will be made to integrate these data into the NHC workstation environment so that they can be utilized and evaluated in near-real time.

Constellation sampling example 1 (resolving TC landfall). A time-lapse simulation comparing CYGNSS and ASCAT coverage of Hurricane Frances (2004) just before its Florida coast landfall is shown in Fig. 5. The simulation was created by projecting satellite coverage predictions for both missions onto the archival storm-track record for Frances. Each frame represents all samples taken within a 3-h interval. The TC inner core is shown as a red-filled circle in each frame. ASCAT, with its relatively narrow swath width, only infrequently samples the inner core, whereas the wider and more dispersed effective swath of the CYGNSS constellation allows for much more frequent sampling (Ruf et al. 2012).

Constellation sampling statistics—Resolving TC life cycle. The simulation used to examine temporal and spatial sampling properties during the Hurricane Frances landfall was extended to the entire 2005 Atlantic hurricane season in a second simulation. In this case, in addition to CYGNSS sampling properties, the sampling by three ocean wind scatterometers [QuikSCAT on NASA SeaWinds, OSCAT on the Indian Space Research Organisation’s (ISRO) *OceanSat-2*, and ASCAT on the European Organisation for the Exploitation of

Meteorological Satellites’s (EUMETSAT) Meteorological Operational (MetOp)] was also modeled. Figure 6 shows the percentage of 3-h intervals over the full hurricane season within which each of the three scatterometers would have sampled the inner-core region of every TC that occurred that year. Also included in the figure is the percentage sampled by the combined OSCAT-and-ASCAT constellation and the percentage that would have been sampled by CYGNSS. CYGNSS has a significantly higher sampling percentage than any single scatterometer and is comparable to the OSCAT-and-ASCAT combination.

Constellation sampling example 2 (wind speed observations). The ability of CYGNSS to resolve the complete wind field of a TC, both the surrounding environmental field and that of the inner core, is illustrated in Fig. 7. Shown is an example of the simulated wind speed measurements made by CYGNSS over a particular 6-h interval in the vicinity of the storm center of the nature run described in Nolan et al. (2013). The spatial sampling is characterized by a large number of interleaved transects along which the winds are measured. They are formed by the trajectories across the ocean surface of the 32 simultaneous specular reflection points being tracked by the CYGNSS constellation. At each reflection point, CYGNSS will measure a DDM and, from it, estimate the wind speed there. The complete time-dependent simulated sampling over the full 13-day life cycle of this nature run is illustrated by an animation available online

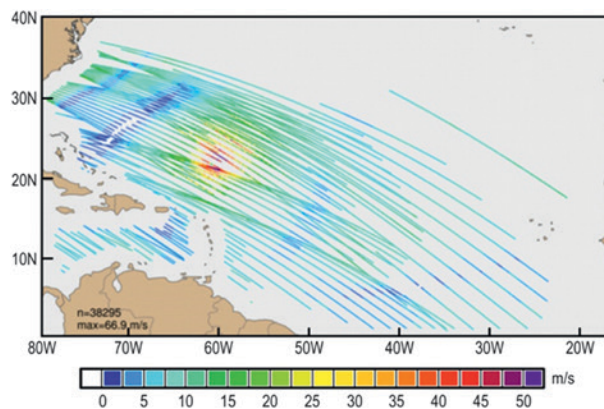


FIG. 7. Simulated wind speeds retrieved by the CYGNSS constellation over a typical 6-h interval in the vicinity of the storm center of the nature run. The simulation includes the effects of all engineering measurement uncertainties as well as the retrieval error associated with the wind speed estimation algorithm. The spatial sampling characteristic of CYGNSS is composed of many interleaved transects formed by the trajectories of the specular reflection points.

TABLE 1. CYGNSS mission scientific data product baseline requirements.

Requirement	Value
Wind speed dynamic range	3–70 m s ⁻¹ as determined by a spatially averaged wind field with 5 × 5 km ² resolution
Wind speed uncertainty	2 m s ⁻¹ retrieval uncertainty for winds less than 20 m s ⁻¹ 10% retrieval uncertainty for winds greater than 20 m s ⁻¹
Precipitation tolerance	Meet dynamic range and uncertainty requirements at rain rates of up to 100 mm h ⁻¹ as determined by a spatially averaged rain field with 5 × 5 km ² resolution
Spatial resolution	25 × 25 km ² or better
Mean revisit time	Less than 12 h
24-h spatial coverage	70% or more of the TC historical tracks

(<http://dx.doi.org/10.1175/BAMS-D-14-00218.2>).

In the animation, measurements made by each of the eight individual spacecraft are distinguished by unique icons. The wind speeds shown in Fig. 7 are those retrieved by CYGNSS and include the effects of expected engineering measurement uncertainties as well as errors associated with the wind speed retrieval algorithm. These results are currently being used in assimilation studies to assess their impact on hurricane intensity and track forecasts.

CONCLUSIONS. The CYGNSS mission is scheduled for launch in October 2016. Its use of multichannel GNSS-R bistatic radar scatterometers, flown on a constellation of eight satellites in a low-inclination orbit, results in a unique ability to measure ocean surface winds in the inner core of tropical cyclones with a revisit time of hours. A summary of the mission’s science measurement requirements is listed in Table 1. It is hoped and expected that this unique dataset will contribute to significant improvements in our understanding of TC inner-core processes and in our ability to model and forecast their development.

ACKNOWLEDGMENTS. The work presented was supported in part by NASA Science Mission Directorate Contract NNL13AQ00C. The authors would also like to thank Dave Nolan for providing the nature run simulation data and Brian McNoldy for producing the spatial sampling image (Fig 7).

REFERENCES

Arguez, A., M. A. Bourassa, and J. J. O’Brien, 2005: Detection of the MJO signal from QuikSCAT. *J. Atmos. Oceanic Technol.*, **22**, 1885–1894, doi:10.1175/JTECH1822.1.

Atlas, R., and Coauthors, 2001: The effects of marine winds from scatterometer data on weather analysis

and forecasting. *Bull. Amer. Meteor. Soc.*, **82**, 1965–1990, doi:10.1175/1520-0477(2001)082<1965:TEOM WF>2.3.CO;2.

—, A. Y. Hou, and O. Reale, 2005a: Application of Sea-Winds scatterometer and TMI-SSM/I rain rates to hurricane analysis and forecasting. *J. Photogramm. Remote Sens.*, **59**, 233–243, doi:10.1016/j.isprsjprs.2005.02.007.

—, and Coauthors, 2005b: Hurricane forecasting with the high-resolution NASA finite volume general circulation model. *Geophys. Res. Lett.*, **32**, L03807, doi:10.1029/2004GL021513.

Brown, D. P., and J. L. Franklin, 2004: Dvorak TC wind speed biases determined from reconnaissance-based “best track” data (1997–2003). *26th Conf. on Hurricanes and Tropical Meteorology*, Miami, FL, Amer. Meteor. Soc., 3D.5. [Available online at https://ams.confex.com/ams/26HURR/techprogram/paper_75193.htm.]

Clarizia, M. P., C. Gommenginger, S. Gleason, M. Srokosz, C. Galdi, and M. di Bisceglie, 2009: Analysis of GNSS-R delay-Doppler maps from the UK-DMC satellite over the ocean. *Geophys. Res. Lett.*, **36**, L02608, doi:10.1029/2008GL036292.

—, C. Ruf, C. Gommenginger, and P. Jales, 2014: Spaceborne GNSS-R minimum variance wind speed estimator. *IEEE Trans. Geosci. Remote Sens.*, **52**, 6829–6843, doi:10.1109/TGRS.2014.2303831.

Gall, R., J. Franklin, F. Marks, E. N. Rappaport, and F. Toepfer, 2013: The Hurricane Forecast Improvement Project. *Bull. Amer. Meteor. Soc.*, **94**, 329–343, doi:10.1175/BAMS-D-12-00071.1.

Garrison, J., S. Katzberg, and M. Hill, 1998: Effect of sea roughness on bistatically scattered range coded signals from the global positioning system. *Geophys. Res. Lett.*, **25**, 2257–2260, doi:10.1029/98GL51615.

—, A. Komjathy, V. Zavorotny, and S. J. Katzberg, 2002: Wind speed measurements using forward scattered GPS signals. *IEEE Trans. Geosci. Remote Sens.*, **40**, 50–65, doi:10.1109/36.981349.

- Gleason, S., 2006: Remote sensing of ocean, ice and land remote sensing using bistatically scattered GNSS signals from low earth orbit. Ph.D. thesis, University of Surrey, 223 pp.
- , 2013: Space-based GNSS scatterometry: Ocean wind sensing using an empirically calibrated model. *IEEE Trans. Geosci. Remote Sens.*, **51**, 4853–4863, doi:10.1109/TGRS.2012.2230401.
- , S. Hodgart, S. Yiping, C. Gommenginger, S. Mackin, M. Adjrad, and M. Unwin, 2005: Detection and processing of bistatically reflected GPS signals from low Earth orbit for the purpose of ocean remote sensing. *IEEE Trans. Geosci. Remote Sens.*, **43**, 1229–1241, doi:10.1109/TGRS.2005.845643.
- , C. Gommenginger, and D. Cromwell, 2010: Fading statistics and sensing accuracy of ocean scattered GNSS and altimetry signals. *J. Adv. Space Res.*, **46**, 208–220, doi:10.1016/j.asr.2010.03.023.
- Houze, R. A., Jr., 2004: Mesoscale convective systems. *Rev. Geophys.*, **42**, RG4003, doi:10.1029/2004RG000150.
- Katzberg, S. J., and J. Dunion, 2009: Comparison of reflected GPS wind speed retrievals with dropsondes in tropical cyclones. *Geophys. Res. Lett.*, **36**, L17602, doi:10.1029/2009GL039512.
- , R. A. Walker, J. H. Roles, T. Lynch, and P. G. Black, 2001: First GPS signals reflected from the interior of a tropical storm: Preliminary results from Hurricane Michael. *Geophys. Res. Lett.*, **28**, 1981–1984, doi:10.1029/2000GL012823.
- , O. Torres and G. Ganoe, 2006: Calibration of reflected GPS for tropical storm wind speed retrievals. *Geophys. Res. Lett.*, **33**, L18602, doi:10.1029/2006GL026825.
- Lin, B., S. J. Katzberg, J. L. Garrison, and B. Wielicki, 1998: Relationship between the GPS signals reflected from sea surface and the surface winds: Modeling results and comparisons with aircraft measurements. *J. Geophys. Res.*, **104**, 20 713–20 727, doi:10.1029/1999JC900176.
- Lowe, S. T., J. L. LaBrecque, C. Zuffada, L. Romans, L. Young, and G. Hajj, 2002: First spaceborne observation of an Earth-reflected GPS signal. *Radio Sci.*, **37**, 7-1–7-28, doi:10.1029/2000RS002539.
- Nesbitt, S. W., E. J. Zipser, and D. J. Cecil, 2000: A census of precipitation features in the Tropics using TRMM: Radar, ice scattering, and lightning observations. *J. Climate*, **13**, 4087–4106, doi:10.1175/1520-0442(2000)013<4087:ACOPFI>2.0.CO;2.
- Nolan, D. S., R. Atlas, K. T. Bhatia, and L. R. Bucci, 2013: Development and validation of a hurricane nature run using the Joint OSSE nature run and the WRF model. *J. Adv. Earth. Model. Syst.*, **5**, 382–405, doi:10.1002/jame.20031.
- O'Brien, A., 2014: End-to-end simulator. CYGNSS Project, Space Physics Research Laboratory Doc. 148-0123, University of Michigan, 24 pp.
- Rickenbach, T. M., and S. A. Rutledge, 1998: Convection in TOGA COARE: Horizontal scale, morphology, and rainfall production. *J. Atmos. Sci.*, **55**, 2715–2729, doi:10.1175/1520-0469(1998)055<2715:CITCHS>2.0.CO;2.
- Rose, R., J. Dickinson, and A. Ridley, 2012: CubeSats to NanoSats; Bridging the gap between educational tools and science workhorses. *2012 IEEE Aerospace Conf.*, Big Sky, MT, IEEE, doi:10.1109/AERO.2012.6187417.
- Ruf, C. S., S. Gleason, Z. Jelenak, S. Katzberg, A. Ridley, R. Rose, J. Scherrer, and V. Zavorotny, 2012: The CYGNSS nanosatellite constellation hurricane mission. *2012 IEEE Int. Geoscience and Remote Sensing Symp.*, Munich, Germany, IEEE, 214–214, doi:10.1109/IGARSS.2012.6351600.
- Schlx, M. G., D. B. Chelton, and M. H. Freilich, 2001: Sampling errors in wind fields constructed from single and tandem scatterometer datasets. *J. Atmos. Oceanic Technol.*, **18**, 1014–1036, doi:10.1175/1520-0426(2001)018<1014:SEIWFC>2.0.CO;2.
- Stephens, G. L., P. J. Webster, R. H. Johnson, R. Engelen, and T. L'Ecuyer, 2004: Observational evidence for the mutual regulation of the tropical hydrological cycle and tropical sea surface temperatures. *J. Climate*, **17**, 2213–2224, doi:10.1175/1520-0442(2004)017<2213:OEFTMR>2.0.CO;2.
- Zavorotny, V., and A. Voronovich, 2000: Scattering of GPS signals from the ocean with wind remote sensing applications. *IEEE Trans. Geosci. Remote Sens.*, **38**, 951–964, doi:10.1109/36.841977.

Find out from the authoritative source

for definitions of meteorological terms.

[What's a dust devil?]



THE AMERICAN METEOROLOGICAL SOCIETY Online Glossary of Meteorology

With over 12,000 meteorological terms,
you'll be able to look up definitions
online any time, any place, anywhere.

<http://glossary.ametsoc.org/wiki>

Also available in hardcover and
CD formats at the AMS Bookstore,
www.ametsoc.org/amsbookstore.



Photo: Sam Christian

A NEW INSTRUMENTED AIRBORNE PLATFORM FOR ATMOSPHERIC RESEARCH

BY PATRICK HAMILL, LAURA T. IRACI, EMMA L. YATES, WARREN GORE, T. PAUL BUI, TOMOAKI TANAKA, AND MAX LOEWENSTEIN

The instrumented Alpha Jet aircraft can respond quickly to unexpected atmospheric conditions, validate satellite retrievals, and carry out pollution studies and flux measurements. Present measurements include profiles of wind, CO₂, CH₄, O₃, and H₂O.

If you watched the documentary television program about climate change, *Years of Living Dangerously*, you might remember the opening scenes in which Harrison Ford walks across the apron of the National Aeronautics and Space Administration (NASA)'s Moffett Federal Airfield and climbs into a sleek olive green airplane to make measurements of atmospheric trace gases over a patch of Nevada desert. In this paper, we describe this unique aircraft, its measurement capabilities, and its future uses as well as presenting a typical flight path and some of the results obtained.

THE AIRPLANE. The Alpha Jet (Fig. 1) is a two-person light subsonic attack jet and advanced trainer developed jointly by Dassault-Breguet and Dornier for the French and German militaries. It is powered by two turbofan jet engines, flies at speeds up to 1,000 km h⁻¹, and has a ferry range of nearly 3,000 km and a ceiling of about 14.5 km. The French Air Force (Armée de l'Air) used the Alpha Jet primarily as a trainer but found that it was “too forgiving” and led to longer learning curves for pilots assigned to combat aircraft that were more difficult to fly. The Alpha Jet is still used by the Patrouille de France, the flight demonstration team of the French Air Force. The Luftwaffe used the Alpha Jet mainly in a light strike role and retired the aircraft in 1997. Production of the airplane ceased in 1991 but it is still in use by the air forces of some 12 countries, including Belgium, Canada, and Portugal. The flight measurement program involving the Alpha Jet at NASA Ames Research Center is called AJAX, an approximate acronym for “Alpha Jet Atmospheric Experiment.”

The modified (demilitarized) Alpha Jet is owned by a private company called H211, LLC, and used by them for pilot training. Since this is no longer a military aircraft, it can land at any commercial field and does not require special permissions. By a Space Act

AFFILIATIONS: HAMILL—NASA Ames Research Center, Moffett Field, and San Jose State University, San Jose, California; IRACI, YATES, GORE, BUI, TANAKA, AND LOEWENSTEIN—NASA Ames Research Center, Moffett Field, California

CORRESPONDING AUTHOR: Patrick Hamill, NASA Ames Research Center, MS 245-3, Moffett Field, CA 94035
E-mail: patrick.hamill@sjsu.edu

The abstract for this article can be found in this issue, following the table of contents.

DOI:10.1175/BAMS-D-14-00241.1

In final form 19 July 2015
©2016 American Meteorological Society



Fig. 1. Alpha Jet in front of hangar at NASA Ames Research Center, Moffett Field, CA.

Agreement between NASA Ames Research Center and H211, the Alpha Jet is stationed at NASA's Moffett Field and can be used by NASA when not required by H211. This somewhat unique public-private collaboration has given us the use of an excellent platform for scientific studies of the atmosphere.

The Alpha Jet flies faster and higher than propeller-driven research aircraft. Its speed is an asset when carrying out various traverses of an interesting area, as one obtains a closer approximation to a "snapshot" than with measurements made with a slower platform. This property was evident during recent measurements of methane emissions from an oil field when the Alpha Jet performed three passes at different altitudes within 20 min. Low-level, fast measurements are useful in making boundary level flux measurements by reducing uncertainty due to the evolution of the atmosphere during the measurement period. Since it was designed as a ground attack airplane, the alpha jet is uniquely suited for safely conducting both high- and low-level atmospheric sampling. In unpopulated regions (desert and marine areas where prescribed lateral offsets are available) it routinely takes measurements below 25 m.

The Alpha Jet can reach the lower stratosphere and we have made ozone and meteorological measurements up to the tropopause at 14 km, but the operation of the Picarro measurement system limits carbon dioxide and methane measurements to altitudes less than about 9 km for reasons described below.

It might be mentioned that jet-powered research aircraft, such as the National Science Foundation

(NSF)/National Center for Atmospheric Research (NCAR) High-Performance Instrumented Airborne Platform for Environmental Research (HIAPER) Gulfstream-V and the NASA Falcon have the same advantages of speed, rate of climb, and high ceiling, as well as significantly greater range and payload. The same is true, for example, of NASA's ER-2, which, however, is seldom flown at altitudes much less than 60,000 ft. Such aircraft are often involved in deployments that involve several scientists, many instruments, and schedules that are determined months

in advance. Perhaps the best comparison to the Alpha Jet is the NASA WB-57, which is also an adapted military airplane. Both are two-seater aircraft, so there is no room on board for instrument specialists. The WB-57 is significantly larger than the Alpha Jet and has a greater payload. They fly at about the same speed and have roughly the same range, but the Alpha Jet has a higher ceiling and a faster rate of climb. The WB-57 is a more general platform that can be adapted to various research projects, whereas the Alpha Jet, at least in its present configuration, has a fixed number of instruments permanently stored in external drop tanks and can be ready to deploy at short notice.

The plane has four wing pods. The outboard pods are fuel tanks. The inboard pods are redesigned fuel tanks mounted at locations originally used for armaments. One of these inboard pods has been repurposed to contain scientific instruments, as shown in Fig. 2, and the second one will be used for future instrumentation. These pods have an available volume of about 0.15 m³ and can carry a 245-kg payload. We are planning to eventually instrument a modified belly tank with a usable volume of 0.08 m³ and a payload of 160 kg.

The Alpha Jet is operated as a "restricted experimental aircraft," which means that it does not require Federal Aviation Administration (FAA) certification when modifications are made to it (as when new instruments are incorporated into the pods). Nevertheless, it must go through a rigorous internal NASA airworthiness and safety review. Science flights are made above or below the commercial flight regions,

and permission is required to fly through them (flight plans must be filed). The aircraft has no deicing mechanisms and cold clouds and lightning storms are avoided.

Aircraft and instrument support is fairly minimal. At present, the Alpha Jet science flights have all been staged out of NASA Ames, but if it should go on deployment to a distant location, the required support would consist of the pilots, an aircraft ground crew of one person, a three-person instrument ground crew, and a ground power cart.

THE INSTRUMENTS. The instruments, as shown in Fig. 2, are presently mounted in the right instrument pod and consist of an ozone monitor, a cavity ring-down spectrometer (to measure concentrations of carbon dioxide, methane, and water vapor), and a Meteorological Measurement System (MMS) to monitor ambient temperature, pressure, and 3D winds. The aircraft is also fitted with GPS and inertial navigation systems. Electrical power in flight can be drawn from a 28-V DC or a 115-V AC, 400-hz supply. Data are recorded for each instrument separately onto a PC card with compact flash.

The standard instrument stainless steel inlets extend 15 cm outside the pod and are backward facing to avoid ram effects and to prevent moisture from entering the system. There is a separate exhaust line.

We now describe the AJAX instruments in terms of their measurements.

Ozone. Ozone mixing ratios are determined with a commercial ozone monitor: 2B Technologies, Inc., Model 205. This instrument utilizes two detection cells: one containing ozone-scrubbed air and the other the sample air. The roles of the cells alternate, allowing for near-continuous measurements. The cells are illuminated with 254-nm UV light and intensity measurements are made simultaneously every 2 s. These are compared to yield ozone mixing ratios. The raw data, taken every 2 s, are averaged over 10 s to reduce the signal to noise ratio, giving an overall uncertainty of 3 ppbv at 10-s resolution.

The monitor has been modified by upgrading the pressure sensor and pump to allow for measurements at high altitudes, including a lamp heater to improve the stability of the UV source and the addition of fans and vibration isolators to control the monitor's physical environment. Calibration tests are performed before and after each flight, using an ozone

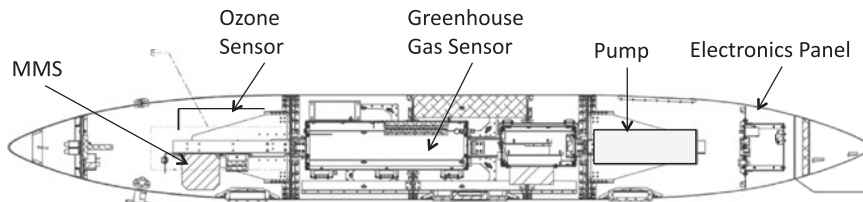


FIG. 2. The pod and its instruments.

calibration source referenced to the National Institute of Standards and Technology (NIST) scale. Technical details are found in Yates et al. (2013).

Carbon dioxide, methane, and water vapor. Three trace species—carbon dioxide, methane, and water vapor—are measured with a cavity ring-down spectrometer (CRDS, Picarro, Inc., Model G 2301-m). The “m” designation means that the instrument was modified for flight by the manufacturer. The AJAX team carried out further modifications; specifically, the instrument was repacked into two separate boxes so that it would fit into the pod, two additional fans and an additional insulation blanket were added, and a filter was added to protect the optics from the deposition of particles (Tadic et al. 2014).

In ring-down spectroscopy, laser light is introduced to a cavity with mirrors at either end, so that the light bounces back and forth, quickly filling the cavity (O’Keefe and Deacon 1988). One of the mirrors is not perfectly reflecting (having a reflectivity of about 99.995%), so that a small fraction of the light leaks out of the cavity. (Our instrument has a 25-cm cavity and light from a laser pulse bounces back and forth some 100,000 times yielding an effective path-length of over 10 km.) The intensity of the transmitted light is given by a Beer’s law relation, expressed in terms of time rather than distance: $I = I_0 \exp(-t/\tau)$. The CRDS mounted in the Alpha Jet uses three wavelengths in the IR at which the three trace gases are highly absorbing; specifically, the lasers are tuned to scan over the individual spectral lines of CO₂ at 1603 nm and CH₄ and H₂O at 1651 nm (Chen et al. 2010). The overall uncertainty ranges from 0.31 to 0.39 ppm for carbon dioxide and from 3.5 to 5.6 ppb for methane. [A detailed description of the instrument precision, repeatability, linearity, and calibration are presented in Tadic et al. (2014).] It might be noted that the instrument requires a pressure difference of at least 135 hPa between the ambient pressure and the pressure in the cavity (about 185 hPa). This limits our greenhouse gas science flight altitudes to pressure levels greater than about 320 hPa ($\leq 9,000$ m). The instrument takes data at 3 Hz, binned to 3 s.

Meteorological Measurement System. The MMS is a NASA–Ames–developed airborne instrument that provides calibrated, science quality, in situ measurements of static pressure, static temperature, and wind in three dimensions. This instrument has been integrated into a number of NASA aircraft including the ER-2, the DC-8, the Global Hawk unmanned aircraft, and now the Alpha Jet. The MMS system is mounted in the nose of the instrumented pod, as shown in Fig. 2. This is the pod with the unpainted ring near the nose, illustrated in Fig. 3.

The MMS instrument consists of three major systems: an air motion sensing system, an inertial navigation system, and a data acquisition system. The basic concepts and instrumentation of the MMS system are as described by Scott et al. (1990), but specific instruments have been updated repeatedly over the years. [For example, the older pressure and temperature transducers have been replaced by a Honeywell Precision Pressure Transducer (PPT) and a Rosemount platinum wire. Details of the MMS are given on the website <http://geo.arc.nasa.gov/sgg/mms>.] Earlier versions of the MMS system were compared with Vaisala radiosonde and radar tracking of balloons in 1986 and comparisons of the wind data with radar-tracked “Jimsphere” balloons were conducted in 1989 (Gaines et al. 1992). In both cases, the results support the MMS measurement accuracy.

The measured parameters are GPS positions, velocities, accelerations, pitch, roll, yaw, heading, angle of attack, angle of sideslip, dynamic total pressure, and total temperature. The primary products of MMS are pressure (precision of ± 0.3 mb with accuracy of

0.5%), temperature (± 0.3 K, 0.2%), horizontal wind (± 1 m s⁻¹, 3.3%), and vertical wind (± 0.3 m s⁻¹). The derived parameters are potential temperature, true airspeed, turbulence dissipation rate, and Reynolds number.

PLANNED INSTRUMENTATION. The instrumentation presently flown on the Alpha Jet gives a significant amount of information on the chemical and physical state of the atmosphere, but planned measurements will allow us to measure to higher altitudes and to measure other important trace species.

AirCore. The AirCore is an innovative yet extremely simple atmospheric sampling system invented by Pieter Tans at the National Oceanic and Atmospheric Administration (NOAA)/Earth System Research Laboratory (ESRL) (Tans 2009; Karion et al. 2010). It consists of a thin, very long, coiled, stainless steel tube (0.64-mm diameter connected to 0.32-mm diameter). The tube is (initially) closed at both ends. Upon reaching maximum altitude, one end of the tube is opened and the enclosed air escapes to the lower pressure environment, effectively evacuating the tube. As the airplane descends, air at lower altitudes (and higher pressures) enters the tube, compressing the higher-altitude air. Thus, the tube contains a record of air at decreasing altitudes (much as an ice core contains a record of ice history). The diffusion of molecules in the tube is extremely slow, so the air at a given location in the AirCore can be specified as air that was originally at a particular altitude. A CO₂ molecule at 208 K will diffuse about 1.6 m day⁻¹. We plan to sample the air

within 3 h following a flight to minimize the effect of diffusion. However, even if the air were not sampled until 24 h after collection, CO₂ would only have diffused 1.6 m in either direction. Thus, the midpoint of each 3.2-m length of the tube can be assumed to contain air representative of a particular altitude. This means that the 150-m tube contains 47 air parcels each representing air from a different altitude (Karion et al. 2010). The AirCore has been evaluated and shown to have measurement precisions for CO₂ and CH₄ that are equal or better than



FIG. 3. Alpha Jet pods. The near pod (with unpainted ring) is the instrumented pod. Note the reflection of the pilot’s helmet in the canopy. (Photograph courtesy of R. Simone.)

detail in Tanaka et al. (2015, manuscript submitted to *IEEE Trans. Geosci. Remote Sens.*) and show excellent agreement between satellite and aircraft measurements.

Johnson et al. (2014) discuss the AJAX methane measurements made on six flights during the DISCOVER-AQ-CA field campaign. These flights were made in the San Francisco Bay Area and the northern San Joaquin Valley. The purpose of the field campaign was to measure methane emissions in urban regions and from livestock in the San Joaquin Valley, which were suspected of being underestimated in the Emission Database for Global Atmospheric Research (EDGAR) emissions inventory (<http://edgar.jrc.ec.europa.eu>). Johnson et al. concluded that the GEOS-Chem model (Bey et al. 2001) using the EDGAR emissions inventory has an overall negative

bias in methane compared to AJAX measurements, particularly during periods when AJAX sampled elevated methane mixing ratios.

The Alpha Jet dedicated two flights to measuring the outflow from the exceptionally large Yosemite (“Rim”) wildfire during the summer of 2013 (Yates et al. 2015, manuscript submitted to *Atmos. Environ.*) and also made measurements of fires in Northern California during the summer of 2014. These measurements are important because in the western United States, wildfires are much more frequent than prescribed burns (ignited by land management programs to reduce the risks of wildfires). However, most current emission sampling is of prescribed burns, and given the differences in fuel, size, and weather conditions, these may not be a suitable proxy for wildfire emissions. Consequently, emission data

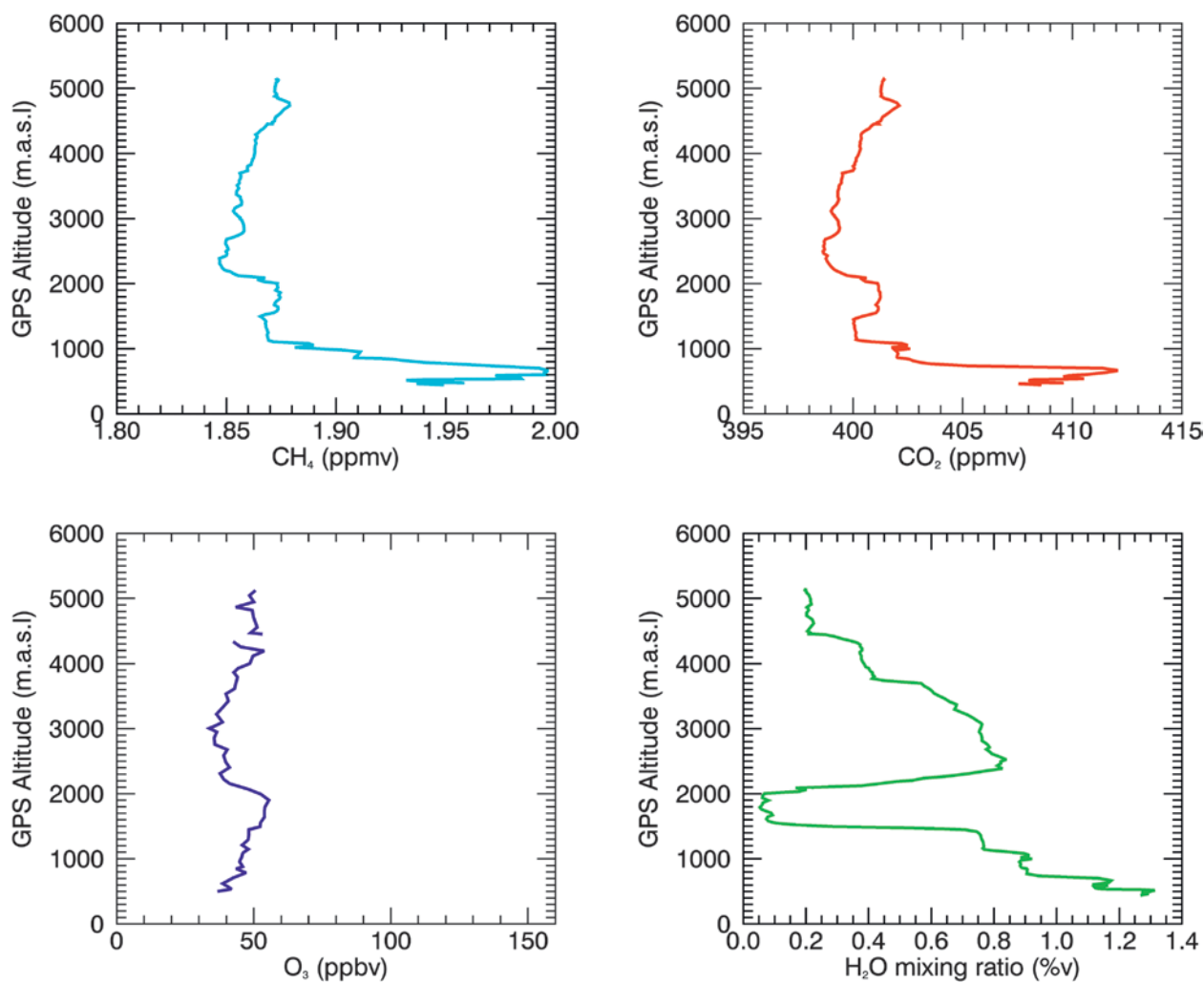


FIG. 5. Profiles of methane, carbon dioxide, ozone, and water mixing ratio during the downward spiral over San Luis Obispo as obtained from Alpha Jet flight 116 (10-s averages for ozone; 3 s for methane, carbon dioxide, and water). Note the strong increases in methane and carbon dioxide at low altitudes.

from wildfires provide valuable information for air quality and fire modeling studies.

The North Pacific midlatitude storm track is a preferred location for deep stratosphere to troposphere transport (Sprenger and Wernli 2003). On two occasions in June and July of 2012, the Alpha Jet was able to capture the distinguishing characteristics (low water vapor, high ozone, high potential vorticity) of such stratosphere to troposphere transport (Yates et al. 2013). The AJAX measurements also indicated that the stratospheric air was significantly depleted in CO_2 , suggesting its use as a nonconventional tracer of stratospheric air. It is interesting to note that the tropopause fold events we observed over California led to surface ozone measurements in Wyoming exceeding the allowed National Ambient Air Quality Standards value, as described in an “Exceptional Event Demonstration Package” prepared by the State of Wyoming Department of Environmental Quality.

A TYPICAL ALPHA JET FLIGHT: TRAJECTORIES AND RESULTS. AJAX flights have been conducted since January 2011 and by June 2015 the Alpha Jet had completed over 160 science flights. To illustrate a typical flight and the data collected we consider flight 116 (5 March 2014) in which the Alpha Jet flew from Moffett Field, over the San Joaquin Valley (at about 8-km altitude) to San Luis Obispo, where it spiraled down. The winds being easterly, the Alpha Jet then flew west from San Luis Obispo toward Monterey Bay with the aim of following the emission plume to the coast. It then returned to Moffett Field. This flight was part of a project called COWGAS organized by Dr. Ira Leifer of Bubbleology Research International, Santa Barbara. It involved multiple platforms to measure methane emissions from a dairy farm operated by the California Polytechnic University.

Figure 4 illustrates a portion of the flight path showing the methane mixing ratio as the Alpha Jet approached San Luis Obispo and spiraled down over the California Polytechnic University Dairy Farm to an altitude of 500 m above sea level. During the downward spiral, the

methane increased from a value of about 1.89 ppm to nearly 2.0 ppm at some 700 m above sea level. Figure 5 presents the vertical profiles of various trace gases measured on board the Alpha Jet. Figure 6 shows a plot of altitude and speed for the entire flight. On this flight, measurements were made of ozone, CO_2 , CH_4 , and water vapor.

CONCLUSIONS. The purpose of this paper is to introduce the scientific community to an instrument platform that is still under development but has already proved its value. When completely instrumented, it will be a rapid response airborne system that can be used to study suddenly occurring events, such as large forest fires or severe air quality events and can be also be used routinely for validation of other aircraft or satellite measurements.

The many successful AJAX flights demonstrate the capabilities of this small, principal investigator-driven, instrumented aircraft measuring program. The system is highly adaptable as illustrated by the response to forest fires described by Yates et al. (2015, manuscript submitted to *Atmos. Environ.*) or the investigation of tropopause folds (Yates et al. 2013). It can be used to carry out routine measurements such as the profiles over the Railroad Valley Playa that supported the CO_2 measurements made by GOSAT. The Alpha Jet can be deployed quickly to essentially any location without being hampered by complicated logistics.

Flight hours on the Alpha Jet can be requested through NASA’s Science Operations Flight Request

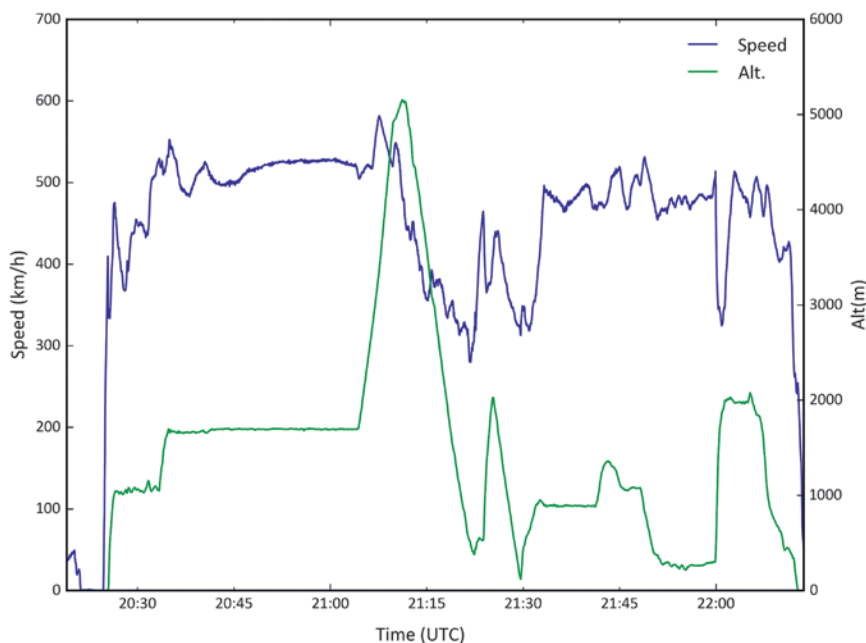


FIG. 6. Speed and altitude plots as a function of time for Alpha Jet flight 116.

System (SOFRS). Scientists who have a serious interest in placing an instrument on the NASA Alpha Jet are invited to contact Dr. Laura Iraci to request a copy of the “Experimenter’s Handbook.”

ACKNOWLEDGMENTS. The authors acknowledge the ongoing support and partnership of H211, LLC, with particular thanks to K. Ambrose, R. Simone, and R. Fisher. Funding for instrumentation and aircraft integration was received from the NASA Ames Research Center Director’s Fund and the NASA Science Innovation Fund. Technical contributions from Z. Young, E. Quigley, A. Trias, and R. Vogler were fundamental to the success of AJAX. The COWGAS project was funded by NASA Grant NNX-13AM21G.

REFERENCES

- Bey, I., and Coauthors, 2001: Global modeling of tropospheric chemistry with assimilated meteorology: Model description and evaluation. *J. Geophys. Res.*, **106**, 23 073–23 095, doi:10.1029/2001JD000807.
- Chen, H. J., and Coauthors, 2010: High-accuracy continuous airborne measurements of greenhouse gases (CO₂ and CH₄) using the cavity ring-down spectroscopy (CRDS) technique. *Atmos. Meas. Tech.*, **3**, 375–386, doi:10.5194/amt-3-375-2010.
- Gaines, S. E., S. W. Bowen, R. S. Hippskind, T. P. Bui, and K. R. Chan, 1992: Comparisons of the NASA ER-2 meteorological measurement system with radar tracking and radiosonde data. *J. Atmos. Oceanic Technol.*, **9**, 210–225, doi:10.1175/1520-0426(1992)009<0210:CO TNEM>2.0.CO;2.
- Johnson, M. S., E. L. Yates, L. T. Iraci, M. Loewenstein, J. M. Tadic, K. J. Wecht, S. Jeong, and M. L. Fischer, 2014: Analyzing source apportioned methane in northern California during Discover-AQ-CA using airborne measurements and model simulations. *Atmos. Environ.*, **99**, 248–256, doi:10.1016/j.atmosenv.2014.09.068.
- Karion, A., C. Sweeney, P. Tans, and T. Newberger, 2010: AirCore: An innovative atmospheric sampling system. *J. Atmos. Oceanic Technol.*, **27**, 1839–1853, doi:10.1175/2010JTECHA1448.1.
- O’Keefe, A., and D. Deacon, 1988: Cavity ring-down optical spectrometer for absorption measurements using pulsed laser sources. *Rev. Sci. Instrum.*, **59**, 2544, doi:10.1063/1.1139895.
- Scott, S. G., T. P. Bui, K. R. Chan, and S. Bowen, 1990: The meteorological measurement system on the NASA ER-2 aircraft. *J. Atmos. Oceanic Technol.*, **7**, 525–540, doi:10.1175/1520-0426(1990)007<0525:TM MSOT>2.0.CO;2.
- Sprenger, M., and H. Wernli, 2003: A Northern Hemispheric climatology of cross-tropopause exchange for the ERA15 time period (1979–1993). *J. Geophys. Res.*, **108**, 8521, doi:10.1029/2002JD002636.
- Tadic, J. M., and Coauthors, 2014: A comparison of in situ aircraft measurements of carbon dioxide and methane to GOSAT data measured over Railroad Valley Playa, Nevada, USA. *IEEE Trans. Geosci. Remote Sens.*, **52**, 7764–7774, doi:10.1109/TGRS.2014.2318201.
- Tans, P. P., 2009: System and method for providing vertical profile measurements of atmospheric gases. U.S. Patent 7597014 B2. [Available online at www.google.com/patents/US7597014.]
- Thome, K., 2001: Absolute radiometric calibration of Landsat 7 ETM+ using the reflectance-based method. *Remote Sens. Environ.*, **78**, 27–38, doi:10.1016/S0034-4257(01)00247-4.
- Tonooka, H., F. D. Palluconi, S. J. Hook, and T. Matsunaga, 2005: Vicarious calibration of ASTER thermal infrared bands. *IEEE Trans. Geosci. Remote Sens.*, **43**, 2733–2746, doi:10.1109/TGRS.2005.857885.
- Toon, G. C., and Coauthors, 2009: Total Column Carbon Observing Network (TCCON). *Advances in Imaging, Optical Society Tech. Digest*, 4–7, doi:10.1364/FTS.2009.JMA3.
- Yates, E. L., and Coauthors, 2013: Airborne observations and modeling of springtime stratosphere-to-troposphere transport over California. *Atmos. Chem. Phys.*, **13**, 12 481–12 494, doi:10.5194/acp-13-12481-2013.
- Yokota, T., Y. Yoshida, N. Eguchi, Y. Ota, T. Tanaka, H. Watanabe, and W. Maksyutov, 2009: Global concentrations of CO₂ and CH₄ retrieved from GOSAT: First preliminary results. *SOLA*, **5**, 160–163, doi:10.2151/sola.2009-041.

AIRCRAFT OBSERVATIONS OF DRY AIR, THE ITCZ, CONVECTIVE CLOUD SYSTEMS, AND COLD POOLS IN MJO DURING DYNAMO

BY SHUYI S. CHEN, BRANDON W. KERNS, NICK GUY, DAVID P. JORGENSEN, JULIEN DELANOË,
NICOLAS VILTARD, CHRISTOPHER J. ZAPPA, FALKO JUDT, CHIA-YING LEE, AND AJDA SAVARIN

The DYNAMO airborne measurements provide new insights into the distinct characteristics of convection, cold pools, water vapor, and air–sea fluxes from the suppressed to active phases of MJO initiation in the Indian Ocean.

The Madden–Julian oscillation (MJO; Madden and Julian 1971, 1972) is known to have a major impact on global weather systems, such as heat waves, tropical cyclones, and winter storms (e.g., Maloney and Hartmann 2000; Zhou et al. 2012). The intraseasonal/planetary time and spatial scales of the MJO make it a critical link between the global weather and climate systems (Zhang 2013). However, current global weather and climate models have little skill in predicting the MJO. The convective initiation of the MJO over the Indian Ocean, which typically consists of suppressed, onset, and active phases of the large-scale equatorial convection (Stephens et al. 2004; Yoneyama et al. 2013), is one of the most challenging problems in predicting the MJO (e.g., Benedict and Randall 2009). A major international field campaign supported by the Dynamics of the Madden–Julian Oscillation (DYNAMO), the Cooperative Indian Ocean Experiment on Intraseasonal Variability (CINDY), the Atmospheric Radiation Measurement Program (ARM) MJO Investigation Experiment (AMIE), and the Littoral

Air–Sea Processes (LASP) programs took place over the Indian Ocean with an intensive observing period (IOP) from 1 October 2011 to 15 January 2012 (Yoneyama et al. 2013). Three MJO events were observed during the IOP of the field program (DYNAMO). A detailed description of the MJO events during DYNAMO can be found in Gottschalck et al. (2013). Here we focus on key observations from aircraft measurements collected during the MJO initiation over the tropical Indian Ocean from November to December 2011.

SCIENCE OBJECTIVES AND MEASUREMENTS OF THE AIRCRAFT MISSIONS IN DYNAMO. The aircraft missions aimed to address three main science objectives of DYNAMO to better understand 1) multiscale convection–environment interactions, 2) water vapor variability and three-dimensional (3D) dynamical and microphysical structure in convective cloud systems, and 3) air–sea fluxes and boundary layer structure in the MJO initiation over the Indian Ocean. The flights were

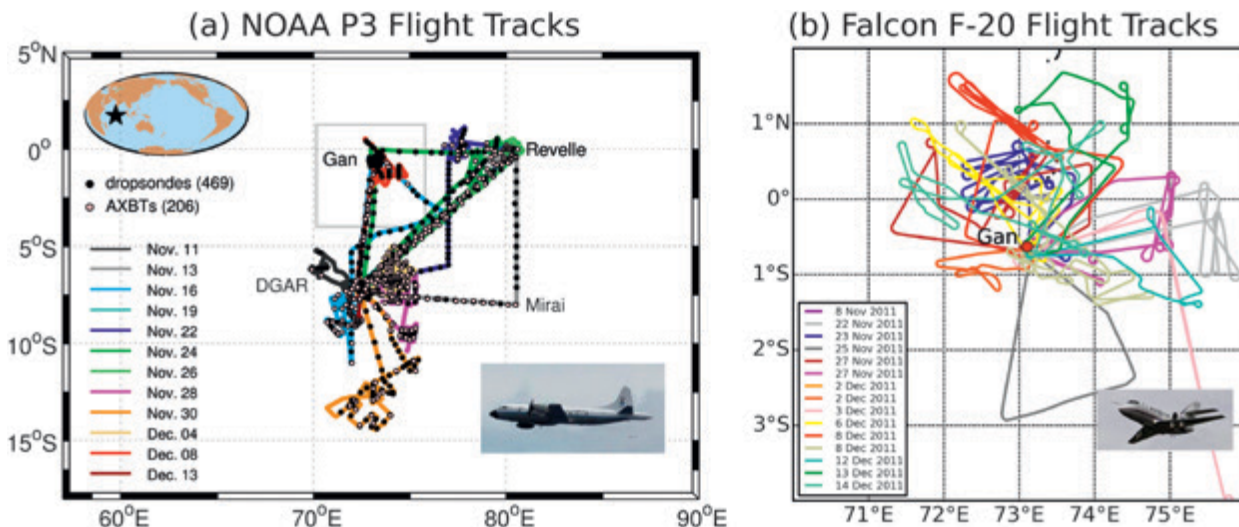


FIG. 1. (a) The NOAA WP-3D aircraft [stationed at Diego Garcia (DGAR)] flight tracks of the 12 missions from 11 Nov to 13 Dec 2011 during DYNAMO. The black dots and open circles indicate air-deployed GPS dropsonde and AXBT locations, respectively. (b) The French Falcon 20 aircraft (stationed at Gan Island) flight tracks of the 15 missions from 22 Nov to 16 Dec 2011 over the region near Gan as marked by the inset in (a). The aircraft missions are color coded by dates.

designed to sample the MJO initiation processes including convective cloud systems and their atmospheric and oceanic environment during all MJO phases, from the convectively suppressed phase to the active phase. This sampling strategy allowed us to address one of the most challenging problems in MJO initiation: the multiscale interaction among convective cloud systems, their large-scale environment, and the upper ocean on time scales from hours to weeks. Summaries of the National Oceanic and Atmospheric

Administration (NOAA) WP-3D and French Falcon 20 aircraft flights, specific objectives, and key measurements of each mission are given in Tables ES1 and ES2, respectively, in the online supplement.

The two aircraft provided finescale, dynamic, mobile measurements to sample the gaps between the stationary ground and ship sites that formed the DYNAMO arrays (Fig. 1). The WP-3D actively pursued the largest convective systems in the DYNAMO domain during the convective missions using primarily its vertically scanning Doppler radar (Jorgensen et al. 1996, 1997). The flight strategies contained various aircraft tracks, including one that allowed the analysis of mesoscale convective systems (MCSs) during each roughly hour-long portion from the Doppler radar reflectivity and velocity (Guy and Jorgensen 2014) and microphysics probes (N. Guy et al. 2015, personal communication). Other WP-3D flight tracks focused on the large-scale environmental conditions, including water vapor, temperature, and winds from transects between the island and ship sites (Kerns and Chen 2014b); the coupled atmosphere–ocean boundary layers; convectively generated cold pools and air–sea fluxes using the global positioning system (GPS) dropsondes; the airborne expendable bathythermographs (AXBTs); and the downward-looking infrared (IR) imaging spectrometer called the Japanese Dynamic Earth Observation by Very Long Baseline Interferometer (JADE) (Table ES1). The French Falcon 20 operated by Service des Avions Français Instrumentés pour la Recherche en Environnement

AFFILIATIONS: CHEN, KERNS, JUDT, AND SAVARIN—Rosenstiel School of Marine and Atmospheric Science, University of Miami, Miami, Florida; GUY—University of Wyoming, Laramie, Wyoming; JORGENSEN—NOAA/National Severe Storms Laboratory, Norman, Oklahoma; DELANOË AND VILTARD—LATMOS, L’Institut Pierre-Simon Laplace, Guyancourt, France; ZAPPA—Lamont-Doherty Earth Observatory, Columbia University, Palisades, New York; LEE—International Research Institute for Climate and Society, Columbia University, Palisades, New York

CORRESPONDING AUTHOR: Dr. Shuyi S. Chen, RSMAS, University of Miami, 4600 Rickenbacker Causeway, Miami, FL 33149
E-mail: schen@rsmas.miami.edu

The abstract for this article can be found in this issue, following the table of contents.

DOI:10.1175/BAMS-D-13-00196.1

A supplement to this article is available online (10.1175/BAMS-D-13-00196.2)

In final form 26 May 2015

©2016 American Meteorological Society

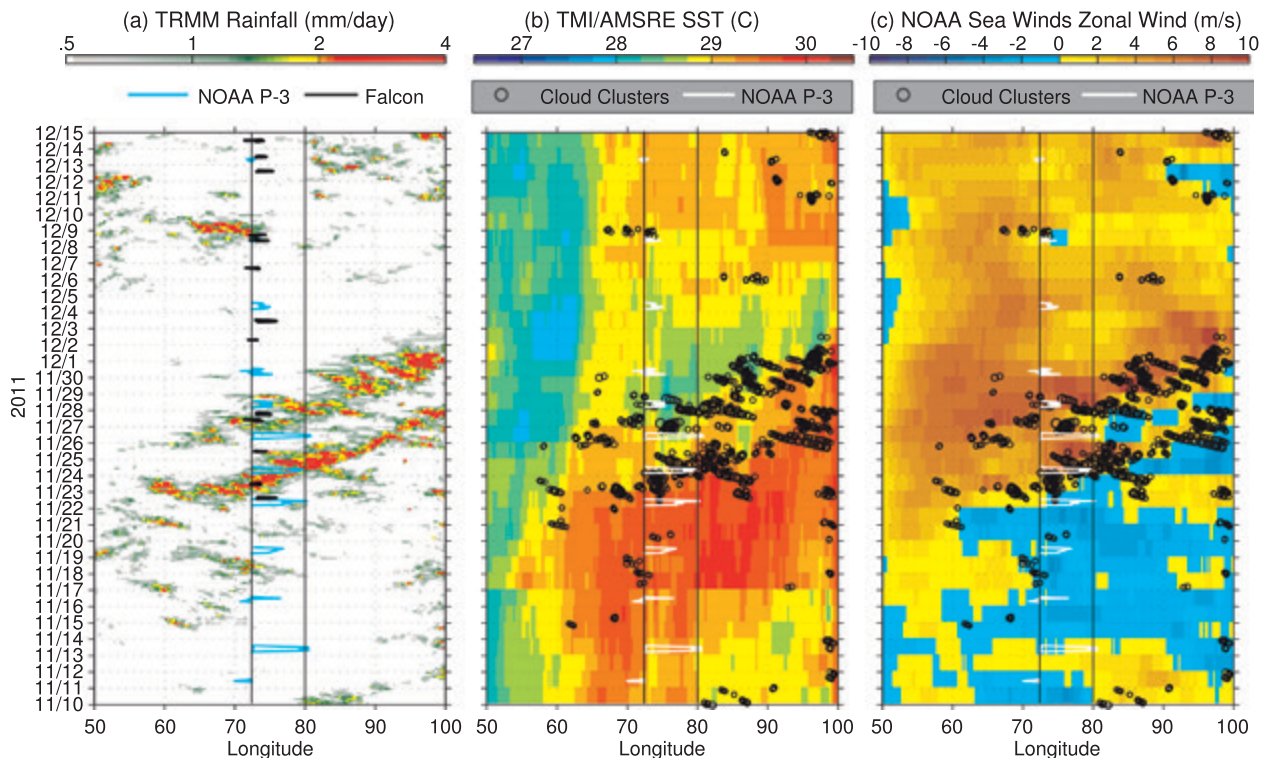


FIG. 2. Time–longitude diagrams of (a) TRMM 3B42 rain rate (color, mm day⁻¹), (b) TRMM/AMSR-E SST (color, °C) overlaid with cloud clusters from *Meteosat-7* IR data, and (c) NOAA SeaWinds zonal surface wind (color, m s⁻¹) from 10 Nov to 15 Dec 2011. The rain rate, SST, and zonal winds are averaged within the tropical latitude zone between 5°S and 5°N. The IR cloud clusters [cloud-top temperature < 208 K] are within the same latitude zone. The size of the black circles is proportional to the size of the observed cloud clusters. The DYNAMO-observing array is within the region between the blue lines (72°–80°E). The WP-3D aircraft tracks are marked in blue in (a) and white in (b) and (c). The Falcon 20 flight tracks are shown by black lines in (a).

(SAFIRE) was equipped with a millimeter-wave Doppler cloud radar and a set of microphysics in situ probes along with the usual environmental measurements (e.g., temperature, relative humidity, and winds; Table ES2). The Falcon 20 aircraft flew mostly near Gan Island (Fig. 1b) and focused on the upper-troposphere ice cloud properties in MCSs. Collectively the two aircraft provided the most comprehensive suite of observations of combined Doppler radar reflectivity and velocity from the lower to the upper troposphere, microphysical properties, convective cold pools, and air–sea fluxes from the GPS dropsondes and AXBTs in tropical oceanic MCSs to date.

LARGE-SCALE CONTEXT OF THE AIRCRAFT OBSERVATIONS. A strong MJO initiation event was observed from 10 November to 15 December 2011 (Yoneyama et al. 2013). An objective cloud-cluster tracking analysis using hourly *Meteosat-7* IR data (based a method described in Chen et al. 1996; Chen and Houze 1997a,b), along with the Tropical Rainfall Measuring Mission (TRMM) 3B42 rain

rate (Huffman et al. 2007), the Advanced Microwave Scanning Radiometer for Earth Observing System (AMSR-E) sea surface temperature (SST), the NOAA SeaWinds surface wind data (Zhang et al. 2006), and the DYNAMO in situ observations, provides a four-dimensional description of the multiscale variability of convective cloud systems and the air–sea fluxes in relation to the MJO initiation over the Indian Ocean. Figure 2 shows the eastward propagation of the large-scale envelope of TRMM precipitation and convective cloud clusters (IR cloud-top temperature < 208 K), changes in SST, and surface winds during the MJO. The cloud clusters became more numerous and increased in size as each MJO event developed. Prior to the onset of the convectively active phase of the MJO in late November 2011, the DYNAMO array is characterized by relatively warm SST and easterly winds (Figs. 2b and 2c). Significant SST cooling and strong near-surface westerly winds occurred during and after the convectively active phase from 25 November to early December. The convective cloud systems are highly correlated with features in the

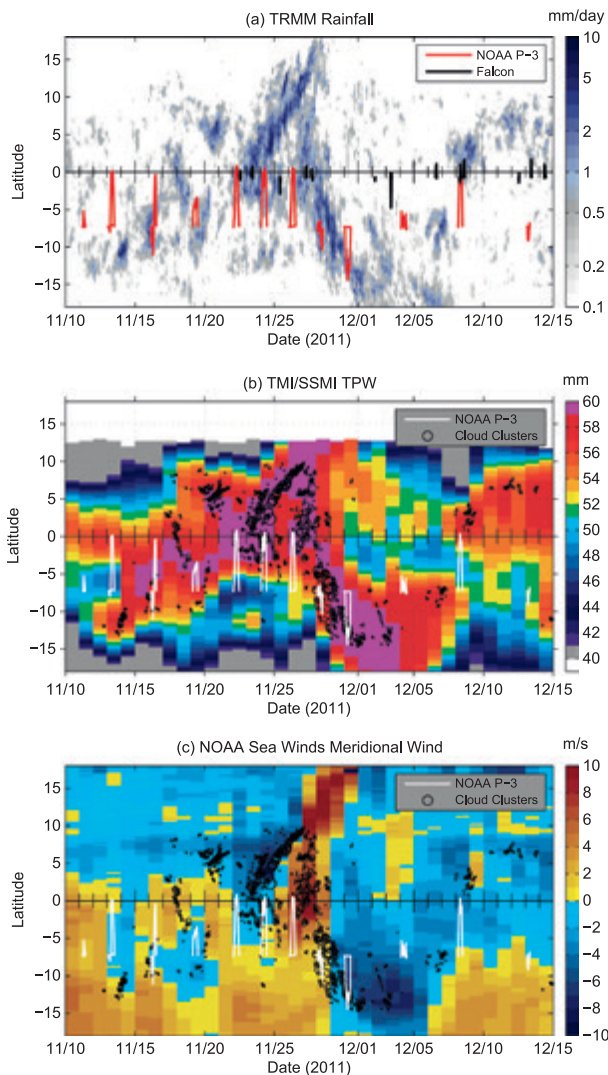


FIG. 3. Time–latitude diagrams of (a) the TRMM 3B42 rain rate (mm day^{-1}), (b) TPW (mm), and (c) NOAA SeaWinds meridional wind component (m s^{-1}) averaged over the DYNAMO array longitude $72^{\circ}\text{--}80^{\circ}\text{E}$ from 10 Nov to 15 Dec 2011. The black circles are the IR ($<208\text{ K}$) cloud clusters. The size of circles is proportional to the size of the cloud clusters. The WP-3D aircraft tracks are marked in red in (a) and white in (b) and (c). The Falcon 20 flight tracks are shown in black lines in (a).

surface winds from the meso and synoptic scale to intraseasonal time scales as seen in the NOAA SeaWinds zonal wind (Fig. 2c), including a complex mix of both local and remote large-scale conditions and impacts of these systems.

The eastward-propagating large-scale convection had two maxima (Fig. 2a). The first one represents the leading edge of the large convective envelope of the MJO (see Fig. 9 in Johnson and Ciesielski 2013). It has been described as being associated with a convectively

coupled Kelvin wave in Gottschalck et al. (2013). The second maximum consisted of mostly westward-propagating large precipitating cloud clusters that may be associated with the equatorial Rossby waves and mixed Rossby–gravity waves (Kiladis et al. 2009). One of the largest westward-propagating systems occurred on 28 November over the DYNAMO array, which was described in detail by Judt and Chen (2014). The distinct rainfall minimum between the two maxima (Fig. 2a) is due to dry air advecting into the equatorial region by Rossby wave gyres that were continually generated as part of the large-scale convective complex of the MJO (Kerns and Chen 2014a,b).

Another interesting feature is the transition of the large-scale convective activity from the intertropical convergence zone (ITCZ) to the equator during MJO initiation (Fig. 3a). Prior to the onset of the equatorial convective activity, deep convection was concentrated within the ITCZ near $8^{\circ}\text{--}10^{\circ}\text{S}$ (Fig. 3a). The convection shifted toward the equator in mid-November. An abrupt northward jump from the ITCZ to the equator occurred on 22 November when a strong dry air intrusion [minimum total precipitable water (TPW) between 5° and 10°S] from the subtropical region south of the DYNAMO array intruded north to 5°S of the equator (Fig. 3b). The dry air intrusion is associated with a maximum in the southerly (equatorward) wind from 15° to 5°S on 21–23 November (Fig. 3c), and with the group of long-lasting, northward-propagating clusters and the associated anomalous northerlies–southerlies couplet (meridional confluence zone) north of the equator from 24 to 27 November (Fig. 3c). These features mark a Rossby Gyre that developed in the active phase of the MJO, which later became Tropical Cyclone 5 (Moum et al. 2014). Another southerly dry air intrusion occurred from 8 to 15 December (Figs. 3b and 3c) but apparently with a less favorable equatorial environment for widespread deep convection in that case.

The WP-3D aircraft sampled all phases of the MJO as well as the ITCZ from 11 November to 13 December, while the Falcon 20 observations captured the convectively active and suppressed phases from 22 November to 14 December near Gan Island, as shown in Figs. 1–3. Examples of the aircraft observations from various large-scale conditions during the MJO initiation are presented in the follow sections.

CONVECTIVE CLOUD SYSTEMS IN SUPPRESSED, TRANSITION, AND ACTIVE PHASES OF MJO. Tropospheric moisture is a major parameter affecting convection during MJO initiation (Kerns and Chen 2014b). Satellite and rawinsonde

observations suggest that synoptic-scale dry air advection plays an important role in convective suppression in the tropics (Yoneyama and Parsons 1999; Kerns and Chen 2014b). The synoptic-scale variability in the wind and the atmospheric moisture fields is a key feature distinct from the different global model forecasts of the late November MJO initiation event during DYNAMO (Kerns and Chen 2014a). Moreover, the interactive processes between convective cloud systems and their large-scale environmental moisture on various scales—for example, equatorial waves—are not well understood. Here we use the

WP-3D Doppler radar and the GPS dropsonde data together with the cloud-cluster tracking analysis using hourly *Meteosat-7* IR data and satellite-observed TPW to provide a four-dimensional description of the multiscale variability of environmental moisture and convective cloud systems during this MJO initiation. Observations from four WP-3D aircraft missions are shown covering the entire MJO initiation from the convectively suppressed phase on 13 November (Fig. 4a), the transition/onset phase on 22 November (Fig. 4b), the active phase on 24 November (Fig. 4c), and the return to the suppressed phase on 8 December

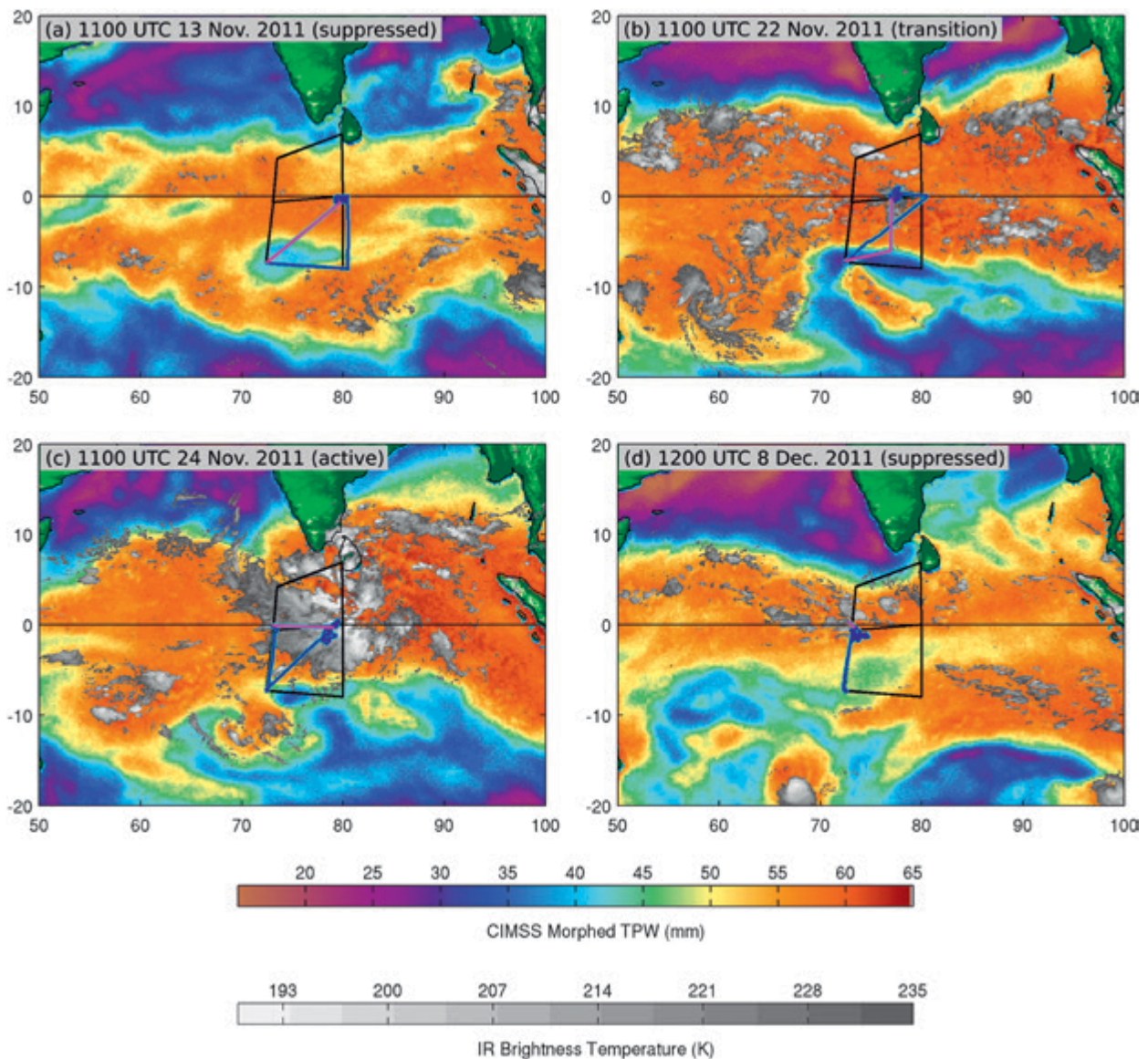


FIG. 4. TPW (color, mm) from the Cooperative Institute for Meteorological Satellite Studies (CIMSS) morphed product and the *Meteosat* IR brightness temperatures (gray, K) for four aircraft missions: (a) 13 Nov (suppressed), (b) 22 Nov (transition), (c) 24 Nov (active), and (d) 8 Dec 2011 (suppressed). The DYNAMO array is drawn in black lines. The WP-3D flight tracks are shown in blue lines. Detailed observations along the flight leg highlighted in magenta will be shown in Figs. 5–8, 12, and 13.

(Fig. 4d). The following three subsections describe the aircraft observations from the transition/onset, active, and suppressed phases of the MJO.

Dry air, ITCZ, and transition from convectively suppressed to active phase of MJO. To address the question of convective organization and its interaction with the large-scale environment during MJO initiation, observations

of convective cloud systems and their immediate surrounding environmental moisture were measured by the airborne Doppler radar, the GPS dropsondes, and flight-level measurements on board the WP-3D aircraft. During the onset of equatorial convection at the early stage of the MJO event from 20 to 23 November, dry air intrusion from the extratropical regions may be instrumental in disrupting the southern ITCZ

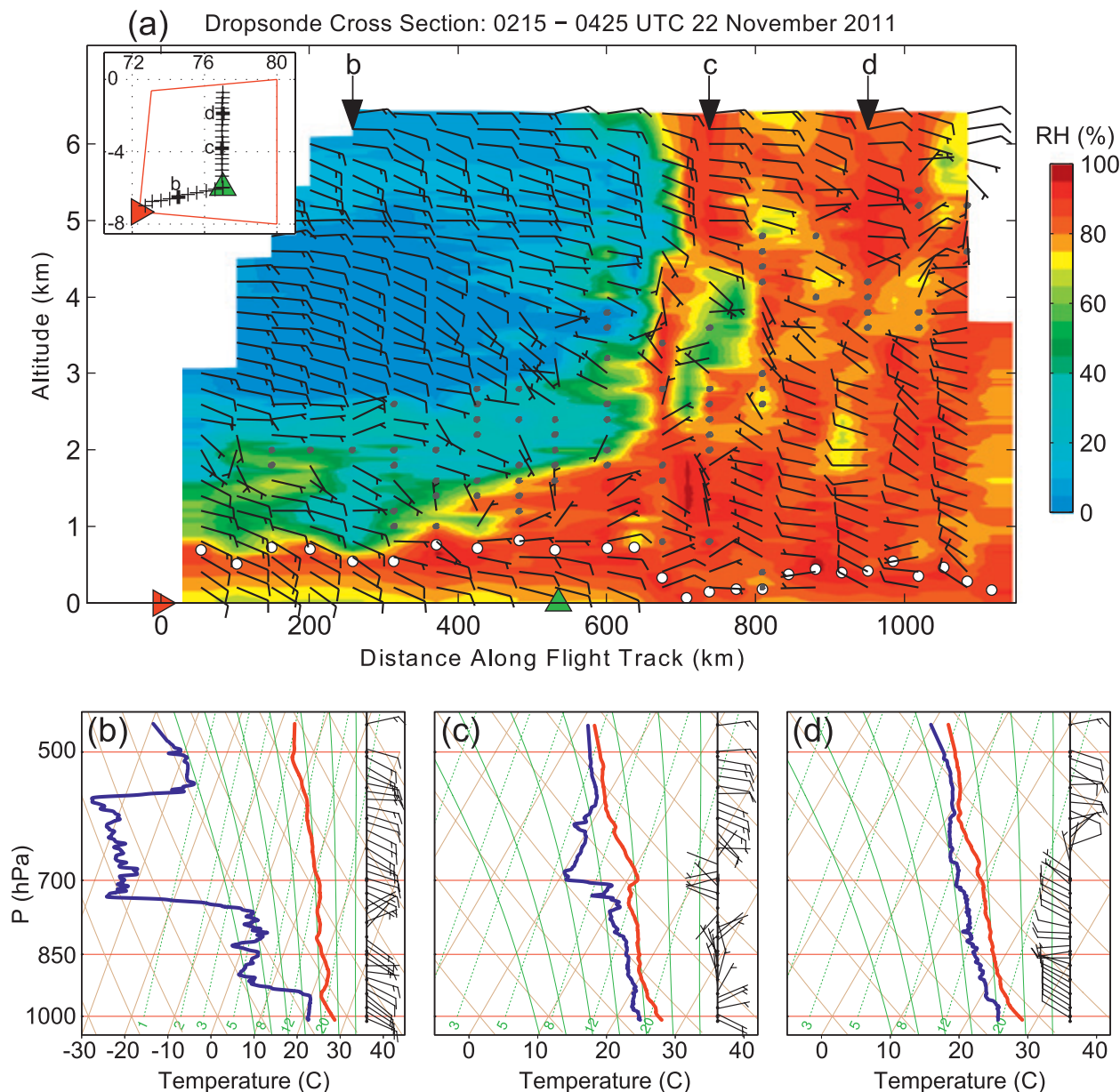


FIG. 5. Dry air intrusion during the transition from the convectively suppressed phase to the active phase of the MJO on 22 Nov 2011 (see Fig. 4b). (a) RH (%) and wind measured by the GPS dropsondes along the WP-3D aircraft track shown on the map (inset) with corresponding locations marked by red and green triangles and dropsonde locations at the black arrows at “b,” “c,” and “d.” White dots represent the height of the atmospheric boundary layer. (b)–(d) Skew T–logp diagrams from dropsondes deployed at three locations marked by the black arrows in (a), showing the contrasting dry air in the south and moist air near the equator. Wind barbs in (a)–(d) show the direction and wind speed of the horizontal wind. Each flag represents 5 m s^{-1} [~ 10 knots (kt); $1 \text{ kt} = 0.51 \text{ m s}^{-1}$].

RAIN, COLD POOLS, AND SEA STATES DURING THE SUPPRESSED AND ACTIVE PHASES OF THE MJO

Rain-induced freshwater pools on the ocean surface and the atmospheric cold pools from convective downdraft driven by evaporation of precipitation can modulate air–sea fluxes and the atmospheric stability that in turn affect convective variability. During the suppressed phase of the MJO, convective rain showers produce cool freshwater lenses over the ocean surface in low-wind conditions (Fig. SBI, top). The SST variability in the vicinity of the rain cell shown in Fig. SBI (top) was captured by the WP-3D aircraft during the DYNAMO field campaign on 16 November 2011 (Fig. 11). Although it is well known that convective rain cells—such as the one shown in Fig. SBI (top)—are numerous, the spatial and temporal scales of the cool freshwater pools and how they may affect the SST and air–sea fluxes are difficult to quantify. In contrast, during the active phase of the MJO, large convective mesoscale systems produced an extensive and deep layer of cold pools from the ocean surface to the atmospheric surface and boundary layers (or above in some cases). Strong winds induced surface waves and white caps (Fig. SBI, bottom) produce strong mixing in the upper ocean and enhanced air–sea fluxes during the active phase of the MJO. The contrasting air–sea interaction processes in the suppressed and active phases of the MJO and their impact on the evolution of MJO initiation need further investigation.



FIG. SBI. (top) Clouds, rain, and calm sea surface during the WP-3D flight near Gan Island on 16 Nov when surface wind speeds were $<5 \text{ m s}^{-1}$. (bottom) Sea surface waves and white caps observed during the WP-3D flight near R/V *Revelle* on 24 Nov when surface wind speeds were $>15\text{--}20 \text{ m s}^{-1}$ during the DYNAMO field campaign over the equatorial Indian Ocean. (Photos by Shuyi S. Chen.)

and forcing convection toward the equator (Kerns and Chen 2014b). Figure 5 shows an example of the dry air and a strong relative humidity (RH) gradient observed by the GPS dropsondes on 22 November, when the convection moved toward the equatorial region in response to the dry air intrusion from the south. The WP-3D flew through the dry air mass on its way to sample the convective cloud systems near the equator (Fig. 4b). The extreme low values of $RH < 10\%$ were observed in the low-midtroposphere near 4° – 5° S (Fig. 5a). Prior to 22 November, the convection in the southern ITCZ was active near 10° S (Fig. 3). This dry air intrusion was found to be responsible for “pushing” convective activity from the southern ITCZ to the equator during the transition/onset of the MJO convective phase (Kerns and Chen 2014b). The GPS dropsondes deployed from WP-3D provided in situ observations of the large-scale environmental moisture and winds as well as the atmosphere boundary layer structure. The depth of the atmosphere boundary layer (defined by the mixed layer using 0.5-K virtual potential temperature gradient) is higher in the dry air region (600–800 km) and lower in the moist region from 5° S to the equator (below 400–500 km) as shown by the white dots in Fig. 5a. The lower-tropospheric wind is easterly in the southern portion of the DYNAMO array with a relatively strong southeasterly component observed by the dropsonde near 7° S, 75° E (Fig. 5a) corresponding to the dry air intrusion (Fig. 4b). The winds changed to low-midtropospheric westerlies from about 4° S to the equator with a transition zone from 6° to 4° S, where a relatively weak midlevel westerly was observed in between the lower- and upper-tropospheric easterlies (Fig. 5a).

The distinct vertical moisture and wind profiles from the extremely dry air environment to the nearly saturated region close to the equator as well as the transition zone are shown clearly by skew T - $\log p$ diagrams from the WP-3D transect on 22 November (Fig. 5). The dry air region was dominated by a relatively strong, deep layer of easterlies, with RH as low as $\sim 10\%$ above 800 hPa (Fig. 5b), whereas the equatorial region had low-midlevel westerlies and upper-level easterlies with RH greater than 90% through a deep layer (Fig. 5d). The sounding collected in the transition zone between the dry and moist areas displayed an interesting “onion”-shaped temperature and dewpoint temperature profile (indicative of subsidence) between 600 and 700 hPa below a nearly saturated melting layer as well as a midlevel westerly wind (Fig. 5c), which displayed a somewhat similar property to those observed in the stratiform rain region of MCSs (e.g., Zipser 1977)

Convective cloud systems and enhanced surface winds in the active phase. Organized MCSs can interact with their large-scale environment through the vertical transport of heat, moisture, and momentum. Previous observations and modeling studies have shown that tropical MCSs can enhance surface westerlies in the MJO during the Tropical Ocean and Global Atmosphere Coupled Ocean–Atmosphere Response Experiment (TOGA COARE; e.g., Houze et al. 2000; Mecham et al. 2005). Midlevel inflow jets developed in the large MCSs can enhance the surface westerlies through melting and evaporative-cooling-driven downward motion and momentum transport in the active phase of the MJO (Jorgensen et al. 1997). During DYNAMO, the onset of the active phase of the MJO and its enhanced westerly winds on 24 November were observed by the in situ GPS dropsonde and Doppler radar measurements from the WP-3D aircraft near the equator (Figs. 4c and 6). A strong westerly jet was associated with the large complex system with multiple MCSs (Fig. 6a) descending from the mid-upper troposphere to the surface (Figs. 6b and 6c). The descending jet coincided with the large areas of the stratiform precipitation as observed by the WP-3D Doppler radar reflectivity and downward velocity as shown in Fig. 6b. Although the type of rear inflow associated with organized MCSs has been observed by Zipser (1977) and Smull and Houze (1987), the very large spatial scale of the descending jet observed by the dropsonde data from 72° to 79° E (>700 km; Fig. 6c) in this case has not been documented prior to DYNAMO. It is interesting to note that, from the Doppler radar reflectivity and velocity data, multiple MCSs were observed along the WP-3D transect from Research Vessel (R/V) *Revelle* to Gan Island (Fig. 6b). The radar reflectivity shows bright bands along the long transect and multiple descending jets, including one from the 1–9-km layer between the 400- and 500-km markers and another 1–5-km layer between 250 and 350 km (Fig. 6b).

The large multi-MCS complex produced a strong and deep cold pool (>4 K in potential temperature depression) extending from the ocean surface up to the 1000-m level (Fig. 6c). Both the enhanced surface westerly wind and the convective cold pools were also captured by the observations at the R/V *Revelle* (Moum et al. 2014). These observations indicate that the MCSs may enhance the surface westerlies during the active phase of the MJO (e.g., Houze et al. 2000), prolong the surface temperature recovery via convective cold pools, and enhance wind-induced upper-ocean mixing (Moum et al. 2014). Thus, these convective upscaling effects of the MCSs may play

an important role in MJO initiation over the tropical Indian Ocean.

Dual aircraft observations of three-dimensional structure of a convective cloud system during the suppressed phase.

The WP-3D and Falcon 20 aircraft flew a coordinated mission on 8 December 2011 (Fig. 4d). An example of the dual aircraft measurements in a convective cloud system near Gan Island is presented here (Fig. 7). The mission was designed to characterize the 3D structure of convective cloud systems, including the dynamic, thermodynamic, and microphysical properties. This is a unique dataset for cloud-resolving model evaluation and verification. Figure 8 shows a cross section along the coincident flight paths that was extracted from the 3D gridded WP-3D X-band (3.22 cm) tail Doppler radar data by projecting the WP-3D data onto the Falcon 20 W-band (3.19 mm) Doppler radar data grid using a bilinear interpolation scheme. Because of the increased sensitivity of the Falcon 20 measurements for smaller precipitation particles, observations where reflectivity was less than 15 dBZ were removed for the WP-3D reflectivity and wind fields. For the preliminary view presented here, the fields were simply overlaid. While wind field magnitudes are very close, it can be seen that minor directional discrepancies exist where the two fields merge. This is not surprising given that each instrument has an

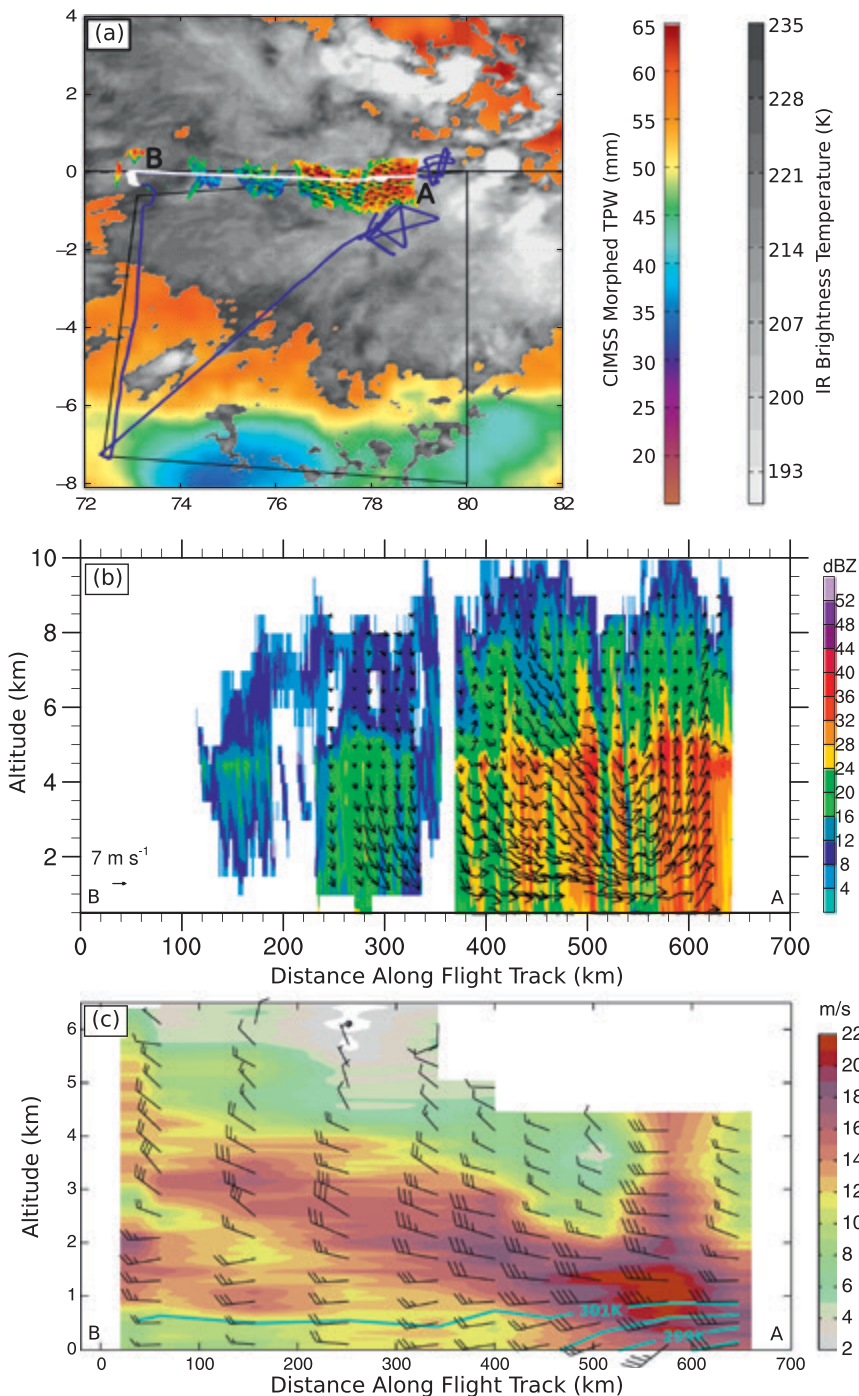


FIG. 6. A large equatorial convective complex with multiple MCSs observed during the active phase of the MJO on 24 Nov: (a) TPW (color, mm) and Meteosat-7 IR (gray, K), overlaid with the WP-3D track (white line) and Doppler radar reflectivity (color, dBZ) and wind at the 2-km level. Vertical sections of (b) show the WP-3D reflectivity and horizontal wind vector and (c) wind speed (color, m s^{-1}) and potential temperature (cyan contours from 298 to 301 K with 1-K intervals) from the dropsondes deployed from the WP-3D along the flight leg B–A near the equator [white line in (a)] from 0810 to 0934 UTC 24 Nov.

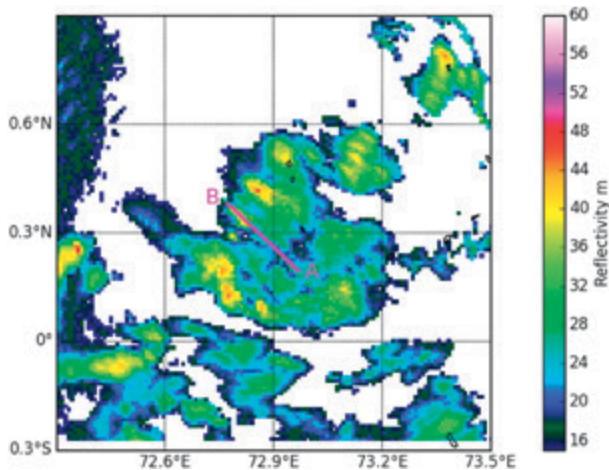


FIG. 7. The coincident flight track of the WP-3D and Falcon 20 aircraft (magenta line) is shown for 0753–0757 UTC 8 Dec 2011. The color contours represent radar reflectivity obtained from the lower fuselage radar aboard the WP-3D.

ideal performance window that becomes decreasingly reliable at this intersection. To improve the analysis going forward, a weighted averaging technique using the magnitudes of reflectivity (or perhaps uncertainties) at each individual point and surrounding eight adjacent neighboring points will be employed to smooth the data at this interface.

The combined vertical cross section of wind shows vertical wind shear within the MCS observed on 8 December (Fig. 8c). This feature is consistent with the observation from the DYNAMO sounding array, which showed strong easterlies in the upper troposphere and moderate westerlies during this time (Johnson and Ciesielski 2013). Understanding how the vertical motion in convective cloud systems interacts with the large-scale horizontal winds in the different phases of the MJO initiation requires synthesis of multiple observational platforms and data sources like in this case.

DISTINCT CONVECTIVE STRUCTURE AND MICROPHYSICS IN THREE MJO PHASES. Sampling from all phases of MJO initiation allowed us to compare the convective structure and microphysical properties of MCSs in different large-scale conditions. The WP-3D Doppler radar reflectivity data were processed from radar convective element (RCE) modules as described in Guy and Jorgensen (2014). Distributions of the height of radar echo tops and the level of maximum reflectivity from the transition/onset phase on 22 November, the convectively active phase on 24 November, and

the convectively suppressed phase on 8 December are shown in Fig. 9. It includes a total of six RCEs with two from each of the three days. Although some echo tops reached 13–14-km height in all cases, the echo tops were mainly below 5–6 km during the suppressed phase on 8 December (Fig. 9c) but higher than 10 km in the transition/onset and active periods from 22 to 24 November (Figs. 9a and 9b). A pronounced maximum in peak reflectivity near the melting level (4.5–5.5 km) indicated stratiform precipitation in the convective onset and active cases (Figs. 9d and 9e), which is in strong contrast to that of the suppressed case (Fig. 9f). The highest echo tops and the largest stratiform region were observed during the active phase on 24 November (Fig. 9b), in agreement with the ground-based observation of Zuluaga and Houze (2013). The dry environment in the suppressed phase (Fig. 4d) may have contributed to the relatively shallower convective cells and the lack of stratiform precipitation in the MCSs of 8 December. A similar relationship between environmental moisture and depth of convection was observed during TOGA COARE (Brown and Zhang 1997).

In situ measurements of water droplets were obtained using a combination of optical spectrometers mounted under the left wing of the WP-3D aircraft. The cloud imaging probe (CIP) and the precipitation imaging probe (PIP) measured the particle size and shape between 25 μm –1.55 mm and 100 μm –6.2 mm, respectively. Data were collected during each flight shown in Fig. 1a, with the exception of 11 November due to system errors. These data were largely collected at flight levels typically from 1500 to 3000 m. Raindrop size distributions (RSDs; Jackson and McFarquhar 2014) were produced for each flight. A three-parameter gamma distribution model was used to fit the RSD data. Analysis was performed using a normalized RSD to reduce the impact of mathematical artifacts possible from the highly correlated nature of the parameters of the gamma distribution fit model and removal of a priori shape constraints.

The observed droplet sizes tended to be larger on 22 and 24 November during the onset and active phases than the suppressed periods on 16 November and 8 December (Fig. 10a). This is consistent with the corresponding convective organization on 22–24 November and 8 December shown in Fig. 9. The onset–active phase was characterized by MCSs with broad stratiform regions and embedded deep convective cells (Guy and Jorgensen 2014). This resulted in an enhanced dependence on ice-phase hydrometeor growth, leading to larger D_m of melted drops and

broadening the distribution. Warm rain microphysics dominated during this regime. The 16 November case was sampled in MCSs from 8° to 10°S within the ITCZ during the suppressed phase and exhibited behavior in between the extremes in contrasting MJO phases. The probability distribution of the generalized intercept parameter (N_w) in Fig. 10b indicated the general similarity of systems observed during DYNAMO: namely, an embedded MCS archetype that tends toward the “transition” state between the classically defined convective and stratiform rain regimes. The 8 December case exhibited slightly greater probabilities of higher N_w , though all were within previous maritime measurement variability. The secondary peak on 8 December corresponds to small particles measured by the CIP.

These data can also be used to calculate reflectivity (Z) and rainfall rate (R) using moments of the RSD spectrum. Calculations of Z - R power-law relationships were found to be similar to those found in previous tropical ocean experiments (e.g., TOGA COARE). The imaging probe dataset also allowed for a unique look at the vertical structure of RSDs, which has been sparsely studied. Further work is underway to develop a full understanding of the RSD variations during DYNAMO measured by aircraft (N. Guy et al. 2015, personal communication).

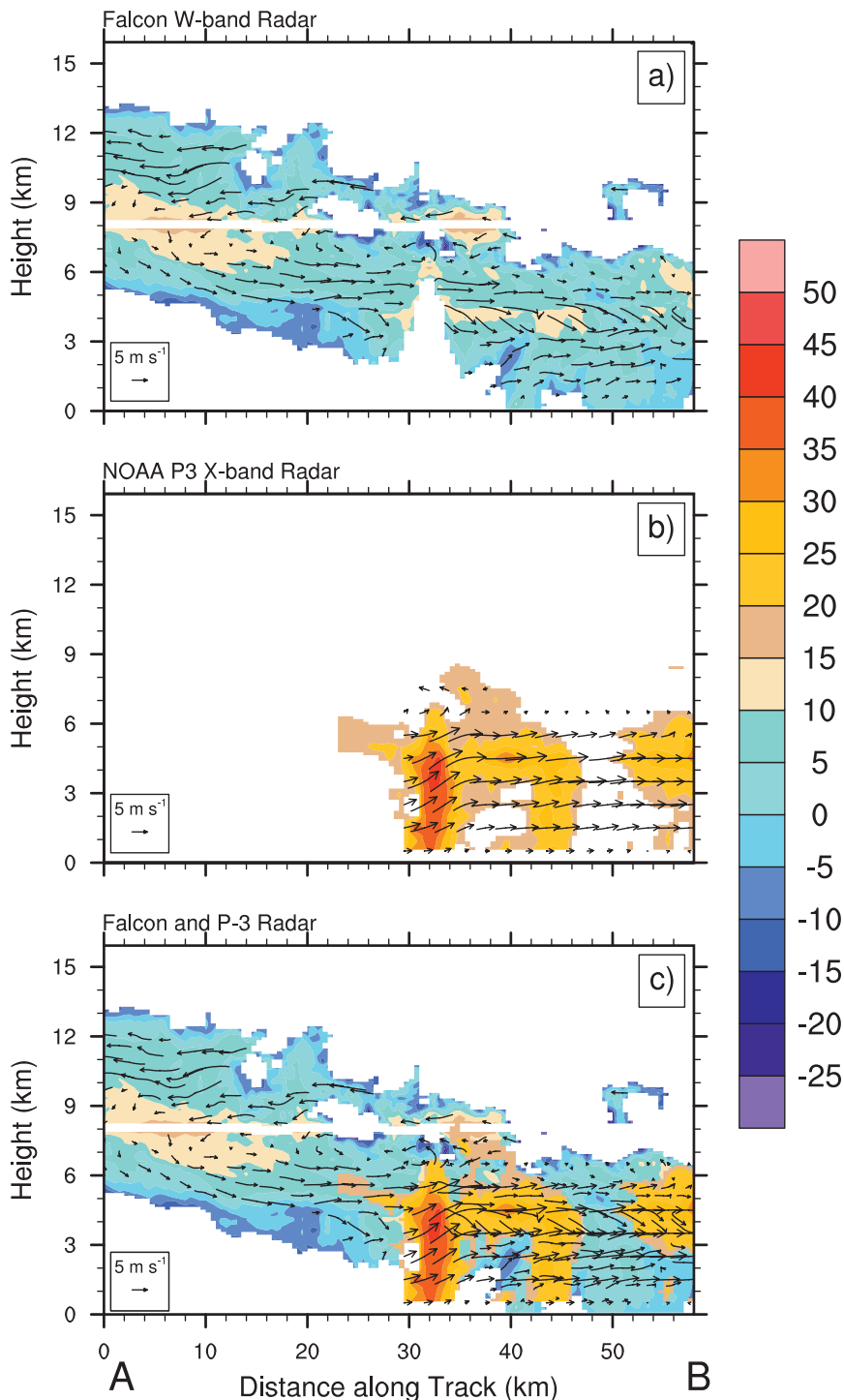


FIG. 8. Vertically pointing (a) Falcon 20 and (b) WP-3D Doppler radar reflectivity (colored contours, dBZ) coincident measurements from 0753 to 0757 UTC 8 Dec 2011 near Gan Island (see Fig. 7) are combined into (c) a coherent vertical cross section. The different radar wavelengths are sensitive to different size particles, allowing for a more detailed picture of the convective system. The overlaid arrows represent 3D wind vectors along the 2D vertical cross section computed from Doppler velocities. Scale for wind vectors is shown in the bottom-left corner of each plot. Values below 15 dBZ are not shown for the WP-3D. The coarse temporal (hence spatial)-resolution WP-3D data are interpolated to the Falcon 20 grid to retain the detailed information provided.

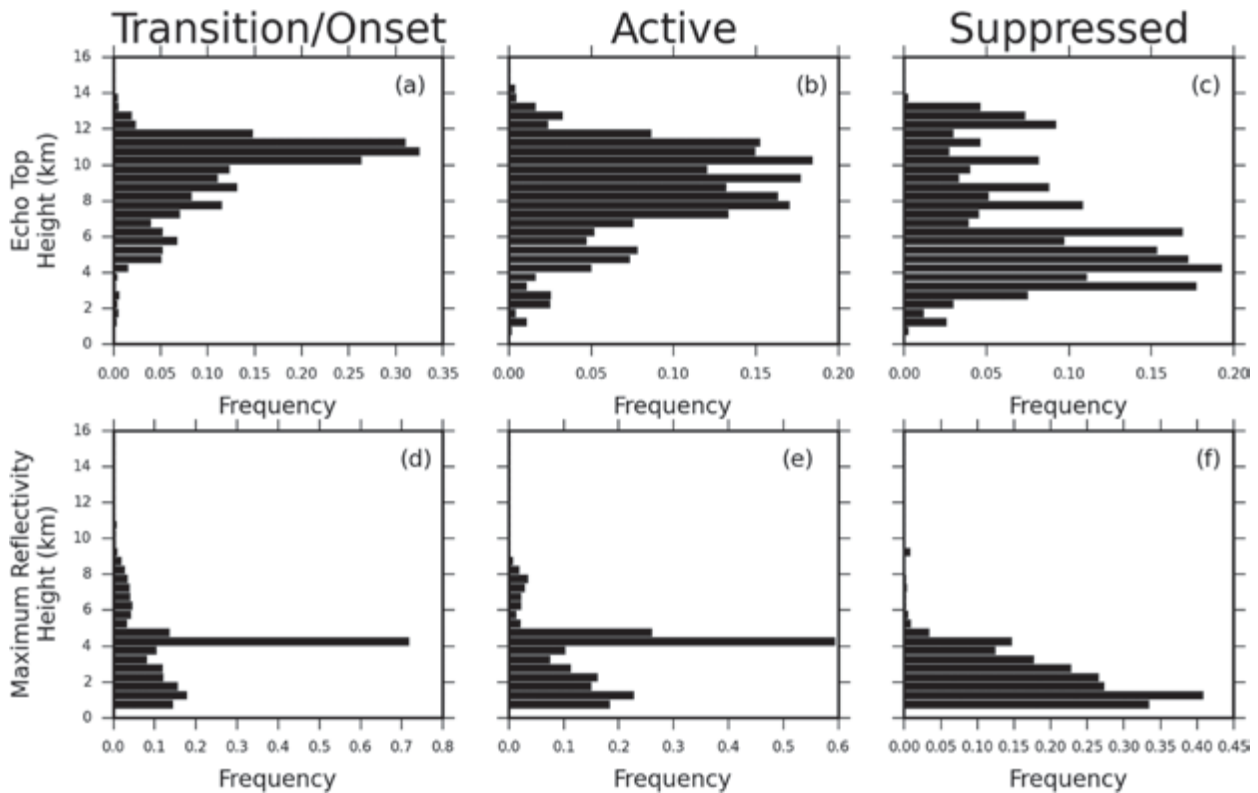


FIG. 9. Frequency of occurrence of (a)–(c) convective echo-top height and (d)–(f) the level of maximum reflectivity observed by the WP-3D Doppler radar during the transition/onset of the equatorial convection on (a),(d) 22 Nov; (b),(e) convectively active phase on 24 Nov; and (c),(f) suppressed phase of the MJO on 8 Dec 2011.

COUPLED OBSERVATIONS OF CONVECTIVELY INDUCED AIR–SEA INTERACTION.

It has been hypothesized that air–sea interaction is one of the important factors affecting the equatorial convective cloud systems and the MJO. Chen and Houze (1997a) identified a bidiurnal cycle of large MCSs, referred to as “diurnal dancing,” during the MJO active phases over the west Pacific warm pool during TOGA COARE. They speculated that the convective cold pools and large cloud shields have contributed to the slow recovery (>24 h) of the SST and the atmospheric boundary layer after a major convective event. Using satellite-derived SST, wind, and rainfall data, Li and Carbone (2012) showed coherent mesoscale patterns in these fields, suggesting that air–sea coupling plays an important role in the observed rainfall and SST variability over the tropics. However, there are no in situ observations to address the physical processes through which the convection interacts with the ocean and how the air–sea interaction processes vary in different phases of the MJO until DYNAMO. Here we use the aircraft data to examine the coherent variability of the air–sea fluxes and convection during the suppressed and active

phases of the MJO over the Indian Ocean. More than 200 collocated GPS dropsonde and AXBT pairs were deployed from the WP-3D aircraft from 11 November to 13 December 2011, which covers the convectively suppressed, transition, and active phases of the MJO.

Convectively induced SST variability. Convective downdrafts and freshwater pools from the rain induce a large spatial and temporal variability in SST, which in turn affects the development of convective cloud systems and air–sea fluxes. During the suppressed phase of the MJO, cool water pools were observed from the infrared camera on board the WP-3D. An example from the WP-3D mission targeting the convective cool pools near Gan Island on 16 November is shown in Fig. 11. The flight track is overlaid on the S-band/Ka-band Dual Polarization, Dual Wavelength Doppler Radar (S-PolKa) reflectivity image, showing isolated small convective cloud systems that the WP-3D was sampling (Fig. 11a). A detailed description of the convective rain cells and associated cold pool signals observed by S-PolKa on 16 November 2011 can be found in Houze et al. (2011). Figures 11b and 11c show a mosaic and spatial series of SST_{skin} variation along

the flight leg marked in red, across a gust front–like feature near convective cells (>40 dBZ; Fig. 11a). The cross-track scale was roughly 1.4 km, and this flight leg spanned roughly 15 km (Figs. 11b and 11c). The small convective systems generated a significant cold pool possibly related to the gust front. Note the two specific features that appear as a pool of cool water and a sharp frontal feature from warm to colder water. The sharp front was detected around 8.5 km into the flight leg. Both of these features may be due to recent rain from the convective cells in the region, as seen in the S-PolKa radar reflectivity (Fig. 11a; see sidebar for additional information on rain, cold pools, and ocean surface during DYNAMO). Although it is difficult to obtain absolute SST_{skin} without ambient measurements, the temperature gradient of nearly 1°C across the flight leg is a robust signal with the effects of window and atmosphere having been removed. Within the cold pool on the ocean surface, the small-scale temperature variability is about $0.1^{\circ}\text{C m}^{-1}$. During the active phase of the MJO, the SST (not shown) is more complex with multiscale variability that may be due to both the convectively induced local winds from downdrafts and rain and is under further investigation.

Upper-ocean and atmospheric boundary layer temperatures, and air–sea fluxes. One of the sampling strategies of the WP-3D aircraft missions was to observe the atmosphere and ocean environments during both the convectively suppressed and active phases of the MJO. Low-level atmospheric and upper-ocean temperatures were observed by the GPS dropsondes and AXBTs deployed concurrently from the WP-3D aircraft from the southwest–northeast transects between Diego Garcia and the R/V *Revelle* during the convectively suppressed period on 13 November (Fig. 12a) and the active phase on 26 November (Fig. 12b). Three main features are noteworthy. First, the upper-ocean temperature is 2° – 3°C warmer during the suppressed phase with weaker winds than the active phase, whereas the atmosphere surface and boundary layer temperatures remained similar. Second, the height of the atmosphere boundary layer (based on the definition of mixed layer using virtual potential temperature $< 0.5\text{ K}$) was higher during the suppressed phase (600–700 m) than in the active phase (500–600 m). Third, there were isolated deep convective clouds along the WP-3D transects on both days, as shown by *Meteosat-7* IR temperatures $< 225\text{ K}$ on 13 November (Fig. 12a) and temperatures $< 215\text{ K}$ on 26 November (Fig. 12c). However, the convective cold pools were stronger during the suppressed phase ($>3^{\circ}\text{C}$ depression; Fig. 12b) than the active phase ($<1.5^{\circ}\text{C}$; Fig. 12d). The dryer midlevel to upper-level

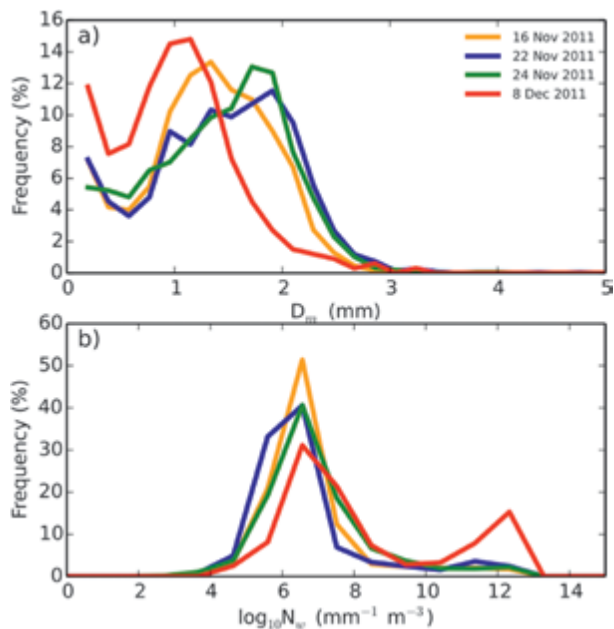


FIG. 10. Probability distributions of (a) mean volume drop diameter and (b) generalized intercept parameter obtained from drop size distributions recorded by the CIP and PIP optical imaging probes aboard the WP-3D aircraft. Suppressed MJO phase/ITCZ on 16 Nov (orange) and 8 Dec (red), MJO onset on 22 Nov (blue), and active MJO phase (green) measurements are shown. The CIP and PIP measurements were made at flight levels typically from 1500 to 3000 m. The corresponding Doppler radar data for 22–24 Nov and 8 Dec are shown in Fig. 9.

environmental moisture may be a contributing factor to the stronger cold pools during the suppressed phase (Savarin et al. 2014).

The air–sea sensible and latent heat fluxes are computed from the GPS dropsonde and AXBT measurements using the COARE bulk flux algorithm (Fairall et al. 2003). The sensible heat flux is larger during the suppressed phase on 13 November than the active phase on 26 November over the regions without the influence of convection (from 100 to 750 km; Figs. 12 and 13a). The large surface temperature difference between the air and sea (2° – 3°C) and the relatively low wind speed ($<5\text{ m s}^{-1}$) are the main reasons for the higher sensible heat flux during the suppressed phase (Fig. 13b). While the difference in the air–sea mixing ratio was larger on 13 November (suppressed conditions), the latent heat flux was larger on 26 November (active phase) due to the higher wind speed (Figs. 13c and 13d).

Convective cold pools and boundary layer recovery. Convectively generated cold pools can suppress convection by cooling and/or drying the surface and

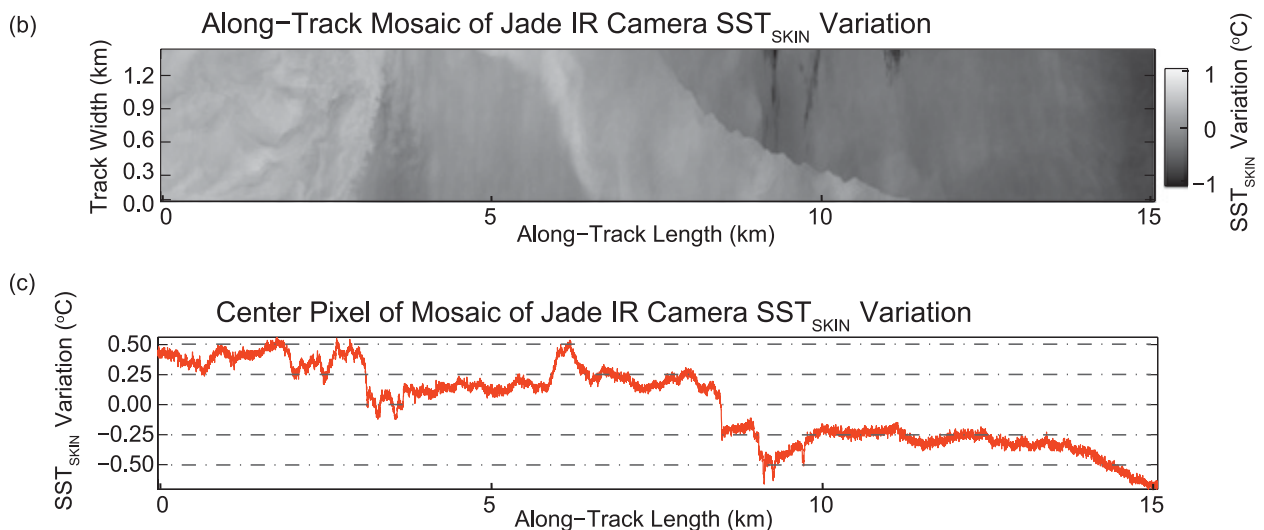
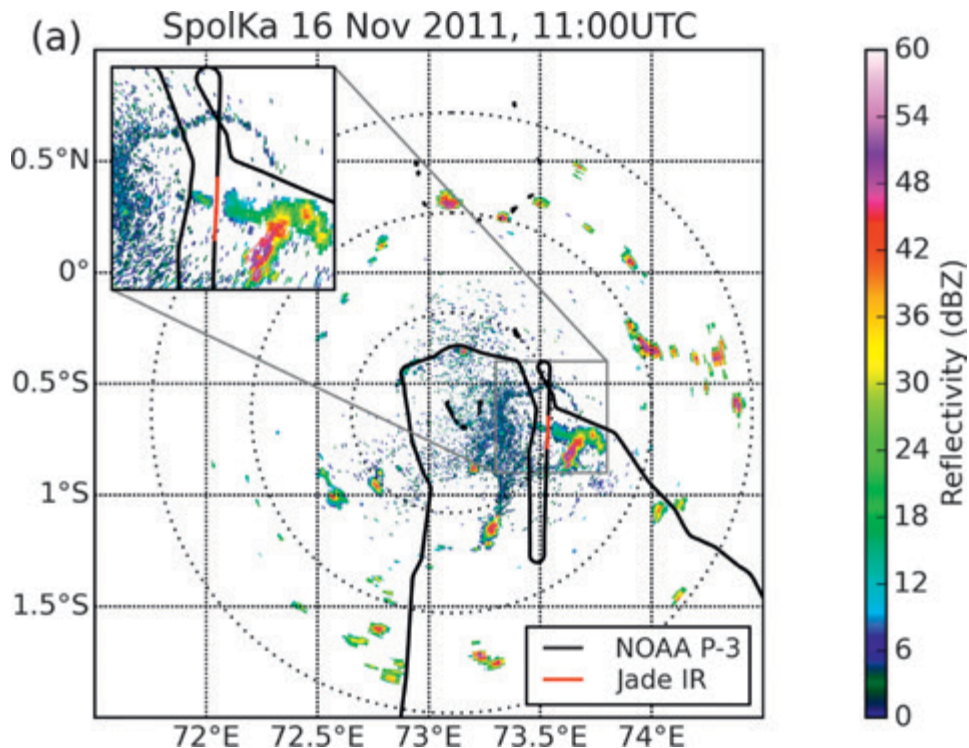


FIG. 11. (a) S-PolKa radar reflectivity at 1100 UTC 16 Nov 2011 (from 0.5° elevation scan) overlaid with the WP-3D flight track (black). The segment of track in red corresponds to 1108:05–1110:00 UTC for the SST_{skin} data shown in (b) and (c). The inset shows a zoomed region near the Jade IR SST measurement. The radial range rings are every 50 km. (b) Mosaic and (c) spatial series of SST_{skin} variation measured from the Jade IR camera on the WP-3D near Gan Island. (Note the large region of cold pool in the mosaic of SST_{skin} .)

boundary layers. Future development of convective cloud systems depends on the recovery of the surface and boundary layers, which is a function of the sunlight and air–sea fluxes. To better understand the air–sea interaction and its impact on convection, we use the aircraft data to investigate both the convectively generated cold pool depth and strength and the

boundary layer recovery time during convectively active and suppressed phases of MJO. The WP-3D Doppler radar data were used to identify the convective cloud and precipitation structures that produced the cold pools. The GPS dropsonde data were used to compute the depth and strength of the cold pools, that is, the depth and intensity of negative buoyancy similar

to that described in Bryan et al. (2005). The air–sea fluxes are computed from the GPS dropsonde and AXBT data. To assess the accuracy of the bulk fluxes, we compared the turbulence sensible and latent heat flux data from R/V *Revelle* that overlapped in time with the WP-3D observations in November–December 2011 (C. Fairall and J. Edson 2015, personal communication). The two air–sea flux datasets matched remarkably well. The boundary layer recovery time is then calculated based on the method used in TOGA COARE (Jorgensen et al. 1997), which is the time for the boundary layer properties to recover from the environmental conditions.

In general, the boundary layer recovery times are positively correlated with the surface wind speed and air–sea fluxes (Figs. 14a, 14c, and 14d). Stronger winds and increased air–sea fluxes reduce the recovery time during the convectively active phase, which indicates a positive feedback between the convection and air–sea fluxes. However, the recovery times are longer (5–24 h) during the suppressed phase on 8 December than during the 22–24 November cases (1–13 h; Fig. 14a). The slower recovery time is related to the environmental lower-tropospheric water vapor (700–50-hPa-layer mean RH; Fig. 14b). The depth of the cold pools varies from less than 100 to over 2000 m. The deepest and strongest cold pools were observed in convective cloud systems during the suppressed phase on 8 December (Savarin et al. 2014), which is consistent with the example shown in Fig. 12. The drier the environment the

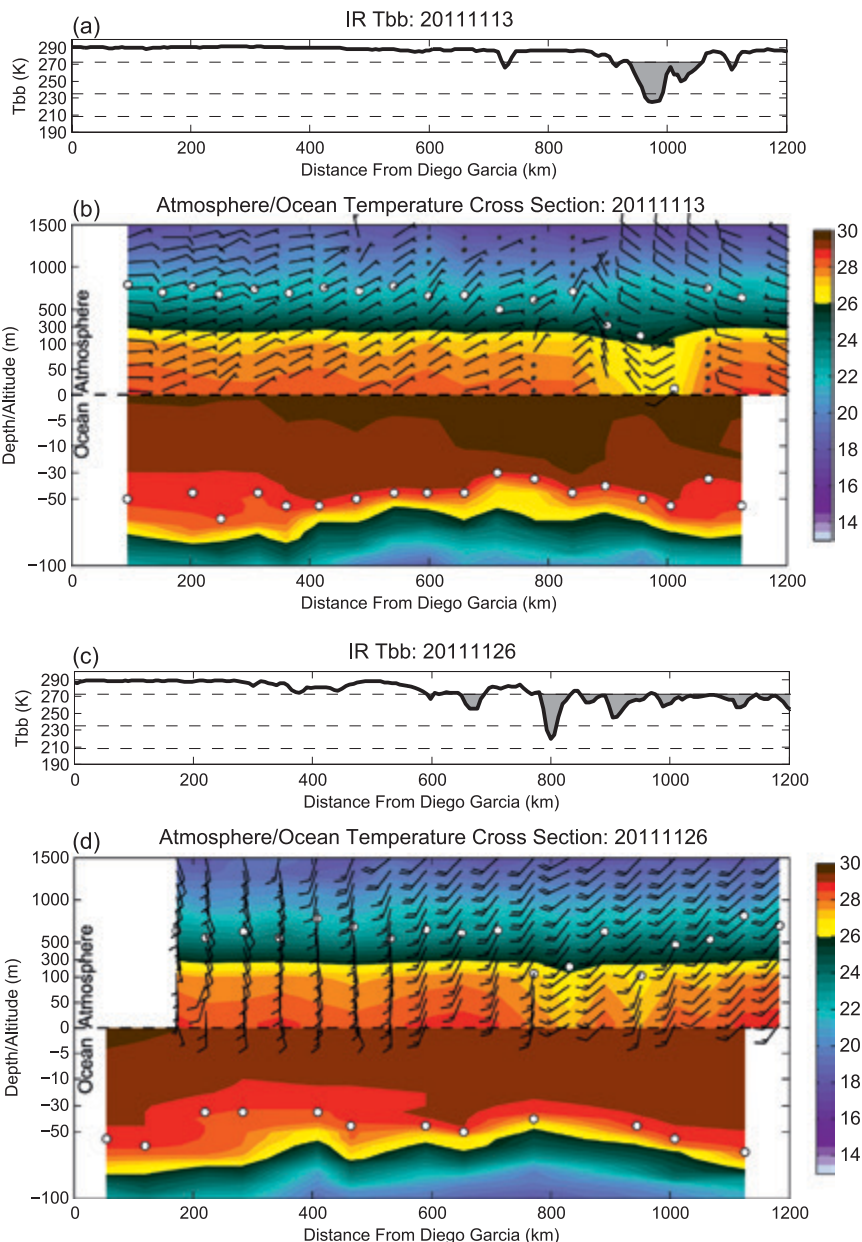


FIG. 12. The *Meteosat-7* IR cloud-top temperatures (K) and the lower-atmospheric and upper-ocean temperatures (color, °C) measured by the GPS dropsondes and AXBTs deployed from the WP-3D aircraft from transects between Diego Garcia and the R/V *Revelle* during the (a),(b) convectively suppressed phase (13 Nov) and (c),(d) active phase (26 Nov) of the MJO. The depths of the atmosphere and upper-ocean mixed layers are shown by white dots. Note that the altitude in the atmosphere and depth in the ocean are shown in different log scales (m). The wind barbs show the horizontal wind directions and speeds.

stronger and deeper the cold pools, which is not unexpected given that dry air entrainment by convection can enhance evaporation and convective downdraft. These results may have important implications for the timing of the postconvection surface/boundary layer recovery during an MJO event.

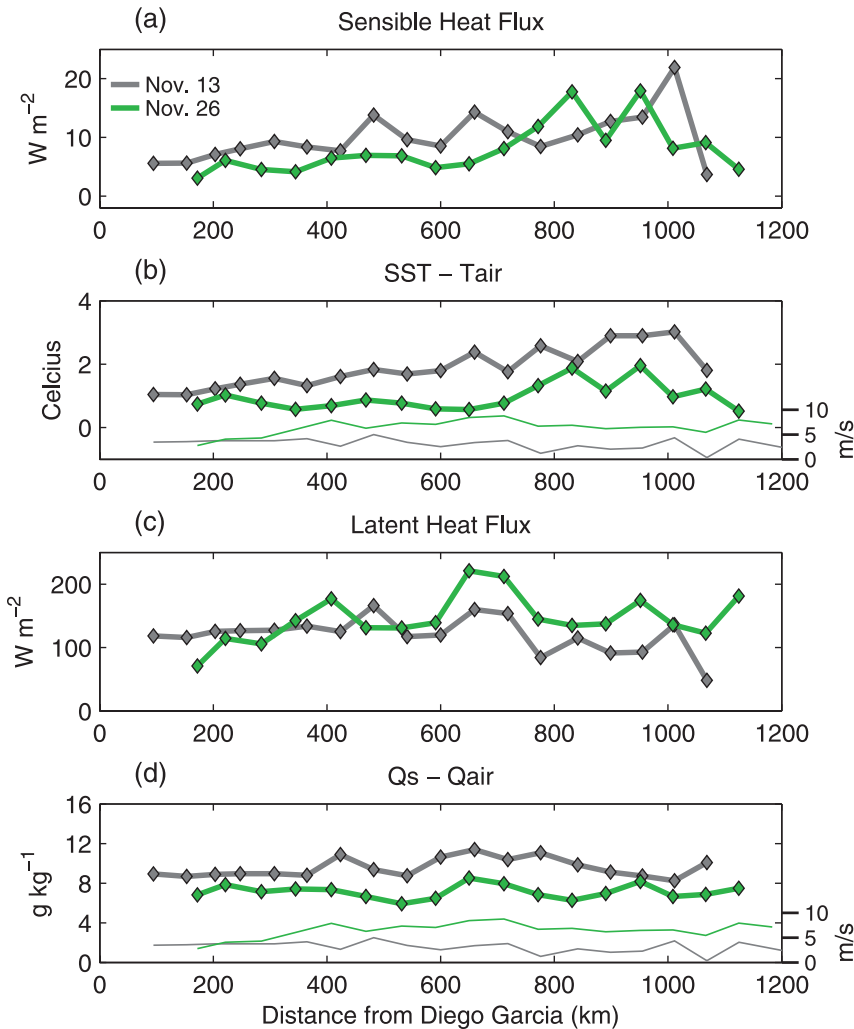


FIG. 13. (a) Air–sea sensible and (c) latent heat fluxes observed using the WP-3D dropsonde and AXBT data from the convectively suppressed phase on 13 Nov (gray) and the active phase on 26 Nov 2011 (green) along the same transects showing in Fig. 12. Corresponding (b) air–sea temperature and (d) specific humidity differences along with the surface wind speeds (m s^{-1} , thin gray and green lines).

CONCLUDING REMARKS. The DYNAMO field campaign collected unprecedented aircraft observations over the tropical Indian Ocean during November–December 2011. The mobility of the aircraft proves to be vital in capturing some key features, such as the spatial distribution of the large-scale water vapor and the small-scale SST variations associated with convective cold pools, filling a gap from the ship- and land-based station observations. These observations, in combination with other DYNAMO land-based, shipborne, and satellite data, have provided invaluable new insights into MJO initiation over the tropical Indian Ocean. A number of emerging science topics are highlighted here:

- Dry air intrusions from the subtropics may suppress convection in the ITCZ, which is favorable for the onset of the equatorial convection during MJO initiation (Figs. 3–5).
- Distinct characteristics were found in the convective structure and microphysical properties of MCSs during the suppressed, transition/onset, and active phases of the MJO (Figs. 9 and 10).
- Convective cold pools are deeper and stronger in MCSs surrounded by the low–midlevel dry air (Figs. 6, 8, and 14) in the suppressed phase, which prolong the atmosphere boundary layer recovery time.
- The atmospheric boundary layer depth and upper-ocean temperature are higher during the suppressed phase than during the active phase, and the air–sea temperature difference and sensible fluxes (Figs. 12 and 13) are larger during the suppressed phase of the MJO.

These topics deserve further investigation. Collectively they highlight the importance of the atmospheric water vapor variability and its impact on organi-

zations and structure of convective cloud systems, as well as their interaction with the ocean through air–sea fluxes on MJO initiation over the tropical Indian Ocean. The aircraft sampling strategy allowed for coherent observations of MCS structure and microphysics using the Doppler radar and microphysics probes and the large-scale atmospheric and ocean environment using the GPS dropsonde and AXBT measurements, which were not available in TOGA COARE. The dual aircraft measurements by the WP-3D and Falcon 20 Doppler radars provided the first 3D reflectivity and velocity observations from 0.5–15.0-km height. The results shown here will help us improve and evaluate high-resolution, cloud-resolving, and

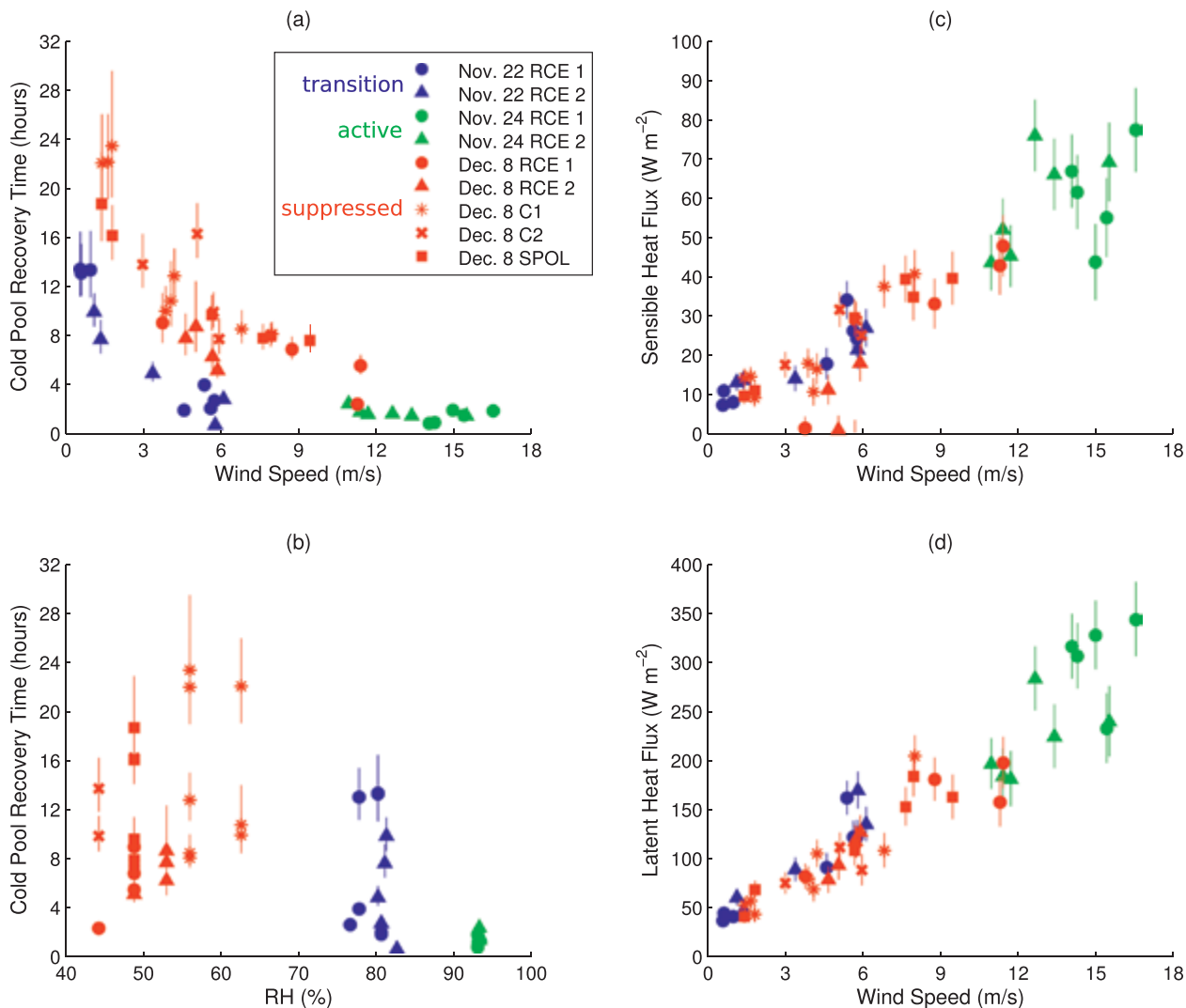


FIG. 14. The WP-3D aircraft observed convective cold pool recovery time varies with (a) wind speed and (b) the 700–500-hPa environment RH averaged over a circular area of 200–500-km radius from each dropsonde. The (c) surface sensible heat and (d) latent heat fluxes varying with wind speed, for individual convective modules from 22 Nov (blue), 24 Nov (green), and 8 Dec 2011 (red), which represent the MJO transition/onset, convectively active, and suppressed phases, respectively. The error bars represent the uncertainty due to SST $\pm 0.5^{\circ}C$ and the range of wind speeds within the lowest 50 m.

coupled atmosphere–ocean models for better prediction of MJO initiation processes in the future. The aircraft data have been organized into an easily accessible form made available online (http://data.eol.ucar.edu/master_list/?project=DYNAMO). It is hoped that they will be used by others in studies for better understanding and predicting the MJO and numerical model evaluation and verification.

ACKNOWLEDGMENTS. We thank our colleagues at the NOAA Aircraft Operations Center (AOC; Jim McFadden, the pilots, aircraft crew, and flight directors) and the NCAR Earth Observing Laboratory (EOL; Jim Moore, José

Meitin, Scot Loehrer, and others), who provided critical support for operating the aircraft from Diego Garcia and Gan during DYNAMO. We are grateful to Patrick Chuang, Mikael Witte, and Bob Black for their help in processing the microphysics data; Scott Brown for collecting the IR SST imaging data; David Trampp, Jeff Kerling, and Qing Wang for the AXBT data; Tammy Weckwerth and Scott Ellis for helping with the aircraft missions using S-PolKa data near Gan Island; Jeff Hawkins for providing the satellite data in real time; Jon Gottschalck and Nick Hall for real-time forecasting support; and Ed Ryan for assisting with the cloud-cluster tracking during DYNAMO. Aircraft- and ground-based radar images were created using the Py-ART

and AWOT software packages courtesy of the Department of Energy ARM Climate Research facility and the NOAA National Severe Storms Laboratory, respectively. Comments and suggestions from three anonymous reviewers and Dr. Brian Mapes helped improve the manuscript significantly. This research was supported by grants from NOAA (NA11OAR4310077), NSF (AGS1062242), and ONR (N000141110562).

REFERENCES

- Benedict, J., and D. A. Randall, 2009: Structure of the Madden–Julian oscillation in the superparameterized CAM. *J. Atmos. Sci.*, **66**, 3277–3296, doi:10.1175/2009JAS3030.1.
- Brown, R. G., and C. Zhang, 1997: Variability of midtropospheric moisture and its effect on cloud-top height distribution during TOGA COARE. *J. Atmos. Sci.*, **54**, 2760–2774, doi:10.1175/1520-0469(1997)054<2760:VOMMAI>2.0.CO;2.
- Bryan, G., D. Ahijevich, C. Davis, S. Trier, and M. Weisman, 2005: Observations of cold pool properties in mesoscale convective systems during BAMEX. *11th Conf. on Mesoscale Processes*, Hyannis, MA, Amer. Meteor. Soc., JP5.12. [Available online at https://ams.confex.com/ams/32Rad11Meso/techprogram/paper_96718.htm.]
- Chen, S. S., and R. A. Houze, Jr., 1997a: Diurnal variation and lifecycle of deep convective systems over the tropical Pacific warm pool. *Quart. J. Roy. Meteor. Soc.*, **123**, 357–388, doi:10.1002/qj.49712353806.
- , and —, 1997b: Interannual variability of deep convection over the tropical warm pool. *J. Geophys. Res.*, **102**, 25 783–25 795, doi:10.1029/97JD02238.
- , —, and B. E. Mapes, 1996: Multiscale variability of deep convection in relation to large-scale circulation in TOGA COARE. *J. Atmos. Sci.*, **53**, 1380–1409, doi:10.1175/1520-0469(1996)053<1380:MVODCI>2.0.CO;2.
- Fairall, C. W., E. F. Bradley, J. E. Hare, A. A. Grachev, and J. B. Edson, 2003: Bulk parameterization of air–sea fluxes: Updates and verification for the COARE algorithm. *J. Climate*, **16**, 571–591, doi:10.1175/1520-0442(2003)016<0571:BPOASF>2.0.CO;2.
- Gottschalck, J., P. E. Roundy, C. J. Schreck III, A. Vintzileos, and C. Zhang, 2013: Large-scale atmospheric and oceanic conditions during the 2011–12 DYNAMO field campaign. *Mon. Wea. Rev.*, **141**, 4173–4196, doi:10.1175/MWR-D-13-00022.1.
- Guy, N., and D. P. Jorgensen, 2014: Kinematic and precipitation characteristics of convective systems observed by airborne Doppler radar during the life cycle of a Madden–Julian oscillation in the Indian Ocean. *Mon. Wea. Rev.*, **142**, 1385–1402, doi:10.1175/MWR-D-13-00252.1.
- Houze, R. A., Jr., S. S. Chen, D. Kingsmill, Y. Serra, and S. E. Yuter, 2000: Convection over the Pacific warm pool in relation to the atmospheric Kelvin–Rossby wave. *J. Atmos. Sci.*, **57**, 3058–3089, doi:10.1175/1520-0469(2000)057<3058:COTPWP>2.0.CO;2.
- , H. C. Barns, D. Hence, and K. Chakravarty, 2011: Convective outbreak near Diego Garcia and cold pools near S-PolKa. DYNAMO Field Catalog. [Available online at http://catalog.eol.ucar.edu/cgi-bin/dynamo/htmlwrap?file_url=/dynamo/report/spolkascientist/20111116/report.SPolKaScientist.20111116.science_summary.html.]
- Huffman, G. J., and Coauthors, 2007: The TRMM Multisatellite Precipitation Analysis (TMPA): Quasi-global, multiyear, combined-sensor precipitation estimates at fine scales. *J. Hydrometeor.*, **8**, 38–55, doi:10.1175/JHM560.1.
- Jackson, R. C., and G. M. McFarquhar, 2014: An assessment of the impact of anti-shattering tips and artifact removal techniques on bulk cloud ice microphysical and optical properties measured by the 2D cloud probe. *J. Atmos. Oceanic Technol.*, **31**, 2131–2144, doi:10.1175/JTECH-D-14-00018.1.
- Johnson, R. H., and P. E. Ciesielski, 2013: Structure and properties of Madden–Julian oscillations deduced from DYNAMO sounding arrays. *J. Atmos. Sci.*, **70**, 3157–3179, doi:10.1175/JAS-D-13-065.1.
- Jorgensen, D. P., T. Matejka, and J. D. DuGranrut, 1996: Multi-beam techniques for deriving wind fields from airborne Doppler radars. *Meteor. Atmos. Phys.*, **59**, 83–104, doi:10.1007/BF01032002.
- , M. A. LeMone, and S. B. Trier, 1997: Structure and evolution of the 22 February 1993 TOGA-COARE squall line: Aircraft observations of precipitation, circulation, and surface energy fluxes. *J. Atmos. Sci.*, **54**, 1961–1985, doi:10.1175/1520-0469(1997)054<1961:SAEOTF>2.0.CO;2.
- Judt, F., and S. S. Chen, 2014: An explosive convective cloud system and its environmental conditions in MJO initiation observed during DYNAMO. *J. Geophys. Res. Atmos.*, **119**, 2781–2795, doi:10.1002/2013JD021048.
- Kerns, B. W., and S. S. Chen, 2014a: ECMWF and GFS model forecast verification during DYNAMO: Multiscale variability in MJO initiation over the equatorial Indian Ocean. *J. Geophys. Res. Atmos.*, **119**, 3736–3755, doi:10.1002/2013JD020833.
- , and —, 2014b: Equatorial dry air intrusion and related synoptic variability in MJO initiation during DYNAMO. *Mon. Wea. Rev.*, **142**, 1326–1343, doi:10.1175/MWR-D-13-00159.1.

- Kiladis, G. N., M. C. Wheeler, P. T. Haertel, K. H. Straub, and P. E. Roundy, 2009: Convectively coupled equatorial waves. *Rev. Geophys.*, **47**, RG2003, doi:10.1029/2008RG000266.
- Li, Y., and R. E. Carbone, 2012: Excitation of rainfall over the tropical western Pacific. *J. Atmos. Sci.*, **69**, 2983–2994, doi:10.1175/JAS-D-11-0245.1.
- Madden, R. A., and P. R. Julian, 1971: Detection of a 40–50 day oscillation in the zonal wind in the tropical Pacific. *J. Atmos. Sci.*, **28**, 702–708, doi:10.1175/1520-0469(1971)028<0702:DOADOI>2.0.CO;2.
- , and —, 1972: Description of global-scale circulation cells in the tropics with a 40–50 day period. *J. Atmos. Sci.*, **29**, 1109–1123, doi:10.1175/1520-0469(1972)029<1109:DOGSCC>2.0.CO;2.
- Maloney, E. D., and D. L. Hartmann, 2000: Modulation of hurricane activity in the Gulf of Mexico by the Madden-Julian Oscillation. *Science*, **287**, 2002–2004, doi:10.1126/science.287.5460.2002.
- Mechem, D. B., S. S. Chen, and R. A. Houze Jr., 2005: Momentum transport processes in the stratiform regions of mesoscale convective systems over the western Pacific warm pool. *Quart. J. Roy. Meteor. Soc.*, **132A**, 709–736, doi:10.1256/qj.04.141.
- Moum, J. N., and Coauthors, 2014: Air–sea interactions from westerly wind bursts during the November 2011 MJO in the Indian Ocean. *Bull. Amer. Meteor. Soc.*, **95**, 1185–1199, doi:10.1175/BAMS-D-12-00225.1.
- Savarin, A., S. S. Chen, B. W. Kerns, and D. P. Jorgensen, 2014: Convective cold pool structure and boundary layer recovery time in DYNAMO. *31st Conf. on Hurricanes and Tropical Meteorology*, San Diego, CA, Amer. Meteor. Soc., 9B.2. [Available online at <https://ams.confex.com/ams/31Hurr/webprogram/Paper245387.html>.]
- Smull, B. F., and R. A. Houze Jr., 1987: Rear inflow in squall lines with trailing stratiform precipitation. *Mon. Wea. Rev.*, **115**, 2869–2889, doi:10.1175/1520-0493(1987)115<2869:RIISLW>2.0.CO;2.
- Stephens, G. L., P. J. Webster, R. H. Johnson, R. Engelen, and T. S. L'Ecuyer, 2004: Observational evidence for the mutual regulation of the tropical hydrological cycle and tropical sea surface temperatures. *J. Climate*, **17**, 2213–2224, doi:10.1175/1520-0442(2004)017<2213:OEFTMR>2.0.CO;2.
- Yoneyama, K., and D. B. Parsons, 1999: A proposed mechanism for the intrusion of dry air into the tropical western Pacific region. *J. Atmos. Sci.*, **56**, 1524–1546, doi:10.1175/1520-0469(1999)056<1524:APMFTI>2.0.CO;2.
- , C. Zhang, and C. N. Long, 2013: Tracking pulses of the Madden–Julian oscillation. *Bull. Amer. Meteor. Soc.*, **94**, 1871–1891, doi:10.1175/BAMS-D-12-00157.1.
- Zhang, C., 2013: Madden–Julian oscillation: Bridging weather and climate. *Bull. Amer. Meteor. Soc.*, **94**, 1849–1870, doi:10.1175/BAMS-D-12-00026.1.
- Zhang, H.-M., J. J. Bates, and R. W. Reynolds, 2006: Assessment of composite global sampling: Sea surface wind speed. *Geophys. Res. Lett.*, **33**, L17714, doi:10.1029/2006GL027086.
- Zhou, S., M. L'Heureux, S. Weaver, and A. Kumar, 2012: A composite study of the MJO influence on the surface air temperature and precipitation over the continental United States. *Climate Dyn.*, **38**, 1459–1471, doi:10.1007/s00382-011-1001-9.
- Zipser, E. J., 1977: Mesoscale and convective-scale downdrafts as distinct components of squall line structure. *Mon. Wea. Rev.*, **105**, 1568–1589, doi:10.1175/1520-0493(1977)105<1568:MACDAD>2.0.CO;2.
- Zuluaga, M. D., and R. A. Houze, 2013: Evolution of the population of precipitating convective systems over the equatorial Indian Ocean in active phases of the Madden–Julian oscillation. *J. Atmos. Sci.*, **70**, 2713–2725, doi:10.1175/JAS-D-12-0311.1.

EYEWITNESS

EVOLUTION OF THE ATMOSPHERIC SCIENCES

by ROBERT G. FLEAGLE

Eyewitness: Evolution of the Atmospheric Sciences describes how the atmospheric sciences were transformed in the span of the author's professional career from its origins in primitive weather forecasting to its current focus on numerical modeling of environmental change. It describes the author's observations of persons, events, and institutions beginning with graduate study during the Second World War and moving on to continuing expansion of the atmospheric sciences and technologies, through development of a major university department, development of new scientific and professional institutions, and to the role that the science of the atmosphere now plays in climate change and other issues of social and political policy.

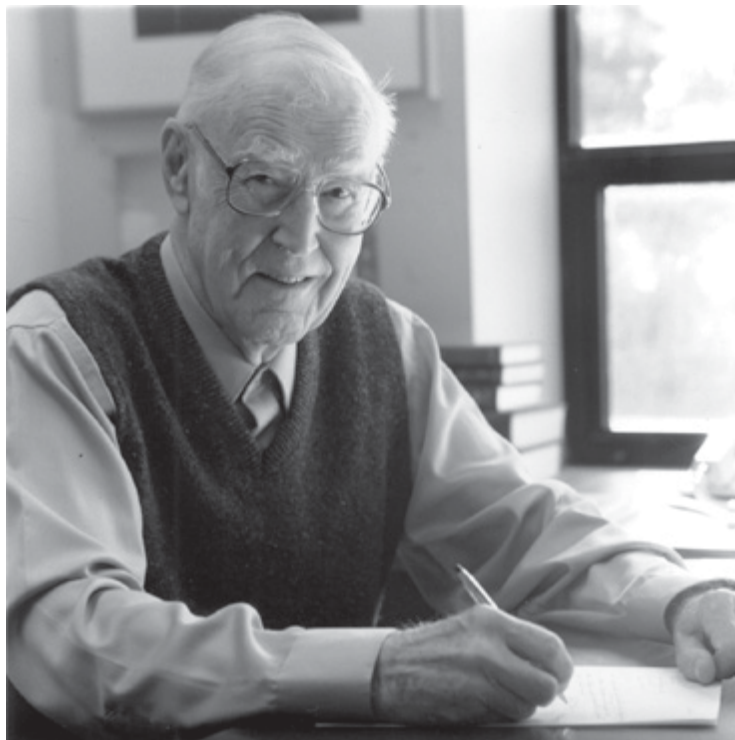


Photo ©Kathy Sauber/University of Washington

EYEWITNESS: EVOLUTION OF THE ATMOSPHERIC SCIENCES

ISBN 1-878220-39-X, 129 pp., hardbound, \$75 list/\$55 member.

Order online: www.ametsoc.org/amsbookstore

or see the order form at the back of this issue.

ABOUT THE AUTHOR

Robert G. Fleagle earned degrees in physics and meteorology at The Johns Hopkins University and New York University and began his professional career in 1948 at the University of Washington (UW). His research has focused on the structure of midlatitude cyclones, the physics and structure of the surface boundary layer, and processes of air-sea interaction. He is the author of about 100 papers published in scientific journals and of books on atmospheric physics and global environmental change. Applications of science to social and political policy have been important motivations for his career and have occupied his attention increasingly as the decades passed.

Fleagle participated at close range in the beginnings and growth of a major university department and of the University Corporation for Atmospheric Research (UCAR). In 1963 and 1964 he served as a staff specialist in the Office of Science and Technology, Executive Office of the President, and in 1977-78 he served as consultant to the National Oceanic and Atmospheric Administration. He has held many administrative posts including chairman of the UW Department of Atmospheric Sciences (1967-77), chairman of the National Academy of Sciences Committee on Atmospheric Sciences (1969-73),

THE DEEP PROPAGATING GRAVITY WAVE EXPERIMENT (DEEPWAVE)

An Airborne and Ground-Based Exploration of Gravity Wave Propagation and Effects from Their Sources throughout the Lower and Middle Atmosphere

BY DAVID C. FRITTS, RONALD B. SMITH, MICHAEL J. TAYLOR, JAMES D. DOYLE, STEPHEN D. ECKERMANN, ANDREAS DÖRNBRACK, MARKUS RAPP, BIFFORD P. WILLIAMS, P.-DOMINIQUE PAUTET, KATRINA BOSSERT, NEAL R. CRIDDLE, CAROLYN A. REYNOLDS, P. ALEX REINECKE, MICHAEL UDDSTROM, MICHAEL J. REVELL, RICHARD TURNER, BERND KAIFLER, JOHANNES S. WAGNER, TYLER MIXA, CHRISTOPHER G. KRUSE, ALISON D. NUGENT, CAMPBELL D. WATSON, SONJA GISINGER, STEVEN M. SMITH, RUTH S. LIEBERMAN, BRIAN LAUGHMAN, JAMES J. MOORE, WILLIAM O. BROWN, JULIE A. HAGGERTY, ALISON ROCKWELL, GREGORY J. STOSSMEISTER, STEVEN F. WILLIAMS, GONZALO HERNANDEZ, DAMIAN J. MURPHY, ANDREW R. KLEKOCIUK, IAIN M. REID, AND JUN MA

The DEEPWAVE experiment employed extensive airborne and ground-based measurements to provide new insights into gravity wave dynamics.

The Deep Propagating Gravity Wave Experiment (DEEPWAVE) was the first comprehensive measurement program devoted to quantifying the evolution of gravity waves (GWs) arising from sources at lower altitudes as they propagate, interact with mean and other wave motions, and ultimately dissipate from Earth's surface into the mesosphere and lower thermosphere (MLT). Research goals motivating the DEEPWAVE measurement program are summarized in Table 1. To achieve our research goals, DEEPWAVE needed to sample regions having large horizontal extents because of large horizontal GW propagation distances for some GW sources.

DEEPWAVE accomplished this goal through airborne and ground-based (GB) measurements that together provided sensitivity to multiple GW sources and their propagation to, and effects at, higher altitudes. DEEPWAVE was performed over and around the GW "hotspot" region of New Zealand (Fig.1, top) during austral winter, when strong vortex edge westerlies provide a stable environment for deep GW propagation into the MLT.

DEEPWAVE airborne measurements employed two research aircraft during a core 6-week airborne field program based at Christchurch, New Zealand, from 6 June to 21 July 2014. The National Science

TABLE 1. Science goals.

<ul style="list-style-type: none"> • Detailed measurements and modeling of GW sources, propagation, momentum fluxes, instabilities, and effects, from their sources in the troposphere into the MLT, in the GW hotspot over New Zealand and Tasmania, and the Southern Ocean.
<ul style="list-style-type: none"> • Understanding GW variations throughout the stratosphere and the implications for momentum flux divergence and drag.
<ul style="list-style-type: none"> • Studies of GW propagation, filtering by mean and large-scale motions, and nonlinear interactions and instabilities impacting GW penetration into the MLT, where GW momentum deposition has major influences on circulation, structure, and variability.
<ul style="list-style-type: none"> • Predictability studies of GW sources, propagation, breaking, and their influences on forecasting.
<ul style="list-style-type: none"> • Characterization of GW sources, scales, amplitudes, intermittency, and momentum transport throughout the atmosphere as inputs to improved GW parameterizations for NWP, climate, and general circulation models.

Foundation (NSF)/National Center for Atmospheric Research (NCAR) Gulfstream V (GV) provided in situ, dropsonde, and microwave temperature profiler (MTP) measurements extending from Earth's surface to ~20 km throughout the core field program (see Table 2). The GV also carried three new instruments designed specifically to address DEEPWAVE science goals: 1) a Rayleigh lidar measuring densities and temperatures from ~20 to 60 km, 2) a sodium resonance lidar measuring sodium densities and temperatures from ~75 to 100 km, and 3) an advanced mesosphere temperature mapper (AMTM) measuring temperatures in a horizontal plane at ~87 km with a field of view (FOV) of ~120 km along track and 80 km cross track. AMTM measurements were augmented by two side-viewing infrared (IR) airglow "wing" cameras also viewing an ~87-km altitude that extended the cross-track FOV to ~900 km. A second aircraft, the DLR Falcon, participated in DEEPWAVE during the last half of the GV measurement interval. It hosted in situ dynamics and chemistry measurements and a downward-viewing aerosol Doppler lidar measuring line-of-sight winds below the Falcon, where aerosol backscatter was sufficient (see Table 2).

Ground-based DEEPWAVE measurements were likewise extensive (see Table 2). Radiosondes were launched at multiple sites, with those at three sites [two on the South Island (SI) western coast and one in the lee of the Southern Alps] providing frequent soundings during intensive observing periods (IOPs), and others launched from Tasmania and Macquarie Island coordinated with research flights (RFs) to support GW and predictability objectives in those regions. A 449-MHz wind profiler (WP) on the South Island western coast measured three-component winds continuously from ~0.5 to ~3–6 km. Additional instruments in the lee of the Southern Alps included 1) a ground-based AMTM measuring the horizontal temperature structure at ~87 km, 2) a Rayleigh lidar measuring temperatures from ~22 to 85 km, 3) two all-sky airglow imagers (ASIs) measuring airglow brightness at several altitudes from ~87 to 96 km, and 4) a Fabry–Perot interferometer (FPI) measuring winds and temperatures centered near ~87 and 96 km. For reference, the various airglow layers observed by the AMTMs, the ASIs, and the FPI all have full-width half maxima (FWHM) of ~7–10 km and may vary in altitude by several kilometers about their nominal

AFFILIATIONS: FRITTS, B. P. WILLIAMS, BOSSERT, MIXA, LIEBERMAN, AND LAUGHMAN—GATS Inc., Boulder, Colorado; SMITH, KRUSE, NUGENT, AND WATSON—Yale University, New Haven, Connecticut; TAYLOR, PAUTET, AND CRIDDLE—Utah State University, Logan, Utah; DOYLE, REYNOLDS, AND REINECKE—Naval Research Laboratory, Monterey, California; ECKERMANN—Naval Research Laboratory, Washington, DC; DÖRNBRACK, RAPP, KAIFLER, WAGNER, AND GISINGER—German Aerospace Center (DLR), Munich, Germany; UDDSTROM, REVELL, AND TURNER—NIWA, Newmarket, Auckland, New Zealand; SMITH—Boston University, Boston, Massachusetts; MOORE, BROWN, HAGGERTY, ROCKWELL, STOSSMEISTER, AND S. F. WILLIAMS—Earth Observing Laboratory, National Center for Atmospheric Research, Boulder, Colorado; HERNANDEZ*—University of Washington, Seattle, Washington; MURPHY

AND KLEKOCIUK—Australian Antarctic Division, Kingston, Tasmania, Australia; REID—University of Adelaide, Adelaide, South Australia, Australia; MA—Computational Physics, Inc., Springfield, Virginia
* Deceased

CORRESPONDING AUTHOR: D. C. Fritts, Boulder GATS Inc., 3360 Mitchell Lane, Boulder, CO 80301
E-mail: dave@gats-inc.com

The abstract for this article can be found in this issue, following the table of contents.

DOI:10.1175/BAMS-D-14-00269.1

In final form 19 May 2015
©2016 American Meteorological Society

altitudes. A second Rayleigh lidar and a meteor radar measuring winds from ~80 to 100 km were deployed at Kingston, Tasmania. Ground-based instrument sites are shown in Fig. 1 (bottom). Figure 2 shows the extent of all DEEPWAVE measurements in altitude and latitude.

DEEPWAVE began with a test flight-planning exercise from 1 to 10 August 2013 to gain experience with forecasting and flight planning and to assess the reliability of such forecasts in preparation for the real field program. This effort, which is summarized and archived online (see appendix A), was judged to be quite successful and led to confidence in the utility of a suite of forecasts and ancillary satellite products in guiding DEEPWAVE IOPs and flight plans.

The DEEPWAVE field program was supported by an extensive operations center at Christchurch International Airport that coordinated all logistical and measurement activities (see appendix B). Forecasting and flight planning was supported by a suite of global, mesoscale, and regional models that proved to be highly valuable and often quite accurate on shorter time scales for final flight planning (see Table 3). These models are now being applied in concert with DEEPWAVE data analysis efforts to answer the science questions posed in Table 1. To aid DEEPWAVE research, a comprehensive DEEPWAVE data archive and management plan has been developed (see appendix A).

MOTIVATIONS. GWs, or buoyancy waves, for which the restoring force is due to negatively (positively) buoyant air for upward (downward) displacements, play major roles in atmospheric dynamics, spanning a wide range of spatial and temporal scales. Vertical and horizontal wavelengths, λ_z and λ_h , respectively, for vertically propagating GWs are dictated by their sources and propagation conditions and range from meters to hundreds and thousands of kilometers, respectively, with typical scales increasing by ~10 times or more from the troposphere to the MLT. Intrinsic frequencies (i.e., with respect to the local flow) vary from the inertial frequency to the buoyancy frequency. GWs at lower frequencies dominate the energy spectra, but higher-frequency GWs have larger vertical group velocities and contribute disproportionately to vertical transports of energy and momentum. As a result, smaller-scale GWs ($\lambda_h \sim 10\text{--}200$ km) have larger impacts on atmospheric circulation, weather, and climate, but their effects are much more challenging to quantify. GW influences typically increase with altitude because decreasing density implies increasing GW amplitudes and effects. Large GW amplitudes

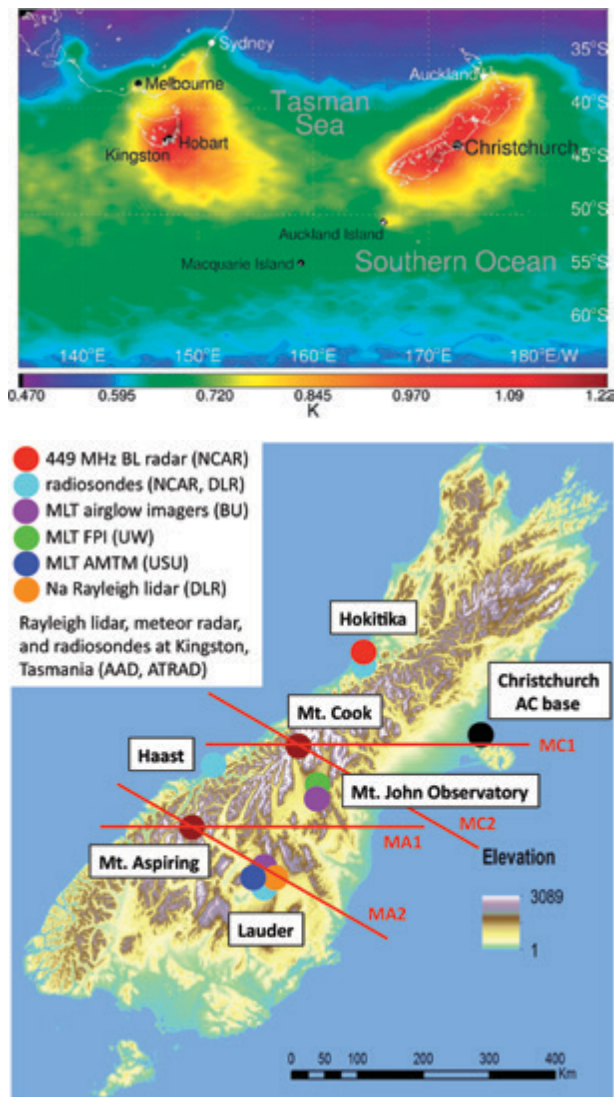


FIG. 1. (top) DEEPWAVE region of airborne and ground-based measurements over New Zealand, Tasmania, the Tasman Sea, and the Southern Ocean. Colors show the GW hotspots in AIRS rms temperature for Jun–Jul 2003–II at 2.5 hPa. (bottom) Ground-based instruments contributing to DEEPWAVE in New Zealand and elsewhere (see legend). The major orographic features are Mt. Cook and Mt. Aspiring, and red lines show flight tracks MCI, MC2, MA1, and MA2, of which MCI and MA2 were used for RF12 and RF22 measurements shown in Figs. 7, 9, and 10.

drive nonlinear (NL) wave–wave and wave–mean flow interactions, instabilities, turbulence, and energy and momentum deposition that result in a strong evolution of the GW spectrum with altitude. These complex dynamics, and their significant dependence on GW sources and the environments through which they propagate, pose major challenges for their parameterizations in global weather and climate models.

TABLE 2. Instruments and capabilities.

Instrument	Variable	Altitude
GV instruments		
Avionics/GPS	$(x, y, z), (U, V, W)$	FL
Gust probe	u, v, w at 25 Hz	FL
279 dropsondes	$V_h(z), q(z), T(z)$	FL–ground
MTP	$T(z)$	FL \pm ~5 km
Rayleigh lidar	$\rho(z), T(z)$	~20–60+ km
Na resonance lidar	$\rho_{Na}(z), T(z)$	~75–100 km
AMTM	$T(x, y), \text{zenith}$	~87 km
Airglow cameras	$I(x, y), \text{side views}$	~87 km
Falcon instruments		
Avionics/GPS	$(x, y, z), (U, V, W)$	FL
Gust probe	u, v, w at 25 Hz	FL
Doppler lidar	$u(x, z), w(x, z)$	~0–10 km
Ground-based instruments		
WP: Hokitika	$(U, V, W)(z)$	~0–4 km
Radiosondes: Haast (51), Hokitika (145), Lauder (98), and at Hobart and South Islands	$V_h(z), T(z), q(z)$	~0–30 km
Rayleigh lidars: Lauder and Kingston	$\rho(z), T(z)$	~20–70 km
AMTM: Lauder	$T(x, y)$	~87 km
ASIs: Lauder and MJO	$I(x, y)$ all sky	~87–96 km
FPI: MJO	V_h, T	~87, 96 km
Meteor radar: Kingston	$V_h(z)$	~80–100 km

Scientific interests and societal needs have motivated many previous studies of GWs from the stable boundary layer and troposphere, through the stratosphere and mesosphere, and into the thermosphere. Among the more important of these are the following:

- 1) GWs pose hazards to people and property; examples include sometimes severe downslope winds and severe turbulence at airline flight altitudes;
- 2) GWs exhibit a wide range of dynamics and effects that play important roles in atmospheric weather and climate from the surface into the MLT, but many of these are poorly understood at present;
- 3) GW motions are incompletely resolved both in global satellite observations and in global numerical weather prediction (NWP) and climate models, and so their effects in large-scale weather and climate models must be parameterized; and
- 4) Inadequate understanding and characterization of GW dynamics and effects have resulted in parameterizations of their effects in NWP and

climate models that are acknowledged to have major deficiencies.

The importance of GWs in multiple atmospheric processes has led to thousands of papers dealing with diverse GW topics including 1) sources; 2) propagation and refraction in variable environments; 3) linear and nonlinear behavior; 4) wave–wave and wave–mean flow interactions; 5) instabilities and turbulence due to large GW amplitudes and superpositions; 6) energy, momentum, and tracer transports; 7) parameterizations of GW effects in large-scale (LS) models; and 8) GW influences on other processes such as convection, cloud microphysics, chemical reactions, and plasma dynamics and instabilities in the ionosphere. Many other papers have addressed important GW roles in oceans, lakes, other planetary atmospheres, and stellar interiors.

PREVIOUS RESEARCH. The scope of GW dynamics and roles is reflected in the many seminal papers, reviews, and books describing these various

TABLE 3. Forecasting and research models. FV = finite volume. DNS = direct numerical simulation and NCEP GFS = National Centers for Environmental Prediction Global Forecast System.

Model	Type, application	Horizontal Resolution		Altitudes
		Operational/ real time	Research	
ECMWF IFS	Global, FC	TL1239 (~16 km)		0–80 km
NCEP GFS	Global, FC	T574 (~23 km)		0–65 km
NIWA/UKMO UM	Global, FC	N768 (~17 km)		0–80 km
NAVGEM	Global, FC, RE	T359 (~37 km)	T119–T425 (~30–110 km)	0–70 km
COAMPS adjoint	Regional, FC, RE	35 km	5–35 km	0–30 km
COAMPS	Regional, FC, RE	5 and 15 km	1–15 km	0–50 km
NZ Limited Area Model (NZLAM)	Regional, FC	12 km		0–80 km
NZ Convective Scale Model (NZCSM)	Regional, FC	1.5 km		0–40 km
WRF (various)	Regional, FC, RE	6 km	2 km	0–45 km
FR linear	Local, FC, RE	0.5–1 km	any	0–100 km
FV DNS	Local, RE		20 m–1 km	0–400 km
Spectral DNS	Local, RE		1–10 m	0–10 km

processes. Examples of those addressing atmospheric GW topics of most relevance to DEEPWAVE science include the following:

- 1) GW linear dynamics, propagation, conservation properties, and fluxes (Hines 1960; Eliassen and Palm 1961; Bretherton 1969a,b; Booker and Bretherton 1967; Gossard and Hooke 1975; Smith 1980; Nappo 2013);
- 2) GW sources, characteristics, and responses (Fritts 1984; Fritts and Alexander 2003);
- 3) GW refraction, mean flow interactions, and responses (Lindzen and Holton 1968; Holton 1982; Garcia and Solomon 1985; Haynes et al. 1991; Sutherland 2010; Bühler 2014);
- 4) GW spectral properties, interactions, instabilities, and saturation (Yeh and Liu 1981; Smith et al. 1987; Hines 1991; Lombard and Riley 1996; Sonmor and Klaassen 1997; Fritts et al. 2009); and
- 5) GW parameterizations for NWP and climate models (Lindzen 1981; Holton 1982; McFarlane 1987; Warner and McIntyre 1996; Hines 1997a,b; Kim et al. 2003; Fritts and Alexander 2003).

Below we provide an overview of previous research on atmospheric GWs, focusing on airborne

measurement programs, but also noting contributions by other ground-based, in situ, and satellite measurements (a number of which were employed during DEEPWAVE). Numerous modeling studies have likewise addressed GW sources, propagation, linear and nonlinear dynamics, and their various effects. However, we will restrict our overview to those

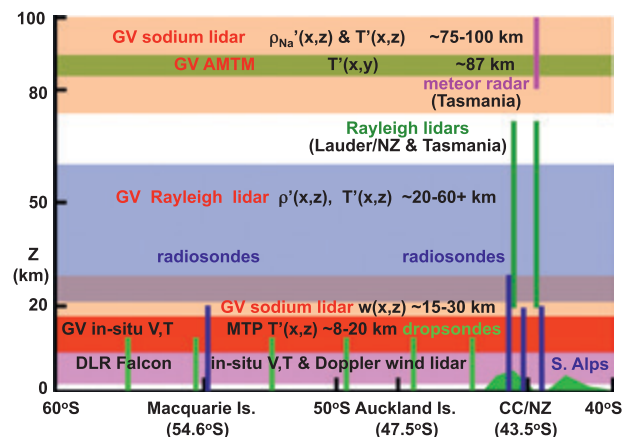


FIG. 2. North-south cross section showing the types of airborne and ground-based instruments contributing to DEEPWAVE measurements and their coverage in latitude and altitude.

efforts performed specifically for comparisons with observational data or which offer a global perspective on resolved GW sources, propagation, and effects.

The earliest studies of mountain waves (MWs) in the 1930s employed balloons and gliders to sample MW flows in North Africa and Europe (e.g., Queney 1936a,b; Küttner 1938, 1939; Manley 1945). These observations provided key insights into the structure of MWs and lee waves and, together with the Sierra Wave Project (see below), motivated initial theoretical advances (e.g., Queney 1947; Scorer 1949; Long 1953, 1955; see also Grubišić and Lewis 2004). Other observations of plasma motions in the ionosphere (now called traveling ionospheric disturbances) motivated the seminal paper by Hines (1960) that provided the theoretical framework for GW propagation throughout the atmosphere. Brief overviews of subsequent GW research using ground-based, in situ, and satellite measurements, accompanying more recent airborne programs, and employing mesoscale and global modeling are provided below.

Ground-based, in situ, and satellite measurements.

Ground-based and in situ measurement capabilities have improved dramatically since the earliest MW studies. Radiosondes have provided evidence of GW sources, scales, amplitudes, intrinsic properties, and fluxes from the surface into the middle stratosphere for many years (e.g., Tsuda et al. 1994; Allen and Vincent 1995; Sato and Dunkerton 1997; Sato and Yoshiki 2008; Geller et al. 2013). Stratospheric superpressure balloon measurements have likewise defined GW intrinsic properties and momentum fluxes (MFs) in the lower stratosphere and, in particular, their intermittency and potential for infrequent, but very strong, GW events to contribute a large fraction of the total momentum flux (e.g., Hertzog et al. 2008; Plougonven et al. 2008, 2013). Rocketborne falling spheres and newer ionization gauges, lidars, and other probes have measured winds, temperatures, and turbulence from ~30 to 100 km and enabled studies of energy dissipation rates due to GW breaking, MW filtering during a stratospheric warming, and anomalous MLT mean structure accompanying strong planetary waves (PWs) in the Southern Hemisphere and other dynamics (e.g., Rapp et al. 2004; Wang et al. 2006; Goldberg et al. 2006).

Multiple types of radars have quantified GW amplitudes, scales, spectral character, momentum fluxes, and evidence of various interaction and instability processes from the troposphere to the MLT for about five decades (e.g., Gossard et al. 1970; Atlas et al. 1970; Woodman and Guillen 1974; Sato and Woodman 1982; Vincent and Reid 1983; Balsley and Garello

1985; Fritts and Rastogi 1985; Fritts and Vincent 1987; Smith et al. 1987; Tsuda et al. 1989, 1990; Sato 1994; Thomas et al. 1999; Pavelin et al. 2001; Luce et al. 2008). Rayleigh and resonance lidars have likewise contributed to the definition of GW properties via measurements of temperatures, winds, and/or metallic species densities from very low altitudes to ~100 km or above (e.g., Chanin and Hauchecorne 1981; Gardner and Voelz 1987; She et al. 1991; Whiteway and Carswell 1994; Williams et al. 2006; Duck et al. 2001; Alexander et al. 2011; Lu et al. 2015). Other optical instruments, especially ASIs and the newer AMTMs, provide valuable information on GW horizontal wavelengths, orientations, phase speeds, and amplitudes, sometimes at multiple altitudes, that contribute greatly to quantification of GW character, propagation, and potential for instability and mean flow interactions (e.g., Gavrilov and Shved 1982; Taylor et al. 1995; Taylor and Hapgood 1988; Hecht et al. 1997, 2001; Walterscheid et al. 1999; Nakamura et al. 2003; Smith et al. 2009; Pautet et al. 2014; Hecht et al. 2014; Fritts et al. 2014).

Multi-instrument measurement programs performed at facilities having extensive ground-based instrument capabilities, such as those that often accompany large radar and/or rocket facilities, have made especially valuable contributions to GW studies. This is because no single instrument can define all of the atmospheric properties and spatial and temporal variability needed to fully quantify the local GW field. Examples of these facilities include the Arctic Lidar Observatory for Middle Atmosphere Research in Norway (69.3°N); the Poker Flat Research Range in Alaska (65.1°N); the Bear Lake Observatory in Utah (42°N); the middle- and upper-atmosphere (MU) radar in Japan (34.9°N); the National Atmospheric Research Laboratory in India (13.5°N); the Equatorial Atmosphere Radar (EAR) in Indonesia (0°); the Jicamarca Radio Observatory in Peru (12°S); the Andes Lidar Observatory in Chile (30.2°S); Buckland Park in Australia (35°S); the Davis (Australia) and Syowa (Japan) Antarctic stations (68.6° and 69°S, respectively); and additional facilities having valuable correlative instrument capabilities in Antarctica, Argentina, Australia, Brazil, Canada, China, France, Germany, India, Puerto Rico, Sweden, and elsewhere.

Measurements of radiances and inferred temperatures by multiple satellite instruments employing limb, sublimb, and nadir viewing have been used to estimate GW temperature variances and momentum fluxes from the lower stratosphere into the MLT for many years. These have provided enticing insights into GWs arising from various sources. In many

cases, however, satellite measurements exhibit strong observational constraints because of line-of-sight averaging or weighting-function depths comparable to, or greater than, the smaller, but important, GW scales. Such measurements nevertheless reveal the larger-scale responses to multiple sources, define the global hotspots of GW activity and their seasonal variations, and on occasion capture very strong GW responses under ideal viewing conditions (e.g., Dewan et al. 1998; Eckermann and Preusse 1999; Ern et al. 2004; Eckermann et al. 2007; Wu and Eckermann 2008; Alexander et al. 2009, 2010; Eckermann and Wu 2012; Geller et al. 2013; Hendricks et al. 2014). Figure 3 shows the measurement capabilities of various satellite viewing geometries compared to DEEPWAVE and the GW wavelengths expected to account for the major GW momentum fluxes. Nadir measurements [e.g., Atmospheric Infrared Sounder (AIRS)] extend to relatively small GW λ_h , but these often fail to capture the smaller- λ_h GW responses inferred to contribute the largest local momentum fluxes (Fritts et al. 2002, 2014; Hertzog et al. 2012). Nadir measurements also often fail to capture larger- λ_h GWs when the GW λ_z is comparable to or smaller than the depth of the weighting function (e.g., Eckermann et al. 2009; Gong et al. 2012).

More recent airborne measurement programs. The next significant airborne measurement program following those in the 1930s was the Sierra Wave Project. This project employed two gliders in 1951/52 and two gliders and two powered aircraft in 1955, together with radiosondes and ground measurements, and yielded a significantly improved understanding of MW structure and related theoretical advances (Grubišić and Lewis 2004). Subsequent MW and lee-wave studies over the Rockies in the 1960s and 1970s used improved instrumentation aboard various aircraft to sample the MW, lee wave, and turbulence environments accompanying MW breaking. These provided more complete descriptions of the flow structures and evolutions and motivated initial modeling of these events (e.g., Kuettner and Lilly 1968; Lilly and Kennedy 1973; Brinkmann 1974; Clark and Peltier 1977; Lilly 1978; Klemp and Lilly 1978; Lilly et al. 1982).

More recent MW airborne studies benefitted from further expanded measurement capabilities, including dropsondes, GPS positioning, and/or the MTP, ground-based instruments, and associated modeling, for example, over the Welsh mountains (Whiteway et al. 2003); over the Alps during the Alpine Experiment (ALPEX), Pyrénées Experiment (PYREX), and Mesoscale Alpine Programme (MAP)

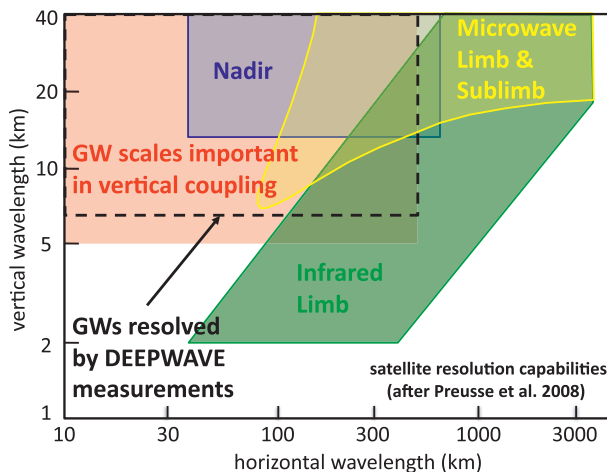


FIG. 3. Schematic of the sensitivity of various satellite measurement techniques to GW horizontal and vertical wavelengths (after Preusse et al. 2008) relative to the GW scales expected to contribute most to GW momentum fluxes throughout the atmosphere (pink). The instrument categories include microwave limb and sublimb (e.g., MLS), infrared limb [e.g., High Resolution Dynamics Limb Sounder (HIRDLS) and SABER], and nadir [e.g., AIRS and Advanced Microwave Sounding Unit (AMSU)]. The range of scales resolved by GW lidars (dashed line) is determined by the altitude coverage of each lidar separately (~30–40 km) and together (~80 km), the length of individual flight segments (~500–2000 km), and the minimum temporal and vertical averaging required for a particular measurement.

(e.g., Bougeault et al. 1990, 2001; Smith et al. 2002; Doyle and Smith 2003; Doyle and Jiang 2006); over the Sierra Nevada during the Terrain-Induced Rotor Experiment (T-REX) (e.g., Grubišić et al. 2008; Smith et al. 2008; Doyle et al. 2011); and elsewhere (e.g., Brown 1983; Whiteway et al. 2003; Doyle et al. 2005). Additional airborne studies explored the influences of MWs on the formation of polar stratospheric clouds at Arctic and Antarctic latitudes (e.g., Carslaw et al. 1998; Eckermann et al. 2006b).

Other airborne programs targeted more general GW responses. The Global Atmospheric Sampling Program (GASP) employed commercial aircraft for global in situ measurements that enabled comparisons of GW responses to various sources (e.g., Nastrom and Fritts 1992; Fritts and Nastrom 1992). The Airborne Lidar and Observations of Hawaiian Airglow 1990 (ALOHA-90) and the Airborne Lidar and Observations of Hawaiian Airglow/Arctic Noctilucent Cloud Campaign 1993 (ALOHA/ANLC-93) measurement programs employed a lidar and ASI to sample GWs extending from the stratosphere into the MLT (Hostetler et al. 1991; Hostetler and Gardner 1994; Swenson et al. 1995). Several airborne measurements

TABLE 4. IOP and research flight focuses and summaries. TW = trailing wave, PF = predictability flight, FL = flight level, SI = South Island, CW = convective waves, FWs = frontal waves, SO = Southern Ocean.

IOP	RF	Date	Primary/secondary targets	Flight summary
1	1	6 Jun	MWs/TWs/PF	Weak GWs/sources expected/verified
2	2	11 Jun	MWs, Tasmania	Weak FL GWs, large amplitudes in MLT
3	3	13 Jun	PF, Tasman Sea	Successful PF
	4	14 Jun	MWs/TWs SI MA2	MWs/TWs at FL, MLT MWs
4	5	16 Jun	MWs/TWs SI MC2	Weak MWs at FL, in stratification and MLT
5	6	18 Jun	MWs over Tasmania	Weak FL responses, possible MWs in MLT
6	7	19 Jun	MWs/CWs/FWs, eastern ocean	Significant/diverse FL/MLT GW activity
7	8	20 Jun	MWs/TWs SI MA1	Weak MWs, FL and MLT
8	9	24 Jun	PF Tasman Sea, MC2	PF, FL MW breaking/turbulence in MLT
	10	25 Jun	MWs/TWs SI MC2	Significant MWs, MLT MWs/CWs
9	11	28 Jun	PF Tasman Sea, SI MC2	CWs, jet stream GWs, MLT GWs/MWs
	12	29 Jun	MWs/TWs SI MC2/MA2	Strong MWs/breaking, MWs in MLT
	F1	30 Jun	MWs SI MA2	Strong, transient MWs; immediately after RF12
	13	30 Jun	MWs/TWs SI MC2/MA2	Similar to RF12, MWs and GWs in MLT
	F2	30 Jun	MWs SI MA2	As for F1, but weaker MWs
	14	1 Jul	MWs/TWs SI MC1	Weak FL MWs, stronger in MLT
CF	F3	2 Jul	Tropopause fold over SI	Moderate GWs near the jet and tropical fold
	15	3 Jul	Lee of SI	Daytime flight, FL measurements only
10	F4	4 Jul	MWs SI MA1	Strong MWs; immediately before RF16
	16	4 Jul	MWs/TWs SI MA1	Largest FL MWs, also MLT MWs
	F5	4 Jul	MWs/TWs SI MA1	Strong MWs; together with RF16
11	17	5 Jul	SO waves (east and south)	Large-scale, large-amplitude GWs in MLT
12	18	7 Jul	PF SO/Tasman Sea	Good jet stream FL and MLT GWs
	19	8 Jul	SO waves	Large-scale, large-amplitude GWs in MLT
13	20	10 Jul	PF/MWs SO SI MC2	Joint with F6, significant MLT GWs
	F6	10 Jul	Intercomparison flight with RF20	Ongoing analysis
	F7	11 Jul	MWs SI MC2	Moderate MWs
	21	11 Jul	MWs/TWs SI MC2	With F7 and F8, FL and MLT MW responses
	F8	11 Jul	MWs SI MC2	Moderate MWs
	F9	12 Jul	MWs SI MC2 and north	Varying/moderate GW responses over SI
	F10	13 Jul	MWs SI MC2 and north	Varying/moderate GW responses over SI
	22	13 Jul	MWs SI MC1	Large-scale/amplitude GWs/MWs in MLT
14	23	14 Jul	SO/island waves	Strong/variable MLT MWs Auckland Island
	24	15 Jul	SO/island waves	Significant GWs in AIRS and MLT
15	F12	16 Jul	MWs SI MC2 and north	Weak MWs, FL and MLT
16	25	18 Jul	SO waves	Strong SI GWs, SO GWs AIRS/MLT
	26	20 Jul	MWs SI along mountains	Weak FL GWs, strong AIRS and MLT
	F13	20 Jul	MWs SI along mountains	Moderate FL GWs; after RF26

also provided evidence of GWs generated by deep convection and their momentum fluxes at flight altitudes (e.g., Kuettner et al. 1987; Pfister et al. 1993; Alexander and Pfister 1995).

Mesoscale and global modeling of GWs. Modeling capabilities for mesoscale and global GW studies have improved dramatically in recent years because of ever-increasing computational resources. As a result, various models have been employed in support of GW measurement programs and to identify GW sources and key dynamics spanning larger spatial scales. Mesoscale models have aided the interpretation of MAP, T-REX, and other airborne MW programs, been employed for intermodel comparisons for several events (e.g., Dörnbrack et al. 2001; Smith et al. 2002; Doyle and Smith 2003; Doyle and Jiang 2006; Doyle et al. 2000, 2011), and assessed the dynamical responses and resolution dependence of airflow over small islands (e.g., Vosper 2015). Global forecast and research models (REs) now achieve spatial resolutions of ~ 25 km or better that enable direct modeling, rather than parameterization, of GWs extending to horizontal scales as small as ~ 100 km. As examples, Yamashita et al. (2010) showed that the European Centre for Medium-Range Weather Forecasts (ECMWF) T799 model described GWs having $\lambda_x > 100$ km that agreed reasonably with a much higher-resolution Weather Research and Forecasting (WRF) Model simulation and AIRS observations of GWs due to a typhoon, exhibited similar GW variance distributions as the Microwave Limb Sounder (MLS), but underestimated GW amplitudes by ~ 2 times compared to Sounding of the Atmosphere using Broadband Emission Radiometry (SABER) measurements. Shutts and Vosper (2011) employed the Met Office (UKMO) and ECMWF global models and a very-high-resolution (4 km) unified model to examine the MW energy and momentum fluxes over the southern Andes. They found a peak in the

fluxes at $\lambda_x \sim 400$ km, with approximately half the fluxes at $\lambda_x < 200$ km. Sato et al. (2012) used a high-resolution middle-atmosphere general circulation model (GCM) to explore the stratospheric dynamics of MWs having $\lambda_x \sim 200$ km and larger arising from the southern Andes. They found that the MWs refract strongly into the polar vortex because of horizontal wind shears and yield downward-propagating responses below ~ 40 km because of nonlinear dynamics at higher altitudes. Similar improvements in characterization of MW and more general GW influences at higher spatial resolution were also found to occur in the Community Atmosphere Model, version 4.0 (CAM4), and the Whole Atmosphere Community Climate Model (WACCM) (Bacmeister et al. 2014; Liu et al. 2014).

FIELD PROGRAM AND EPO OVERVIEW.

The DEEPWAVE field program was complex and was made possible by the participation of a large number of individuals from the NSF principal investigator (PI) teams, NCAR, Naval Research Laboratory (NRL), DLR, National Institute of Water and Atmosphere Research (NIWA), Australian Antarctic Division (AAD), and other colleagues and students in New

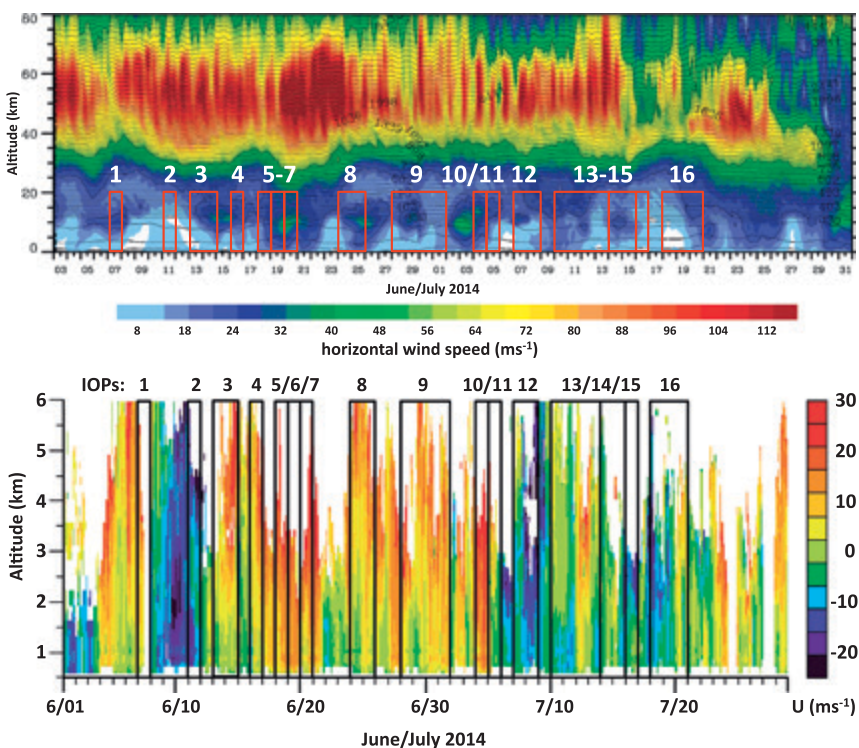


FIG. 4. DEEPWAVE IOPs (red rectangles with white labels) shown with respect to (top) the large-scale ECMWF horizontal winds and potential temperatures (contours) and (bottom) the Hokitika WP eastward 6-h mean winds throughout the DEEPWAVE field program.

Table 5. GB-IOP (no coincident RF) Lauder lidar/AMTM GW summaries. T' = temperature fluctuations, MF = momentum flux, I' = intensity fluctuations, and SS = small scale.

GB-IOP	Date	GW responses, MW forcing, and large-scale influences
GB1	30 May	~20–60-km MWs and other GWs, apparent correlation with T
GB2	31 May	Slow ~60-km GWs with strong, sharp “front” and cooling/brightening
GB3	1 Jun	MWs ~80 km moderated by larger-scale wave with large T' , $U' \sim 10 \text{ m s}^{-1}$
GB4	2 Jun	Very strong MWs ~ 15–80 km, large MFs, little evidence of instabilities
GB5	11 Jun	Apparent bore or NL wave train with sharp T increase thereafter
GB6	12 Jun	Strange behavior in MLT
GB7	15 Jun	Strong AMTM I' and T' modulation in MLT
GB8	18 Jun	MWs and other responses in MLT
GB9	19 Jun	Lots of MLT GWs, MWs not dominant—coordinate with RF7
GB10	21 Jun	Very strong MWs ~ 15–80 km, large MFs, instabilities, weak MW forcing
GB11	22 Jun	Lots of GW responses, multiple SS events in MLT
GB12	23 Jun	Lots of GW responses, multiple SS events in MLT
GB13	26 Jun	Large linear/nonlinear MWs, SS instabilities in MLT
GB14	28 Jun	Strong SS MWs and instabilities in MLT
GB15	4 Jul	Strong complex GWs in MLT, mostly westward propagation
GB16	10 Jul	Large-amplitude, transient SS MWs ~ 10–100 km, very large SS MFs
GB17	14 Jul	Large-amplitude, transient SS MWs ~ 30–40 km, very large MFs, north-west–southeast alignment
GB18	16 Jul	Significant SS GW activity, some MWs
GB19	17 Jul	Strong, coherent, sustained SS MWs ~ 20–30 km, north-northwest–south-southeast alignment
GB20	18 Jul	Significant, persistent SS and LS MWs, north-northwest–south-southeast alignment
GB21	31 Jul–2 Aug	Very large MW event in Lauder–Rayleigh lidar observations
GB22	14–15 Aug	Very large MW event in Lauder–Rayleigh lidar observations

Zealand, Australia, and Austria. Altogether, over 100 people contributed to various aspects of the program. DEEPWAVE participants and their roles are listed in appendix D. The various tasks included aircraft logistics, operations and maintenance, ground-based instrument installations, weather forecasting and updates, flight planning and debriefs, personnel scheduling, education and public outreach (EPO) activities, and local outreach. Most activities were performed during daytime, but, because of the extensive use of the new GV lidars and imagers, most research flights and all ground-based optical measurements were performed at night. The major components of the program are discussed further below.

Weather forecasting, briefings, and updates. Daily weather forecasting began each morning, with efforts coordinated by a lead forecaster and contributed to by a team including scientists, students, and NIWA staff using local weather observations and forecasts

and mesoscale and global forecast models (FCs; see Table 3). The forecast models often proved to be quite accurate on short time scales and hence very valuable for these purposes. The focus was on events having GW responses expected to penetrate into the stratosphere and MLT and weather impacting GV operations. Weather briefings occurred each day at 1300 local time (LT) [0100 universal time (UT)] and typically reviewed the weather for that day (if there was a research flight scheduled) and 1–3 days out for flight planning purposes. On days having research flights scheduled, an additional weather update was also provided ~2 h before flight departure.

Flight planning. Flight planning typically involved submission of flight proposals by individuals or teams designed to address specific DEEPWAVE science questions. Occasionally, flight plans looked farther ahead and anticipated a combination of flights, for example, predictability and verification or successive

sampling of a multiday event. Often, alternative flight proposals were merged to optimize the expected results and/or address common measurement goals. A subcommittee of scientists that changed weekly determined the final flight plan in the event of competing proposals. The selected flight plan was then sent to the Earth Observing Laboratory (EOL) team for review and feedback.

Research flights and large-scale context. All research flights [RFs and Falcon research flights (FFs)] for the GV and the Falcon were part of an IOP ranging from 1 to 4 days to facilitate coordination with ground-based measurements. GV flight durations ranged up to ~9 h and flight distances ranged up to ~8,000 km. Falcon flights had maximum durations and lengths of ~3.5 h and ~3,000 km, respectively. The large majority of RFs and FFs were performed at high altitudes, ~12–13.7 km for the GV and ~10–11 km for the Falcon. For the GV, this was done for fuel efficiency and because the GV lidars were not allowed to operate at lower altitudes. Both aircraft also performed a number of flight segments at lower altitudes to sample interesting events on various occasions. MW flights targeted strong and weak forcing to span a range of responses at higher altitudes. The IOPs, dates, research targets, and flight summaries for all RFs flown during DEEPWAVE are listed in Table 4.

IOPs are shown in the context of the large-scale ECMWF horizontal winds from 0 to 80 km in Fig. 4 (top). The dominant feature is the polar night jet with a maximum wind often exceeding 100 m s^{-1} at ~50–60 km that is presumably modulated in strength by PWs on time scales of ~5–10 days. The poleward

jet associated with frontal systems exhibits episodic maxima of ~30–50 m s^{-1} at ~8–12 km on similar time scales. Also seen in the second half of July are two intervals in which the polar night jet decreases, first to ~60 m s^{-1} (~15–20 July) and then to ~30 m s^{-1} (beginning ~29 July). These intervals accompany significant enhancements in the zonal wavenumber 1-PW amplitude that yield both a weak stratospheric warming and westward wind perturbations that account for the weaker ECMWF winds at these times.

Ground-based measurements. As noted above, DEEPWAVE was supported by extensive ground-based measurements. The WP operated continuously

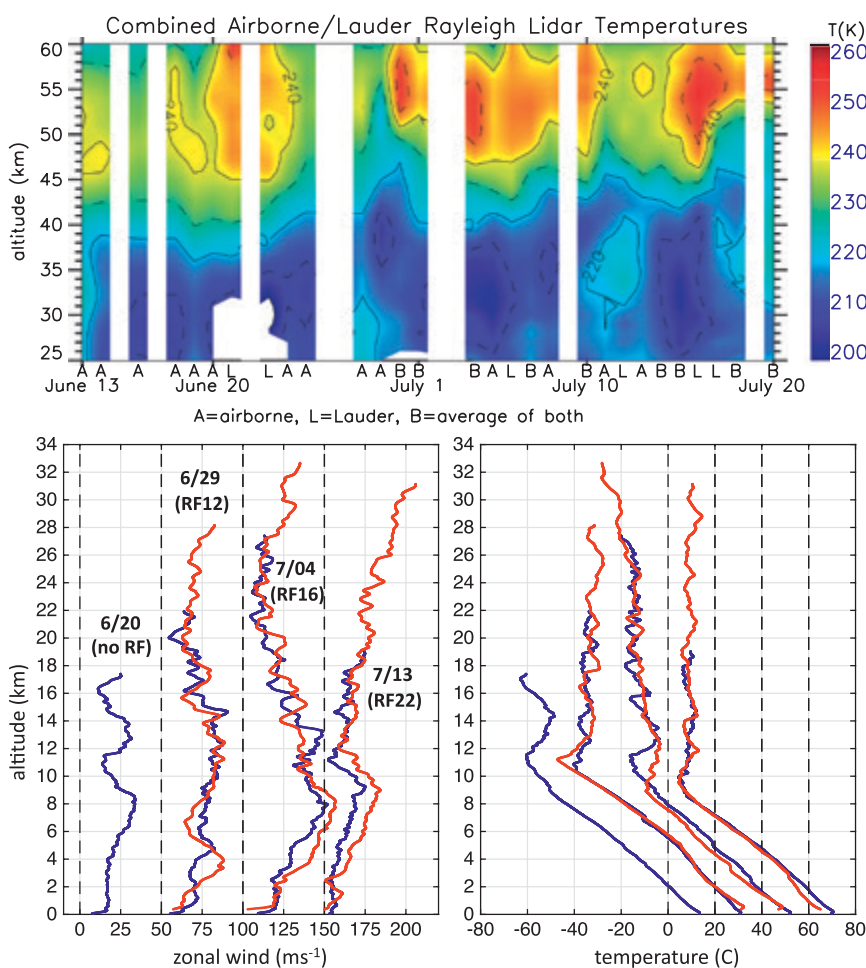


FIG. 5. (bottom) Radiosonde zonal wind and temperature profiles at Hokitika (blue) and Lauder (red) at 2307 UT 20 Jun (as best available data for 21 Jun), 1053 and 1129 UT 29 Jun (RF7), 1403 and 1440 UT 4 Jul (RF16), and 1059 and 0238 UT 13 Jul (RF22), respectively. (top) RF-mean and/or nightly mean temperatures obtained with the GV airborne and Lauder ground-based Rayleigh lidars from 13 Jun to 20 Jul that reveal the variability of mean temperatures and atmospheric stability over South Island during DEEPWAVE. Note the code at bottom that specifies which lidar(s) contributed each day. Winds and temperatures on successive days are offset by 50 m s^{-1} and 20°C , respectively.

from 28 May to 28 July. Radiosondes were launched daily at Hokitika from 24 May to 18 July, at Lauder from 13 June to 1 August, at a higher cadence during IOPs at these sites and at Haast, and at Hobart and Macquarie Island to support flights or predictability objectives in those areas. The AMTM, ASIs, and FPI at Lauder and Mt. John Observatory (MJO) performed routine nighttime observations spanning the DEEPWAVE core measurement interval. The DLR lidar at Lauder operated from 19 June to 6 November. The Kingston lidar operated in coordination with GV flights over Tasmania and the Tasman Sea, and the meteor radar at Kingston operated continuously beginning 10 June. The altitudes sampled by these various instruments are shown with vertical bars in Fig. 2. Additional ground-based IOPs were designated on nights for which interesting responses were observed that correlated with the forecast models and measurements at lower altitudes. These events are listed in Table 5.

Four examples of radiosonde measurements at Hokitika and Lauder relevant to specific cases discussed further below are shown in Fig. 5 (bottom). Shown in Fig. 5 (top) are RF-mean or nightly mean temperatures obtained with the GV airborne and Lauder Rayleigh lidars for each available measurement over South Island. These illustrate some of the diversity of GW propagation environments from the surface to 60 km during the DEEPWAVE program.

EPO activities. DEEPWAVE EPO efforts had two primary objectives: 1) to increase the awareness of students in kindergarten–grade 12 of the field of atmospheric science by exposing them to research methods through engaging presentations and interactions with early-career scientists and 2) to increase public awareness of the DEEPWAVE science objectives and societal benefits

on an international level. The program consisted of targeted student enrichment activities including 10 presentations to 565 middle and high school students; Internet-based outreach efforts that included 11 educational web pages with 2,000 views in a 104-day period, 15 Facebook posts, blog posts, and tweets from postdoctoral scholars in the field; a research aircraft public open house with over 250 visitors; media visits resulting in several high-profile pieces broadcast in New Zealand; and various printed information. Additionally, 26 undergraduate and graduate (grad) students from eight organizations and universities were directly involved with DEEPWAVE research and operations, gaining valuable experience in observational fieldwork.

INITIAL MEASUREMENTS AND RESULTS.

Initial DEEPWAVE data analysis efforts are addressing

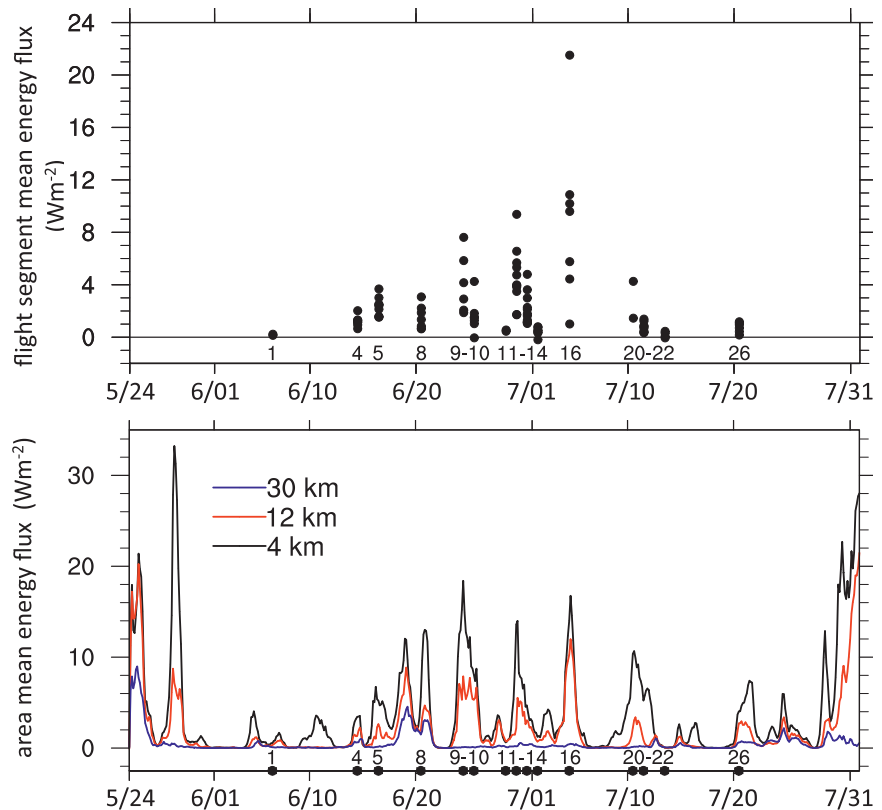


FIG. 6. (top) Flight-level vertical energy fluxes $\langle p'w' \rangle$ computed for each GV MW flight segment over South Island throughout the DEEPWAVE field program. Note the large variability accompanying the largest RF mean energy fluxes and largest-amplitude MWs. **(bottom)** Regional vertical energy fluxes over South Island computed from WRF constrained by ECMWF IFS initial conditions at 4, 12, and 30 km as a guide to MW dissipation with altitude due to variable MW forcing and environments. Numerical designations along the x axis in the bottom panel show the RFs for which GV flight-level energy fluxes are displayed in the top panel.

a number of topics and yielding a variety of tantalizing results. Example “first results” that will be discussed briefly below include 1) strong variability of MW energy fluxes among, and within, the various MW flights; 2) evidence of MW breaking at flight altitudes; 3) predictability targeting and influences; 4) MWs arising from weak forcing attaining large amplitudes at higher altitudes; 5) strong three-dimensional (3D) MW responses at high altitudes over Auckland Island; 6) GWs in the stratosphere apparently generated within the jet stream; 7) responses to weak MW forcing over several days that yielded intermittent MW breaking in the MLT; and 8) comparisons of DEEPWAVE measurements with model forecasts and AIRS temperature observations.

MW flight-level responses and predictability. An initial assessment of MW propagation employing GV flight-level (FL) MW energy flux estimates $\langle p'w' \rangle$ (where p' and w' are the in situ GV measurements of pressure and vertical velocity perturbations, and brackets denote horizontal averaging) for each MW RF is shown in Fig. 6 (top). WRF Model estimates of these fluxes at 4, 12, and 30 km for initial conditions specified by the ECMWF Integrated Forecasting System (IFS) model are shown in Fig. 6 (bottom) and were computed following Kruse and Smith (2015). The WRF GW energy flux maxima typically accompany frontal systems that bring strong lower-level flow over South Island. RF energy fluxes are positive (negative) for upward (downward) MW propagation, suggesting strong variability in MW strength and propagation within individual MW events. Modeled energy fluxes suggest variable MW propagation and dissipation at higher altitudes depending on the MW forcing strengths and propagation environments. The numbered circles on the x axis in Fig. 6 (bottom) are the RFs for which computed energy fluxes are shown in the top panel.

One of the strongest MW events during DEEPWAVE occurred during RF12 on 29 June. The GV flew a box pattern with repeated flight segments over Mt. Aspiring

and Mt. Cook. Data from segments 14 and 22 along Mt. Aspiring flight-track 2 (MA2; see Fig. 1) are shown in Fig. 7. Most notable are the very different responses separated by only 1.5 km in altitude. At 12.2 km, the along-track wind accelerated to 25 m s^{-1} and then decelerated to 12 m s^{-1} over the high terrain. At 13.7 km, the disturbance was stronger and decelerated to $\sim 0 \text{ m s}^{-1}$, which is expected to accompany wave breaking. The vertical velocity fields (top panel) were also different at the two levels. At 12.2 km, these mostly showed a quasi-periodic train of small-scale (SS) waves downwind of the highest orography. These were likely trapped waves having small energy and momentum fluxes. At 13.7 km, a burst of high-frequency turbulence occurred over the high terrain, likely accompanying wave breaking.

An example of the predictability component of DEEPWAVE is illustrated in Fig. 8 for 13 June 2014 (RF3). The Coupled Ocean–Atmosphere Mesoscale Prediction System (COAMPS) forecast and adjoint models (Amerault et al. 2008; Doyle et al. 2014) were used to compute the forecast sensitivity to the initial state, and these regions of high sensitivity were targeted for additional dropwindsonde (DWS) observations. As an example, the color shading in the Tasman Sea (Fig. 8a) highlights the upstream regions where the 24-h COAMPS forecast kinetic energy in the lowest 1 km above the surface in the gray box is most sensitive to the initial-state 700-hPa u -wind

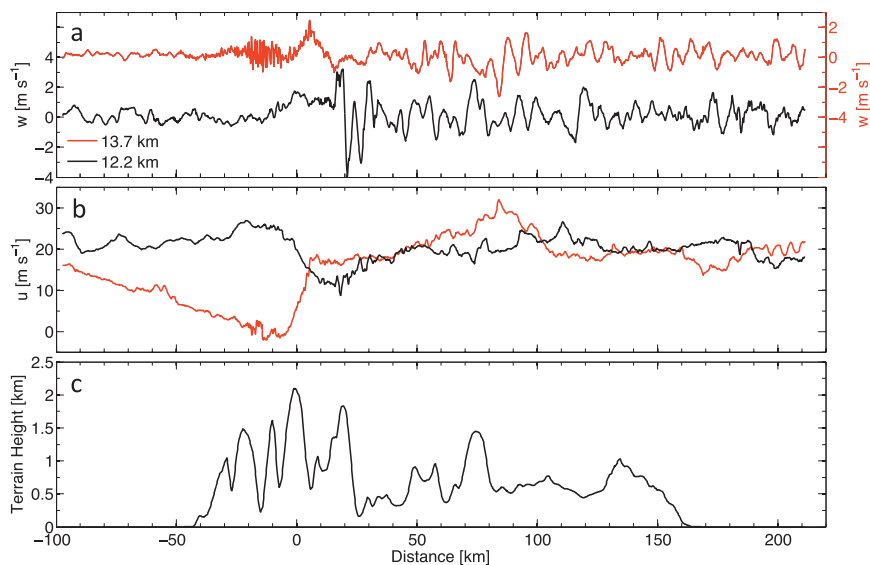


FIG. 7. GV flight-level gust-probe data from RF12 on 29 Jun. Two flight segments over Mt. Aspiring along MA2 (see Fig. 1) are shown: segment 14 at $z = 12.2$ km (black) and segment 22 at $z = 13.7$ km (red). Shown are (a) vertical velocities, (b) along-track cross-mountain wind speed, and (c) terrain height. Note that the GV passed through a region of MW breaking on segment 22 where the MW velocity exactly cancelled the along-track mean wind.

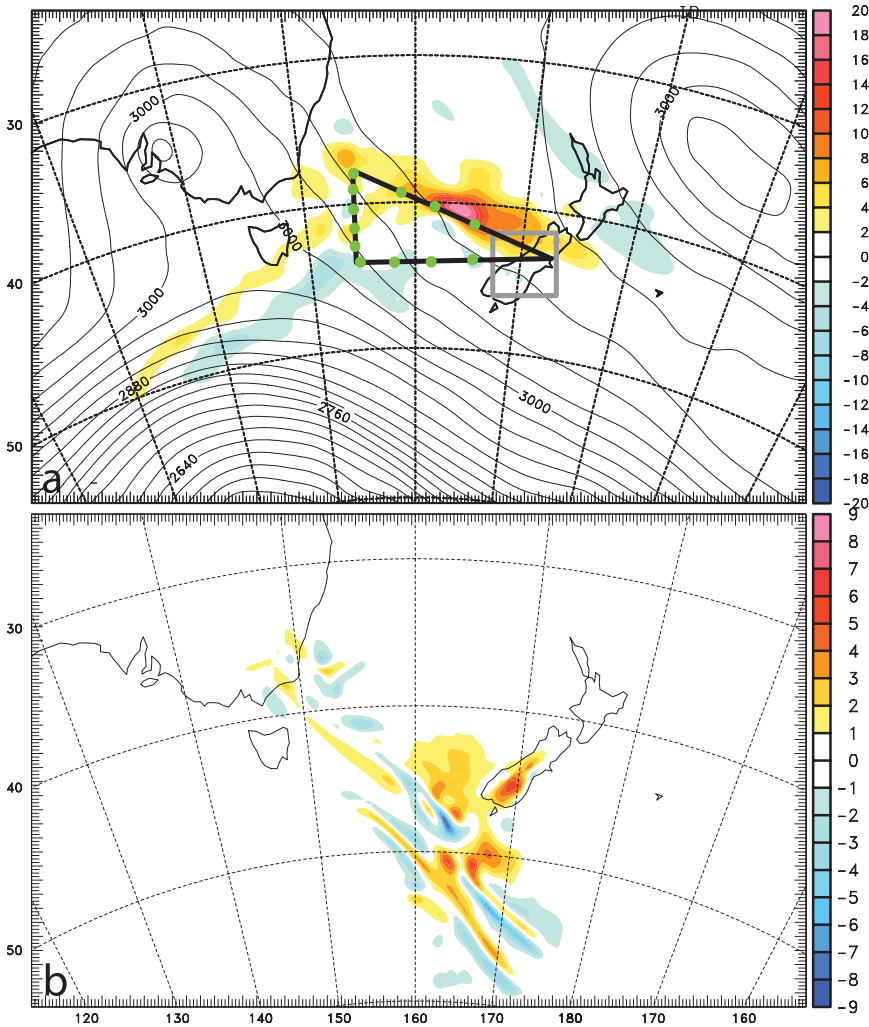


FIG. 8. (a) The sensitivity of the 24-h COAMPS forecast kinetic energy in the lowest 1 km above the surface (gray box) to the initial-state 700-hPa U -wind component at 0600 UTC 13 Jun 2014 (color scale with interval of $2 \times 10^{-3} \text{ m s}^{-1}$). (b) The evolved perturbations (m s^{-1}) based on the scaled sensitivity after 24 h of integration at 800 hPa near the crest-level height for the U -wind component valid at 0600 UTC 14 Jun. The GV flight track and DWSs (green dots) are shown in (a). The 700-hPa geopotential height analysis is shown in (a) with an interval of 30 m. The sensitivities in (a) are scaled by 10^5 km^{-3} .

component. The sensitive regions most strongly influence MW launching and amplitudes over South Island 24 h later. Green dots along the flight track show the DWS deployments for this assessment. The evolved perturbations (24 h) based on the sensitivity scaled to a maximum of 1 m s^{-1} at the initial time (Fig. 8b) exhibit a maximum over South Island with growth of ~ 10 times for the u -wind component perturbations in this case. The GV flight the following day on 14 June served as the verification flight to assess the degree to which the targeted DWSs improve the prediction of MWs over South Island.

MW responses in the stratosphere and MLT accompanying weak surface forcing. A major surprise during the DEEPWAVE field program was the observation of large-amplitude, breaking MWs in the MLT on a night that the flight planning team had elected not to fly a MW mission because of the forecast of weak MW forcing conditions. This quickly sensitized the team to conditions for which weak surface forcing can nevertheless lead to large MW amplitudes at high altitudes potentially because of the largely linear MW propagation and an absence of instabilities and breaking in the stratosphere, in contrast to strong forcing events (e.g., Fig. 7).

One example of these MW dynamics was observed during RF22 (13 July), a case having weak cross-mountain flow and MW forcing but favorable vertical propagation conditions with strong eastward winds through the stratosphere and above. A subset of observations from the GV lidars and the AMTM and wing cameras is shown in Figs. 9 and 10. Figures 9c and 9d show two successive cross sections along Mt. Cook flight-track 1 (MCI; see Fig. 1) of strato-

spheric temperatures from 20 to 60 km and sodium density perturbations obtained with the GV lidars. Figures 9a and 9b show corresponding cross sections of sodium mixing ratios for the same two cross sections. Rayleigh lidar temperatures are shown together with perturbation temperature contours from the ECMWF IFS that contributed significantly to DEEPWAVE flight planning and were interpolated to the GV location in space and time for this comparison. Note, in particular, the very close agreement of the MW scales and phase structures between the GV lidar data and a composite of IFS

analyses and 1-h predictions, including the MW growth with altitude and the changing MW vertical wavelength λ_z accompanying the stronger winds extending to ~ 60 km and above. The major differences are that the IFS results underpredict (by ~ 2 – 5 times) the large-scale MW amplitudes, and they appear not to capture some of the smaller-scale MWs contributing to the lidar temperature perturbations above ~ 40 km.

At higher altitudes, sodium mixing ratios measured by the GV sodium lidar reveal very large vertical displacements because of the smaller-scale MWs and other GWs. Peak-to-peak displacements as large as ~ 3 – 8 km imply these smaller-scale GWs have $T' \sim 5$ – 20 K or more and very large momentum fluxes. Rough estimates based on the observed GW scales and amplitudes measured on RF22 are ~ 100 – 500 $\text{m}^2 \text{s}^{-2}$ or larger, which are ~ 1 – 2 decades larger than the expected mean values at these altitudes (e.g., Fritts and Alexander 2003; Fritts et al. 2014).

An example of a combined GV AMTM and wing camera cross-mountain image of OH airglow brightness is shown in Fig. 10a for the vertical cross section shown in Fig. 9d. This reveals the same $\lambda_h \sim 200$ – 300 -km MW seen by the Rayleigh lidar and multiple additional MWs and other GWs at smaller horizontal wavelengths, $\lambda_h \sim 30$ – 80 km, at ~ 87 km. Additional horizontal cross sections of the IFS horizontal divergence at 2 hPa (~ 43 km) at 0900 UT (Fig. 10b), and AIRS brightness temperature (radiance) perturbations at 2 hPa (Figs. 10c and 10d) suggest that the GV imagers observed the upward extension of the larger- and smaller-scale MW field seen by the GV lidars. The IFS vertical and horizontal cross sections in Figs. 9 and 10 captured both the vertical and horizontal structures of the large-scale MW and the associated trailing waves (TWs) for this event quite well.

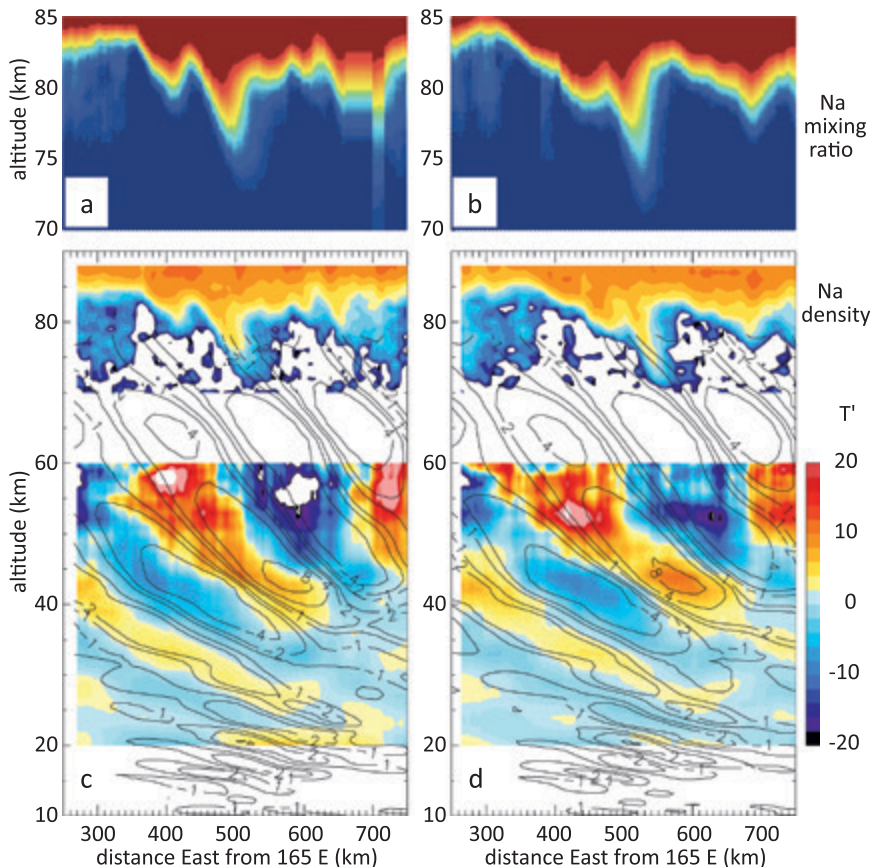


FIG. 9. GV lidar along-track vertical cross sections for the final two South Island flight segments of RF22 along MCI (see Fig. 1) on 13 Jul. Seen are large-scale, $\lambda_h \sim 200$ – 300 km, MWs in the stratosphere and other smaller-scale, $\lambda_h \sim 30$ – 80 km, MWs and GWs in the upper stratosphere and MLT accompanying weak orographic forcing. (c),(d) Rayleigh lidar T' from 20 to 60 km and sodium lidar densities from 70 to 88 km. (a),(b) Sodium mixing ratios that clearly reveal vertical air parcel displacements. The Rayleigh lidar T' fields are shown with T' contours predicted by the ECMWF IFS and interpolated to the GV locations and measurement times.

Jet stream GW responses. Jet streams also represented a significant source of larger-scale GWs predicted by the NWP models during DEEPWAVE. Thus, several flights over the Southern Ocean (SO) specifically targeted these GWs. An example of one cross section through an apparent jet-generated GW, and its prediction by the IFS model, is shown in Fig. 11. As seen in the MW observations on RF22 (Fig. 9), Rayleigh lidar temperature measurements again reveal surprising agreement in the GW spatial structures and refraction with altitude with the changing environment. But again, GW amplitudes tended to be underestimated by the model fields interpolated to the GV locations and measurement times by up to ~ 2 times or more. While our initial comparisons employed only the IFS model, we note that other global and regional models supporting DEEPWAVE achieved similar successes in

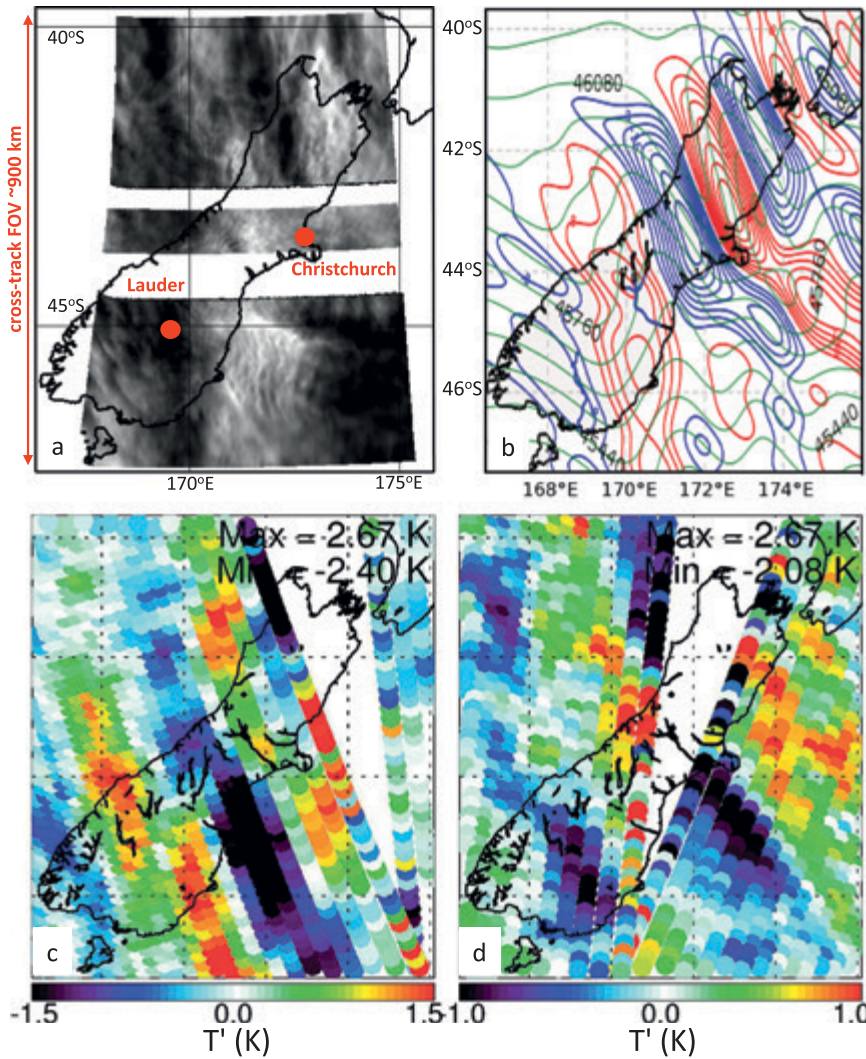


FIG. 10. (a) Full GV AMTM and wing camera flight segment image of airglow brightness at ~ 87 km for the final east-west flight segment over Mt. Cook obtained between 0833 and 0911 UT 13 Jul during RF22 along MCI (see Fig. 1). Note the large-scale ($\lambda_h \sim 200\text{--}300$ km) MW having phases aligned slightly north-northwest-south-southeast and the smaller-scale GWs that are most evident in the brighter regions of the large-scale MW. ECMWF IFS horizontal divergence at 2 hPa (~ 43 km) at (b) 0900 UT (red positive, blue negative) and AIRS brightness temperature (radiance) perturbations (K) in swath nadir geometry from AIRS channel 74 at 2 hPa on 13 Jul during the (c) ascending and (d) descending *Aqua* overpasses of South Island. At these times, South Island lies between the outer scan edges of the AIRS swath imagery from successive satellite overpasses, separated by ~ 98 min and occurring at ~ 0141 and ~ 0319 UT (ascending) and ~ 1248 and 1427 UT (descending).

characterizing GW responses to the various sources for which the GW spatial scales were well resolved. These comparisons will be highlighted in future papers.

MW responses over small islands. Given the potentially strong MW responses at higher altitudes to flow over small SO island orography (e.g., Alexander

and Grimdsell 2013), several DEEPWAVE flights overflew SO islands when deep MW forcing was expected. An example of these measurements over and in the lee of Auckland Island by the GV imagers on RF23 with strong surface flow from the northwest is shown in Fig. 12a. This image reveals ship wave temperature structure at ~ 87 km having a dominant $\lambda_h \sim 40$ km and evidence of a stronger trailing wave response to the north, likely resulting from filtering by the intervening winds. The GV AMTM also revealed a peak amplitude of $T' \sim 20$ K or larger immediately in the lee of Auckland Island. A MW response computed with the NRL Fourier-Ray (FR) linear model (Eckermann et al. 2006a) using upstream forcing profiles from NWP models and GV DWSs for this day captures some key features of the observed MLT MW field (wavelength and approximate amplitude) in Fig. 12b. Three GV passes over Auckland Island $\sim 3\text{--}4$ h later revealed breaking and instabilities that destroyed the MW field at ~ 87 km. As for RF22 (Fig. 9), the large amplitude and small λ_h of this response also imply a very large, but spatially localized, MW momentum flux.

MW breaking observed on 21 June. Finally, we illustrate ground-based MW observations

that alerted the team to the importance of weak forcing events at high altitudes. This event occurred near the end of an interval of sustained weak MW forcing first observed on RF7 on 19 June to the southeast of South Island (e.g., AIRS images show continuous large-scale MW and trailing wave responses in the middle stratosphere throughout this interval).

Three images of OH (~ 87 km) temperatures obtained with the AMTM at Lauder at 30-min intervals are shown in Figs. 13a–c. These reveal relatively stationary MWs exhibiting $\lambda_h \sim 10$ –70 km, phases oriented largely north (N)–south (S), and maximum $T' > 20$ K. The images also exhibit pronounced “sawtooth” patterns in the temperature fields seen as gradual decreases in temperature from warm to cold followed by sudden transitions back to warm in progressing from east to west that are indicative of GW nonlinearity, including steepening, overturning, and breaking. The Lauder AMTM images cover only a portion of the larger-scale MW response also seen simultaneously by the Lauder ASI (Fig. 13d) and by AIRS ~ 2 h later (Fig. 13e), both of which indicate that these MWs extend well upstream and downstream

of the orographic source. They also appear for only ~ 1 h on this day, suggesting that filtering by variable winds at these or lower altitudes must modulate these MLT responses, given that the AIRS responses are essentially continuous throughout ~ 4 days. As noted for the MWs seen on RF22 and RF23 discussed above, these strong breaking MWs over Lauder must likewise have very large momentum fluxes extending in this case over a large area.

SUMMARY. The DEEPWAVE field program was successfully executed because of the major efforts by many people and organizations (see appendix D) and an unprecedented and comprehensive suite of airborne and ground-based instrumentation (see Figs. 1 and 2; Table 2). DEEPWAVE was also the first research program to systematically measure GW dynamics arising from various sources in the troposphere and stratosphere to altitudes of dissipation extending up to ~ 100 km. DEEPWAVE measured GWs generated by orography, jet streams, frontal systems, deep convection, and secondary generation processes and spanned a range of forcing, propagation, and dissipation conditions. The various DEEPWAVE measurements led to

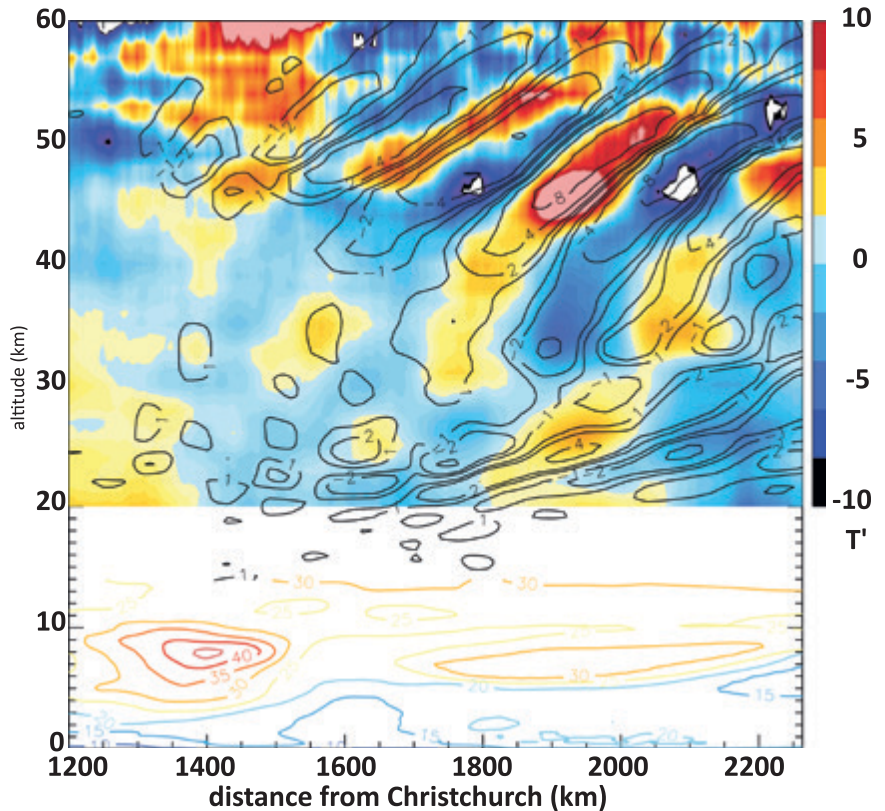


FIG. 11. As in Figs. 9c and 9d, except showing apparent stratospheric GW responses to a jet stream observed on RF25 on 18 Jul. ECMWF horizontal winds (m s^{-1}) are shown with colored contours below 15 km.

the initial identification of a large number of anticipated research targets (see Tables 4 and 5) and also yielded a number of surprises. These include the following:

- 1) highly variable MW energy fluxes at flight altitudes for weak and strong forcing;
- 2) the interruption of vertical MW propagation and resulting absence or strong attenuation of MWs at higher altitudes in cases of strong forcing and breaking in the stratosphere;
- 3) the detection of secondary GW generation in regions of strong MW breaking;
- 4) the potential for MWs due to weak forcing to penetrate to very high altitudes and achieve very large amplitudes and momentum fluxes;
- 5) the penetration of MWs having very small horizontal wavelengths of $\lambda_h \sim 10$ –30-km to ~ 80 –100-km altitudes under weak forcing conditions;
- 6) the generation of ship wave patterns due to small islands at small scales and large amplitudes in the MLT;
- 7) the ubiquitous presence of larger-scale GWs from nonorographic sources in the stratosphere and mesosphere;

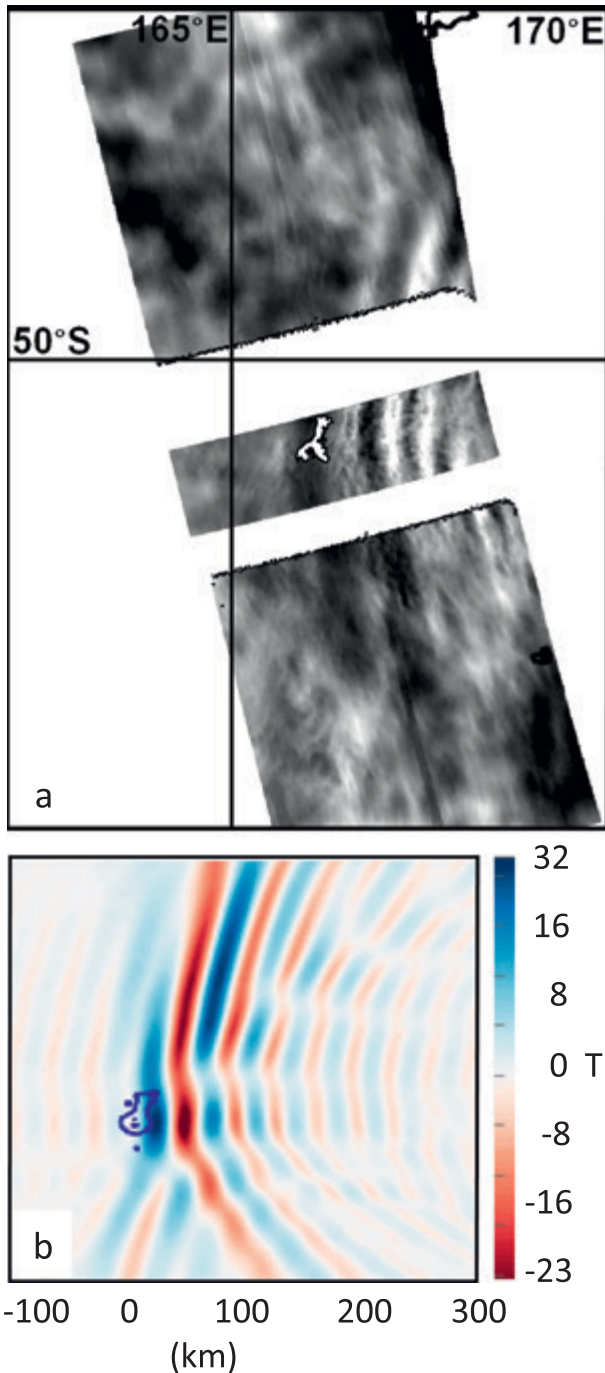


FIG. 12. As in Fig. 10a, but for (a) the first flight segment across Auckland Island on RF23. Note the strong MW and trailing wave responses in the lee and largely north of the orography. The dominant response occurs at $\lambda_h \sim 40$ km and the peak amplitude is $T' > 20$ K. (b) An example of the FR model prediction of this MW response at 85.5 km in an environment provided by the Navy Global Environmental Model (NAVEM), which agrees reasonably with the observed MW phase structure and amplitude.

- 8) strong and coherent responses to orography and other GW sources at larger scales that were often remarkably consistent with the predictions of mesoscale and global models employed in DEEPWAVE forecasting and analysis efforts; and
- 9) regions of initial condition sensitivity diagnosed from adjoint models were nearly always in areas of very active weather including jet streaks, fronts, and convection that played a prominent role in GW launching the following day.

Initial conclusions from our DEEPWAVE measurements include confirmation of 1) the important roles of multiple sources of larger-scale large-amplitude GWs ($\lambda_h \sim 200\text{--}300$ km or larger) that readily penetrate to higher altitudes; 2) the frequent refraction of larger-scale GWs into the polar vortex, including large-scale trailing MWs; 3) the importance of environmental wind and temperature fields in defining their evolving characteristics and the altitudes to which they penetrate; and 4) links between GW sources and characteristics at higher altitudes. Initial DEEPWAVE observations and analyses also suggest that smaller-scale GWs 1) arise preferentially from orography, deep convection, and secondary GW generation in the stratosphere; 2) readily penetrate into the stratosphere and mesosphere under suitable propagation conditions; 3) are less likely to exhibit strong refraction into the polar vortex; 4) often attain very large amplitudes at higher altitudes; and 5) typically dominate the total momentum fluxes in these regions.

DEEPWAVE measurements also have implications for modeling of GWs arising from various sources. The high-resolution mesoscale and global models that supported DEEPWAVE appear to capture important aspects of MW generation and propagation when the MW scales are well resolved. The global models also perform well in defining the character of GW responses to various sources for larger-scale GWs. Compared to FL and lidar stratospheric measurements, however, these models typically underestimated the measured GW amplitudes in the stratosphere and above.

Specific questions suggested by initial DEEPWAVE observations and modeling that further studies will attempt to resolve include the following:

- 1) How do environmental conditions modulate the deep propagation of GWs from various sources?
- 2) What roles do nonlinear dynamics and instabilities play in interrupting GW penetration to higher altitudes?

- 3) Which GW sources and spatial scales contribute most to total momentum fluxes as a function of altitude, and can these be quantified by current models and satellite measurements?
- 4) Which GW sources and spatial scales account for the largest latitudinal transport of momentum?
- 5) What dynamics account for the spatial and temporal intermittency of energy and momentum fluxes at different altitudes?
- 6) What are the dynamics and consequences of multiscale GW superpositions throughout the lower and middle atmosphere?

Our DEEPWAVE research team is actively pursuing multiple research topics and we anticipate that a number of results will be available to the community in the near future.

ACKNOWLEDGMENTS.

The DEEPWAVE program was made possible through financial and/or in-kind support from many U.S. and international organizations, including NSF, NCAR/EOL, NRL, DLR, NIWA, AAD, the New Zealand MET Service, PAE Ltd., ECMWF, and NOAA-NCEP. Many individuals also contributed greatly in various ways (see appendix D). Financial support for U.S. participants was provided by NSF under Grants AGS-1261619 and AGS-1338646 (GATS); AGS-1338655 (Yale University); AGS-1061892 and AGS-1338666 (Utah State University); AGS-1338309 and AGS-1343097 (Boston University); and AGS-1338557 (CPI). The NRL investigators (Doyle, Eckermann, Reinecke, and Reynolds) are supported by the

Chief of Naval Research through the NRL Base Program (PE 0601153N). We are indebted to Kerry Chuck and Phil Ambler for their very able assistance with airport logistics in Christchurch and to John Robinson and his very helpful NIWA staff at Lauder.

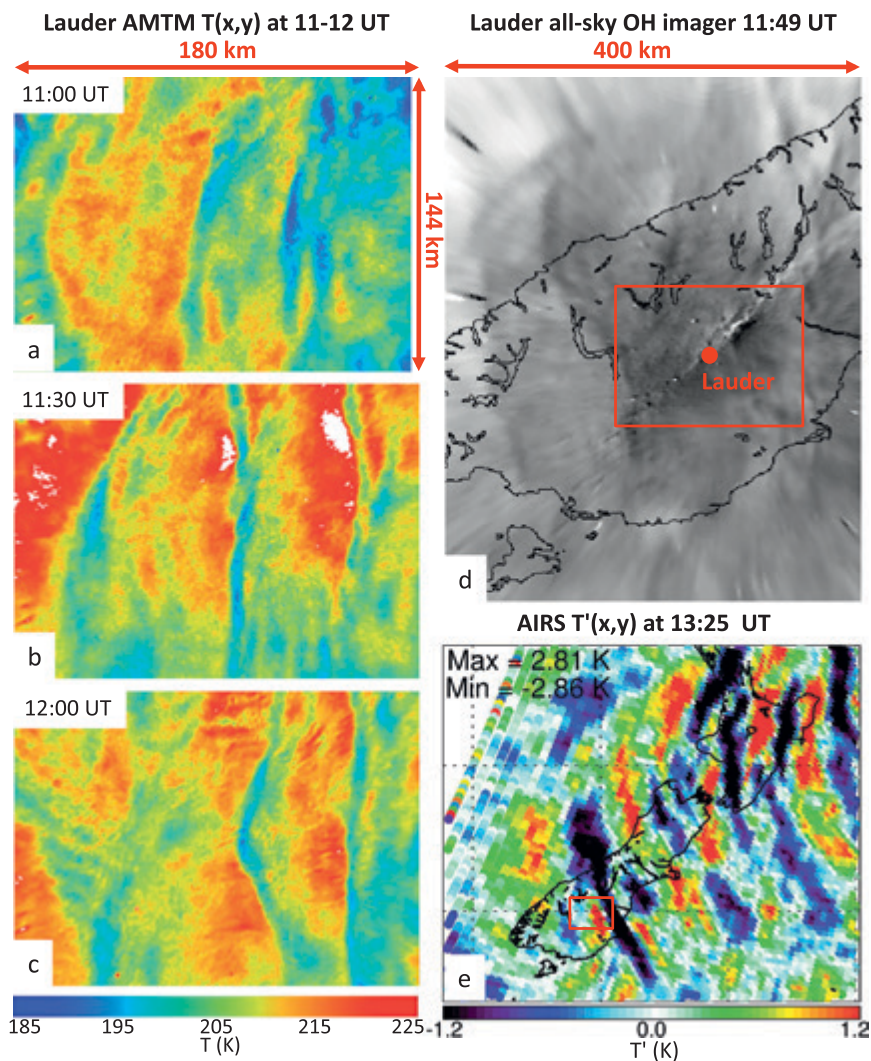


FIG. 13. Lauder AMTM images ($180 \text{ km} \times 144 \text{ km}$) of MW breaking at $\sim 82 \text{ km}$ at (a) 1100, (b) 1130, and (c) 1200 UT 21 Jun under weak orographic forcing conditions (see the first radiosonde profile in Fig. 5). The AMTM images reveal MW responses at $\lambda_h \sim 10\text{--}70 \text{ km}$ that vary on time scales of $\sim 5\text{--}10 \text{ min}$. The larger-scale MWs achieve temperature amplitudes of $T' \sim 20 \text{ K}$ or larger; the smaller-scale MWs exhibit amplitudes of $T' \sim 5\text{--}10 \text{ K}$. (d) A coincident OH brightness image from the Boston University ASI at Lauder at $\sim 82 \text{ km}$ from the Lauder airglow imager that reveals that the AMTM images (dashed red rectangle with Lauder at the center) show only a portion of a large-scale MW response extending over a region larger than the southern South Island. (e) AIRS brightness temperature (radiance) perturbations in swath nadir imagery from channel 74 at $\sim 2 \text{ hPa}$ or 43 km at 1325 UT on descending *Aqua* overpass of South Island (red rectangle shows AMTM image location). Lauder AMTM and AIRS images show very similar large-scale MW responses and suggest coherent propagation of these MWs from the surface into the MLT.

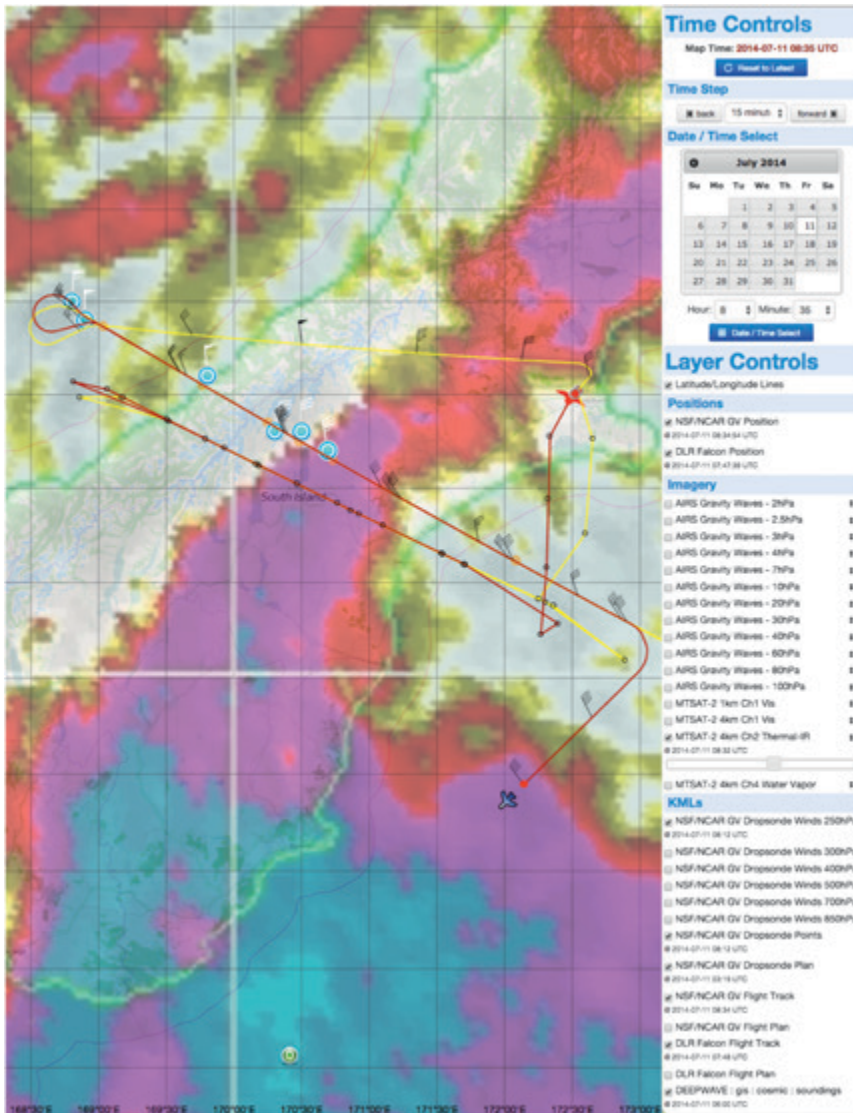


FIG. A1. Catalog maps tool display of NSF/NCAR GV and DLR Falcon flight information during flights on Jul 11. The background is from the *Multifunctional Transport Satellite-2 (MTSAT-2)* satellite channel 2 IR image. Flight tracks for each aircraft are overlaid with aircraft icons indicating their current positions as of 0835 UTC. Wind barbs (black) are depicted at 10-min intervals along the GV flight track indicating measured flight-level winds. The blue and white circles indicate the position of DWS launch points and the white wind barbs indicate DWS winds at 250 hPa. The green and white circle south of Dunedin indicates a Constellation Observing System for Meteorology, Ionosphere and Climate (COSMIC) radio occultation sounding point. Skew T plots for DWS and COSMIC data are viewable by clicking on the location circles.

APPENDIX A: DATA MANAGEMENT, FIELD CATALOG, AND ACCESS.

Development and maintenance of a comprehensive data archive is a critical step in meeting the scientific objectives of DEEPWAVE. The goal is to make the dataset and documentation available to the scientific community as soon as possible following the DEEPWAVE field program via a permanent DEEPWAVE web page. This web page

is available online (at www.eol.ucar.edu/field_projects/deepwave). The web page includes information on operations, logistics, facilities, instrumentation, mailing lists, meetings and presentations, education and outreach, and data management throughout the DEEPWAVE program.

EOL will maintain a DEEPWAVE data management portal that provides a long-term archive and access to DEEPWAVE datasets for the DEEPWAVE PIs and the scientific community (http://data.eol.ucar.edu/master_list/?project=DEEPWAVE), including the main archive at EOL and DEEPWAVE archives at other organizations. EOL will also ensure that “orphan” datasets (i.e., smaller regional and local networks) will remain available through the EOL DEEPWAVE archive. DEEPWAVE data will be available to the scientific community through a number of designated DEEPWAVE Data Archive Centers (DDACs), coordinated by NCAR/EOL and the main archive website noted above.

General users will have free and open access to all DEEPWAVE data, subject to procedures at the various DDACs and the terms of the DEEPWAVE data policy. Key elements of this policy include the following: 1) timely submission of preliminary and final data to an archive; 2) exclusive access

to the DEEPWAVE datasets by DEEPWAVE science team members from 29 January 2015 to 29 January 2016; 3) full public data access on 1 February 2016; 4) prompt notification of data providers and offers of coauthorship or attribution by data users; and 5) proper dataset citation using digital object identifiers (DOIs) and acknowledgment of DEEPWAVE data including the project name, data providers, and funding agencies.

Table C1. DEEPWAVE participants and their roles. GATS = Global Atmospheric Technologies and Sciences. USU = Utah State University. ASPEN = Atmospheric Sounding Processing Environment. AVAPS = Airborne Vertical Atmospheric Profiling System.

Organization	Participants	DEEPWAVE roles
GATS Inc.	Dave Fritts	Lead PI, NSF/NCAR GV
	Bifford Williams	GV lidar PI and operator
	Katrina Bossert	Grad student, GV lidar operator
	Tyler Mixa	Grad student, Integrated Sounding System (ISS)/FC
	Ruth Lieberman	PW analyses
	Brian Laughman	GW modeling
Yale University	Ron Smith	Co-PI, NSF/NCAR GV
	Alison Nugent, Chris Kruse, and Campbell Watson	Grad student, FC
	Azusa Takeishi	Grad student, ISS support
	Christine Tsai	Undergrad student
USU	Mike Taylor	Co-PI, GV, PI AMTM
	Dominique Pautet	Instrument scientist, AMTM
	Neal Criddle	Grad student, Lauder AMTM
	Yucheng Zhao	Scientist, GW analyses
NRL, Monterey	Jim Doyle	Co-PI, FC/modeling
	Carolyn Reynolds	Scientist, FC/modeling
	Alex Reinecke	Scientist, FC/modeling
NRL, Washington D.C.	Steve Eckermann	Co-PI, modeling
DLR, Germany	Markus Rapp	DLR PI, Falcon and GB
	Andreas Dörnbrack	DLR co-PI, Falcon and GB
NIWA, New Zealand	Michael Uddstrom	NIWA co-PI, FC
NCAR/EOL	Jim Moore and Vidal Salazar	NCAR operations director
	Lou Lussier and Pavel Romashkin	GV project manager
	Scotty McClain, Bo LeMay, Lee Baker, and Ed Ringleman	GV pilot
	Stuart Beaton, Al Cooper, and Jorgen Jensen	GV instrument scientist/QC
	Kip Eagan, Kyle Holden, Bill Irwin, Brent Kidd, Jason Morris, and Aaron Steinbach	GV aircraft mechanic
	John Cowan and John Munnerlyn	GV aircraft technician
	Julie Haggerty	GV MTP scientist
	Kelly Schick	GV MTP specialist
	Chris Webster	GV software engineer
	Kate Young	GV ASPEN specialist
	Clayton Arendt, Terry Hock, Nick Potts, and Laura Tudor	GV AVAPS engineer/technician
	Bill Brown	ISS project manager
	John Militizer, John Sobtzak, and Charlie Martin	ISS engineer

Table C1. Continued.

Organization	Participants	DEEPWAVE roles
NCAR/EOL	Timothy Lim, Jennifer Stanbridge, and Lou Verstraete	ISS technician
	Gary Granger	ISS support
	Chrissy Fladung	RAF administrator
	Greg Stossmeister	Field catalog manager
	Janine Aquino and Erik Johnson	Field catalog support
	Mike Paxton, Ted Russ, and Brandon Slaten	System administrator
	Steve Williams	Data management
	Alison Rockwell	EPO specialist
DLR, Germany	Andrea Hausold	DLR Falcon project manager
	Florian Gebhardt, Andreas Giez, Michael Grossrubatcher, Nico Hannemann, Christian Mallaun, Philipp Weber, Roland Welsler, Alexander Wolf, and David Woudsma	DLR Falcon operations
DLR, University of Mainz (*)	Fernando Chouza-Keil, Sonja Gisinger, Peter Hoor (*), Stefan Kaufmann, Mareike Kentner, Teresa Klausner, Michael Lichtenstern, Stefan Müller (*), Stephan Rahm, Anja Reiter, Philipp Reutter (*), Monika Scheibe, Romy Schlage, Hans Schlager, Patrick Vrancken, Christiane Voigt, and Benjamin Witschas	DLR Falcon science team
DLR	Christian Büdenbender, Bernd Kaifler, Natalie Kaifler, and Benedikt Ehard	Lauder–Rayleigh lidar
University of Innsbruck, University of Munich (Δ), DLR (*)	Martina Bramberger, Markus Garhammer (Δ), Sonja Gisinger (*), Tanja Portele, and Maria Siller	Lauder radiosonde team
NIWA	Mike Revelle and Richard Turner	Forecasting
	Tony Bromley	Haast sounding support
University of Innsbruck	Johannes Wagner	Grad student, FC/modeling
Computational Physics Inc.	Jun Ma and Dave Broutman	Scientist, FC
University of Canterbury	Joe Chen, Ben Jolly, Jordan Miller, Simon Parson, David Stevens, and Kate Walsh	Student, ISS support
Australian Antarctic Division	Damian Murphy, Andrew Klekociuk, and Peter Love	Kingston meteor radar and lidar
Boston University	Steve Smith	Lauder and MJO ASIs
University of Washington	Gonzalo Hernandez and Michael McCarthy	MJO FPI
University of Adelaide	Iain Reid, Andrew Mackinnon, and Andrew Spargo	Kingston meteor radar
St. Cloud State University	Brian Billings	Scientist, surface observations/photography
	Tashiana Osborne	Grad Student, ISS support
New Zealand Meteorological Service	Peter Kreft and Tony Qualye	
Millersville University	Mike Charnick	Grad student, FC
Australian Bureau of Meteorology	Michael Joyce, David Nottage, Greg Roff, and Keon Stevenson	Radiosondes, Hobart, Tasmania, and Macquarie Island

An online DEEPWAVE field catalog (<http://catalog.eol.ucar.edu/deepwave>) was hosted by EOL during the DEEPWAVE field program to support mission planning, product displays, documentation of activities, and “browse” tools for use in postfield analyses. The DEEPWAVE field catalog can access and replay flight missions and supports real-time mission coordinator and geographical information system (GIS) catalog maps display tools. The 2013 DEEPWAVE flight planning exercise is documented online (http://catalog.eol.ucar.edu/deepwave_2013). An example of the field catalog maps display is shown for reference in Fig. A1.

APPENDIX B: DEEPWAVE FIELD OPERATIONS. Operational support for the DEEPWAVE field program included several major components. The DEEPWAVE Operations Center and aircraft support were located at the U.S. Antarctic Program (USAP) Christchurch International Airport (CHC). Major logistical support was provided by PAE Ltd., the local New Zealand contractor funded by NSF. The project occupied two buildings and adjacent ramp space and served as the focus for aircraft support, forecasting and in-field science analyses, logistics, and communications. Broadband Internet access facilitated communications with remote participants in New Zealand and elsewhere.

The major deployments of ground-based instruments and aircraft for DEEPWAVE occurred over the period from late May to early August 2014, though several instruments or capabilities remained up to several months longer at Lauder. More information on these efforts and related activities can be found online (www.eol.ucar.edu/field_projects/deepwave).

The science leadership, operations coordinators, and facility project managers were key components of the DEEPWAVE in-field management team. DEEPWAVE had a daily planning meeting (DPM) 7 days a week to discuss relevant operations issues, resources and status, science objective status, current weather and outlook, and PI science mission proposals. An interesting aspect of DEEPWAVE was that all GV flights but one were conducted at night to allow the new GV optical instruments to perform optimally. The DPM was convened at 0100 UTC (1300 LT) 7 days a week to allow participation by as many groups as possible across 10 time zones. ReadyTalk web conferencing linked participants with full audio and video capabilities. The DPMs led to the definitions of the various IOPs and RF and GB measurement scheduling.

Real-time support for the project including tracking of, and interactions with, the GV utilizing the

DEEPWAVE field catalog and the EOL/Research Aviation Facility (RAF) Aeros and catalog maps tools for displaying real-time aircraft position, flight-level data displays, satellite and model data overlays, dropsonde launches and plots, and lidar and AMTM data sharing.

A unique aspect of DEEPWAVE was the ability to make real-time dropsonde deployment decisions at specific points over New Zealand and widely over the Southern Ocean. These data were relayed via satellite to the ground for quality control and processing by EOL-trained student participants before forwarding to the Global Telecommunications System for assimilation into global weather center model forecasts.

APPENDIX C: DEEPWAVE PARTICIPANTS AND ROLES. Table C1 shows the DEEPWAVE participants and their roles during the experiment.

REFERENCES

- Alexander, M. J., and L. Pfister, 1995: Gravity wave momentum flux in the lower stratosphere over convection. *Geophys. Res. Lett.*, **22**, 2029–2032, doi:10.1029/95GL01984.
- , and A. W. Grimsdell, 2013: Seasonal cycle of orographic gravity wave occurrence above small islands in the Southern Hemisphere: Implications for effects on the general circulation. *J. Geophys. Res. Atmos.*, **118**, 11 589–11 599, doi:10.1002/2013JD020526.
- , S. D. Eckermann, D. Broutman, and J. Ma, 2009: Momentum flux estimates for South Georgia Island mountain waves in the stratosphere observed via satellite. *Geophys. Res. Lett.*, **36**, L12816, doi:10.1029/2009GL038587.
- , and Coauthors, 2010: Recent developments in gravity-wave effects in climate models and the global distribution of gravity-wave momentum flux from observations and models. *Quart. J. Roy. Meteor. Soc.*, **136**, 1103–1124, doi:10.1002/qj.637.
- Alexander, S. P., A. R. Klekociuk, and D. J. Murphy, 2011: Rayleigh lidar observations of gravity wave activity in the winter upper stratosphere and lower mesosphere above Davis, Antarctica (69°S, 78°E). *J. Geophys. Res.*, **116**, D13109, doi:10.1029/2010JD015164.
- Allen, S. J., and R. A. Vincent, 1995: Gravity wave activity in the lower atmosphere: Seasonal and latitudinal variations. *J. Geophys. Res.*, **100**, 1327–1350, doi:10.1029/94JD02688.
- Amerault, C., X. Zou, and J. Doyle, 2008: Tests of an adjoint mesoscale model with explicit moist physics on the cloud scale. *Mon. Wea. Rev.*, **136**, 2120–2132, doi:10.1175/2007MWR2259.1.

- Atlas, D., J. I. Metcalf, J. H. Richter, and E. E. Gossard, 1970: The birth of “CAT” and microscale turbulence. *J. Atmos. Sci.*, **27**, 903–913, doi:10.1175/1520-0469(1970)027<0903:TBOAMT>2.0.CO;2.
- Bacmeister, J. T., M. F. Wehner, R. B. Neale, A. Gettelman, C. Hannay, P. H. Lauritzen, J. M. Caron, and J. E. Truesdale, 2014: Exploratory high-resolution climate simulations using the Community Atmosphere Model (CAM). *J. Climate*, **27**, 3073–3099, doi:10.1175/JCLI-D-13-00387.1.
- Balsley, B. B., and R. Garello, 1985: The kinetic energy density in the troposphere, stratosphere, and mesosphere: A preliminary study using the Poker Flat MST radar in Alaska. *Radio Sci.*, **20**, 1355–1361, doi:10.1029/RS020i006p01355.
- Booker, J. R., and F. P. Bretherton, 1967: The critical layer for internal gravity waves in a shear flow. *J. Fluid Mech.*, **27**, 513–539, doi:10.1017/S0022112067000515.
- Bougeault, P., A. Jansa Clar, B. Benech, B. Carissimo, J. Pelon, and E. Richard, 1990: Momentum budget over the Pyrénées: The PYREX experiment. *Bull. Amer. Meteor. Soc.*, **71**, 806–818, doi:10.1175/1520-0477(1990)071<0806:MBOTPT>2.0.CO;2.
- , and Coauthors, 2001: The MAP special observing period. *Bull. Amer. Meteor. Soc.*, **82**, 433–462, doi:10.1175/1520-0477(2001)082<0433:TMSOP>2.3.CO;2.
- Bretherton, F. P., 1969a: Waves and turbulence in stably stratified fluids. *Radio Sci.*, **4**, 1279–1287, doi:10.1029/RS004i012p01279.
- , 1969b: Momentum transfer by gravity waves. *Quart. J. Roy. Meteor. Soc.*, **95**, 213–243, doi:10.1002/qj.49709540402.
- Brinkmann, W. A. R., 1974: Strong downslope winds at Boulder, Colorado. *Mon. Wea. Rev.*, **102**, 592–602, doi:10.1175/1520-0493(1974)102<0592:SDWABC>2.0.CO;2.
- Brown, P. R. A., 1983: Aircraft measurements of mountain waves and their associated momentum flux over the British Isles. *Quart. J. Roy. Meteor. Soc.*, **109**, 849–865, doi:10.1002/qj.49710946211.
- Bühler, O., 2014: *Waves and Mean Flows*. Cambridge University Press, 360 pp.
- Carlsaw, K. S., and Coauthors, 1998: Particle microphysics and chemistry in remotely observed mountain polar stratospheric clouds. *J. Geophys. Res.*, **103**, 5785–5796, doi:10.1029/97JD03626.
- Chanin, M.-L., and A. Hauchecorne, 1981: Lidar observation of gravity and tidal waves in the stratosphere and mesosphere. *J. Geophys. Res.*, **86**, 9715–9721, doi:10.1029/JC086iC10p09715.
- Clark, T. L., and W. R. Peltier, 1977: On the evolution and stability of finite-amplitude mountain waves. *J. Atmos. Sci.*, **34**, 1715–1730, doi:10.1175/1520-0469(1977)034<1715:OTEASO>2.0.CO;2.
- Dewan, E. M., and Coauthors, 1998: MSX satellite observations of thunderstorm-generated gravity waves in mid-wave infrared images of the upper stratosphere. *Geophys. Res. Lett.*, **25**, 939–942, doi:10.1029/98GL00640.
- Dörnbrack, A., M. Leutbecher, J. Reichardt, A. Behrendt, K.-P. Müller, and G. Baumgarten, 2001: Relevance of mountain wave cooling for the formation of polar stratospheric clouds over Scandinavia: Mesoscale dynamics and observations for January 1997. *J. Geophys. Res.*, **106**, 1569–1581, doi:10.1029/2000JD900194.
- Doyle, J. D., and R. B. Smith, 2003: Mountain waves over the Hohe Tauern: Influence of upstream diabatic effects. *Quart. J. Roy. Meteor. Soc.*, **129**, 799–823, doi:10.1256/qj.01.205.
- , and Q. Jiang, 2006: Observations and numerical simulations of mountain waves in the presence of directional wind shear. *Quart. J. Roy. Meteor. Soc.*, **132**, 1877–1905, doi:10.1256/qj.05.140.
- , and Coauthors, 2000: An intercomparison of model-predicted wave breaking for the 11 January 1972 Boulder windstorm. *Mon. Wea. Rev.*, **128**, 901–914, doi:10.1175/1520-0493(2000)128<0901:AOMPW>2.0.CO;2.
- , M. Shapiro, Q. Jiang, and D. Bartels, 2005: Large-amplitude mountain wave breaking over Greenland. *J. Atmos. Sci.*, **62**, 3106–3126, doi:10.1175/JAS3528.1.
- , and Coauthors, 2011: An intercomparison of T-REX mountain-wave simulations and implications for mesoscale predictability. *Mon. Wea. Rev.*, **139**, 2811–2831, doi:10.1175/MWR-D-10-05042.1.
- , C. Amerault, C. A. Reynolds, and P. A. Reinecke, 2014: Initial condition sensitivity and predictability of a severe extratropical cyclone using a moist adjoint. *Mon. Wea. Rev.*, **142**, 320–342, doi:10.1175/MWR-D-13-00201.1.
- Duck, T. J., J. A. Whiteway, and A. I. Carswell, 2001: The gravity wave–Arctic stratospheric vortex interaction. *J. Atmos. Sci.*, **58**, 3581–3596, doi:10.1175/1520-0469(2001)058<3581:TGWASV>2.0.CO;2.
- Eckermann, S. D., and P. Preusse, 1999: Global measurements of stratospheric mountain waves from space. *Science*, **286**, 1534–1537, doi:10.1126/science.286.5444.1534.
- , and D. L. Wu, 2012: Satellite detection of orographic gravity-wave activity in the winter subtropical stratosphere over Australia and Africa. *Geophys. Res. Lett.*, **39**, L21807, doi:10.1029/2012GL053791.
- , D. Broutman, J. Ma, and J. Lindeman, 2006a: Fourier-ray modeling of short wavelength trapped lee waves observed in infrared satellite imagery near Jan

- Mayen. *Mon. Wea. Rev.*, **134**, 2830–2848, doi:10.1175/MWR3218.1.
- , A. Dörnbrack, S. B. Vosper, H. Flentje, M. J. Mahoney, T. P. Bui, and K. S. Carslaw, 2006b: Mountain wave–induced polar stratospheric cloud forecasts for aircraft science flights during SOLVE/THESEO 2000. *Wea. Forecasting*, **21**, 42–68, doi:10.1175/WAF901.1.
- , J. Ma, and D. L. Wu, 2007: A three-dimensional mountain wave imaged in satellite radiance throughout the stratosphere: Evidence of the effects of directional wind shear. *Quart. J. Roy. Meteor. Soc.*, **133**, 1959–1974, doi:10.1002/qj.187.
- , L. Hoffman, M. Hopfner, D. L. Wu, and M. J. Alexander, 2009: Antarctic NAT PSC belt of June 2003: Observational validation of the mountain wave seeding hypothesis. *Geophys. Res. Lett.*, **36**, L02807, doi:10.1029/2008GL036629.
- Eliassen, A., and E. Palm, 1961: On the transfer of energy in stationary mountain waves. *Geophys. Publ.*, **22**, 1–23.
- Ern, M., P. Preusse, M. J. Alexander, and C. D. Warner, 2004: Absolute values of gravity wave momentum flux derived from satellite data. *J. Geophys. Res.*, **109**, D20103, doi:10.1029/2004JD004752.
- Fritts, D. C., 1984: Gravity wave saturation in the middle atmosphere: A review of theory and observations. *Rev. Geophys.*, **22**, 275–308, doi:10.1029/RG022i003p00275.
- , and P. K. Rastogi, 1985: Convective and dynamical instabilities due to gravity wave motions in the lower and middle atmosphere: Theory and observations. *Radio Sci.*, **20**, 1247–1277, doi:10.1029/RS020i006p01247.
- , and R. A. Vincent, 1987: Mesospheric momentum flux studies at Adelaide, Australia: Observations and a gravity wave/tidal interaction model. *J. Atmos. Sci.*, **44**, 605–619, doi:10.1175/1520-0469(1987)044<0605:MMFSAA>2.0.CO;2.
- , and G. D. Nastrom, 1992: Sources of mesoscale variability of gravity waves. Part II: Frontal, convective, and jet stream excitation. *J. Atmos. Sci.*, **49**, 111–127, doi:10.1175/1520-0469(1992)049<0111:SO MVOG>2.0.CO;2.
- , and M. J. Alexander, 2003: Gravity dynamics and effects in the middle atmosphere. *Rev. Geophys.*, **41**, 1003, doi:10.1029/2001RG000106.
- , S. A. Vadas, and Y. Yamada, 2002: An estimate of strong local gravity wave body forcing based on OH airglow and meteor radar observations. *Geophys. Res. Lett.*, **29**, doi:10.1029/2001GL013753.
- , L. Wang, J. Werne, T. Lund, and K. Wan, 2009: Gravity wave instability dynamics at high Reynolds numbers. Part II: Turbulence evolution, structure, and anisotropy. *J. Atmos. Sci.*, **66**, 1149–1171, doi:10.1175/2008JAS2727.1.
- , and Coauthors, 2014: Quantifying gravity wave momentum fluxes with mesosphere temperature mappers and correlative instrumentation. *J. Geophys. Res. Atmos.*, **119**, 13 583–13 603, doi:10.1002/2014JD022150.
- Garcia, R. R., and S. Solomon, 1985: The effect of breaking gravity waves on the dynamical and chemical composition of the mesosphere and lower thermosphere. *J. Geophys. Res.*, **90**, 3850–3868, doi:10.1029/JD090iD02p03850.
- Gardner, C. S., and D. G. Voelz, 1987: Lidar studies of the nighttime sodium layer over Urbana, Illinois: 2. Gravity waves. *J. Geophys. Res.*, **92**, 4673–4694, doi:10.1029/JA092iA05p04673.
- Gavrilov, N. M., and G. M. Shved, 1982: Study of internal gravity waves in the lower thermosphere from observations of the nocturnal sky airglow [OI] 5577 Å in Ashkhabad (translation). *Ann. Geophys.*, **38**, 789–803.
- Geller, M. A., and Coauthors, 2013: A comparison between gravity wave momentum fluxes in observations and climate models. *J. Climate*, **26**, 6383–6405, doi:10.1175/JCLI-D-12-00545.1.
- Goldberg, R. A., and Coauthors, 2006: The MacWAVE program to study gravity wave influences on the polar mesosphere. *Ann. Geophys.*, **24**, 1159–1173, doi:10.5194/angeo-24-1159-2006.
- Gong, J., D. L. Wu, and S. D. Eckermann, 2012: Gravity wave variances and propagation derived from AIRS radiances. *Atmos. Chem. Phys.*, **12**, 1701–1720, doi:10.5194/acp-12-1701-2012.
- Gossard, E. E., and W. H. Hooke, 1975: *Waves in the Atmosphere*. Developments in Atmospheric Science Series, Vol. 2, Elsevier Scientific, 456 pp.
- , J. H. Richter, and D. Atlas, 1970: Internal waves in the atmosphere from high-resolution radar measurements. *J. Geophys. Res.*, **75**, 3523–3536, doi:10.1029/JC075i018p03523.
- Grubišić, V., and J. M. Lewis, 2004: Sierra Wave Project revisited: 50 years later. *Bull. Amer. Meteor. Soc.*, **85**, 1127–1142, doi:10.1175/BAMS-85-8-1127.
- , and Coauthors, 2008: The Terrain-Induced Rotor Experiment. *Bull. Amer. Meteor. Soc.*, **89**, 1513–1533, doi:10.1175/2008BAMS2487.1.
- Haynes, P. H., C. J. Marks, M. E. McIntyre, T. G. Shephard, and K. P. Shine, 1991: On the “downward control” of extratropical diabatic circulations by eddy-induced mean zonal forces. *J. Atmos. Sci.*, **48**, 651–678, doi:10.1175/1520-0469(1991)048<0651:OT COED>2.0.CO;2.

- Hecht, J. H., R. L. Walterscheid, D. C. Fritts, J. R. Isler, D. C. Senft, C. S. Gardner, and S. J. Franke, 1997: Wave breaking signatures in OH airglow and sodium densities and temperatures: 1. Airglow imaging, Na lidar, and MF radar observations. *J. Geophys. Res.*, **102**, 6655–6668, doi:10.1029/96JD02619.
- , —, and R. Vincent, 2001: Airglow observations of dynamical (wind shear-induced) instabilities over Adelaide, Australia, associated with atmospheric gravity waves. *J. Geophys. Res.*, **106**, 28 189–28 197, doi:10.1029/2001JD000419.
- , and Coauthors, 2014: The life cycle of instability features measured from the Andes Lidar Observatory over Cerro Pachon on March 24, 2012. *J. Geophys. Res. Atmos.*, **119**, 8872–8898, doi:10.1002/2014JD021726.
- Hendricks, E. A., J. D. Doyle, S. D. Eckermann, Q. Jiang, and P. A. Reinecke, 2014: What is the source of the stratospheric gravity wave belt in austral winter? *J. Atmos. Sci.*, **71**, 1583–1592, doi:10.1175/JAS-D-13-0332.1.
- Hertzog, A., G. Boccaro, R. A. Vincent, F. Vial, and P. Cocquerez, 2008: Estimation of gravity-wave momentum fluxes and phase speeds from quasi-Lagrangian stratospheric balloon flights. Part II: Results from the Vorcore campaign in Antarctica. *J. Atmos. Sci.*, **65**, 3056–3070, doi:10.1175/2008JAS2710.1.
- , M. J. Alexander, and R. Plougonven, 2012: On the intermittency of gravity wave momentum flux in the stratosphere. *J. Atmos. Sci.*, **69**, 3433–3448, doi:10.1175/JAS-D-12-09.1.
- Hines, C. O., 1960: Internal atmospheric gravity waves at ionospheric heights. *Can. J. Phys.*, **38**, 1441–1481, doi:10.1139/p60-150.
- , 1991: The saturation of gravity waves in the middle atmosphere. Part II: Development of Doppler-spread theory. *J. Atmos. Sci.*, **48**, 1361–1379, doi:10.1175/1520-0469(1991)048<1361:TSOGWI>2.0.CO;2.
- , 1997a: Doppler-spread parameterization of gravity-wave momentum deposition in the middle atmosphere. Part 1: Basic formulation. *J. Atmos. Sol.-Terr. Phys.*, **59**, 371–386, doi:10.1016/S1364-6826(96)00079-X.
- , 1997b: Doppler-spread parameterization of gravity-wave momentum deposition in the middle atmosphere. Part 2: Broad and quasi-monochromatic spectra, and implementation. *J. Atmos. Sol.-Terr. Phys.*, **59**, 387–400, doi:10.1016/S1364-6826(96)00080-6.
- Holton, J. R., 1982: The role of gravity wave induced drag and diffusion in the momentum budget of the mesosphere. *J. Atmos. Sci.*, **39**, 791–799, doi:10.1175/1520-0469(1982)039<0791:TROGWI>2.0.CO;2.
- Hostetler, C. A., and C. S. Gardner, 1994: Observations of horizontal and vertical wave number spectra of gravity wave motions in the stratosphere and mesosphere over the mid-Pacific. *J. Geophys. Res.*, **99**, 1283–1302, doi:10.1029/93JD02927.
- , —, R. A. Vincent, and D. Lesicar, 1991: Spectra of gravity wave density and wind perturbations observed during ALOHA-90 on the 25 March flight between Maui and Christmas Island. *Geophys. Res. Lett.*, **18**, 1325–1328, doi:10.1029/91GL01150.
- Kim, Y.-J., S. D. Eckermann, and H.-Y. Chun, 2003: An overview of the past, present and future of gravity-wave drag parameterization for numerical climate and weather prediction models. *Atmos.–Ocean*, **41**, 65–98, doi:10.3137/ao.410105.
- Klemp, J. B., and D. K. Lilly, 1978: Numerical simulation of hydrostatic mountain waves. *J. Atmos. Sci.*, **35**, 78–107, doi:10.1175/1520-0469(1978)035<0078:NSO HMW>2.0.CO;2.
- Kruse, C. G. and R. B. Smith, 2015: Gravity wave diagnostics and characteristics in mesoscale fields. *J. Atmos. Sci.*, **72**, 4372–4392, doi:10.1175/JAS-D-15-0079.1.
- Kuettner, J. P., and D. K. Lilly, 1968: Lee waves in the Colorado Rockies. *Weatherwise*, **21**, 180–197, doi:10.1080/00431672.1968.9932819.
- , P. A. Hildebrand, and T. L. Clark, 1987: Convection waves: Observations of gravity wave systems over convectively active boundary layers. *Quart. J. Roy. Meteor. Soc.*, **113**, 445–467, doi:10.1002/qj.49711347603.
- Küttner, J., 1938: Moazagotl und Föhnwelle. *Beitr. Phys. Atmos.*, **25**, 79–114.
- , 1939: Zur Entstehung der Föhnwelle. *Beitr. Phys. Atmos.*, **25**, 251–299.
- Lilly, D. K., 1978: A severe downslope windstorm and aircraft turbulence induced by a mountain wave. *J. Atmos. Sci.*, **35**, 59–77, doi:10.1175/1520-0469(1978)035<0059:ASDWAA>2.0.CO;2.
- , and P. J. Kennedy, 1973: Observations of a stationary mountain wave and its associated momentum flux and energy dissipation. *J. Atmos. Sci.*, **30**, 1135–1152, doi:10.1175/1520-0469(1973)030<1135:OOAS MW>2.0.CO;2.
- , J. M. Nicholls, P. J. Kennedy, J. B. Klemp, and R. M. Chervin, 1982: Aircraft measurements of wave momentum flux over the Colorado Rocky Mountains. *Quart. J. Roy. Meteor. Soc.*, **108**, 625–642, doi:10.1002/qj.49710845709.
- Lindzen, R. S., 1981: Turbulence and stress owing to gravity wave and tidal breakdown. *J. Geophys. Res.*, **86**, 9707–9714, doi:10.1029/JC086iC10p09707.
- , and J. R. Holton, 1968: A theory of the quasi-biennial oscillation. *J. Atmos. Sci.*, **25**, 1095–1107,

- doi:10.1175/1520-0469(1968)025<1095:ATOTQB>2.0.CO;2.
- Liu, H.-L., J. M. McInerney, S. Santos, P. H. Lauritzen, M. A. Taylor, and N. M. Pedatella, 2014: Gravity waves simulated by high-resolution Whole Atmosphere Community Climate Model. *Geophys. Res. Lett.*, **41**, 9106–9112, doi:10.1002/2014GL062468.
- Lombard, P. N., and J. J. Riley, 1996: Instability and breakdown of internal gravity waves. I. Linear stability analysis. *Phys. Fluids*, **8**, 3271–3287, doi:10.1063/1.869117.
- Long, R. R., 1953: Some aspects of the flow of stratified fluids. I. A theoretical investigation. *Tellus*, **5**, 42–58, doi:10.1111/j.2153-3490.1953.tb01035.x.
- , 1955: Some aspects of the flow of stratified fluids. III. Continuous density gradients. *Tellus*, **7**, 341–357, doi:10.1111/j.2153-3490.1955.tb01171.x.
- Lu, X., X. Chu, W. Fong, C. Chen, Z. Yu, B. R. Roberts, and A. J. McDonald, 2015: Vertical evolution of potential energy density and vertical wave number spectrum of Antarctic gravity waves from 35 to 105 km at McMurdo (77.8°S, 166.7°E). *J. Geophys. Res. Atmos.*, **120**, 2719–2737, doi:10.1002/2014JD022751.
- Luce, H., M. Yamamoto, S. Fukao, and K. Sato, 2008: High-resolution observations with MU radar of a KH instability triggered by an inertia–gravity wave in the upper part of the jet stream. *J. Atmos. Sci.*, **65**, 1711–1718, doi:10.1175/2007JAS2346.1.
- Manley, G., 1945: The helm wind of Crossfell, 1937–1939. *Quart. J. Roy. Meteor. Soc.*, **71**, 197–219, doi:10.1002/qj.49707130901.
- McFarlane, N. A., 1987: The effect of orographically excited gravity wave drag on the general circulation of the lower stratosphere and troposphere. *J. Atmos. Sci.*, **44**, 1775–1800, doi:10.1175/1520-0469(1987)044<1775:TEOOEG>2.0.CO;2.
- Nakamura, T., T. Aono, T. Tsuda, A. G. Admiranto, E. Achmad, and Suranto, 2003: Mesospheric gravity waves over a tropical convective region observed by OH airglow imaging in Indonesia. *Geophys. Res. Lett.*, **30**, 1882, doi:10.1029/2003GL017619.
- Nappo, C. J., 2013: *An Introduction to Atmospheric Gravity Waves*. 2nd ed. International Geophysics Series, Vol. 85, Academic Press, 276 pp.
- Nastrom, G. D., and D. C. Fritts, 1992: Sources of mesoscale variability of gravity waves. Part I: Topographic excitation. *J. Atmos. Sci.*, **49**, 101–110, doi:10.1175/1520-0469(1992)049<0101:SOMVOG>2.0.CO;2.
- Pautet, P.-D., M. J. Taylor, W. R. Pendleton Jr., Y. Zhao, T. Yuan, R. Esplin, and D. McLain, 2014: An advanced mesospheric temperature mapper for high-latitude airglow studies. *Appl. Opt.*, **53**, 5934–5943, doi:10.1364/AO.53.005934.
- Pavelin, E., J. A. Whiteway, and G. Vaughants, 2001: Observation of gravity wave generation and breaking in the lowermost stratosphere. *J. Geophys. Res.*, **106**, 5173–5179, doi:10.1029/2000JD900480.
- Pfister, L., S. Scott, M. Loewenstein, S. Bowen, and M. Legg, 1993: Mesoscale disturbances in the tropical stratosphere excited by convection: Observations and effects on the stratospheric momentum budget. *J. Atmos. Sci.*, **50**, 1058–1075, doi:10.1175/1520-0469(1993)050<1058:MDITTS>2.0.CO;2.
- Plougonven, R., A. Hertzog, and H. Teitelbaum, 2008: Observations and simulations of a large-amplitude mountain wave breaking over the Antarctic Peninsula. *J. Geophys. Res.*, **113**, D16113, doi:10.1029/2007JD009739.
- , —, and L. Guez, 2013: Gravity waves over Antarctica and the Southern Ocean: Consistent momentum fluxes in mesoscale simulations and stratospheric balloon observations. *Quart. J. Roy. Meteor. Soc.*, **139**, 101–118, doi:10.1002/qj.1965.
- Preusse, P., S. D. Eckerman, and M. Ern, 2008: Transparency of the atmosphere to short horizontal wavelength gravity waves. *J. Geophys. Res.*, **113**, D24104, doi:10.1029/2007JD009682.
- Queney, M. P., 1936a: Recherches relatives a l'influence du relief sur les éléments météorologiques (1). *Meteorologie*, 334–353.
- , 1936b: Recherches relatives a l'influence du relief sur les éléments météorologiques (suite). *Meteorologie*, 453–470.
- , 1947: Theory of perturbations in stratified currents with application to air flow over mountain barriers. Department of Meteorology, University of Chicago Miscellaneous Rep. 23, 81 pp.
- Rapp, M., B. Strelnikov, A. Müllemann, F.-J. Lübken, and D. C. Fritts, 2004: Turbulence measurements and implications for gravity wave dissipation during the MaCWAVE/MIDAS summer rocket program. *Geophys. Res. Lett.*, **31**, L24S07, doi:10.1029/2003GL019325.
- Sato, K., 1994: A statistical study of the structure, saturation and sources of inertio-gravity waves in the lower stratosphere observed with the MU radar. *J. Atmos. Terr. Phys.*, **56**, 755–774, doi:10.1016/0021-9169(94)90131-7.
- , and R. F. Woodman, 1982: Fine altitude resolution radar observations of stratospheric turbulent layers by the Arecibo 430 MHz radar. *J. Atmos. Sci.*, **39**, 2546–2552, doi:10.1175/1520-0469(1982)039<2546:FAROOS>2.0.CO;2.
- , and T. J. Dunkerton, 1997: Estimates of momentum flux associated with equatorial Kelvin and gravity waves. *J. Geophys. Res.*, **102**, 26 247–26 261, doi:10.1029/96JD02514.

- , and M. Yoshiki, 2008: Gravity wave generation around the polar vortex in the stratosphere revealed by 3-hourly radiosonde observations at Syowa station. *J. Atmos. Sci.*, **65**, 3719–3735, doi:10.1175/2008JAS2539.1.
- , S. Tateno, S. Watanabe, and Y. Kawatani, 2012: Gravity wave characteristics in the Southern Hemisphere revealed by a high-resolution middle-atmosphere general circulation model. *J. Atmos. Sci.*, **69**, 1378–1396, doi:10.1175/JAS-D-11-0101.1.
- Scorer, R. S., 1949: Theory of waves in the lee of mountains. *Quart. J. Roy. Meteor. Soc.*, **75**, 41–46, doi:10.1002/qj.49707532308.
- She, C. Y., J. R. Yu, J. W. Huang, C. Nagasawa, and C. S. Gardner, 1991: Na temperature lidar measurements of gravity wave perturbations of wind, density and temperature in the mesopause region. *Geophys. Res. Lett.*, **18**, 1329–1331, doi:10.1029/91GL01517.
- Shutts, G. J., and S. B. Vosper, 2011: Stratospheric gravity waves revealed in NWP model forecasts. *Quart. J. Roy. Meteor. Soc.*, **137**, 303–317, doi:10.1002/qj.763.
- Smith, R. B., 1980: Linear theory of stratified hydrostatic flow past an isolated mountain. *Tellus*, **32**, 348–364, doi:10.1111/j.2153-3490.1980.tb00962.x.
- , S. Skubis, J. D. Doyle, A. S. Broad, C. Kiemle, and H. Volkert, 2002: Mountain waves over Mont Blanc: Influence of a stagnant boundary layer. *J. Atmos. Sci.*, **59**, 2073–2092, doi:10.1175/1520-0469(2002)059<2073:MWOMBI>2.0.CO;2.
- , B. K. Woods, J. Jensen, W. A. Cooper, J. D. Doyle, Q. F. Jiang, and V. Grubisic, 2008: Mountain waves entering the stratosphere. *J. Atmos. Sci.*, **65**, 2543–2562, doi:10.1175/2007JAS2598.1.
- Smith, S. A., D. C. Fritts, and T. E. VanZandt, 1987: Evidence for a saturated spectrum of atmospheric gravity waves. *J. Atmos. Sci.*, **44**, 1404–1410, doi:10.1175/1520-0469(1987)044<1404:EFASSO>2.0.CO;2.
- , J. Baumgardner, and M. Mendillo, 2009: Evidence of mesospheric gravity-waves generated by orographic forcing in the troposphere. *Geophys. Res. Lett.*, **36**, L08807, doi:10.1029/2008GL036936.
- Sonmor, L. J., and G. P. Klaassen, 1997: Toward a unified theory of gravity wave stability. *J. Atmos. Sci.*, **54**, 2655–2680, doi:10.1175/1520-0469(1997)054<2655:TAUTOG>2.0.CO;2.
- Sutherland, B. R., 2010: *Internal Gravity Waves*. Cambridge University Press, 377 pp.
- Swenson, G. R., M. J. Taylor, P. J. Espy, C. Gardner, and X. Tac, 1995: ALOHA-93 measurements of intrinsic AGW characteristics using airborne airglow imager and ground-based Na wind/temperature lidar. *Geophys. Res. Lett.*, **22**, 2841–2844, doi:10.1029/95GL02579.
- Taylor, M. J., and M. A. Hapgood, 1988: Identification of a thunderstorm as a source of short period gravity waves in the upper atmospheric airglow emissions. *Planet. Space Sci.*, **36**, 975–985, doi:10.1016/0032-0633(88)90035-9.
- , Y. Y. Gu, X. Tao, C. S. Gardner, and M. B. Bishop, 1995: An investigation of intrinsic gravity wave signatures using coordinated lidar and nightglow image measurements. *Geophys. Res. Lett.*, **22**, 2853–2856, doi:10.1029/95GL02949.
- Thomas, L., R. M. Worthington, and A. J. McDonald, 1999: Inertia-gravity waves in the troposphere and lower stratosphere associated with a jet stream exit region. *Ann. Geophys.*, **17**, 115–121, doi:10.1007/s005850050741.
- Tsuda, T., T. Inoue, D. C. Fritts, T. E. VanZandt, S. Kato, T. Sato, and S. Fukao, 1989: MST radar observations of a saturated gravity wave spectrum. *J. Atmos. Sci.*, **46**, 2440–2447, doi:10.1175/1520-0469(1989)046<2440:MROOAS>2.0.CO;2.
- , Y. Murayama, M. Yamamoto, S. Kato, and S. Fukao, 1990: Seasonal variation of momentum flux in the mesosphere observed with the MU radar. *Geophys. Res. Lett.*, **17**, 725–728, doi:10.1029/GL017i006p00725.
- , —, H. Wiryosumarto, S. W. B. Harijono, and S. Kato, 1994: Radiosonde observations of equatorial atmospheric dynamics over Indonesia: 2. Characteristics of gravity waves. *J. Geophys. Res.*, **99**, 10 507–10 516, doi:10.1029/94JD00354.
- Vincent, R. A., and I. M. Reid, 1983: HF Doppler measurements of mesospheric momentum fluxes. *J. Atmos. Sci.*, **40**, 1321–1333, doi:10.1175/1520-0469(1983)040<1321:HDMOMG>2.0.CO;2.
- Vosper, S. B., 2015: Mountain waves and wakes generated by South Georgia: Implications for drag parameterization. *Quart. J. Roy. Meteor. Soc.*, **141**, 2813–2827, doi:10.1002/qj.2566.
- Walterscheid, R. L., J. H. Hecht, R. A. Vincent, I. M. Reid, J. Woithe, and M. J. Hickey, 1999: Analysis and interpretation of airglow and radar observations of quasi-monochromatic gravity waves in the upper mesosphere and lower thermosphere over Adelaide, Australia (35°S, 138°E). *J. Atmos. Sol.-Terr. Phys.*, **61**, 461–478, doi:10.1016/S1364-6826(99)00002-4.
- Wang, L., D. C. Fritts, B. P. Williams, R. A. Goldberg, F. J. Schmidlin, and U. Blum, 2006: Gravity waves in the middle during the MaCWAVE winter campaign. *Ann. Geophys.*, **24**, 1209–1226, doi:10.5194/angeo-24-1209-2006.
- Warner, C. D., and M. E. McIntyre, 1996: On the propagation and dissipation of gravity wave spectra through a realistic middle atmosphere.

- J. Atmos. Sci.*, **53**, 3213–3235, doi:10.1175/1520-0469(1996)053<3213:OTPAADO>2.0.CO;2.
- Whiteway, J. A., and A. I. Carswell, 1994: Rayleigh lidar observations of thermal structure and gravity wave activity in the high Arctic during a stratospheric warming. *J. Atmos. Sci.*, **51**, 3122–3136, doi:10.1175/1520-0469(1994)051<3122:RLOOTS>2.0.CO;2.
- , E. G. Pavelin, R. Busen, J. Hacker, and S. Vosper, 2003: Airborne measurements of gravity wave breaking at the tropopause. *Geophys. Res. Lett.*, **30**, 2070, doi:10.1029/2003GL018207.
- Williams, B. P., D. C. Fritts, C. Y. She, G. Baumgarten, and R. A. Goldberg, 2006: Gravity wave propagation, tidal interaction, and instabilities in the mesosphere and lower thermosphere during the winter 2003: MaCWAVE rocket campaign. *Ann. Geophys.*, **24**, 1199–1208, doi:10.5194/angeo-24-1199-2006.
- Woodman, R. F., and A. Guillen, 1974: Radar observations of winds and turbulence in the stratosphere and mesosphere. *J. Atmos. Sci.*, **31**, 493–505, doi:10.1175/1520-0469(1974)031<0493:ROOWAT>2.0.CO;2.
- Wu, D. L., and S. D. Eckermann, 2008: Global gravity wave variances from Aura MLS: Characteristics and interpretation. *J. Atmos. Sci.*, **65**, 3695–3718, doi:10.1175/2008JAS2489.1.
- Yamashita, C., H.-L. Liu, and X. Chu, 2010: Gravity wave variations during the 2009 stratospheric sudden warming as revealed by ECMWF-T799 and observations. *Geophys. Res. Lett.*, **37**, L22806, doi:10.1029/2010GL045437.
- Yeh, K. C., and C. H. Liu, 1981: The instability of atmospheric gravity waves through wave-wave interactions. *J. Geophys. Res.*, **86**, 9722–9728, doi:10.1029/JC086iC10p09722.

NEW FROM AMS BOOKS!

The Thinking Person's Guide to Climate Change

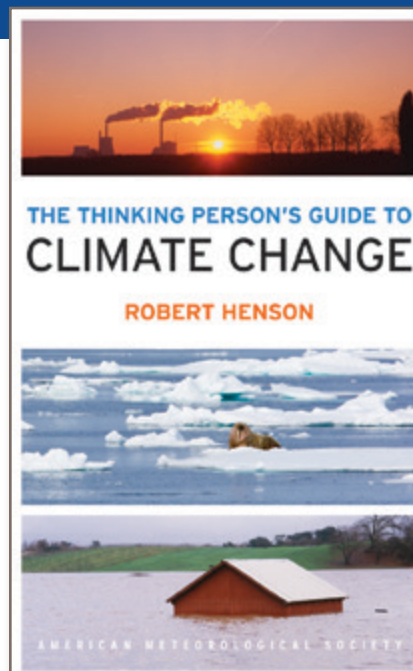
Robert Henson

Expanded and updated from Henson's *Rough Guide to Climate Change*, 3rd edition (no longer in print), combining years of data with recent research, including conclusions from the Fifth Assessment Report of the Intergovernmental Panel on Climate Change, the Guide breaks down the issues into straightforward categories:

- Symptoms, including melting ice and extreme weather
- Science, laying out what we know and how we know it
- Debates, tackling the controversy and politics
- Solutions and Actions for creating the best possible future

© 2014, 516 pages, paperback
ISBN: 978-1-878220-73-7

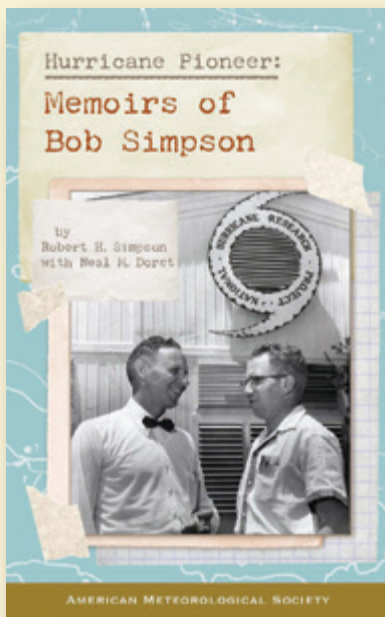
List price: \$30 AMS Member price: \$20



AMS BOOKS

RESEARCH APPLICATIONS HISTORY

➤ bookstore.ametsoc.org



HURRICANE PIONEER

Memoirs of Bob Simpson

Robert H. Simpson with Neal M. Dorst

In 1951, Bob Simpson rode a plane directly into the wall of a hurricane—just one of his many pioneering explorations. This autobiography of the first director of the National Hurricane Research Project and co-creator of the Saffir-Simpson Hurricane Scale starts with childhood remembrance and ends in first-hand account of a revolutionary

© 2014, PAPERBACK
 ISBN: 978-1-935704-75-1
 LIST \$30 MEMBER \$20



CLIMATE CONUNDRUMS

What the Climate Debate Reveals About Us

William B. Gail

This is a journey through how we think, individually and collectively, derived from the climate change debate. With wit and wisdom, Gail explores several questions: Can we make nature better? Could science and religion reconcile? Insights from such issues can help us better understand who we are and help

© 2014, PAPERBACK
 ISBN: 978-1-935704-74-4
 LIST \$30 MEMBER \$20

Browse online at
ametsoc.org/bookstore

FREE SHIPPING
 for AMS Members!

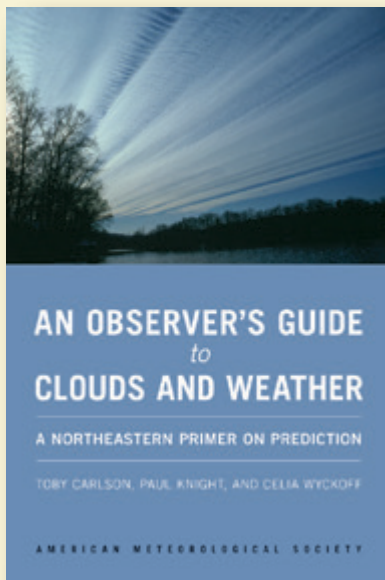
AN OBSERVER'S GUIDE TO CLOUDS AND WEATHER

A Northeast Primer on Prediction

Toby Carlson, Paul Knight, and Celia Wyckoff

With help from Penn State experts, start at the beginning and go deep. This primer for enthusiasts and new students alike will leave you with both refined observation skills and an understanding of the complex science behind the weather: the ingredients for making reliable predictions of your own.

© 2014, PAPERBACK
 ISBN: 978-1-935704-58-4
 LIST \$35 MEMBER \$20



AMS BOOKS

AMS Books are available to groups and booksellers, and desk copies may be obtained, through our distributor The University of Chicago Press: 1-800-621-2736 or custserv@press.uchicago.edu.

THE CAUSES OF FOEHN WARMING IN THE LEE OF MOUNTAINS

BY ANDREW D. ELVIDGE AND IAN A. RENFREW

A first quantitative investigation into the causes of foehn warming in the lee of mountain ranges demonstrates the importance of three physical mechanisms, including one previously neglected.

Societal and environmental impacts of the warming experienced in the lee of mountains, known as the foehn warming effect, are significant and diverse. This warming can be spectacular (e.g., 25°C in an hour; Richner and Hächler 2013) and is typically accompanied by a decrease in humidity and accelerated downslope winds. The notoriety of these foehn winds has led to recognition by various local terms: among others, the Chinook and Santa Ana of North America and the Zonda of Argentina. The warmth brought by the foehn has implications for agriculture, ecosystems, and climate systems. It can increase the risk of avalanches or floods (Barry 2008), melt glaciers, and contribute to ►

Rotor cloud revealing overturning and turbulence above the lee slopes of the Antarctic Peninsula during a foehn event (Case A in this study). Photo by A. Elvidge.

the disintegration of ice shelves (Cook et al. 2005; Kuipers Munneke et al. 2012). Foehn windstorms regularly cause damage to property and infrastructure (Whiteman and Whiteman 1974; Richner and Hächler 2013), and the combination of warm, dry air and high wind speeds promotes the ignition and rapid spread of wildfires (Westerling et al. 2004; Gedalof et al. 2005; Sharples et al. 2010). In California, Santa Ana winds are responsible for the majority of major wildfires, including 12 fires in October 2003 that burnt an area of over 300,000 ha, causing more than \$1 billion (U.S. dollars) in property damage (Westerling et al. 2004; Ahrens 2012). Accurate forecasting of foehn events is a challenge for hazard assessment and management, one that is made significantly harder by a lack of quantitative understanding of the causes of foehn warming.

PARADIGMS OF THE FOEHN. Traditionally foehn winds are defined as any “warm, dry wind descending in the lee of a mountain range” (Brinkmann 1971, p. 230; Ahrens 2012; Barry 2008). However, this definition begs two critical questions: 1) what is the foehn warm and dry relative to and 2) why is the foehn warm and dry? While such imprecision is perhaps appropriate in describing something that is an everyday occurrence for many, it also reflects the difficulty in concisely defining a phenomenon that is not fully understood. Indeed Brinkmann (1971, p. 238) challenges his own definition (above) by concluding, “Since the search for the definition of a phenomenon is, by necessity, the search for its cause, and since the true causes are still poorly understood, the question remains: what is foehn?” Recent advances have provided the tools to better understand foehn flows, and they support a Lagrangian definition as the framework for investigation (cf. WMO 1992); for example, the

foehn is a downslope wind in the lee of a mountain that is accelerated, warmed, and dried as a result of the orographic disturbance on the prevailing flow.

The first scientific accounts put forward two mechanisms for foehn warming and drying, for example, Hann (1901); also see Beran (1967), Barry (2008), and Richner and Hächler (2013). The first is the sourcing of foehn air from higher, potentially warmer and dryer altitudes upwind of the mountain barrier due to the blocking of low-level flow by the mountain. This mechanism is here termed *isentropic drawdown* and is illustrated in Fig. 1a. Note that *isentropic drawdown* is likely to be associated with the drawdown of drier air too, though there may be occasions when leeside drying does not accompany leeside warming (e.g., Gaffin 2002). Flow blocking is characteristic of a non-linear flow regime, where the speed of the approaching stably stratified flow is insufficient for ascent from low levels over the mountain (Smith 1990). The second is the more well-known “thermodynamical” foehn theory, whereby cooling during uplift on the windward slopes promotes condensation, cloud formation, and subsequently precipitation leading to moisture removal and irreversible latent heating (the *latent heating and precipitation* mechanism; Fig. 1b). Considerable orographic uplift and cloud formation are characteristic of a linear flow regime, where the approaching flow is strong enough to overcome buoyancy forces and ascend from low levels over the mountain (Smith 1990). These two mechanisms have been widely discussed in the literature (e.g., Scorer 1978; Seibert 1990; Richner and Hächler 2013). However, two other foehn mechanisms also exist: turbulent sensible heating and drying of the low-level flow via *mechanical mixing* (Fig. 1c) above rough, mountainous terrain in a stably stratified atmosphere (Scorer 1978; Ólafsson 2005) have always been dismissed as unimportant or, more commonly, simply neglected, and *radiative heating* (Fig. 1d) of the low-level lee side due to the dry, cloud-free foehn conditions (Hoinka 1985; Ólafsson 2005) tends not to have been explicitly considered as a foehn mechanism.

Interestingly, for several decades *isentropic drawdown* was all but lost as an explanation for the foehn effect as the more textbook-friendly *latent heating and precipitation* mechanism was preferred, becoming a classic example of thermodynamics changing the weather (Seibert 1990; Richner and Hächler 2013). In fact, in popular media and nonacademic scientific articles, this bias is still common. This is despite some recent case studies qualitatively indicating that latent heating is of secondary importance (Seibert 1990; Ólafsson 2005), in contrast to others that indicate the opposite (Seibert

AFFILIATIONS: ELVIDGE AND RENFREW—School of Environmental Sciences, University of East Anglia, Norwich, United Kingdom

CORRESPONDING AUTHOR: Dr. A. D. Elvidge, Atmospheric Processes and Parameterizations, Met Office, FitzRoy Road, Exeter, Devon, EX1 3PB, United Kingdom
E-mail: andy.elvidge@metoffice.gov.uk

The abstract for this article can be found in this issue, following the table of contents.

DOI:10.1175/BAMS-D-14-00194.1

In final form 24 April 2015
©2016 American Meteorological Society



This article is licensed under a [Creative Commons Attribution 4.0 license](https://creativecommons.org/licenses/by/4.0/).

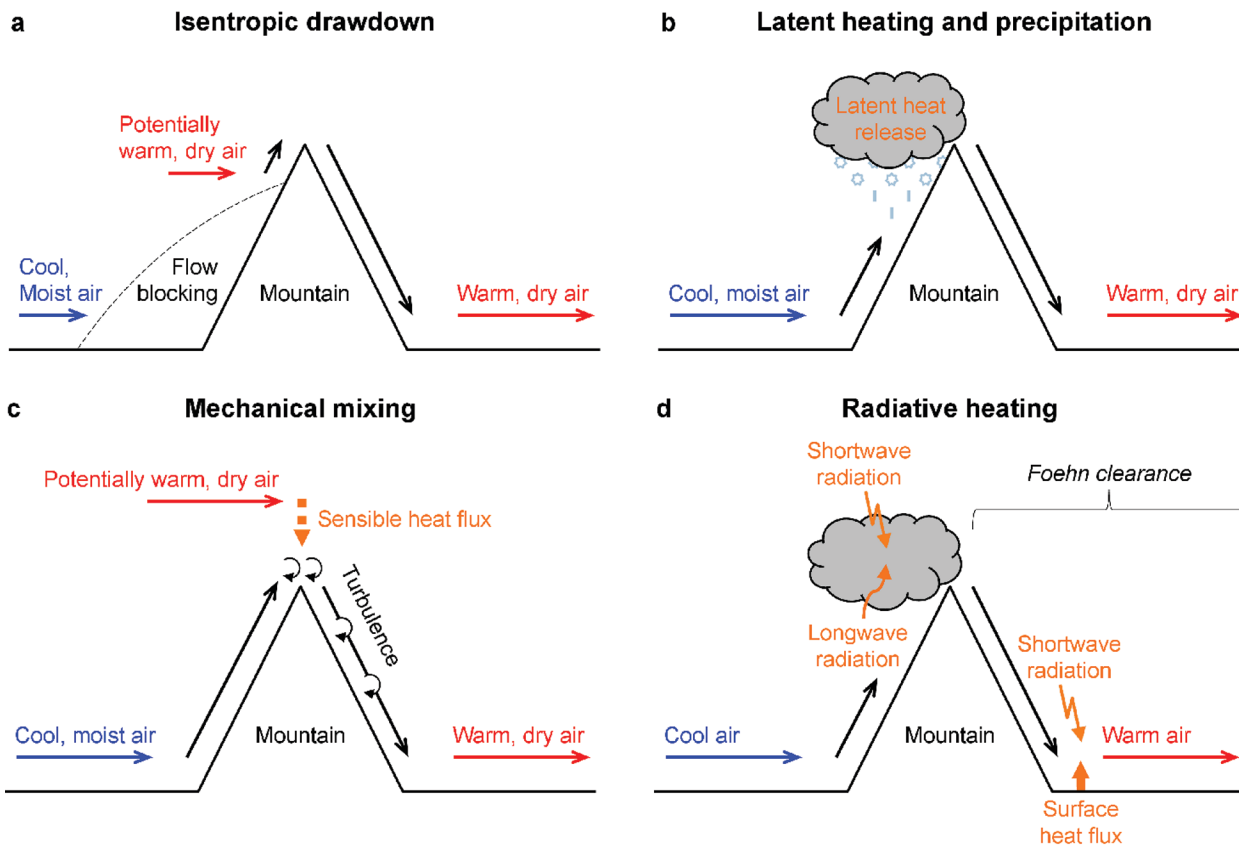


FIG. 1. Foehn warming mechanisms. (a) Upwind of the mountain, cool, moist air can be blocked allowing potentially warmer, drier air to be advected isentropically down the lee slopes. (b) Without flow blocking, there is ascent on the windward slopes so the air cools, leading to condensation and latent heat release that reduces the cooling; precipitation removes the condensed water so that descent on the lee side is dry, which increases the (pressure related) warming leading to higher leeside temperatures. (c) As cool, moist air passes over the mountain, it will mix mechanically with the overlying air mass; for a statically stable atmosphere, this is potentially warmer (and usually drier) and so corresponds to a turbulent flux of sensible heat into the foehn flow (and a turbulent flux of moisture out of it). (d) Associated with the mechanisms described in (a)–(c), there is often clear, dry air on the downwind slopes, the “foehn clearance,” and cloud on the upwind slopes; this situation encourages radiative flux convergence and thus warmer air on the lee side.

et al. 2000; Richner and Hächler 2013). Here, for the first time, we are able to quantitatively address the question “what causes foehn warming?” We employ a novel Lagrangian heat budget model that uses trajectories from high-resolution numerical model output to focus on three representative case studies.

AN IDEAL NATURAL LABORATORY. The Antarctic Peninsula provides one of the best natural laboratories in the world for the study of foehn: it presents a consistently high (up to ~2300 m), broad (~100 km), and long (~1500 km) quasi-2D barrier to the prevailing westerly flow, with homogeneous and relatively smooth upwind (maritime) and downwind (ice shelf) surface boundaries (see Fig. 2). The three foehn events examined have westerly flow across the peninsula onto the Larsen C Ice Shelf (LCIS) and

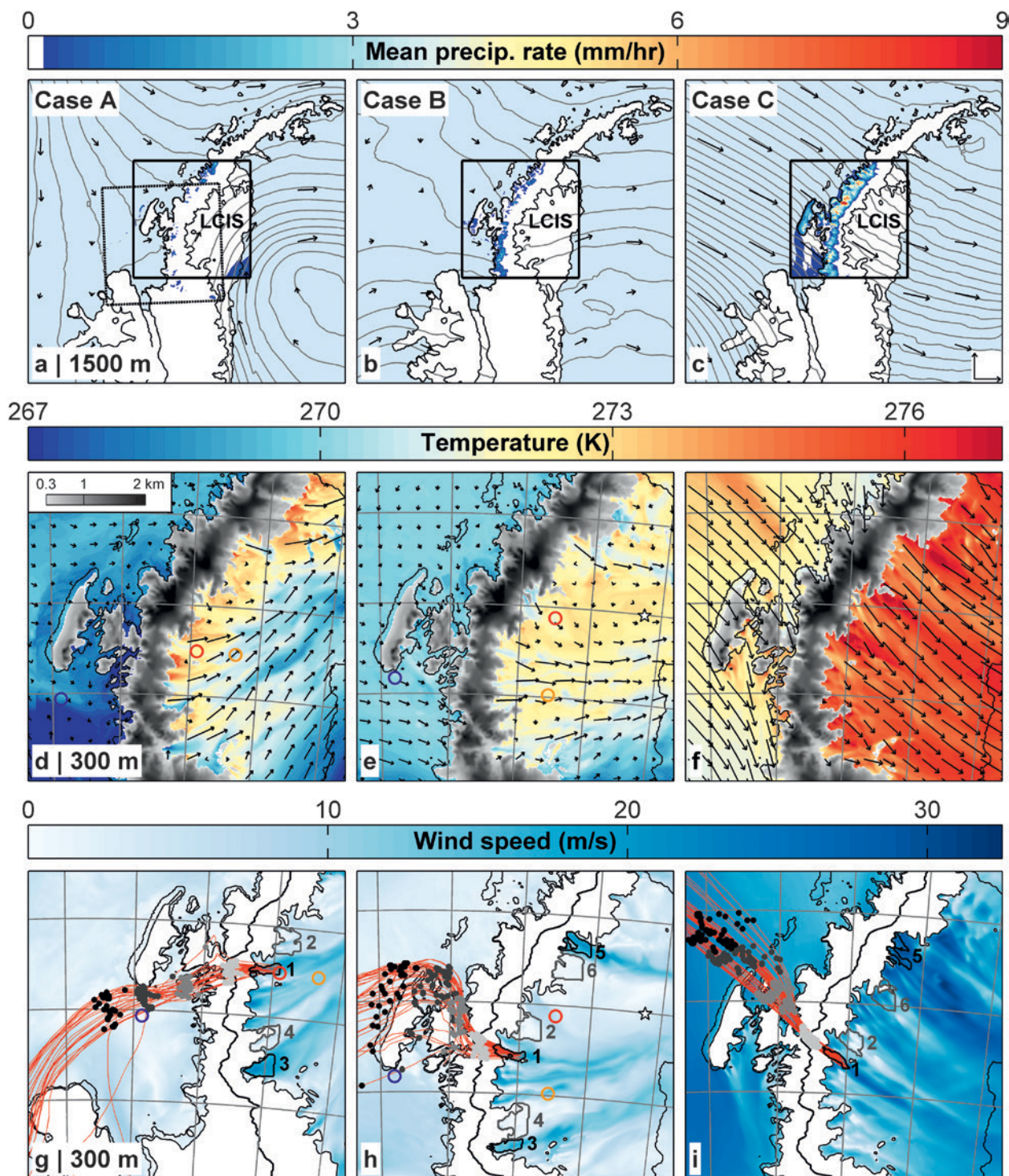
occurred during the austral summer of 2010/11. Two of them (cases A and B) are documented by aircraft observations (Elvidge et al. 2015, 2016), and all three have been simulated using the Met Office Unified Model (see sidebar on “Observations and simulations of three westerly events”).

Upwind (west) of the peninsula, cases A and B were characterized by relatively weak upwind flow, while in case C a large-scale pressure gradient drove strong northwesterly flow across the barrier (Figs. 2a–c). The weak winds of case A combined with a statically stable atmosphere and an elevated inversion (~1,250 m) to produce a strongly nonlinear flow regime (Elvidge et al. 2016), in which considerable flow blocking is associated with little orographic precipitation (Fig. 2a). Conversely, the strong winds and weaker static stability of case C lead to a relatively linear flow

regime with considerable orographic uplift and high precipitation rates (peaking at ~ 12 mm h $^{-1}$; Fig. 2c). Case B resides somewhere between the two in terms of flow regime linearity and precipitation (Fig. 2b).

At low levels above the LCIS, southwesterly to northwesterly foehn winds are apparent in all three cases (Figs. 2d–f). In contrast to climatology, conditions to the east of the peninsula are warmer

than those to the west, implying foehn warming. For case A, the warming (up to 5 K) and also drying are apparent in observations taken from aircraft profiles (Fig. 3). Here, the upwind profile used for temperature was flown 4–5 h prior to the two downwind profiles (see sidebar on “Observations and simulations of three westerly events”), roughly reflecting the time taken for air to cross the barrier. Note that



in both the observations and the model simulation leeside temperatures decrease with distance downwind of the mountains (Figs. 2d, 3a). For case B, aircraft observations again show warmer conditions on the lee side of the mountain range, indicating a foehn event. Unfortunately the profiles here are not Lagrangian; the upwind profile was flown 1–2 h after the downwind profiles.

The evolution of foehn conditions at the eastern reaches of the LCIS during case B is illustrated by a time series of atmospheric soundings in Fig. 4. On the evening of 26 February 2011, conditions are stagnant and cool over the ice shelf. Over the course of 27 February, westerly winds throughout the depth of

the lower atmosphere bring about a warming (3–4 K between 200 and 500 m) and drying, as illustrated by the downward-sloping potential temperature and specific humidity contours with time. Note that below ~200 m, a surface-forced diurnal variation is superposed on the foehn signature.

The numerical model generally performs well in its simulation of cases A and B. In Fig. 3, the model reproduces both upwind and downwind profiles of temperature and humidity to a high degree of accuracy (typically within 0.5 K and 0.2 g kg⁻¹), especially at low levels. This implies the model is able to accurately capture the warming of air parcels as they cross the peninsula. Further downwind of the

OBSERVATIONS AND SIMULATIONS OF THREE FOEHN EVENTS

Aircraft measurements were made by an instrumented De Havilland Canada Twin Otter aircraft [for details see Fiedler et al. (2010)]. Observations from two flights on 5 February 2011 (case A) and one flight on 27 January 2011 (case B) are shown in Fig 3. For Case A, aircraft data comprise upwind profiles at 1130 and 1330 UTC over Marguerite Bay (blue circle in Figs. 2d,g marks the locations) and downwind profiles at 1530 and 1600 UTC over LCIS and Whirlwind Inlet (orange and red circles in Figs. 2d,g). Note that the first upwind profile for humidity is not available owing to an instrument malfunction, so the second upwind profile is shown in Fig. 3. Case B aircraft data comprise an upwind profile at 1800 UTC over Marguerite Bay (blue circle in Figs. 2e,h) and downward profiles at 1600 and 1630 UTC over the LCIS (red and orange circles in Figs. 2e,h). Further aircraft observations are

shown in Elvidge et al. (2015, 2016). During case B, Vaisala radiosondes were launched from a camp toward the eastern reaches of the LCIS (star in Figs. 2e,h) at 1800 UTC on 26 January, and then 6 hourly between 1200 UTC on 27 January and 0600 UTC on 28 January 2011.

The Met Office Unified Model (the MetUM), version 7.6, MetUM, version 7.6, which is used for operational numerical weather prediction and climate prediction (Davies et al. 2005), has been used [configured following Elvidge et al. (2015)]. Our highest-resolution domain has a grid spacing of 1.5 km and 70 vertical levels. Such high resolution was necessary to adequately resolve the complex flow fields and large vertical velocities generated by the Antarctic Peninsula's steep and complex orography. This model and configuration has previously demonstrated considerable skill in reproducing the key features of westerly

foehn flow over the peninsula (Elvidge et al. 2015, 2016) and other strong wind events near steep orography (Orr et al. 2014). The MetUM 1.5-km simulations were initiated at 0600 UTC 4 February 2011 for case A, 1800 UTC 26 January 2011 for case B, and 0600 UTC 15 November 2010 for case C. Each was nested within a larger regional domain with 4-km grid spacing initiated 6 h earlier, which in turn was nested within a global domain with 25-km grid spacing. The majority of analysis presented is from the MetUM 1.5-km simulations. In addition to the standard 1.5-km domain, a southwest-shifted domain was used in case A, where necessary, to avoid the premature departure of back trajectories (see Fig. 2). Note each of these case A simulations was nested within the same 4-km simulation and reproduced the same major flow features (where there was an overlap), that is, comparable foehn warming, jets, and wakes.

FIG. 2. Three foehn events over the Antarctic Peninsula simulated by a high-resolution numerical weather prediction model. All plots show conditions in cases (left) A, (middle) B, and (right) C at the time of back trajectory initiation. (a)–(c) Pressure (contours every 1 hPa) and wind vectors at 1500 m MSL for the 4-km-resolution model domain; insets are mean precipitation rates for the 1.5-km resolution model domains. LCIS is marked. The scaling vectors in (c) illustrate 20 m s⁻¹ [for panels (a)–(f)]. (d)–(f) Temperature (shading) and wind vectors at 300 m MSL for the 1.5-km-resolution domain. Model topography is shaded in gray. (g)–(i) Wind speed at 300 m MSL and also the peninsula's topographic crest as a bold line for the 1.5-km-resolution domain [the southwest-shifted domain in (g)]. On the lee side, six regions are outlined, three of which (in black) correspond to inlets that experience foehn jets; the other three (in gray) correspond to wake areas to the north (N of) or south (S of) each inlet. The regions are labeled as follows: 1) Whirlwind Inlet, 2) N of Whirlwind Inlet, 3) Mobil Oil Inlet, 4) N of Mobil Oil Inlet, 5) Cabinet Inlet, and 6) S of Cabinet Inlet. Back trajectories (red lines) are plotted from WI, with the grayscale dots marking points 0, 50, 100, and 150 km upwind of the peninsula's crest along the back trajectories. Note only every fourth back trajectory is shown. Colored circles and stars are locations for Figs. 3 and 4.

peninsula, in situ changes in winds, temperature, and humidity during case B are also generally well simulated (Fig. 4). The model captures the transition between cool, moist, and stagnant conditions to warmer, drier foehn conditions with stronger, westerly winds, followed by the weakening of winds and stabilizing of temperatures and humidities on the morning of 28 February 2011. There are some shortcomings: for example, the model overestimates low-level humidities prior to the foehn event and exaggerates static stability and vertical humidity gradients throughout case B. More evidence of this model's generally high level of skill in reproducing these foehn events can be found in two recent publications: Elvidge et al. (2015) provide validation of

upwind conditions, the broad-scale foehn warming, and the structure and magnitude of foehn winds for cases A and B. Elvidge et al. (2016) provide validation of orographic gravity waves and turbulence over the mountains for case A.

In all three cases, the leeside low-level wind field is distinguished by a series of jets emanating from the mouths of major inlets on the peninsula's east coast, separated by regions of weaker flow, termed here "wakes" (Figs. 2g–i). These "foehn jets" (Elvidge et al. 2015) are characterized by higher wind speeds than upwind, the flow having been accelerated across the mountains. They are the result of gap flows (Mayr et al. 2007) through mountain passes along the peninsula's crest (Elvidge et al. 2015). The jets are generally cooler (Figs. 2d–f) and moister than adjacent wake regions because of a dampening of the foehn effect, a consequence of the lower terrain traversed by the gap flows (Elvidge et al. 2015). Back trajectories for jets emanating from Whirlwind Inlet (WI) (Figs. 2g–i) show a clustering in space that is typical of the jets and wakes and suggest a common upwind source region. It also implies that average back trajectories can be treated as representative of the foehn flow impacting that region. Note that the Lagrangian model used for calculating the back trajectories is described in the sidebar on "Lagrangian modeling." Figure 5 shows the mean back trajectory characteristics for all three cases for Whirlwind Inlet. It reveals various features in the Lagrangian evolution of a foehn air parcel: upwind ascent on approaching the peninsula, leeside descent, a net drawdown of flow and/or diabatic warming, and moisture loss across the barrier. These features are illustrative of each of the jet and wake regions and thus the foehn flow in general.

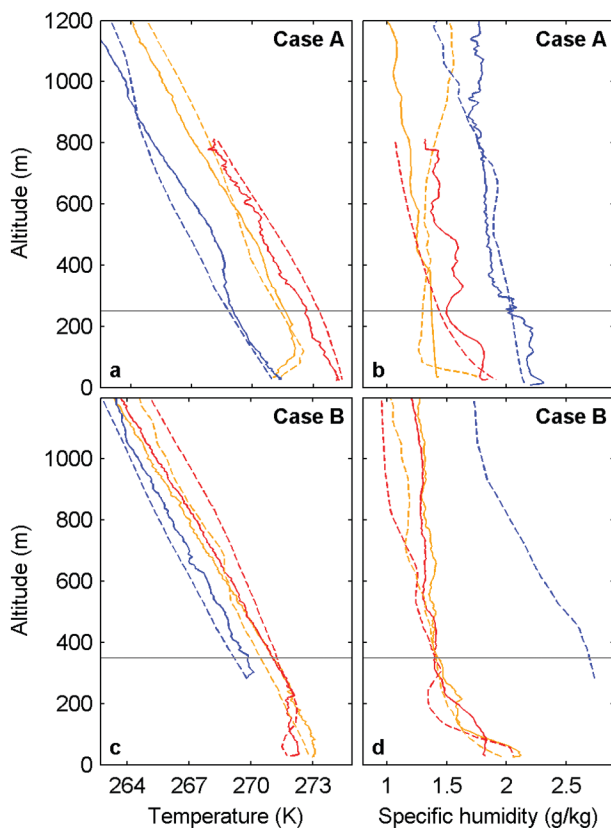


FIG. 3. Profiles of temperature and specific humidity upwind and downwind of the Antarctic Peninsula. The profiles are from instrumented aircraft observations (solid lines) and corresponding model output (dashed lines) for cases A and B. The upwind profiles (from Marguerite Bay) are plotted in blue, and the downwind profiles are plotted in red and orange. The locations of the profiles are marked in appropriate panels of Fig. 2 as circles of the same color. Note that, owing to an instrument malfunction, the observed upwind humidity profile is not available for case B. The horizontal gray lines mark the altitude of back trajectory initialization.

QUANTIFYING FOEHN WARMING. Figure 6a illustrates the key features of a novel Lagrangian heat budget model devised to quantify and attribute foehn warming contributions to particular foehn mechanisms. The model follows an air parcel from point B (upwind) to point C near the surface in the immediate lee of the peninsula where the foehn flow has the most impact and where the back trajectories are initiated. Point B is in undisturbed flow and so must be further upwind than the Rossby radius of deformation (Hunt et al. 2001), which is ~ 150 km here (Elvidge et al. 2015). Point A is below point B and at the same height as C.

The *foehn warming* is the temperature change induced by the orographic disturbance, defined as $\Delta^{FT} \approx T_C - T_A$, where T_C is the mean trajectory

temperature at C and T_A is the mean temperature at A (at the time the trajectories pass B). It is the sum of five contributions (Fig. 6a), four of which can be equated directly to the foehn mechanisms of Fig. 1. The *isentropic draw-down* contribution $\Delta^{ID}T$ is due to the sourcing of air from point B, rather than A, and so is the mean difference in θ between trajectories at B and simultaneous conditions at A. The other three mechanisms can be determined from Lagrangian air parcel changes. The *latent heating and precipitation* contribution Δ^{LHT} is due to changes in $\theta - \theta_e$, with convergence indicating latent heat gain (from condensation or freezing) and divergence indicating latent heat loss (from evaporation or melting). Changes in air parcel θ_e reflect the remaining diabatic contributions from *mechanical mixing* leading to sensible heating $\Delta^{SH}T$ and *radiative heating* $\Delta^{RH}T$. These two mechanisms can be isolated by computing $\Delta^{RH}T$ along the foehn trajectories using numerical model output. Note that $\Delta^{RH}T$ is not shown as—

together with convective contributions to $\Delta^{SH}T$ (see sidebar on “Lagrangian modeling”)—it is insignificant in our cases (contributing less than 0.1 K of leeside warming), probably as a result of the large solar zenith angles and the clear, dry air. The final contribution to the temperature budget is associated with any foehn-induced cross mountain pressure gradient Δ^{APT} . During a foehn event, a leeside low pressure anomaly is generated as a result of foehn warming and flow blocking (Gaffin 2009), which leads to a minor leeside cooling contribution.

Foehn temperature anomalies and warming contributions by each mechanism are shown in Figs. 6b–d for the three cases and six regions. Case A

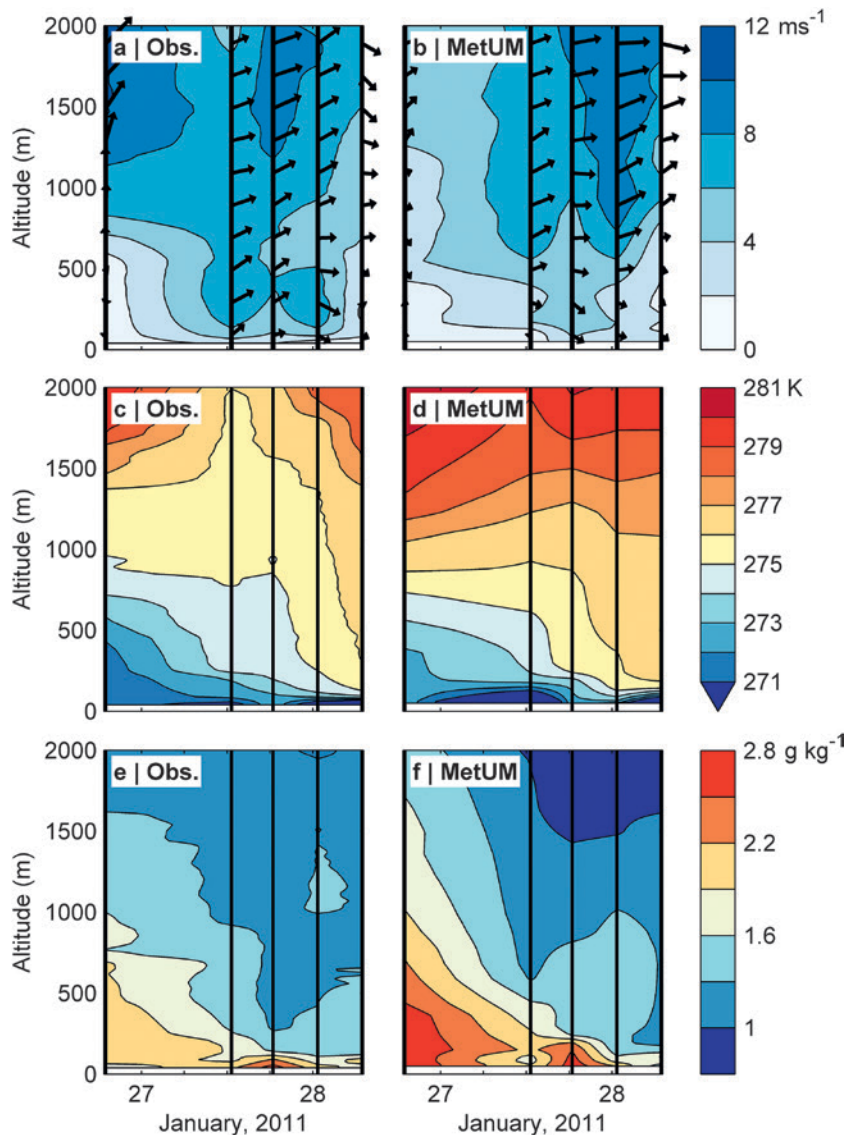


FIG. 4. Incursion and evolution of foehn conditions above the LCIS during case B. Time series of (a),(b) wind velocity, (c),(d) potential temperature, and (e),(f) specific humidity interpolated from five soundings (vertical black lines) from radiosondes released from near the eastern edge of the LCIS (star in Figs. 2e,h) and from corresponding model profiles. Vectors in (a) and (b) indicate wind speed and horizontal wind direction (e.g., a rightward-pointing arrow denotes a westerly wind).

generally exhibits the greatest leeside warming, with Δ^FT between 1.7 and 5.1 K, compared to 1.1–3.6 K in case B and 1–3.7 K in case C. The trajectory-derived temperature changes are consistent with the observed and simulated low-level near-Lagrangian warming shown in Fig. 3 (case A) and in situ warming shown in Fig. 4 (case B), albeit for a location farther east on the ice shelf. Note the foehn warming is generally greater in the wake regions than the adjacent jet regions.

In case A, *isentropic drawdown* is the dominant mechanism, consistent with having the highest

source altitude for foehn air out of the three cases (evident for WI in Figs. 5a,d,g and for all regions in Figs. 6b–d). These contributions are the largest of any of the mechanisms, peaking at 8 K south of the Cabinet Inlet (CI) wake. In case C, *latent heating and precipitation* is the dominant mechanism, consistent with having the highest upwind humidities (Figs. 5c,f,i) and greatest orographic uplift (Figs.

5a,d,g) and, as a result, the greatest precipitation rates (Figs. 2a–c) and moisture losses of the three cases. In case B, there is no single dominant mechanism. Sensible heating due to *mechanical mixing* provides the largest contribution in two of the five regions, peaking at ~2 K north of WI. This reflects greater orographic uplift (of potentially cool air over rough orography) than in case A together with less precipitation due to drier air than in case C (Figs. 5f,i). Note in case B, WI trajectories undergo sensible heating throughout their approach to the Antarctic Peninsula, perhaps owing to turbulent mixing over the rough terrain of Adelaide Island (Fig. 2h). In general, the jet regions have similar, but smaller, foehn heating contributions to the adjacent wake regions; that is, they experience a dampened foehn effect.

Taking an overview of the 15 heat budgets shown, it is clear that all three foehn warming mechanisms are important. The two established mechanisms of *isentropic drawdown* and *latent heating and precipitation* contribute the largest single warming contributions of 8 K during case A and 4 K during case C and are each the dominant mechanism in 6 out of 15 cases. *Mechanical mixing* is also important, providing over 20% of the total warming in 7 out of 15 cases and being the dominant mechanism in 3 cases. In only 5 out of 15 cases is its magnitude less than 20% of the total warming. Clearly, none of the three mechanisms can be neglected, and therefore each must be well represented for accurate simulation and prediction of foehn events. This suggests that a detailed analysis of the representation of each mechanism has the potential to pinpoint the problems that can still exist in numerical weather prediction forecasts of foehn flows (Richner and Hächler 2013).

It should be noted that *mechanical mixing* contributions will be dependent on the subgrid-scale turbulence scheme employed (Zängl et al. 2004). The model we are using [the Met Office’s Unified Model (MetUM); see sidebar on “Observations and simulations of three westerly events”] employs a nonlocal 1D turbulence scheme (Lock et al. 2000) that has been extensively tested against observations and is highly competitive in terms of its performance (e.g., Svensson et al. 2011; Boutle et al. 2014). This scheme has previously shown considerable skill in complex terrain, enabling realistic representation of temperature variability in valley cold pools, where vertical turbulent heat transport is found to dominate the heat budget (Vosper et al. 2013, Vosper et al. 2014). In this suite of experiments, those that employed the 1D turbulence scheme were found

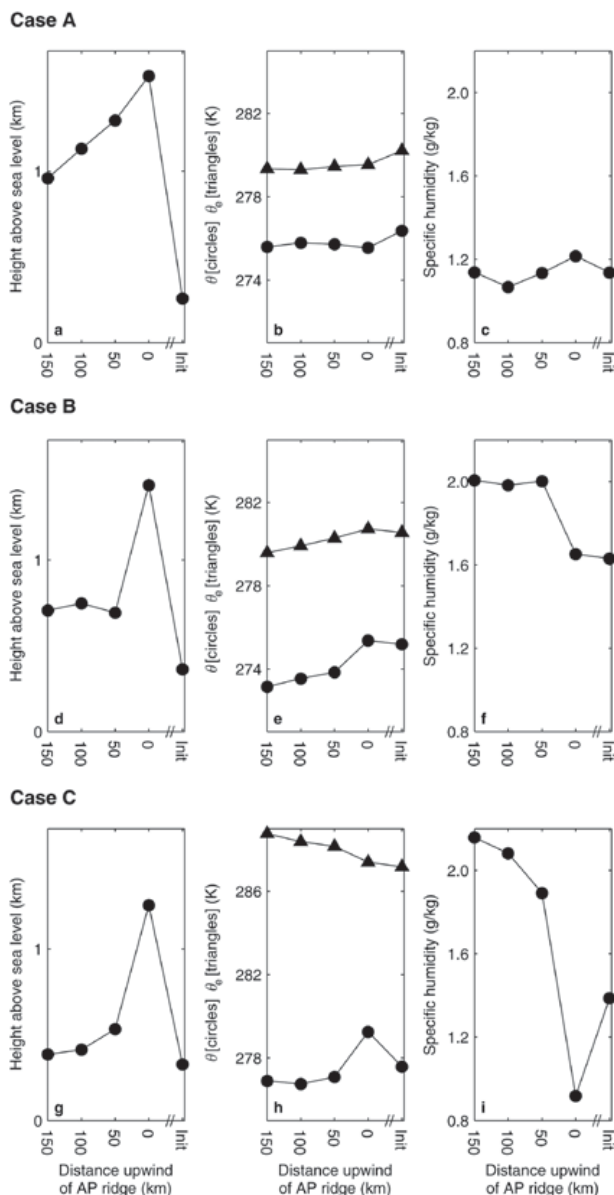
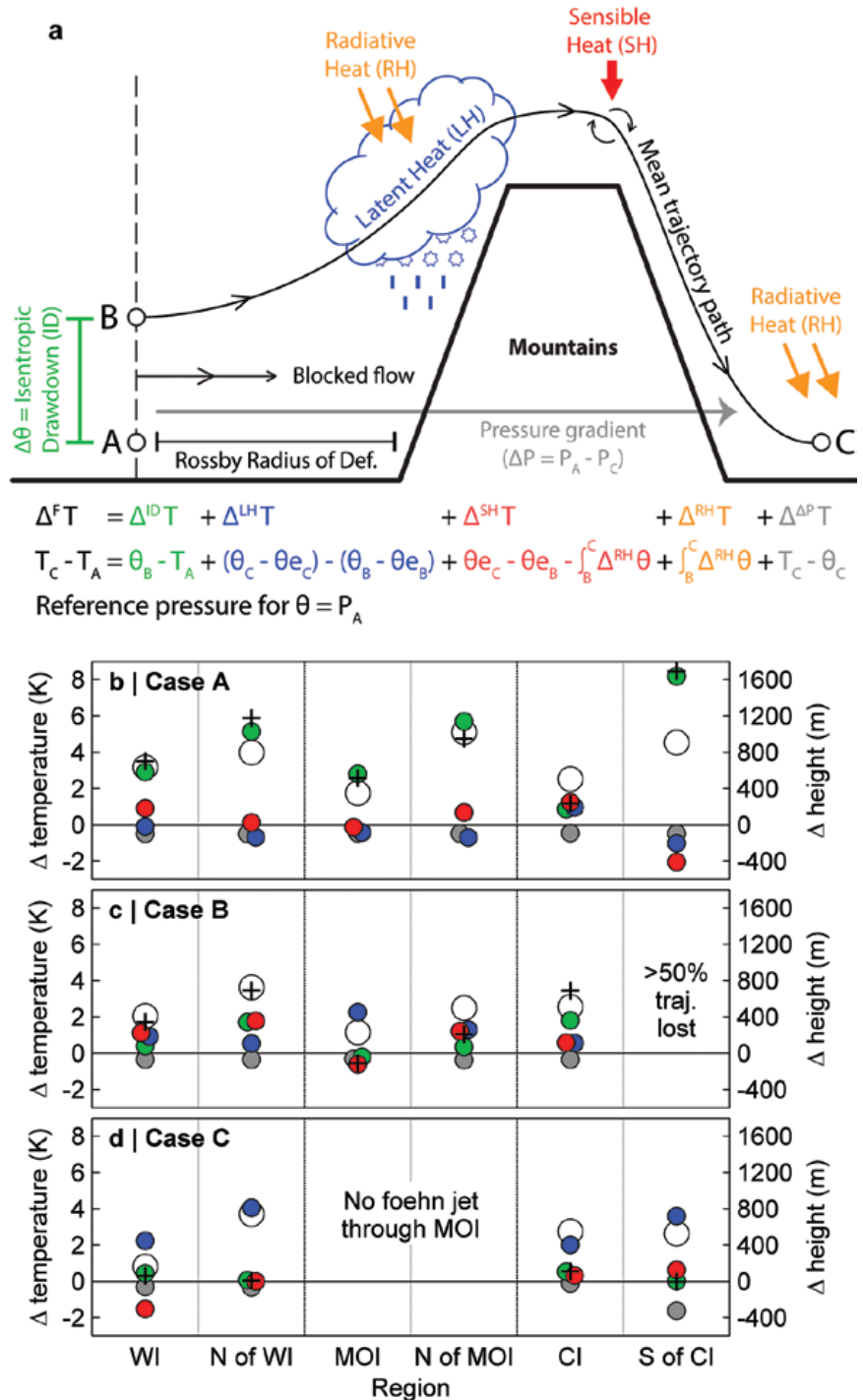


FIG. 5. Mean air parcel properties following back trajectories during foehn events. The air parcel properties shown are height above MSL, potential temperature (θ , circles), equivalent potential temperature (θ_e , triangles), and specific humidity. Mean back trajectory properties are plotted against distance upwind of the peninsula’s crest and initiated in the jet region of Whirlwind Inlet.

to yield near-identical results to those using a 3D Smagorinsky scheme (S. Vosper 2015, personal communication). The proven skill of the turbulence scheme we use, along with the model's success in simulating temperatures in the immediate lee of the peninsula (see, e.g., Fig. 3)—implying no large or systematic discrepancy in any one term—provides confidence that our new foehn warming paradigm is well founded. We acknowledge, however, that there is some uncertainty with this contribution; for example, modeled turbulent kinetic energy in foehn flows has previously been found to be underestimated (Lothon et al. 2003; Richner and Hächler

2013), implying an underestimate in the *mechanical mixing*-driven sensible heating contribution. In future work, we will examine the sensitivity of the heating contributions to the parameterization of turbulence further. An appropriate representation of turbulence in foehn flows has the potential to improve their prediction and that of related hazards, potentially mitigating adverse societal impacts (e.g., Meyers and Steenburgh 2013).

FIG. 6. Foehn heating contributions. (a) Lagrangian heat budget model for an air parcel passing over a mountain, from point B to point C, and experiencing the following foehn warming mechanisms: *isentropic drawdown* $\Delta^{ID}T$ (green), *latent heating and precipitation* Δ^{LHT} (blue), *sensible heating due to mechanical mixing* Δ^{SHT} (red), *radiative heating* Δ^{RHT} (orange), and *pressure gradient-related cooling* Δ^{APT} (gray). These contributions sum to a total foehn heating $\Delta^F T$; see text for further details. (b)–(d) The foehn heating contributions as a change in temperature (K). The total foehn warming is plotted as a large open circle (○) and the heating contributions are color coded: *isentropic drawdown* (●), *latent heating and precipitation* (●), *sensible heating through mechanical mixing* (●), and *pressure gradient cooling* (●). The *radiative heating* contribution is negligible. Also shown is the cross-peninsula descent (+). Note that the circles are sometimes offset to improve clarity. The 15 foehn flow heat budgets over three case studies and six back trajectory initiation regions (see Figs. 2g–i).



LAGRANGIAN MODELING

The trajectory model Lagranto (Wernli and Davies 1997) is employed to provide a Lagrangian analysis of the cross-peninsula flow. MetUM 1.5-km data were used as input for the calculation of back trajectories initiated at every grid point within assigned regions to the east (lee side) of the peninsula at 1000 UTC 5 February 2011 during case A, 0000 UTC 28 January 2011 during case B, and 2200 UTC 15 November 2010 during case C. These times coincide roughly with a peak in the foehn warming; other trajectory analysis, with slightly different trajectory initiation times and from the southwesterly domain, yielded similar results. Lagranto is run backward in time for up to 24 h at a resolution of 3 min; a small time step was necessary because of the high spatial resolution of the simulations. The evolution of physical variables along these Lagrangian paths is then evaluated. The trajectory initiation regions consist of three inlets subject to foehn jets, Whirlwind Inlet

(WI), Mobil Oil Inlet (MOI), and Cabinet Inlet (CI), and three wake regions, to the north of WI (N of WI) and MOI (N of MOI) and to the south of CI (S of CI) (see Fig. 2). For case A, data from the southwest-shifted domain are used as input for trajectories that were initiated within the four southernmost regions. For case B, more than 50% of the S of CI trajectories are lost owing to an unphysical intersection with the orography (Elvidge et al. 2015b; Miltenberger et al. 2013) and so an analysis of these is not possible. For case C, trajectories are not initiated within the MOI and N of MOI regions as there was little cross-peninsula flow here (as apparent in Fig. 2f), and for the CI and S of CI trajectories, distances of 50 and 100 km upwind (respectively) are used for the undisturbed flow (rather than the usual 150 km) owing to the exit of trajectories from the model domain.

The Lagrangian heat budget model used to quantify foehn warming

contributions is outlined in the main text; however, a couple of additional details are noted here. First, θ_e along the trajectories is conserved for latent heat exchange owing to condensation and evaporation (Bolton 1980) and also owing to freezing and melting. These latter phase changes are important in our case studies owing to significant cloud ice contents; virtually all precipitation above the peninsula falls as snow rather than rain. Consequently, $\Delta^{LH}T$ is the net effect on Lagrangian temperature changes owing to all latent heat processes. Second, in addition to orographically driven mechanical mixing with potentially warmer air, contributions toward $\Delta^{SH}T$ could conceivably be due to sensible heat exchange from the surface, which depends on radiatively driven changes in surface temperature. This surface-derived contribution is negligible in our cases owing to stable stratification but in general should be considered.

CONCLUSIONS. A novel heat budget model employed in an ideal natural laboratory has provided the first quantitative evaluation of the causes of foehn warming, demonstrating that either of the established foehn warming mechanisms (*isentropic drawdown* and *latent heating and precipitation*), as well as a previously neglected mechanism (*mechanical mixing* due to turbulence), can be chiefly responsible for leeside warming. This discovery suggests a new paradigm for foehn warming in the lee of mountains is required, one in which all three of these heating mechanisms are important and any can dominate. In addition, a fourth mechanism (*radiative heating*), found to be unimportant here (at most 0.1 K), cannot always be discounted and may be significant in other foehn-prone regions, for example, where radiative fluxes are greater. The importance of each mechanism depends upon the orographically forced flow dynamics and meteorological conditions and so varies from case to case. Previous assertions on the dominance of one mechanism over another must be the result of regional or case study specifics and are not general. Indeed, future work should include the application of our Lagrangian heat budget model to foehn winds elsewhere in the world and also to idealized cases to establish the general applicability of our new paradigm.

ACKNOWLEDGMENTS. The authors thank J. C. King, A. Orr, T. Lachlan-Cope, M. Joshi, and G. W. K. Moore for useful discussions and comments. We acknowledge invaluable help with the numerical modelling from M. Weeks, S. Webster, S. Vosper, S. L. Gray, and M. Sprenger. The simulations were carried out on the joint Met Office/NERC MONSooN computing system. We acknowledge the support of the British Antarctic Survey's air unit and field operations team in obtaining the aircraft observations—in particular the leadership of Tom Lachlan-Cope—as well as A. Kirchgaessner, P. Kuipers-Munnke, and J. C. King for the radiosonde data. This research was funded by NERC (NE/G014124/1) as part of the Orographic Flows and Climate over the Antarctic Peninsula (OFCAP) project.

REFERENCES

- Ahrens, C. D., 2012: *Meteorology Today: An Introduction to Weather, Climate, and the Environment*. Cengage Learning, 640 pp.
- Barry, R. G., 2008: *Mountain Weather and Climate*. 3rd ed. Cambridge University Press, 506 pp.
- Beran, D. W., 1967: Large amplitude lee waves and chinook winds. *J. Appl. Meteor.*, **6**, 865–877, doi:10.1175/1520-0450(1967)006<0865:LALWAC>2.0.CO;2.

- Bolton, D., 1980: The computation of equivalent potential temperature. *Mon. Wea. Rev.*, **108**, 1046–1053, doi:10.1175/1520-0493(1980)108<1046:TCOEPT>2.0.CO;2.
- Boutle, I. A., J. E. J. Eyre, and A. P. Lock, 2014: Seamless stratocumulus simulation across the turbulent gray zone. *Mon. Wea. Rev.*, **142**, 1655–1668, doi:10.1175/MWR-D-13-00229.1.
- Brinkmann, W. A. R., 1971: What is a foehn? *Weather*, **26**, 230–240, doi:10.1002/j.1477-8696.1971.tb04200.x.
- Cook, A. J., A. J. Fox, D. G. Vaughan, and J. G. Ferrigno, 2005: Retreating glacier fronts on the Antarctic Peninsula over the past half-century. *Science*, **308**, 541–544, doi:10.1126/science.1104235.
- Davies, T., M. J. P. Cullen, A. J. Malcolm, M. H. Mawson, A. Staniforth, A. A. White, and N. Wood, 2005: A new dynamical core for the Met Office's global and regional modelling of the atmosphere. *Quart. J. Roy. Meteor. Soc.*, **131**, 1759–1782, doi:10.1256/qj.04.101.
- Elvidge, A. D., I. A. Renfrew, J. C. King, A. Orr, and T. A. Lachlan-Cope, M. Weeks, and S. L. Gray, 2015: Foehn jets over the Larsen C Ice Shelf, Antarctica. *Quart. J. Roy. Meteor. Soc.*, **141**, 698–713, doi:10.1002/qj.2382.
- , —, —, —, —, 2016: Foehn warming distributions in nonlinear and linear flow regimes: A focus on the Antarctic Peninsula. *Quart. J. Roy. Meteor. Soc.*, doi:10.1002/qj.2489, in press.
- Fiedler, E. K., T. A. Lachlan-Cope, I. A. Renfrew, and J. C. King, 2010: Convective heat transfer over thin ice covered coastal polynyas. *J. Geophys. Res.*, **115**, C10051, doi:10.1029/2009JC005797.
- Gaffin, D. M., 2002: Unexpected warming induced by foehn winds in the lee of the Smoky Mountains. *Wea. Forecasting*, **17**, 907–915, doi:10.1175/1520-0434(2002)017<0907:UWIBFW>2.0.CO;2.
- , 2009: On high winds and foehn warming associated with mountain-wave events in the western foothills of the southern Appalachian mountains. *Wea. Forecasting*, **24**, 53–75, doi:10.1175/2008WAF2007096.1.
- Gedalof, Z., D. L. Peterson, and N. J. Mantua, 2005: Atmospheric, climatic, and ecological controls on extreme wildfire years in the northwestern United States. *Ecol. Appl.*, **15**, 154–174, doi:10.1890/03-5116.
- Hann, J., 1901: *Lehrbueh der Meteorologic*. 1st ed. Leipzig, 805 pp.
- Hoinka, K. P., 1985: What is a foehn clearance? *Bull. Amer. Meteor. Soc.*, **66**, 1123–1132, doi:10.1175/1520-0477(1985)066<1123:WIAFC>2.0.CO;2.
- Hunt, J. C. R., H. Olafsson, and P. Bougeault, 2001: Coriolis effects on orographic and mesoscale flows. *Quart. J. Roy. Meteor. Soc.*, **127**, 601–633, doi:10.1002/qj.49712757218.
- Kuipers Munneke, P., M. R. van den Broeke, J. C. King, T. Gray, and C. H. Reijmer, 2012: Near-surface climate and surface energy budget of Larsen C Ice Shelf, Antarctic Peninsula. *Cryosphere*, **6**, 353–363, doi:10.5194/tc-6-353-2012.
- Lock, A. P., A. R. Brown, M. R. Bush, G. M. Martin, and R. N. B. Smith, 2000: A new boundary layer mixing scheme. Part I: Scheme description and single-column model tests. *Mon. Wea. Rev.*, **128**, 3187–3199, doi:10.1175/1520-0493(2000)128<3187:ANBLMS>2.0.CO;2.
- Lothon, M., A. Druilhet, B. Bénéch, B. Campistron, S. Bernard, and F. Said, 2003: Experimental study of five föhn events during the Mesoscale Alpine Programme: From synoptic scale to turbulence. *Quart. J. Roy. Meteor. Soc.*, **129**, 2171–2193, doi:10.1256/qj.02.30.
- Mayr, G. J., and Coauthors, 2007: Gap flows: Results from the Mesoscale Alpine Programme. *Quart. J. Roy. Meteor. Soc.*, **133**, 881–896, doi:10.1002/qj.66.
- Meyers, M. P., and W. J. Steenburgh, 2013: Mountain weather prediction: Phenomenological challenges and forecast methodology. *Mountain Weather Research and Forecasting*, F. K. Chow, S. F. J. De Wekker, and B. J. Snyder, Eds., Springer, 1–34.
- Miltenberger, A. K., S. Pfahl, and H. Wernli, 2013: An online trajectory module (version 1.0) for the nonhydrostatic numerical weather prediction model COSMO. *Geosci. Model Dev.*, **6**, 1989–2004, doi:10.5194/gmd-6-1989-2013.
- Ólafsson, H., 2005: The heat source of the foehn. *Hrvat. Meteor. Časopis*, **40**, 542–545.
- Orr, A., T. Phillips, S. Webster, A. D. Elvidge, M. Weeks, J. S. Hosking, and J. Turner, 2014: Met Office Unified Model high-resolution simulations of a strong wind event in Antarctica. *Quart. J. Roy. Meteor. Soc.*, **140**, 2287–2297, doi:10.1002/qj.2296.
- Richner, H., and P. Hächler, 2013: Understanding and forecasting Alpine foehn. *Mountain Weather Research and Forecasting: Recent Progress and Current Challenges*, F. K. Chow, S. F. J. De Wekker, and B. J. Snyder, Eds., Springer, 219–260.
- Scorer, R. S., 1978: *Environmental Aerodynamics*. Vol. 815. Ellis Horwood, 488 pp.
- Seibert, P., 1990: South foehn studies since the ALPEX experiment. *Meteor. Atmos. Phys.*, **43**, 91–103, doi:10.1007/BF01028112.
- , H. Feldmann, B. Neininger, M. Bäuml, and T. Trickl, 2000: South foehn and ozone in the eastern Alps—Case study and climatological

- aspects. *Atmos. Environ.*, **34**, 1379–1394, doi:10.1016/S1352-2310(99)00439-2.
- Sharples, J. J., G. A. Mills, R. H. D. McRae, and R. O. Weber, 2010: Foehn-like winds and elevated fire danger conditions in southeastern Australia. *J. Appl. Meteor. Climatol.*, **49**, 1067–1095, doi:10.1175/2010JAMC2219.1.
- Smith, R. B., 1990: Why can't stably stratified air rise over high ground? *Atmospheric Processes over Complex Terrain, Meteor. Monogr.*, No. 45, Amer. Meteor. Soc., 105–107.
- Svensson, G., and Coauthors, 2011: Evaluation of the diurnal cycle in the atmospheric boundary layer over land as represented by a variety of single-column models: The second GABLS experiment. *Bound.-Layer Meteor.*, **140**, 177–206, doi:10.1007/s10546-011-9611-7.
- Vosper, S., E. Carter, H. Lean, A. Lock, P. Clark, and S. Webster, 2013: High resolution modelling of valley cold pools. *Atmos. Sci. Lett.*, **14**, 193–199, doi:10.1002/asl2.439.
- , J. K. Hughes, A. P. Lock, P. F. Sheridan, A. N. Ross, B. Jemmett-Smith, and A. R. Brown, 2014: Cold-pool formation in a narrow valley. *Quart. J. Roy. Meteor. Soc.*, **140**, 699–714, doi:10.1002/qj.2160.
- Wernli, B., and H. C. Davies, 1997: A Lagrangian-based analysis of extratropical cyclones. I: The method and some applications. *Quart. J. Roy. Meteor. Soc.*, **123**, 467–489, doi:10.1002/qj.49712353811.
- Westerling, A. L., D. R. Cayan, T. J. Brown, B. L. Hall, and L. G. Riddle, 2004: Climate, Santa Ana winds and autumn wildfires in southern California. *Eos, Trans. Amer. Geophys. Union*, **85**, 289–296, doi:10.1029/2004EO310001.
- Whiteman, C. D., and J. G. Whiteman, 1974: A historical climatology of damaging downslope windstorms at Boulder, Colorado. NOAA Tech. Rep. ERL 336-APCL 35, 62 pp.
- World Meteorological Organization, 1992: *International Meteorological Vocabulary*. Vol. 182. World Meteorological Organization, 784 pp.
- Zängl, G., B. Chimani, and C. Häberli, 2004: Numerical simulations of the föhn in the Rhine Valley on 24 October 1999 (MAP IOP 10). *Mon. Wea. Rev.*, **132**, 368–389, doi:10.1175/1520-0493(2004)132<0368: NSOTFI>2.0.CO;2.

CLIMATE CHANGE/POLICY

“This book is timely because global climate change policy is a mess.... Drawing on concrete examples and a broad range of social science theory, this book convincingly makes the case for a social learning approach to both adaptation and emissions mitigation.”

— Steve Rayner, James Martin Professor of Science and Civilization, University of Oxford

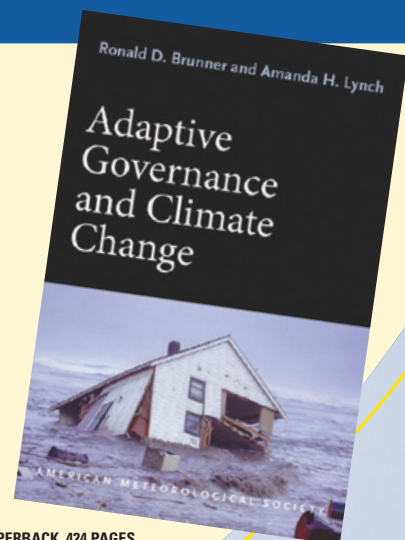
Adaptive Governance and Climate Change

RONALD D. BRUNNER AND AMANDA H. LYNCH

As greenhouse gas emissions and temperatures at the poles continue to rise, so do damages from extreme weather events affecting countless lives. Meanwhile, ambitious international efforts to cut emissions have proved to be politically ineffective or infeasible. There is hope, however, in adaptive governance—an approach that has succeeded in some communities and can be undertaken by others around the globe.

In this book:

- A political and historical analysis of climate change policy
- How adaptive governance works on the ground
- Why local, bottom-up approaches should complement global-scale negotiations



© 2010, PAPERBACK, 424 PAGES

ISBN: 978-1-878220-97-4

AMS CODE: AGCC

LIST \$35 MEMBER \$22

AMS BOOKS

RESEARCH APPLICATIONS HISTORY

www.ametsoc.org/amsbookstore

Radar and Atmospheric Science: A Collection of Essays in Honor of David Atlas

Edited by Roger M. Wakimoto and Ramesh Srivastava



This monograph pays tribute to one of the leading scientists in meteorology, Dr. David Atlas. In addition to profiling the life and work of the acknowledged “Father of Radar Meteorology,” this collection highlights many of the unique contributions he made to the understanding of the forcing and organization of convective systems, observation and modeling of atmospheric turbulence and waves, and cloud microphysical properties, among many other topics. It is hoped that this text will inspire the next generation of radar meteorologists, provide an excellent resource for scientists and educators, and serve as a historical record of the gathering of scholarly contributions honoring one of the most important meteorologists of our time.

Radar and Atmospheric Science: A Collection of Essays in Honor of David Atlas

Aug 2003. Meteorological Monograph Series, Vol. 30, No. 52;
270 pp, hardbound; ISBN 1-878220-57-8; AMS code MM52.

Price \$75.00 list/\$55.00 member

To place an order point your Web browser to
www.ametsoc.org/amsbookstore

AMS BOOKS

RESEARCH APPLICATIONS HISTORY

RADAR AND ATMOSPHERIC SCIENCE:
A COLLECTION OF ESSAYS IN HONOR OF
DAVID ATLAS



Edited by

Roger M. Wakimoto
Ramesh C. Srivastava

Published by the American Meteorological Society

AMS BOOKS

RESEARCH

APPLICATIONS

HISTORY

AMS MEMBERS GET FREE

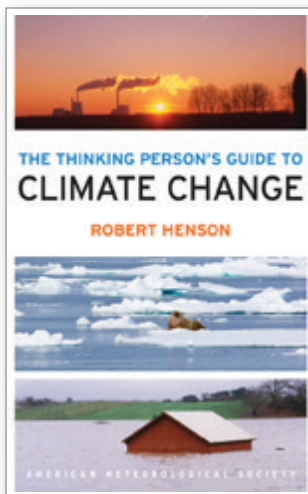
CLIMATE

The Thinking Person's Guide to Climate Change

ROBERT HENSON

This fully updated and expanded revision of *The Rough Guide to Climate Change* combines years of data with recent research. It is the most comprehensive overview of climate science, acknowledging controversies but standing strong in its stance that the climate is changing—and something needs to be done.

© 2014, PAPERBACK, 520 PAGES,
ISBN: 978-1-935704-73-7
LIST \$30 MEMBER \$20

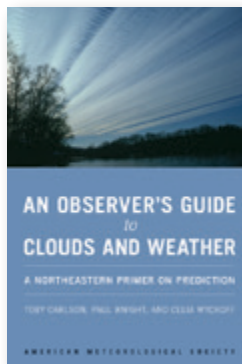


GUIDES

An Observer's Guide to Clouds and Weather:

A Northeastern Primer on Prediction

TOBY CARLSON, PAUL KNIGHT,
AND CELIA WYCKOFF



With help from Penn State experts, start at the beginning and go deep. This primer, intended for both serious enthusiasts and new meteorology students, will leave you with both refined observation skills and an understanding of the complex science behind the weather: the ingredients for making reliable predictions of your own. It connects fundamental meteorological concepts with the processes that shape

weather patterns, and will make an expert of any dedicated reader.

© 2014, PAPERBACK, 210 PAGES,
ISBN: 978-1-935704-58-4 LIST \$30 MEMBER \$20

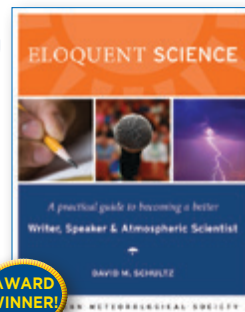
Eloquent Science: A Practical Guide to Becoming a Better Writer, Speaker, and Atmospheric Scientist

DAVID M. SCHULTZ

The ultimate communications manual for undergraduate and graduate students as well as researchers in the atmospheric sciences and their intersecting disciplines.

© 2009, PAPERBACK, 440 PAGES,
ISBN 978-1-878220-91-2

LIST \$45 MEMBER \$30

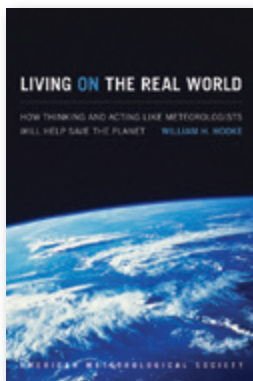


Climate Conundrums: What the Climate Debate Reveals about Us

WILLIAM B. GAIL

This is a journey through how we think, individually and collectively, about humanity's relationship with nature, and more. Can we make nature better? Could science and religion reconcile? Gail's insights on such issues help us better understand who we are and find a way forward.

© 2014, PAPERBACK, 240 PAGES,
ISBN: 978-1-935704-74-4 LIST \$30 MEMBER \$20



Living on the Real World: How Thinking and Acting Like Meteorologists Will Help Save the Planet

WILLIAM H. HOOKE

Meteorologists focus on small bits of information while using frequent collaboration to make decisions. With climate change a reality, William H. Hooke suggests we look to the way meteorologists operate as a model for how we can solve the 21st century's most urgent environmental problems.

© 2014, PAPERBACK, 272 PAGES, ISBN 978-1-935704-56-0 LIST \$30 MEMBER \$22

TEXTBOOK

Midlatitude Synoptic Meteorology: Dynamics, Analysis, and Forecasting

GARY LACKMANN

This textbook links theoretical concepts to modern technology, facilitating meaningful application of concepts, theories, and techniques using real data.

©2011, PAPERBACK, 360 PAGES,
ISBN 978-1-878220-10-3

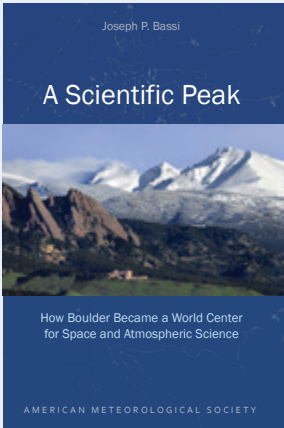
LIST \$100 MEMBER \$75 STUDENT MEMB. \$65



Midlatitude Synoptic Meteorology Teaching CD
More than 1,000 PowerPoint Slides.

© 2013, CD, ISBN 978-1-878220-27-1 LIST \$100 MEMBER \$75

To order: bookstore.ametsoc.org, 617-226-3998, or use the order form in this magazine



A Scientific Peak:
How Boulder Became a World Center for Space and Atmospheric Science

JOSEPH P. BASSI

How did big science come to Boulder, Colorado? Joe Bassi introduces us to the characters, including Harvard sun-Earth researcher Walter Orr Roberts, and the unexpected brew of politics, passion, and sheer luck that during the Cold War era transformed this "Scientific Siberia" to home of NCAR and NOAA.

© 2015, PAPERBACK, 264 PAGES, ISBN: 978-1-935704-85-0

LIST PRICE: \$35.00 MEMBER PRICE: \$25.00

HISTORY



Taken by Storm, 1938:
A Social and Meteorological History of the Great New England Hurricane
LOURDES B. AVILÉS

The science behind the 1938 Hurricane, which hit New England unannounced, is presented here for the first time along with new data that sheds light on the motivations of the Weather Bureau forecasters. This compelling history successfully weaves science, historical accounts, and social analyses to create a comprehensive picture of the most powerful and devastating hurricane to hit New England to date.

© 2013, HARDCOVER, 288 PAGES, ISBN: 978-1-878220-37-0

LIST \$40 MEMBER \$30

METEOROLOGICAL MONOGRAPH SERIES

AMS Meteorological Monographs Vols. 1-55 (1947-2010) are available via Springer at springer.com/ams, with select volumes available in print via AMS at bookstore.ametsoc.org. Starting in 2016 with Vol. 56, new monographs will be open access, available via the AMS Journals Online site.



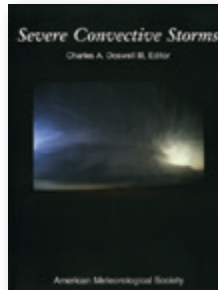
Synoptic-Dynamic Meteorology and Weather Analysis and Forecasting: A Tribute to Fred Sanders

EDITED BY LANCE F. BOSART AND HOWARD B. BLUESTEIN



Northeast Snowstorms (Volume I: Overview, Volume II: The Cases)

PAUL J. KOCIN AND LOUIS W. UCCELLINI



Severe Convective Storms

EDITED BY CHARLES A. DOSWELL III

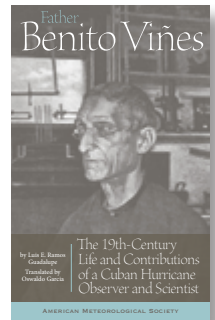
Father Benito Viñes: The 19th-Century Life and Contributions of a Cuban Hurricane Observer and Scientist

LUIS E. RAMOS GUADALUPE
TRANSLATED BY OSWALDO GARCIA

Before Doppler radar and weather broadcasts, Spanish Jesuit Benito Viñes (1837-1893) spent decades observing the skies at Belen Observatory in colonial Cuba. Nicknamed "the Hurricane Priest," Viñes taught the public about the weather and developed the first network of weather observation stations in the Caribbean, groundwork for the hurricane warning systems we use today.

© 2014, PAPERBACK, 172 PAGES

ISBN: 978-1-935704-62-1 LIST \$20 MEMBER \$16



Hurricane Pioneer: Memoirs of Bob Simpson

ROBERT H. SIMPSON AND NEAL DORST



In 1951, Bob Simpson rode a plane into a hurricane—just one of the many pioneering exploits you'll find in these memoirs. Bob and his wife Joanne are meteorological icons: Bob was the first director of the National Hurricane Research Project and a director of the National Hurricane Center. He helped to create the Saffir-Simpson Hurricane Scale; the public knows well his Categories 1-5. Proceeds from this book help support the AMS's K. Vic Ooyama Scholarship Fund.

© 2015, PAPERBACK, 156 PAGES

ISBN: 978-1-935704-75-1 LIST \$25 MEMBER \$20



Booksellers, groups, or for examination copies:

The University of Chicago Press:
1-800-621-2736 (US & Canada)
773-702-7000 (all others)
custserv@press.uchicago.edu



AMS MEMBERS GIVE A GREAT GIFT AT A GREAT PRICE

Looking for the perfect present for the weather enthusiast in your life? Want to make a valuable contribution to your local library or community college? Send a subscription to *Weatherwise* magazine (calendar year) for just \$24.95*—That's nearly 50% off the list price!

Written for a general audience, *Weatherwise* offers a colorful and nontechnical look at recent discoveries in meteorology and climatology. Check out the latest table of contents at www.weatherwise.org.

Want your own? Then order a personal subscription at the same great price.



Contact Member Services by e-mail at amsmem@ametsoc.org or by phone at 617-227-2425 to place all of your *Weatherwise* orders today!

*Cost for delivery outside of the U.S. is \$40.95. *Weatherwise* is available to AMS Members through a cooperative agreement with Taylor & Francis Group LLC, the publishers of *Weatherwise*.

45 BEACON

LETTER FROM HEADQUARTERS

You Can Propose a Session for the Next Annual Meeting

At the recent 96th AMS Annual Meeting in New Orleans, I heard several people suggest that AMS should allow individuals to propose sessions for the meeting. The comments supported the notion of a “bottom up” approach to creating the program rather than what some view as the “top down” structure provided by the STAC committees that organize the various conferences that make up the Annual Meeting.

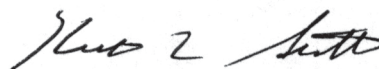
The opportunity to propose and lead sessions at the Annual Meeting has been available for years, but perhaps not in the way some were looking for or expecting, and that option has probably not been promoted as much as it could have been. Since the AMS Annual Meeting is organized as a collection of conferences and symposia—rather than a much larger collection of individual sessions—the calls to propose sessions have been part of the calls for papers within those conferences and symposia. Thus, someone interested in organizing a session on a specific topic is encouraged to consider having that session as part of one of the existing conferences or symposia already in place for the meeting. This is usually possible given the wide array of topics and subdisciplines covered by the various conferences and symposia, and doing so makes it more likely that attendees who are focusing on a specific area of interest will be made aware of the session. (In a sense, one can think of each conference or symposia as representing a “track” within the larger meeting. Thus, a session organized on some aspect of hydrology, for example, logically falls into the “track” represented by the Hydrology Conference.)

It is possible to create a stand-alone session or a new special symposium to host sessions that do not logically fit within an existing conference or symposium. Examples of that from the most recent Annual Meeting were the special sessions on U.S.-International Partnerships or the Special Symposium

on Hurricane Katrina. In some cases, there are symposia that began as a special session but grew to become a symposium series due to interest and demand in that topic area. The Symposium on the Prediction of the Madden-Julian Oscillation, the fourth of which occurred this past January, is one example of several.

If you are interested in proposing a session for the next Annual Meeting (in Seattle, next January 22–26), it is very straightforward to do so. The Annual Meeting section of the AMS website provides the list of conferences and symposia currently planned for the meeting. The call for papers of each includes information on how to propose a session. For topics that do not fit under an existing conference or symposium, proposals can be made to the Annual Meeting Program Committee as well as to the Annual Meeting Oversight Committee, two groups of volunteers who provide overall guidance on the meeting. You can contact AMS Director of Meetings Claudia Gorski (cgorski@ametsoc.org) for more information. In all cases, the proposal should be made by May 2 so that, if approved, the session can be incorporated into the planning for the meeting.

Sessions proposed by members who are not serving on the relevant STAC committees have been an important part of the AMS Annual Meeting for years. I hope that broader recognition of this option will lead to even broader session topics at AMS meetings in coming years and engagement with a larger cross-section of the AMS community.



KEITH L. SEITTER, CCM
EXECUTIVE DIRECTOR

[Editor's Note: The following post is adapted from William Hooke's blog, *Living on the Real World* (www.livingontherealworld.org). Hooke is the former director of the AMS Policy Program and currently a senior policy fellow.]

Weather Stories that Will Endure throughout 2016 and Beyond

Originally posted on January 2, 2016

Weather has figured in the news as we close out 2015 and enter 2016. For example, writing in the *Washington Post*, Darryl Fears and Angela Fritz note that:

“From the top of the world to near the bottom, freakish and unprecedented weather has sent temperatures soaring across the Arctic, whipped the United Kingdom with hurricane-force winds and spawned massive flooding in South America.

The same storm that slammed the southern United States with deadly tornadoes and swamped the Midwest, causing even greater loss of life, continued on to the Arctic. Subtropical air pulled there is now sitting over Iceland, and at what should be a deeply sub-zero North Pole, temperatures on Wednesday appeared to reach the melting point—more than 50 degrees above normal. That was warmer than Chicago. . .

. . .Thousands of miles south, in the center of Latin America, downpours fueled by the Pacific Ocean's giant El Niño pattern have drenched regions of Paraguay, Argentina, Brazil and Uruguay . . .

. . .Up and down the U.S. East Coast, this month will close as the hottest December on record. In much of the Northeast into Canada, temperatures on Christmas rose into the 70s—tricking bushes and trees into bloom in many locations . . .

. . .Almost two dozen levees along the Mississippi River are considered at risk, and forecasts are calling for record or near-record crests of the river and tributaries that feed it. Nearly 450 river-gauges have hit flood stage since Monday . . .

. . .Although river levels will begin to drop over the weekend, the floodwaters will continue to move downstream on the Mississippi through mid-January . . .”

The journalists go on to discuss conditions in Europe. They could have expanded their story to cover weather impacts in Asia, where the El Niño has contributed to record-breaking haze and air pollution, and more.

ON-AIR METEOROLOGY

10 QUESTIONS WITH . . .

A new series of profiles celebrating AMS Certified Broadcast Meteorologists and Sealholders



Samantha Mohr
WXIA 11 Alive
Atlanta, Georgia

What inspired you to go into broadcasting? Opportunity inspired me. At age 19, I was asked to audition for a local weather position while involved a community theater production of *Camelot* in my hometown of Columbus, Georgia. Luckily, I landed the role and it was at WRBL Monday through Friday at 11 p.m. It might sound strange that I'd be doing weather at age 19 on a nightly newscast, but at that time they were looking for young women to work in newsrooms.



How do you want to be remembered? That I knew how to connect with viewers and tell a really good weather story.

What's been your most difficult moment on-air? Doing a live shot in Arizona at nine-plus-months pregnant. It was in over 100-degree heat in late October! I gave birth the next day.

Such individual events capture our attention, but only briefly. They will be superseded by others as the year 2016 plays out. However, behind and towering over these episodes and those that lie ahead are several weather meta-stories, which will endure, not just for the year, but for decades to come. You might have your own additional or better list; here are four candidate examples.

AWARENESS. Fears and Fritz are justified in labeling this present weather “freakish,” but in the larger scheme of things, the world’s weather is and always has been so. No two days’ weather are ever the same, and the Earth system is continually and forever accomplishing much of its business through extremes. For millennia, in fact for millions of years, we’ve had correspondingly unusual weather. What’s new is that we’re only now able to observe and fully comprehend weather manifested in remote regions of the world as well as weather’s global connectedness. For this we owe thanks to global satellite coverage and a host of other surface-based observing technologies of unprecedented diagnostic power. We’re like the blind person who’s suddenly gained sight. We’re undergoing the greatest flowering of awareness and understanding since the mid-1800s, when the

telegraph (the Victorian Internet) first allowed us to piece together a picture of weather patterns and their movement. *Everything* is going to look exotic for the next century or so. We should enjoy this time; it’ll be a sad day when and if the novelty wears off, when we lose our capacity for wonder about the Earth system—its nature and workings, its raw power and majesty, its enchanting beauty.

Weather will continue to amaze for decades.

SENSITIVITY/VULNERABILITY. Here’s a twenty-first century irony. We’re increasingly vulnerable to weather even as our personal exposure to heat and cold, sun and rain is in decline. Most of us are in the virtual workplace of information technology, which itself is embedded in the virtual climate of the heated/air-conditioned office. Even so, we’ve been forced to acknowledge our increasing sensitivity and changing vulnerability to weather, and especially extremes and even lesser departures from so-called “normals.” The big challenge here is the emerging mismatch between (1) the time-horizon of our strategies and investments for producing food, maintaining water and energy supplies, transporting people and goods, and a weather-sensitive economy; and (2) the time-horizon on which we can anticipate the threats

Who has been your biggest role model? Karen Maginnis of CNN fame because she always shows grace under pressure.

What do you think the next “big thing” is in weather reporting? Personalized forecasts delivered by weathercasters in hologram form upon request . . . like the holograms in *Minority Report*.

What is the best thing about what you do? I most enjoy telling an interesting story that engages and enlightens.

How would you define the value of the AMS seal programs? The seal programs keep us informed and accountable.

What’s one thing people would be surprised to learn about you? I competed in my first Iron Girl Triathlon at age 50 in Lake Tahoe and competed at Miss America as Miss Georgia in 1985. I also have a website where I feature the stories of former Miss America state title holders (www.afterthecrown.com).

If you weren’t a broadcaster, what do you think you would be? An orthodontist. I am obsessed with teeth!

What music should be the soundtrack for your job? “I Love a Rainy Night” by Eddie Rabbitt followed by “Pocketfull of Sunshine” by Natasha Bedingfield.

Samantha Mohr received her AMS Television Seal of Approval in 1993. For more information on AMS Certification Programs, go to www.ametsoc.org.

weather and climate, and their associated effects on water, pose to those plans and ventures. We're in essence flying blind. We're placing bets at the poker table without looking at our own hand or those of the other players.

This is a recent development. In human experience prior to the past ten thousand years, we were nomads and hunter-gatherers. We could respond as needed to seasonal and weather shifts and their consequences for the availability of food and water. Our interdependent, increasingly urbanized world is now totally reliant on a complex critical infrastructure that is not a single system but an interwoven system of systems, whose performance under weather and climate variability is only poorly understood.

The global investments aggregate to many trillions of dollars, and they presuppose that the infrastructure will remain useful and serviceable for many decades. Weather of unanticipated severity and climate change and variability are already exposing shortcomings in the original vision. For example, investments in the infrastructure needed to extract and distribute fossil fuels look suspect in light of the need to limit global warming. Dependence of agricultural yields on irrigation and pesticides looks unsustainable as unintended consequences of these practices emerge and their associated energy demands grow. The return on investment in coastal infrastructure is threatened by the prospect of sea level rise.

We've also newly reduced our room for error and uncertainty. Even as recently as 200 years ago, most societies were rural and agricultural, and compensated for weather vulnerability by building generous margins into the system and relying on muddle-through strategies that would never be *optimal* for any given weather scenario, but would always be *adequate*. Not so today. In developed societies, this is because margin has come to be associated with waste. Examples of deliberate decisions to reduce margin are seen in electricity, where deregulation and use of regional power grids has allowed a reduction in "excess" generating capacity; in agriculture, where schedules for crop planting and harvest are worked out between farmers and buyers months in advance, and food is delivered to supermarkets only hours before consumers buy it; and in fragile transportation systems, where carrying capacity can plummet in inclement weather. In the undeveloped world, zero-margin is imposed by the richer nations—for example, encouraging farmers to grow cash crops for foreign consumption (coffee, soybeans, palm oil, even flowers . . .) versus food for domestic, in-country use.

We're going to be flying blind in all these respects for some time. Unforeseen societal sensitivity to weather and climate will be a growing news story for the remainder of this century.

NEW OPTIONS. Recent years have seen the emergence of questions such as, "Okay, your weather forecasts have improved. But how much do such improvements actually contribute to reduced property loss or improved business continuity in the face of severe weather? Given that the public often lacks options for self-protection in the face of danger, or fails to understand or respond to your warnings, how many lives do you actually save?"

Assessing the *value* of weather, water, and climate forecasts and outlooks will continue to be problematic, but one aspect of this narrative is beginning to change, and change favorably. The options for action in the face of changes in weather on all time and space scales are growing in number and effectiveness.

We have information technology to thank. It's not just that IT has vastly advanced our ability to translate our observations of what the Earth system is doing *now* to what it is *about to do next*. Today's IT allows us to provide that information to those in harm's way or those who stand to benefit from favorable windows of opportunity *in time for them to act*. That possibility has engendered a lot of creative rejiggering of every sector of society to take fullest advantage of the information. The transportation sector has long been moving in this direction. Airlines now cancel and reschedule flights based on weather forecasts, rather than allowing their fleets to be snowbound. Ocean routing has long guided ship operations. Truckers use information on road weather to schedule the deliveries and develop workarounds. Other sectors are following this lead. Electricity consumers ranging from homeowners to industrial concerns are allowing utilities to vary their electricity use to offset bumps in demand. Utilities in turn use weather information to assess the availability of wind and solar power on the grid. Retailers use weather forecasts to increase sales of everything from snowplows to umbrellas while keeping inventories low. The military uses weather, water, and climate information to assess threats ranging from Somali pirates, to terrorists, to instability created by displaced populations. In many of these applications, we are seeing growing means for computer to talk to computer directly, eliminating the middleman (or woman).

Much more creativity is coming. Each advance in weather forecasting triggers tipping points where new

real-time responses to weather become economically viable. And so-called Big Data—the increasing ability for cloud-based IT architectures to integrate multiple, diverse high-volume, high-velocity data streams to provide impact-based decision support—will add unprecedented value to tomorrow’s weather, climate, and water information.

ACCOUNTABILITY. Growing Earth-system awareness, recognition of vulnerabilities, and realization of new options will attract the attention of journalists. Increasingly, the press and the public will demand the right to life in the face of hazards (as represented by warnings and options for action) not limited to the richest in society but extending to the poorest and most disadvantaged. People worldwide will want homes that are the safest place to be during hazardous weather, not points of embarkation for evacuation. They’ll want jobs to return to after hazards have come and gone. They’ll come to expect continuity of critical services in the face of hazards, including electricity and water, but extending to

transportation and schools, health care, and more. They’ll insist that natural hazards not trigger environmental disasters.

As the press and the public realize the possibilities, they’ll demand performance, from both political and business leaders and in turn from the meteorologists, hydrologists, oceanographers, and others—whether government or private forecasters, whether scientists or broadcast meteorologists. Take the disgruntlement over the past several years about the performance of U.S. weather predictions relative to those coming from Europe; the frustration over so-called “missed” forecasts of heavy snow, when the weather patterns in question were accurately depicted but perhaps displaced by a few miles, etc. That’s just a foretaste of what’s coming.

And the legal profession may not be far behind. Likely the tempo and complexity of litigation will pick up markedly over the first half of the twenty-first century.

Weather, water, and climate. Awareness, sensitivity/vulnerability, new options, and demands for accountability.

Headline news.

ABOUT OUR MEMBERS

Bob Breck, chief meteorologist at Fox affiliate WVUE in New Orleans, retired in March, with **David Bernard** taking over the position. As Bernard transitioned to chief meteorologist, **Shelby Latino** took over for him on the FOX 8 *Morning Edition*.

Bernard joined WVUE in November and has nearly 25 years of weather forecasting experience. Before starting at WVUE, he spent nine years as chief meteorologist for WFOR Miami.

New Orleans was Bernard’s home from 1997 to 2005, when he was the morning meteorologist for CBS affiliate WWL. From 1993 to 1997, he gained experience forecasting at TV stations in the Tornado Alley region of the Texas Panhandle and Oklahoma. A native of Houston, Bernard graduated from the University of Texas at Austin and attended Mississippi State University. He is also a member of the National Weather Association and a former member of the AMS Board of Broadcast Meteorology.

Latino is a native of Southeast Louisiana who attended Mississippi State University to earn her degree

in professional meteorology. During the summer of her junior year, she had the opportunity to intern with Breck and learn his forecasting and storytelling techniques.

Meteorologist **Andrew Chung** has joined the First Warn 5 weather team in Rio Grande Valley, Texas. Originally from Miami, Andrew received his B.S. in meteorology and a minor in mathematics from Florida State University in 2000. In 2004, Andrew moved to Texas to become a meteorologist at KBTB in Beaumont/Port Arthur, where he forecasted tropical storms and hurricanes.

In 2008, Andrew left Southeast Texas to join the weather team at KVIA in El Paso. While in El Paso, he had the chance to forecast a variety of weather events like dust storms and snow. In 2010, Andrew took a weather position at KVUE in Austin, where he had the opportunity to forecast flash flooding and ice storms. After more than four years in Central Texas, Andrew returned to the Rio Grande, joining the KRGV weather team.

IN MEMORIAM

DAVID ATLAS
1924–2015

SIGMUND FRITZ
1914–2015

JOHN KNAUSS
1925–2015

JIM SLIPEC
1961–2015

66TH INTERNATIONAL SCIENCE AND ENGINEERING FAIR

Pittsburgh, Pennsylvania, May 11–15, 2015

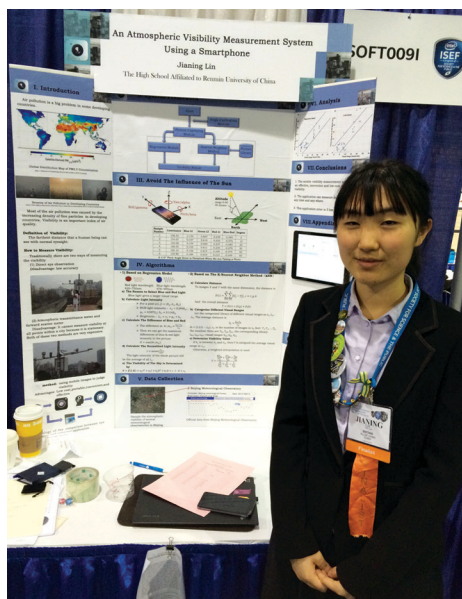
On May 14, 2015, the AMS presented awards to six high school students participating in the 66th International Science and Engineering Fair (ISEF) in Pittsburgh, Pennsylvania. These awards, ranging from \$500 to \$2,000, recognized outstanding student work in atmospheric science–related projects.

The Society for Science and the Public’s ISEF (sponsored by Intel) is the pinnacle event in a yearlong process of local, regional, state, and national science fairs. More than 1,700 students from the United States, its territories, and over 70 additional countries participated in the event held at the David E. Lawrence Convention Center.

The AMS was among 64 professional, industrial, educational, and governmental organizations providing judges to administer special awards at the ISEF. The AMS judging team included Fred McMullen and Alicia Miller of the National Weather Service Forecast Office in Pittsburgh, Pennsylvania. Charles Holliday, 16th Weather Squadron, Offutt Air Force Base, Nebraska, served as judge chairman.

The ISEF includes 20 disciplinary categories ranging from animal sciences to robotics and intelligent machines. Often, AMS award winners come from the core Earth and environmental sciences category. However, AMS judges may find atmospheric-related projects in other categories, such as mathematics, systems software, physics and astronomy, embedded systems, and engineering mechanics, as well as energy and plant science. This year’s top winner, Jianing Lin, was a competitor in the systems software category.

AMS exhibit competition this year featured research in urban heat island effects, El Niño modeling, tropical cyclone climatology, polar vortex weakening, satellite



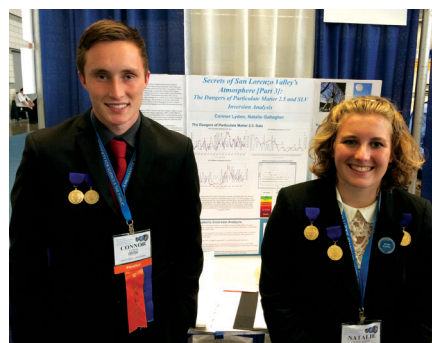
First Place: Jianing Lin, The High School Affiliated to Renmin University of China, Beijing, China: “An Atmospheric Visibility Measurement System Using Smartphone.”

analysis of volcanic ash plumes, affordable surface weather instrumentation, air quality studies, and atmospheric visibility measurements. Projects also encompassed other subjects such as sea ice variability and wind impacts on forest fire spread. Of the total individual projects at the ISEF, those related to atmospheric sciences represented almost 1% of the exhibits.

The level of sophistication in candidate projects at ISEF is quite high. The majority of the students receive guidance from professional scientists as well as use of selected datasets and facilities at federal institutions and universities. The AMS judging team must sort out how much the student participated in the design of the

experiment and in the data analysis. The final, critical steps in the judging process are the multiple student interviews, which give the individual judges the opportunity to determine the degree of each student’s knowledge, technical skill, and creative ability.

The Society awards monetary recognition to the top three winners. All winners receive certificates of achievement. In addition,



Second Place: Connor Burke Lydon and Natalie Gallagher, San Lorenzo Valley High School, Felton, California: “Secrets of San Lorenzo Valley’s Atmosphere, Part Three: The Dangers of Particulate Matter 2.5 and SLV Inversion Analysis.”

the Society provides each student with a one-year associate membership (with subscription to either the *Bulletin* or *Weatherwise*). Each student also receives an AMS Journal/*Bulletin* Archive DVD from the previous year. For widespread recognition, all ISEF participants with projects related to AMS interests receive lapel pins and reference cards.

First-Place Award: **Jianing Lin**, 16, of the High School affiliated to Renmin University of China in Beijing, China, received the AMS special award of \$2,000 for the best atmospheric exhibit at the ISEF. Her work was titled “An Atmospheric Visibility Measurement System Using Smartphone.”

Second-Place Award: The team of **Connor Burke Lydon**, 18, and **Natalie Gallagher**, 17, both of San Lorenzo Valley High School in Felton, California, garnered the AMS second-place award of \$1,000 for their exhibit, “Secrets of San Lorenzo Valley’s Atmosphere, Part Three: The Dangers of Particulate Matter 2.5 and SLV Inversion Analysis.”

Third-Place Award: The team of 17-year-olds **Pedro Otavio Liberato Rocha** and **Lucas Moraes**, both of the Federal Institute of Education, Science and Technology-Mato Grosso do Sul, in Campo Grande, Brazil, and **Eduardo da Silva Campos**, 19, of Antonietta and Leon Feffer School in São Paulo, Brazil, secured the AMS third-place award of \$500. Their project was titled

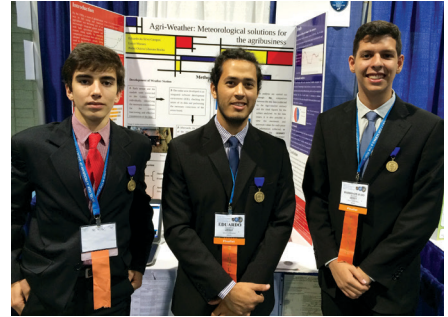
“Agri-Weather: Meteorological Solutions for the Agribusiness.”

Honorable Mention Winners: **Tsai-Ju Yu**, 18, National Lo-Tung Senior High School, Luodong Township, Yilan County, Chinese Taipei, for her exhibit “Impact of Eyjafjallajökull Volcano Eruption on Atmospheric Temperature in 2010”;

Jesse Tan Zhang, 17, Fairview High School, Boulder, Colorado, for his project, “The Effect of the Atlantic Ocean on Polar Vortex Weakening”;

and **Emma Camille Barbin**, 16, Saint Joseph’s Academy in Baton Rouge, Louisiana, for her work “The Effect of the Atlantic Multidecadal Oscillation on the Accumulated Cyclone Energy and Annual Storm Counts of Atlantic Tropical Storms and Hurricanes.”

—CHARLES HOLLIDAY



Third place: **Pedro Otavio Liberato Rocha** and **Lucas Moraes**, **Federal Institute of Education, Science and Technology-Mato Grosso do Sul, Campo Grande, Brazil**; and **Eduardo da Silva Campos**, **Antonietta and Leon Feffer School, São Paulo, Brazil**: “Agri-Weather: Meteorological Solutions for the Agribusiness.”

2015 Science Fairs

The AMS awards *Certificates of Outstanding Achievement* to student exhibitors for creative scientific endeavor in the areas of atmospheric and related oceanic and hydrologic sciences at regional and state fairs affiliated with the Intel International Science and Engineering Fair. Listed below are AMS award winners from the 2015 fairs.

ALABAMA

ALABAMA SCIENCE AND ENGINEERING FAIR

McKenna Tharpe, Stanhope Elmore High School, “Rain, Acid Rain, How Does Your Garden Grow?”
Maggie Knight, Alabama School of Fine Arts, “Correcting Ocean Acidification with Potassium Carbonate”

ARIZONA

YOUTH ENGINEERING AND SCIENCE FAIR

Heaven Murphy, Huachuca City School, “Has There Been a Significant Changing Climate

throughout My Thirteen Years in Sierra Vista, Arizona?”

ARKANSAS

CENTRAL ARKANSAS REGIONAL SCIENCE AND ENGINEERING FAIR

Matt Cole, Little Rock Central High School, “Do Sunspots Affect Hurricanes?”

NORTHWEST ARKANSAS REGIONAL SCIENCE AND ENGINEERING FAIR

Ryan Waldrop, Alma High School, “Future Forecast”

SOUTHWESTERN ENERGY ARKANSAS SCIENCE AND ENGINEERING FAIR

Matt Cole, Little Rock Central High School, "How Sunspots Affect Hurricane Intensity"

CALIFORNIA

MONTEREY COUNTY SCIENCE AND ENGINEERING FAIR

Kyle Groves, Salinas High School, "Sizzling the Atmosphere: Detecting Sudden Ionospheric Disturbances"

CONTRA COSTA SCIENCE AND ENGINEERING FAIR

Eric Zhou and Jacob Bronshteyn, Monte Vista High School, "The Effect of Adding a Plant Based Biological Filtration Compartment on the Chemical Filtration Ability of Media and Cloth Fibers"

Hannah Howard, Deer Valley High School, "The Effect of Salt Water Intrusion on Agriculture"

SANTA CRUZ COUNTY SCIENCE AND ENGINEERING FAIR

Natalie Gallagher and Connor Lydon, San Lorenzo Valley High School, "Secrets of San Lorenzo Valley's Atmosphere Part 3: A Dual Study of Atmospheric Pressure Systems and the Dangers of Particulate Matter 2.5"

Audrey Webb, Pacific Collegiate School, "Thermal Microcosm"

COLORADO

DENVER METRO REGIONAL SCIENCE AND ENGINEERING FAIR

Chereen Zahner, Cherry Creek High School, "Can Adding Water Absorbing Materials to Top Soil Help Retain Water for Plant Growth during Drought Conditions?"

Vindhya Pasupuleti, Cherry Creek High School, "Do the Environmental Factors of a Tropical Climate versus a Desert Climate Affect the Vitamin C Levels of Navel Oranges Grown There?"

LONGS PEAK SCIENCE AND ENGINEERING FAIR

Jordan Eskaw, Windsor Charter Academy Middle School, "What's in the Air up There?"

Claire McHenry, Knowledge Quest Academy, "Water Stabilization"

CONNECTICUT

CONNECTICUT SCIENCE AND ENGINEERING FAIR

Adina Katz, Southern Connecticut Hebrew Academy, "Analysis of Increased CO₂ levels in Ocean Water and Effect on Crustaceans' and Bivalves' Growth"

Hunter Kirkman, St. Rose of Lima School, "The Effect of Water Depth and Beach Surface on the Onshore Height of a Tsunami"

Ingrid Schwarz and Quennie Callanta, Hamden Middle School, "Wind Power: How the Shape of the Blade Affects the Amount of Power Produced"

DELAWARE

DELAWARE VALLEY SCIENCE FAIR

Alexa Ornstein, Marine Academy of Tech/Environmental Science, "Terrapin Nest Site Soil Assessment for the Establishment of 'Turtle Gardens'"

James Tralie, Upper Dublin High School, "Microclimates: Is More Created than Just Artificial Turf?"

Andrew Lloyd, Charter School of Wilmington, "Correlations Between Weather and Crime Rates"

Nivetha Karthikeyan, High Technology High School, "Predicting Power Outputs of Wind Turbines on Highways"

Kerri McBride, McBride Homeschool, "Investigating Metal-Oxide Laminates to Solve Wind Turbine Radar Interference: A National Security and Meteorologists' Problem"

Michelle Farina, Bishop Shanahan High School, "Cruising Crustaceans: Analysis of Triops Locomotion"

Grace Cocanower, Marine Academy of Tech/Environmental Science, "Comparing Local Drainage Basins in Barnegat Bay Watershed"

Adkash Pillai, William Allen Middle School, "The Effect of El Niño (ENSO) on Hurricanes and Storms in the Atlantic Basin"

Anna Kozielski, Alloway Township School, "Save our Sea"

Nancy Sohlberg, Cedarbrook Middle School, "How Does Rain Affect Water Contamination?"

FLORIDA

BIG SPRINGS REGIONAL SCIENCE FAIR

Kayla N. Gandy, West Port High School, "Structure Danger"

Jordan Tobar, North Marion High School, "Exposed Beaches vs. Beaches with Plants"

EAST PANHANDLE REGIONAL SCIENCE AND ENGINEERING FAIR

Camille Miles, Niceville High School, “Triple the Fun in the Sun”

INDIAN RIVER REGIONAL SCIENCE AND ENGINEERING FAIR

Rebecca Holden, Vero Beach High School, “Solar Effect on Climate Change”

LAKE REGIONAL SCIENCE AND ENGINEERING FAIR

Lauren Schneider and Katie Beason, Eustis High School, “Measuring Dissolved Oxygen and pH Levels in Freshwater”

LOCKHEED MARTIN MANATEE RSEF

Ryan Johnston, Manatee High School, “Effect of Acid Rain on Plants”

SARASOTA REGIONAL SCIENCE, ENGINEERING, AND TECHNOLOGY FAIR

Nhu Le, Sarasota High School, “Optimized Boron Infused Carbon Nanosponges on Traditional Booms for Oil Spill Clean-up”

SOUTH FLORIDA REGIONAL SCIENCE AND ENGINEERING FAIR

Olivia de Olazarra, Westminster Christian School, “The Effect of Rhizophora mangle Upon Ocean pH Levels”

Alejandro Bermudez, Rockway Middle School, “Thermal Expansion of Water as it Applies to Rising Sea Levels”

Victor Ceballos, North Miami Senior High School, “How Well Is It Buffered?”

STATE SCIENCE AND ENGINEERING FAIR OF FLORIDA

MaryAlice D. Young, San Jose Catholic Grade School, “Sunscreen SPF Effectiveness in the Presence of UVB Rays from the Sun and Artificial Light”

Charlie M. Taylor, The Villages Charter High School, “Impact of Climate Irregularities on Pinus Elliottii Ring Chronologies”

THOMAS ALVA EDISON KIWANIS SCIENCE & ENGINEERING FAIR

Jack Webb, home schooled, “The Altering of Weather Patterns to Diminish or Neutralize Tropical Cyclones”

THREE RIVERS REGIONAL SCIENCE AND ENGINEERING FAIR

Tyler Lyon, Surfside Middle School, “Solar Powered Water Heater”

Nicholas Thorpe, Merritt Brown Middle School, “Up on the Roof”

GEORGIA

ATLANTA PUBLIC SCHOOLS DISTRICT WIDE SCIENCE & ENGINEERING FAIR

Maxwell Rafferty and Amber Thomas, H. W. Grady High School, “Desalination Technology and the California Drought”

GEORGIA SCIENCE & ENGINEERING FAIR

Ally Carpenter, Chapel Hill High School, “Comprehensive Analyses of Atmospheric Data and Instrumentation”

HENRY REGIONAL SCIENCE AND ENGINEERING FAIR

Craig Worley, Luella High School, “Is There a Correlation between Hydropower Efficiency and Flap Arrangement”

ROCKDALE MAGNET SCHOOL FOR SCIENCE AND TECHNOLOGY

Tiffany Adjmul and Alliyah Hill, Rockdale Magnet School for Science and Technology, “Optimizing Removal of Crude Oil from Marine Environments”

HAWAII

HAWAII DISTRICT SCIENCE AND ENGINEERING FAIR

James Iaukea, Pahoia High and Intermediate School, “Which Way Does the Wind Blow When the Lava Flows?”

ILLINOIS

CHICAGO PUBLIC SCHOOLS CITY SCIENCE FAIR

Anaam Ahmed, Lake View High School, “Polyacrylamide for Water Conservation”

Carmelo Lattuca, Kennedy High School, “Hurricanes and Temperature”

ILLINOIS JUNIOR ACADEMY OF SCIENCE

Mia Taft, Pleasant Plains Middle School, “Hot Air Balloons”

Ben Rogers, St. Agnes School, “How Composting Waste Impacts Greenhouse Gas Emissions”

INDIANA

LAFAYETTE REGIONAL SCIENCE AND ENGINEERING FAIR

Shelly Tan, Lafayette Jefferson High School, "Nature vs Nurture: A New Mechanism for Pesticide Resistance"

Abigail Lammers, Lafayette Jefferson High School, "The Interaction of Copper and Metallothioneins in Seed Development"

NORTHEASTERN INDIANA TRI-STATE REGIONAL SCIENCE FAIR

Patel Zarna, East Noble High School, "Function of Anemometer Affected by the Size of its Blades"

NORTHERN INDIANA REGIONAL SCIENCE AND ENGINEERING FAIR

Andrea Guzman, Marian High School, "Adaptation of Dengue Virus Vectors to Environmental Stressors"

Mary Rice, Saint Matthew Cathedral School, "Hot or Cold: What is the Ideal Environment for Optimal Energy Production of a Solar Cell?"

TRI-STATE SCIENCE AND ENGINEERING FAIR

Kimber Schnarr, Jasper Middle School, "Where Will Derechos Form Next?"

Jonathan Reid, FJ Reitz High School, "Cooking Without Fire"

IOWA

EASTERN IOWA SCIENCE AND ENGINEERING FAIR

Kelsey Bryant, Central Lee High School, "The Effectiveness of Moringa Oleifera in Purification of Turbid Water Phase III"

Priya Khanolkar, Keokuk High School, "The Efficacy of Algae with the Process of Water Purification"

WESTERN IOWA SCIENCE AND ENGINEERING FAIR

Bryn Groff, Sheldon High School, "Sunlight, Sun Bright"

KENTUCKY

LOUISVILLE REGIONAL SCIENCE AND ENGINEERING FAIR

Bennett Schramko, Ballard High School, "Do Hurricanes Cool the Ocean?"

LOUISIANA

LOUISIANA SCIENCE AND ENGINEERING FAIR

Emma Barbin, St. Joseph's Academy, "The Effect of the Atlantic Multidecadal Oscillation on the Accumulated Cyclone Energy and Annual Storm Counts of Atlantic Tropical Storms and Hurricanes"

Ateshi Bhatt, Baton Rouge Magnet High School, "What Can be Done to Increase the Amount of Oil that Is Moved Through a Pump?"

MARYLAND

ANNE ARUNDEL COUNTY REGIONAL SCIENCE AND ENGINEERING FAIR

Adriana Pena, Bates Middle School, "When Air Masses Collide"

BALTIMORE SCIENCE FAIR

Zachary Byrd, Baltimore Polytechnic Institute, "Study of Droplet Impact on Superhydrophobic Surfaces"

Samuel Chan, La Salle Academy, "Droplet Experiments for Early Illness Detection"

FREDERICK COUNTY SECONDARY SCIENCE AND ENGINEERING FAIR

Brin K. Strause, Urbana Middle School, "Don't Acid Rain on My Outdoor Parade: National, Local and Habitat Studies of the Effects of Acid Rain in Outdoor Recreation Settings"

Mahnour Sultan Khan, Tuscarora High School, "Effect of Arctic Sea Ice on the Length of Winter in the USA"

MASSACHUSETTS

BCC/RENSELAER REGION III SCIENCE AND ENGINEERING FAIR

Victor F. Cai, N. Attleboro High School, "Adaptive Power Load Forecast Using Reference Day and Weather Model"

Mitchell R. Green, Foxborough Charter School, "Verbal Pool Biochemistry"

MINNESOTA

MINNESOTA REGIONAL SCIENCE AND ENGINEERING FAIR

Elaine Adams and Ella Haefner, Loyola Catholic School, "The Effect of Current Concentrations of Triclosan in Minnesota Waterways on Daphnia Magna"

Abigail Butler, Sibley East High School, “Monitoring Pollutants in the Lower Minnesota Watershed and Evaluating the Efficiency of Various Types of Buffer Zones”

Vicky Erickson, New Prauge High, “Significant Decrease Difference of Air Pollution in Five Areas with a Homemade Air Purifier”

SOUTHEASTERN MINNESOTA/WESTERN WISCONSIN REGIONAL SCIENCE AND ENGINEERING FAIR

Sean Wittenberg, Winona Senior High School, “Using Offshore Wind Turbines to Reduce Wind Speed and Storm Surge of Hurricanes”

MISSISSIPPI

MISSISSIPPI REGION VI SCIENCE & ENGINEERING FAIR

Adara Rutherford, Hancock High School, “Seasonal Variation of Water Quality in the Bay of St. Louis and the MS Sound”

Michael Forgione, home schooled, “The Effect of Microplastics on Photosynthesis in an Aquatic Plant”

MISSOURI

MASTODON FAIR

Jacob Maples, Maples Home School, “Harnessing the Power of the Wind”

SOUTHEAST MISSOURI REGIONAL SCIENCE FAIR

Megan Engelen, Immaculate Conception School, “Using Nature to Predict Winter Weather”

MONTANA

BILLINGS CLINIC SCIENCE EXPO

Alex LeSueur, Billings West High School, “Effects of Acid Rain on Seed Germination”

MONTANA REGION II SCIENCE FAIR

Bridgett Olson and Ciara Coxe, Simms High School, “Fukushima Nuclear Meltdown Effect on Montana”

MONTANA SCIENCE FAIR

Danelle Toren, Simms High School, “Temperature Lapse of the Tropopause in Montana”

NEVADA

ELKO COUNTY SCIENCE FAIR

Elizabeth Andreozzi, Elko High School, “Acid Rain and Ocean Acidification”

NEW JERSEY

MERCER SCIENCE AND ENGINEERING FAIR

Josephine Yi, Hamilton High East, “Measuring Sky Glow”

NORTH JERSEY REGIONAL SCIENCE FAIR

Greg Jacob, Bergen County Academies, “Aqua Monitoring System”

Bryant Tseng-Wei Lee Kaitlyn Ann Espiritu Kang Min Shin, Tenafly High School, “SO₂ Pollution Index by Identification of Lichen Specimens”

NEW MEXICO

CENTRAL NEW MEXICO SCIENCE AND ENGINEERING RESEARCH CHALLENGE

Lucas Gatterman, Albuquerque Institute of Math & Science, “How Does Salinity Affect Oil Spills?”

Kayla Alarcon, Rio Rancho High School, “The Relationship between the Biodiversity of the Benthic Macroinvertebrates and the Water Quality”

NEW YORK

NEW YORK STATE SCIENCE AND ENGINEERING FAIR

Anja Kenagy, Half Hollow Hills High School East, “Investigation of Pelagic Zones Demonstrates Species Specific Hg Bio-magnification”

Dominick Prudente, Oceanside High School, “The Effects of Simulated Storm Surge on Benthic Nutrient Fluxes in Mill River, a Eutrophic Tidal Creek”

UTICA COLLEGE REGIONAL SCIENCE FAIR

Ammar Arnautovic, Utica Academy of Science, “The Hidden Power of Cow Manure”

Peter Burrirt, Poland Central School, “Does Wood Really Burn?”

NORTH DAKOTA

NORTHEAST NORTH DAKOTA SCIENCE FAIR

Oliver Dalmi, Schroeder Middle School, “Rotation of the Earth”

NORTH DAKOTA STATE SCIENCE FAIR

Ryan Muggli, Grant County Junior High, “Wind Power: Is It Worth It?”

OHIO

NORTHEASTERN OHIO SCIENCE AND ENGINEERING FAIR

Norn Htaw, Roswell Kent Middle School, "Surface Temperature: A Yearly Comparison of Sites"
Mai See Lor, Roswell Kent Middle School, "Retention Phenomenon of Urban Heat Island Effect: Comparative Study between Urban and Rural Site"
Anja Koprivicia, St. Anthony of Padua Elementary, "A Local Look at Warming Up"
Lillian Heywood, Lakewood Catholic Academy, "The Solar Angle"

OKLAHOMA

CENTRAL OKLAHOMA REGIONAL SCIENCE AND ENGINEERING FAIR

Rosalinda Espinosa, Dove Science Academy, "The Moon and the Tides"
Daphne Millspaugh, Rosary Catholic School, "Relationship between Time of Night and Skyglow"

EAST CENTRAL OKLAHOMA REGIONAL SCIENCE AND ENGINEERING FAIR

Riley Morgan, Wewoka Middle School, "A Study of Moon Phases and Seafloor Geography Using Neap and Spring Tidal Range Data"
Parker Henderson, Latta High School, "Is There a Connection between Hydraulic Fracturing and the Increase of Earthquakes in Oklahoma?"

NORTHWESTERN OKLAHOMA REGIONAL SCIENCE FAIR

Cannon Carnagey and Dason Mason, Vici Public School, "Solar Angles"

OREGON

AARDVARK SCIENCE EXPOSITION

Bryan To, Oregon Episcopal School, "How the Mass or the Surface Area Affects the Melting of Ice"
Zoe Hardister, Ky Bissell, and Joanna Cloutier, Oregon Episcopal School, "Global Warming Effects on Organisms"

BEAVERTON HILLSBORO SCIENCE EXPO

Erin Tallman, Liberty High School, "The Musical Sonification of Alaskan Weather Data"
Swati Garg, Westview High School, "Effects of UV Light on Development of Antibiotic Resistance in *Seeatia Marcescens*"
Stuti Garg, Westview High School, "Serratia Marcescens Prodigiosin Under the Effects of Active Ingredients in Sunscreen and Ultraviolet Light"

Jenny Li, Southridge High School, "The Variance of Light Pollution in Relation to Distance from an Urban City Center"

CENTRAL OREGON COMMUNITY COLLEGE REGIONAL SCIENCE EXPO

Jocelynn Smith, Grant Union High School, "Effects of Temperature on Fish Growth"
Sam Anderton, Trinity Lutheran School, "Denitrification of Rivers Through Dams"

CENTRAL WESTERN OREGON SCIENCE EXPO

Kestrel Bailey, Tillamook High School, "The Feasibility of Removing Holden Creek Tidegates to Reduce Municipal Flooding in Tillamook, Oregon"

CREST JANE GOODALL SCIENCE SYMPOSIUM

Ellie Jones and Katies Jones, West Linn High School, "Mercury Levels in a Salt Marsh in North Carolina"
Angela Garrett and Olivia Klugman, Wilsonville High School, "Effects of Pollution on Macroinvertebrate Colonization in Small Northwest Streams"

PENNSYLVANIA

NORTH MUSEUM SCIENCE AND ENGINEERING FAIR

Drew Wolf, Ephrata Middle School, "Blown Away"
PITTSBURGH REGIONAL SCIENCE AND ENGINEERING FAIR

Hyun-Young Kim and Richard Kwon, Pine-Richland High School, "Harmonies of the World"
Calley Neelan, Saint Joseph High School, "Storm Water Management"
Rohun Agarwal and Elizabeth Siefert, Winchester Thurston School, "Gorlov/Tesla Hybrid Water Turbine"
Gerry Chen, Fox Chapel Area High School, "Tesla Turbine Optimization"

READING-BERKS SCIENCE AND ENGINEERING FAIR

Alexia Dunsky, Muhlenberg Middle School, "What Happened to the Ice Caps?"
Curt Mauger, Oley Valley Middle School, "Does Acid Rain Affect Aquatic Species?"

PUERTO RICO

SAN JUAN REGIONAL SCIENCE AND ENGINEERING FAIR

Sean McNally, Heights Middle School, "Catholic Protection and Water Quality 2"
Iszea Blackwater, Tibbetts Middle School, "Tornado Box"

SOUTH CAROLINA

CSRA REGIONAL SCIENCE AND ENGINEERING FAIR

Lillian Acree, Davidson Fine Arts High School, "What Are the Levels of Carcinogens and Chemicals Present in the Reid Creek Water and the August Canal Pumping Station in Comparison to EPA Guidelines?"

Lleylanna Stewart, Westside High School, "How Harmful are Local Acid Rain Levels to Plants?"

LOWCOUNTRY REGIONAL SCIENCE AND ENGINEERING FAIR

Nathan Gates and Zach McKinleym, The Georgetown School of the Arts and Sciences, "Study of the Correlation between Nekton Abundance and Biological/Meteorological Variables (1994–1998)"

Lochlyn Hejl, The Georgetown School of the Arts and Sciences, "Puddles and Pavement"

SOUTH DAKOTA

NORTHERN SOUTH DAKOTA SCIENCE AND MATHEMATICS FAIR

Dylan Schneider, Simmons Middle School, "What Type of Bat Makes The Ball Go Farther?"

Cindy Venegas-Mata, Central High School, "The Effect of Corbicula Fluminea on Nitrate and Phosphate Levels in Water"

TENNESSEE

CUMBERLAND PLATEAU REGIONAL SCIENCE AND ENGINEERING FAIR

Caleb Velker, home schooled, "Tsunami Protection"

SOUTHERN APPALACHIAN SCIENCE AND ENGINEERING FAIR

Kurt Cantrell, Pittman Center Elementary School, "The Power of pH"

Kayla Allison, Maryville Junior High School, "Infiltration Rates of Different Material Types"

TEXAS

ALAMO REGIONAL SCIENCE AND ENGINEERING FAIR

De'Everett Ross, Howell Middle School, "What Effect Does Temperature Have on the Formation of Tornadoes?"

Lia Gomez, Jay Science Academy, "A Twenty Four Hour Water Sampling of the Rio Grande"

UTAH

SALT LAKE VALLEY SCIENCE AND ENGINEERING FAIR

Anthony Cheng, Hillcrest High School, "Modeling and Analyzing Melting Arctic Sea Ice with Percolation Theory"

Hannah Bennett, Stansbury High School, "Solar Weather and Climate Change: An Investigation of Interrelationships of Coronal Mass Ejections, the Sunspot Cycle and Terrestrial Weather"

SOUTHERN UTAH SCIENCE AND ENGINEERING FAIR

Andrus Jackson, SUCCESS Dixie, "Biodiesel: The Fuel of the Future"

VIRGINIA

BLUE RIDGE HIGHLANDS REGIONAL SCIENCE FAIR

Ashley Jordan and Austin Owen, Southwest Virginia Governors' School, "The Correlation between Surface Temperature and Arctic Sea Ice Thickness"

SHENANDOAH VALLEY REGIONAL SCIENCE FAIR

Jennie Cuddeback, James Wood High School, "The Effect of Geographic Region on Weather Forecast Accuracy"

Erin Fosnacht, Shenandoah Valley Governor's School, "A Simple Formula for Predicting Radiation Fog"

WASHINGTON

MID-COLUMBIA REGIONAL SCIENCE AND ENGINEERING FAIR

Juan Casas, Sunnyside High School, "Biomimetic Sequestration of Anthropogenic Carbon Dioxide"

Mitali Kumar, West Valley Junior High School, "What Is the Effect of Seasonal Changes and Sampling Location on Stream Water Quality Tests?"

WISCONSIN

BADGER STATE SCIENCE AND ENGINEERING FAIR

Ameerah Ahmad, Divine Savior Holy Angels, "Aspen's Tolerance to Herbivory in Different Environments"

Amol Rajes, James Madison Memorial High School, "Leaf Matching Algorithms: An Exploratory Study"

UNIVERSITY OF MILWAUKEE SCIENCE AND ENGINEERING FAIR

Elanor Huffman, University School of Milwaukee, "How Varying Updrafts Affect Tornado Activity"

INTERNATIONAL

BRAZIL

FEIRA BRASILEIRA DE CIÊNCIAS E ENGENHARIA

Isabela Chahade Sibanto Simoes and Rafaela Kehdi Buazar, Escola Lourenco Castanho, “Rivers Urban Resources: A Slightly Explored Resource”

Diego Ciquini Chaves da Silva and Caue Paiva da Rocha, St. James International School, “Urban Influence in a Valley Bottom Environment through the Water Qualities Analysis”

Kevyn Danuway Oliveira Alves, Escola Estadual 11 de Agosto, “Diminution of Air Pollution through and Air Purifier Ecological”

Rebeca Rocha da Silva and Yuri Carvalho Teixeira, E.E.F.M. Jose de Borba Vasconcelos, “Chemistry and the Environment: The Use of Activated Carbon from Coconut in Improving Water Quality”

CHINA

CHINA ADOLESCENTS SCIENCE AND TECHNOLOGY INNOVATION CONTEST

Yuan Liu, Beijing No.3 Middle School, “Remote Sensing Monitoring and Environmental Impact Analysis of the Changing Area of the Glacier in the Middle Section of Tian Shan”

Yudi Wang, Beijing No. 2 Railway Middle School, “A Campus Haze Automatic Detection Cable Robot and the Haze Removal System”

Yukun Ge, Beijing Zhongguancun High School, “Preliminary Comparative Study on the Coral Reef Ecosystem’s Health Status of Luhuitou in Hainan Sanya and that of Houhai Lake”

Wangshu Liu, The Experimental High School Attached to Beijing Normal University, “A Preliminary Study on Primary and Middle School Students’ Living Environment Monitoring under Haze in Beijing and Countermeasures”

SICHUAN SCIENCE FAIR

Matthew Li, Max Pinaud, and Shua Noh, Quality Schools International: Chengdu, “Hybrid Air Purifier”

RUSSIA

RUSSIA SCIENCE FAIR

Kashapov Aleksandr, Lyceum #13, “Training Robotic Weather Station”

TAIWAN

TAIWAN INTERNATIONAL SCIENCE FAIR

Pin-Yun Lin, Zi-Rong Huang, and Wei-Shiang Huang, Changhua County; Yang Ming Junior High School, “A Study to Simply Use the Sunlight Polarization Message to Calculate the Longitude and the Latitude of the Observer’s Location”

AMS MEMBERS AND CHAPTERS

CALIFORNIA

LOS ANGELES COUNTY SCIENCE AND ENGINEERING FAIR

The Los Angeles AMS Chapter again (going on three decades) supported the LA County Science & Engineering Fair at the Pasadena Convention Center, held on March 27, 2015. Scott Moore and AMS member Steve Ladouchy, two members of the chapter, judged the best weather-related projects in the Junior and Senior divisions (middle and high schools).

After much deliberation, they decided to award the top prize (a one-year subscription to *Weatherwise* and an invitation to the chapter’s annual banquet for the students’ families) to Hoyt Dong, a tenth grader from South Pasadena High School, California. His project was “Understanding the Role of Climatic Variables on Isotopic Ratios of Rainwater.” Hoyt used $^1\text{H}/^2\text{H}$ and $^{18}\text{O}/^{16}\text{O}$ ratios to differentiate input variables on rainwater. He found that water from storms that had prolonged rainfall (rained out) had a different isotopic ratio than rainwater from shorter or recent rainfall events. Hoyt collaborated with Dr Wu of the California Institute of Technology on the project.

In the Junior Division, prize winner Stacey Bedolla, an eighth grader from St. Joseph in Long Beach, built a “Tornado Chamber” and experimented on the model design. The impressive tornado funnel used water and dry ice, a plexiglass chamber with slits, and a small motor fan on top. Honorable mention in the Junior Division went to Esmeralda Roque, a seventh grader from Luther Burbank Math, Science & Technology Magnet in Los Angeles, for her project, “Is an El Niño Event Occurring This Year?” Roque took numerous water temperature measurements in the Santa Monica Bay during the winter of 2015 and compared them with normal SSTs.

NEW YORK

NIAGARA REGIONAL SCIENCE AND ENGINEERING FAIR

Andrew Ross, president of the Western New York Chapter and AMS member, served as judge for the fair in Ontario, Canada. Certificates were awarded to Ryan Minor from St. Elizabeth School for his project, “Wind Speed of Tornadoes,” and to Hannah Robertson from Grand Ave. Elementary School for her project, “Snow Go.”

SOUTH CAROLINA

SOUTH CAROLINA REGION II SCIENCE AND ENGINEERING FAIR

A team of judges from the Palmetto Chapter consisting of Dan Miller, Doug Anderson, and Whitney Smith of the National Weather Service office in Columbia; Robert Buckley of Savannah River National Laboratory; and Greg Quina and Wes Behrend of the South Carolina Department of Health and Environmental Control, judged the meteorology and atmospheric science-related projects and selected a first- and second-place winner and an honorable mention.

The first-place prize went to Noah Adams, a fifth-grader from Harmony School in Columbia, with a project titled “Which Weather Station Should You Choose?” His project examined the accuracy of forecasted high and low temperatures by several Columbia area television stations. He stated that doing the project promoted his interest in meteorology.

The second-place prize went to, Caitlin Kunchur, a seventh-grader from Dutch Fork Middle School in Columbia, with a project titled “A Windy Day. . .” and “pull” forces on objects”, in which she observed Bernoulli’s principle by examining how wind from a fan moved an object.

An honorable mention was given to sixth-grader Brianna Hinchee of Kelly Mill Middle School near Columbia for her project, “Pacific Ocean Pollution,” in which she attempted to simulate an oceanic pollution gyre.

At the awards ceremony on March 22, 2015, the winners each received an official AMS Certificate of Achievement. The first-place winner also received *The AMS Weather Book: The Ultimate Guide to America’s Weather* by Jack Williams. The second-place winner received the *National Audubon Society Field Guide to North American Weather* by David Ludlum.

NEW! PRINT & CD FORMATS

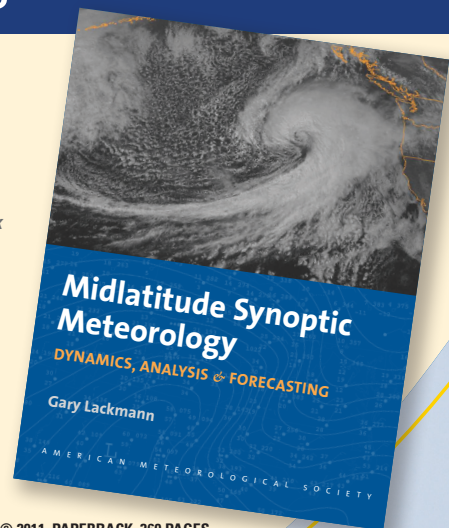
“Professor Lackmann has prepared an excellent synthesis of quintessential modern midlatitude synoptic-dynamic meteorology.”

— LANCE BOSART, Distinguished Professor, Department of Atmospheric and Environmental Sciences, The University of Albany, State University of New York

Midlatitude Synoptic Meteorology: Dynamics, Analysis, and Forecasting

GARY LACKMANN

The past decade has been characterized by remarkable advances in meteorological observation, computing techniques, and data-visualization technology. *Midlatitude Synoptic Meteorology* links theoretical concepts to modern technology and facilitates the meaningful application of concepts, theories, and techniques using real data. As such, it both serves those planning careers in meteorological research and weather prediction and provides a template for the application of modern technology in the classroom.



© 2011, PAPERBACK, 360 PAGES
 Digital edition also available
 ISBN: 978-1-878220-10-3
 AMS CODE: MSM
 LIST \$100 MEMBER \$75
 STUDENT \$65

Instructors: Midlatitude Synoptic Teaching CD, containing over 1,000 lecture slides, is now available!

AMS BOOKS

RESEARCH APPLICATIONS HISTORY

www.ametsoc.org/amsbookstore 617-226-3998

NEW MEMBERS

The Council has approved the election of the following candidates to the grade of **Full Member**:

Ori Adam	Yizhe Bu	Chad A. Dumas	Eric Jacobsen
Elizabeth Adams	Michael S. Buban	Alice DuVivier	Raymond Jefferson, Jr.
Katherine Adams	Jeremy L. Buckles	Karl H. Eggestad	Janelle Jenniges
Yakov Afanasyev	Kevin C. Burns	Daniel C. Eiblum	Reginald E. Johnson
Graeme Aggett	Brandie M. Cantrell	Chris Ellis	Matthew D. Jones
Gonzalo A. Agudelo, Jr.	Tyler W. Case	Richard M. Forbes	Paul E. Kamis
Benjamin S. Albright	Stephen G. Castleberry	Jennifer Fowler	Thomas Kane
Rafael Ameller	Stefan F. Cecelski	Carol Freeman	Boosik Kang
Bill Anderson	Hui-Ling Chang	Hatsuki Fujinami	Loryn Kasten
Brandon L. Anderson	Xingchao Chen	Peter Furze	Edward Keible
Jesse Anschutz	Xiuhong Chen	Carlos F. Gaitan	Patrick J. Kelly
Tracey Anthony	Jean-Paul Chretien	Patrick N. Gatlin	Jonathan A. Kemp
Brian Argrow	Thomas Chubb	Ali Gholizadeh Touchaei	Glenn Kerr
Kelli A. Armstrong	Edward Cokely	James S. Gilbert	LeRoy E. Klet
Jessica Arnoldy	Bob Cook	Paul W. Goree	Peter Knox
Andrew M. Badger	Chris J. Cox	Robert J. Gottlieb	Jasper F. Kok
Kevin S. Bartlett	Leo Pio D'Adderio	Christian Michael Grams	Gabriel Kooperman
Brett M. Basarab	Erin Dagg	Benjamin W. Green	Andrew C. Kren
Jonathan M. Bass	Frank J. Dale	Anna G. Hallar	James M. Kurdzo
Sean Benedict	Robert P. Dale	Amy R. Halloran	Emma L. Kuster
Jamie Beyore	Gabrielle A. Deabler	Erik Hankin	Nicholas D. Kyper
Aubry Bhattarai	Frank B. DeFina	Kirstin Harnos	Tristan S. L'Ecuyer
Thomas A. Birkland	Joseph W. DelliCarpini	Andrew Hastings-Black	Miguel Angel Labiano
Ellis Blandford	Ryan A. Dennis	Francis J. Hickey	Orli Lachmy
Bryan D. Blankenship	Tyler Dewvall	John Hickey	Yang Lang
Angela C. Bliss	Stephanie DiVito	Cameron R. Homeyer	Temple R. Lee
Rodrigo J. Bombardi	Robert K. Doe	Chris Hovanic	Mark Leifer
Christina E. Bonfanti	Dianna Dollar	Marcus Hylton	Sihan Li
Tim Bonin	Angela Q. Downing	Andrew P. Ingersoll	Christina E. Liaskos
Adam R. Brown	Hailiang Du	Brandon A. Ivey	Tanja Likso

The Executive Committee has approved the election of the following candidates to the grade of **Affiliate Member**:

Vanessa N. Foord	Mary E. Voice	Larry T. Winstone
------------------	---------------	-------------------

The Executive Committee has approved the election of the following candidates to the grade of **Associate Member**:

Surafel Abebe	Rex Horner	Gianmarc Manzione	Rachel S. Thomas-Medwid
Philip Abraham	Seth Jonas	Jinny Nathans	Matthew Tucker
Jim Chenery	Joey R. Jones	Ana Cristina Palmeira	Carter J. Tull
Brady Dennis	Steve Kagen	Prathap Ramamurthy	James Waddell
William A. Edmundson	Raphael A. Kauffman	Matthew Schwartz	Chris White
Shea Gibson	Deborah Lidl	Justin P. Stow	Joseph R. Zarba
Alex Gittens	Keitapu Maamaatuaiahutapu	Charles E. Strub	

NEW MEMBERS

Juan Lora	Rachael M. Penton	Chris Schmidt	Brian J. Vanderwende
Thomas Loridan	Oscar Peralta	Jaclyn Schmidt	Danielle C. Verdon-Kidd
Hua Lu	Natalie Perlin	Christopher J. Schultz	Tanner R. Verstegen
Donald Lucas	Aaron T. Perry	David Schwartzman	Brian J. Viner
Shaun P. Lynch	Anders Persson	Ali Shahin	Aiko Voigt
Joseph P. Markiewicz III	Michael J. Peterson	Kayvon Sharghi	Jeffrey Walker
Katherine L. McCaffrey	Katie Pitts	Xiaoming Shi	Hao Wang
Emily M. McGuire	Sally H. Potter	Shraddhanand Shukla	Mingjun Wang
Douglas B. McRoberts	Francisco Javier Quiroz	Michael Siemann	Mark E. Weber
Ryan S. Metzger	Todd A. Radenbaugh	Adam K. Simkowski	Tyler Wehr
Jennifer Meyers	Elisa Raffa	Jeffrey W. Simmons	Chris Weldon
Shiguang Miao	Shannon L. Rees	Morgan Simms	Eric Wendoloski
Leonilo C. Millanes	Jefferson J. Rhoads	Patrick S. Skinner	Keith C. White
John R. Mioduszewski	Rick Rhoton	Brianne K. Smith	Shannon White
Thomas D. Moore	Stephen Richart	Soemduth Sowdagur	Justin C. Wilkerson
Kalon W. Morris	Sarah E. Ringerud	Shobha Sriharan	Austin Winfield
Kenneth R. Morris	Britley Ritz	Kayla E. St. Germain	Andrew C. Winters
Collin Ray Myers	Kimberly J. Roberts	Derek P. Starkenburg	Rachael Witter
James Negus	Jared D. Robinson	Fulvio Stel	Samantha Wnek
Chris Nelson	Robert M. Robinson	Kial D. Stewart	Gifford J. Wong
Kevin J. Nelson	Rebecca A. Rogers	Sarah E. Stewart	Jin-Han Xie
Marta M. Nelson	Tom Rolfson	Abigail E. Stimach	Kara M. Yedinak
Jennifer Newman	Tom Rolinski	Brian R. Strahl	Janet K. Yokobata-Ando
Benjamin Noll	Kirsten Roth	Cedrick L. Stubblefield	Yueyue Yu
Stephen A. Ogden	William F. Rowland	Ryan Sullivan	Valery A. Yudin
Holly J. Oldoryd	Gregory Sadowy	Jill E. Szwed	Steven G. Zareski
Debasish PaiMazumder	Alexander Saltman	Shuaiqi Tang	Jonathan A. Zawislak
Andrea Paparelli	Hannah Sankey	Xiaodong Tang	Jianting Zhang
Gil Passwaters	Urs Schaefer-Rolffs	Kristen A. Tronvig	Seth Zuckerman
Jill Peeters			

The Executive Committee has approved the election of the following candidates to the grade of **Associate Member—K–12 Teacher**:

Debra Brice

Katherine C. F. Jones

Brian Ludwig

The Executive Committee has approved the election of the following candidates to the grade of **Associate Member—Precollege Student**:

Kiley Allen

Richard Duncan

Nathan LaLonde

Julia M. Schinik

Grant Bilderback

Connor Eshelman

Sarah B. Monte

Kyrek Charles Tommell

Jarrett T. Braden

Jacob Ettinger

Samuel Panatera

Trent N. Tougas

Daniel J. Butler

Poushali Ghosh

Harrison P. Rademacher

NEW MEMBERS

The Executive Committee has approved the election of the following candidates to the grade of **Student Member**:

Doyeon Ahn	Stuart Bivens	Samantha J. Cook	Jaime E. Firster
Juyone G. Akinmulewo	Miles C. Bliss	Rachael Coons	Kaitlynn E. Fish
Mohamed M. Al Sabri	Rachel Bobyak	Timothy D. Corrie III	Kalen Fisher
Gary A. Alexander	Isaiah Bordelon	Joshua L. Coupe	Allison A. Fitzpatrick
Katherine Alexander	Steven M. Boring	Kelsey R. Cowen	Joseph M. Fitzwater
Abdullah Ali	Hallie Boyer	Joshua K. Cozart	William Flamholtz
Michael E. Allcock	Brandon P. Brady	Ellen C. Creecy	Austen R. Flannery
Thomas D. Allison	Kathleen E. Brady	Isa M. Cruz	Samuel L. Foley
Mohammed A. Almashaykhi, Jr.	Miles Brkovich	Malekai Cullen	Steven D. Foster, Jr.
Lydia Almquist	Gabriel Bromley	Brennon Cupp	Brandon Fox
Alice Alpert	Ari H. Brown	Chastity Curry	Kimberly M. Frauhammer
Margo Anderson	Shawna J. Browning	Cheng Da	Rachel M. Frazier
Claire E. Andrew	Peyton L. Brudi	Jordan E. Darensbourg	Tyler Fricker
Margo S. Andrews	Steven Buckner	Thibaut Dauhut	Luke Friess
Frederic Anglade	Jennifer Bukowski	Cameron D. Dauterive	Keenan Fryer
Michael P. Angus	Ryan Bunker	Benjamin Davis	Rachel Gaal
Zachary Aronson	Amy K. Burnett	Thomas C. Day	Anne H. Gale
Julia Arthur	Derek Burns	Connor Dearth	Lan Gao
Jared L. Ashmore	Randi M. Burns	Gregory DeBoe	Oluwayemi A. Garuba
Sara Ates	Erica Burrows	Stacey L. Denson	Dillon Gaudet
Michael Autovino	Eric Burton	Emery Dhanens	Maxwell A. Gawryla
Emily Baalman	Ana B. Cabrera	Ying Dong	Kevin M. Gaynor
Amanda A. Babcock	Christian Campo	John M. Dopieralla	James T. Gebhardt, Jr.
Amanda Back	Dylan Card	Elizabeth M.B. Doran	Cara L. Geiger
Amarou Bah	Cody D. Carlin	Renee Dorwart	Keon L. Gibson
Mandy Bailey	Elizabeth Carlisle	Michelle A. Dovel	Zachary Gilchrist
Jordan L. Baker	Brian J. Carroll	Matthew Dross	Kyle Gill
Nicholas H. Balderas	Jacob D. Carstens	Yajuan Duan	Daniel Giltner
Justin T. Ballard	Dominic M. Cartina	Daniel DuBois	Amalia W. Gjerloev
Alek Balvanz	Armani L. Cassel	Daniel Edie	Aaron G. Glazer
James R. Barham	Douglas Catharine	Brett M. Edwards	Kate Godfrey
Brooke Barker	Sam O. Cauley	Stephanie M. Eilts	Amanda G. Goluszka
Gerardo Barreda	Victoria R. Cavaliere	Dean J. Eisenmann	Liliana Gonzalez
Daniela Barrios	Joseph E. Cebulko	Janae Elkins	Samuel L. Gould
Ryan Bartholomew	Caitlin L. Cervac	Jacob Elliott	David Grabbs, Jr.
Randy D. Bartoshevich	Hoa-Po Chang	Alexander M. Elmore	Matthew R. Green
Christopher Battisto	Kimberly Channell	Michelle Elmore	Jennifer Greenwood
Paul T. Bauer	Hans W. Chen	Haadi ElSaawy	Katelyn Griffith
Barbara Becker	Shao Wen Chen	Abraham M. Endalamaw	Adam S. Grimes
Erika C. Beddings	Xiaodong Chen	Bryan N. Engelsen	Declan Gruber
Jordan T. Benjamin	Will Cheung	Chris Ertl	Austin J. Guarniere
Joseph R. Bennett	Jason Chou	Kenyatta L. Esters	Erin K. Guidry
Rebecca R. Bennett	Jordan I. Christian	Daniel Estes	Timothy J. Gunkel
Kevin Bente	Peter G. Clark	Montana Etten-Bohm	Chandler J. Gyorke
Valerie Bernstein	Rebecca J. Clemmer	Madeline F. Evans	Janelle Hakala
Michael I. Biddinger	Andrew K. Cloninger	Christopher R. Everhart	Vanessa M. Haley
Kevin S. Biehl	Casey Cloud	James E.J. Eyre	Dolly Hall
Devin M. Biggs	Christopher D. Colacito	Mariama A. Feaster	Andrew Hamilton
Christina Billos	Andrew J. Colantoni	Edwin J. Feliu	Rawan Hammad
Erika H. Birnbaum	Michael Coleal	Deidra Fey	Danbi Han
	Sarah K. Coleman	Shireen M. Fikree	Jonathan R. Hansford

NEW MEMBERS

Cassie Happel	Kyle Jola	Tyler C. Leicht	Marissa J. McGinty
Daniel Harp	Alesha R. Jones	Sarah L. Levesque	Karess McGrath
Sarah M. Harris	Erin Jones	Michael Levine	Elin McIlhattan
David R. Harrison	Austin Jordan	Todd M. Lewis	Madeline McKenna
Jessica E. Harryman	Kailey Joyce	Xiaofei Li	Dallas M. McKinney
Theodore MI Hartman	Vance Joyner	Yi Li	John McMahan
Melinda Hatt	Sydney Jupitz	Joseph W. Lilek	Devore'a D. McMillian
Amanda Hazelton	Yuki Kanno	Yuna Lim	Chelsea R. Mealey
Sarah Heitzman	Marie Elaine M. Keim	Stephanie Lin	Jackson Mehringer
Sarah Henderson	Mitchell K. Kelleher	Jakob Lindaas	Lucy Melcher
Stephanie Hernandez	Mary C. Kelley	Jie Liu	Lilliana Mendoza
Harold J. Hersback	Maura A. Kelly	Matthew Livingston	Andrea Meyer
Tara Hersey	Kyle R. Kenney	Meagan T. Longenbaugh	Scott Meyer
Casey Hilgenbrink	Jessica Keune	Erica C. Lopez	Bradley J. Michel
Melvin J. Hill, Jr.	Jamal J. Keyes	Amy E. Lovely	Natalie Midzak
James Hlywiak	Brittany Keys	Patrick Luce	Haylie N. Mikulak
Hung Chak Ho	Benjamin M. Kiel	Casey Luddy	Douglas E. Miller
Dial Hoang	Heather Kimball	Samuel Luthi	Kerry N. Mindiak
Sabrina M. Hodge	Austin T. King	Nicholas D. Lybarger	Shapour S. Mirzadeh, Jr.
Noni A. Hodges-Flakes	Mark E. Kleinwechter	Chen-Geng Ma	Sarah E. Mitchell
Connor S. Hoelscher	Rudolf Klucik	Raya Maday	Sarah Mitman
Allison Hogikyan	Kyle A. Knight	Chloe E. Magee	Kaitlyn K. Moffett
John R. Holloway	Lydia Knox	Alexa Maines	Ivana M. Molina
Chaopeng Hong	Mary G. Knutson	Aurel Malapani	Griffin S. Mooers
Andrea N. Honor	Drew W. Koeritzer	Samantha Malcom	Cody R. Moore
Ben F. House III	Kathrine M. Koncel	Garima Malhotra	Sergio A. Mora
Vanessa Hower	Corinne J. Konoza	Danielle Mallon	Anjelica Moreno
CareyAnne Howlett	Tsambika M. Kostas	Mikayla Malone	Nick Morgan
Huancui Hu	Matthew Koszuta	Douglas J. March	Jala Morrow
Yipeng Huang	Stephen J. Kreller	Angelica M. Marchi	Ehsan Mosadegh
Brianna Hue	Nicholas Kronlage	Daniela H. Marin	Changhong Mou
Daniel M. Hueholt	Kaitlyn N. Krzyzaniak	Joseph M. Marino	Jennifer Munsey
Robert T. Hughes	Ashley Kubera	Timothy O. Markle	Elisa Murillo
Alexis Hunzinger	Abigail R. Kugland	Nick Markopoulos	Nkosi M. Muse
Tyler C. Hutcherson	McKenzie Kulseth	Benjamin R. Martin	Jacob Myers
Corey A. Ingles	Jerry J. Kung	Katelyn M. Martin	Kate Nagel
Amy Ip	Peter Kvietauskas	Nathan R. Martin	Asmi M. Napitu
Emily K. Ireland	Lukasz Kyzywon	Gerard Masalias Huguet	Antonio Negron
Rezwon Islam	Noe Labrado	Jason P. Maska	Stewart D. Negron, Jr.
Maria Jacobson	Emilee J. Lachenmeier	Mickenzie T. Mason	Dan Nelson
Mozhdeh Jamei	Chavelly N. Lamolli	Scott Matuszewski	Stephanie M. Neumann
Megan C. James	Collin J. Landry	Seth P. Maughan	Brady E. Newkirk
Olivia Jancse	Jessica A. Langlois	Catherine A. Maxwell	Brittany Newman
Josh Jansen	Sarah E. Larkin	Thomas O. Mazzetti	Cameron J. Nixon
Rachel Jennings	Jennifer N. Larson	Maxwell McAllister	Eber Nolasco-Martinez
Steven M. Jester	Marissa Lautenbacher	Megan I. McAuliffe	Mackenzie Nuthals
Anya Johnson	Scott LaVoise	Alexander T. McAvoy	Jonathan E. O'Brien
April Johnson	Quinn Lease	Taylor McCann	Cecilia O'Connor
Benjamin K. Johnson	Chung-Rui Lee	Michael T. McCarthy	John P. Obee
Geoffrey Johnson	Su Jeong Lee	Stephen McCoy	
Erica A. Joch	Yeonjin Lee	Jessica McDonald	

(continued)

NEW MEMBERS

The Executive Committee has approved the election of the following candidates to the grade of **Student Member**:

Rachel O'Donnell	Lu Ren	Kyle A. Sisco	Danielle M. Uliano
Oluwaseun O. Ojimi	Jennifer R. Renee	Alexandra C. Skinner	Atene F. Ulimasao
Jon Oleson	Dante A. Ricci	Chadrick D. Skyberg	Peter J. Ulm
Benjamin Oquinn	Kevin T. Richer	Nick Slaughter	Usaama A. Van
Margaret M. Orr	Abby Rinderer	Michael Slifer	Stephanie Van Oppen
Zachary M. Osborne	Alexis D. Rivera	Dylan Smith	Cole Vaughn
Olabosipo O. Osibanjo	Matthew Roberts	Jane Smyth	Shaquille Vaxter
Olivia R. Ostwald	Sarena D. Robertson	Tyler Snider	Thomas Verheyde
Gregory J. Ottino	Benjamin D. Rodenkirch	Dalton S. Snyder	Nicholas J. Vertz
Sujan Pal	Aaron J. Rodriguez	Miriam Sobrevilla	Selina Vinski
Kimberly J. Palmer	Shawn Rosenthal	Jacob V. Sojda	Alex Vukadinovic
Emily Paltz	Adam Roser	Karla M. Soto Perez	Charles Wammock
Elizabeth Palumbi	Edmar Ruano	Erik Sousa	Jiandong Wang
Sandip N. Palve	Paolo Ruggieri	Greg Lee Sova	Zaiyu Wang
Pratik Patel	Jan Ryherd	Kendra L. Spalding	Beverly A. Watson
Casey R. Patrizio	Atousa Saberi	Alexander Spearow	Hunter Weber
Leilani D. Paxton	Bavand Sadeghi	Trenton W. Spencer	Jordan Wells
Steven Peak	Leslie A. Salazar	Hannahle J. Spitze	Joseph Wermter
James C. Perkins	Ricky Santana	Alexander Staarmann	Michael E. Wessler
Frances Peyton	Silvia Regina Santos Da Silva	Mark A. Stalcup	Daniel T. Wheatley
Marshall Pfahler	Swarnali Sanyal	Alyssa M. Stansfield	Charles White
Jordan V. Pino	Charles Sayre	Daniel Steigerwald	Taylor Whitney
Ryan Plumley	Michael Scanlan	Melanie Steinberg	Jordan K. Wilkes
Camden T. Plunkett	Daniel Schmidt	Christopher Stickney	Ayesha Wilkinson
Jacqueline Poglodek	Frederick Schmidt	Raymond Sukhdeo	Asiah N. Williams
Catherine Pomposi	Krysta M. Schoenecker	Lu Sun	Malik J. Williams
Diana M. Pop	Emily J. Schuitema	Sarah Szymborski	Matt Wilson
Joshua W. Port	Eric M. Schumacher	Azusa Takeishi	Samuel Wilson
Steven E. Potter	Emma L. Scott	Skye K. Takkett	Steve Wolbach
Destiny Pounds	Trevor G. Scott	Wenfu Tang	Zachary S. Wolfff
Amanda L. Powell	Jeremiah R. Secrest	Kevin A. Tardi	Blake Woodring
Kristen Pozsonyi	Chamaka S. Senarath	Caitlynn Taylor	Alex Woolum
Christina A. Prestine	Jessica Sergeant	Natalie Teale	Eric Wright
Kevin C. Prince	Nicholas G. Servetas	Kevin Thiel	Samantha G. Wright
Vanessa Przybylo	Gabrielle Seymore	Jonathan Thielen	Zheng Wu
Nannan Qin	Tamara Sharp	Callum F. Thompson	Khairunnisa Yahya
Ana Quevedo	Kyle Shaw	Brandon J. Thorne	Keiko Yamamoto
Andrew K. Racki	Jennifer Shepard	Kendall Timmons	Ruikai Yan
Christopher R. Ramirez	Krystal Sherland	Shelbi Tippet	Huizhen Yu
Bhavesh Ramkorun	Kathleen C. Sherman	Kayleen Torres	Shanshui Yuan
Emily K. Ramnarine	Zachary S. Sherman	MacLane Townsend	Angela Zabler
Noman Rasheed	Cole Shimek	Brittany J. Toy	Kinsey Zarske-Williamson
Ashley Ravenscraft	Kayla M. Shipley	George A. Trail	Yidiana Zayas Rivera
Matthew G. Reagan	Andrew R. Shipotofsky	Alexa J. Trischler	Colton Zercher
Matthew Reardon	Sisam Shrestha	Sarah Trojniak	Shipeng Zhang
Alexander Reed	Austin M. Silva	Britney Truempy	Xiang Zhang
Erin M. Regan	Kerrie M. Simmons	Eli J. Turasky	Qianjin Zheng
Stephanie E. Reichlin	Harrison Sincavage	Dylan Turner	Katelyn Zigner
Karly J. Reimel			

NEW MEMBERS

The Council has approved the election of the following candidate to the grade of **Full Member with Student Privileges**:

Michael Allen	Raleigh Grysko	Zachary Moon	Eirik Mikal Samuelsen
Hendrik Andersen	Boyan Gu	Kyle J. Morganti	Steven R. Schill
Alexander Burton	Cameron Hardin	Jacob Muller	Derek Schroeter
Carly Cassidy	Michael A. Herrera	Marissa Nowakowski	Rick Schulte
Hui Christophersen	James W. Holton	Renee L. Obringer	Matthew O. Seedorf
Jad Edlebi	Kellen Jones	Chijioke R. Okolionya	Yasuhiro K. Shinohara
Marwa Mohamed Ho	Joey R. Krastel	Qi Ouyang	Itinderjot Singh
El-Sayed	Kayla M. LeDuc	Diane Palko	Koninika Tanzim, Jr.
Jared E. Fauque	Casey M. Lehecka	Max Pike	Derek Thompson
Brady S. Ferster	Yen-Heng Lin	Katie Prichard	Corey Tober
Steven Fons	Feiyu Lu	Rebecca Prosser	Chong-Chi Tong
James P. Fowler	Megan Maloney	Scott Purdy	Hunter A. Tubbs
John P. Fowler	Sophie L. Mayne	Travis R. Reddick	Yi Wang
Alexander F. Fox	Johnathan Metz	Samantha Rumler	Joshua D. White
Maria E. Frediani	Jessica Mirrielees	Manuel A. Salgado	Celeste Wrye
William Frey	Brandon Molyneux	Vicente Salinas	Daniel Yeager
Alexander Goldstein	Emily Monroe		

NEW FROM AMS BOOKS!

A Scientific Peak: How Boulder Became a World Center for Space and Atmospheric Science

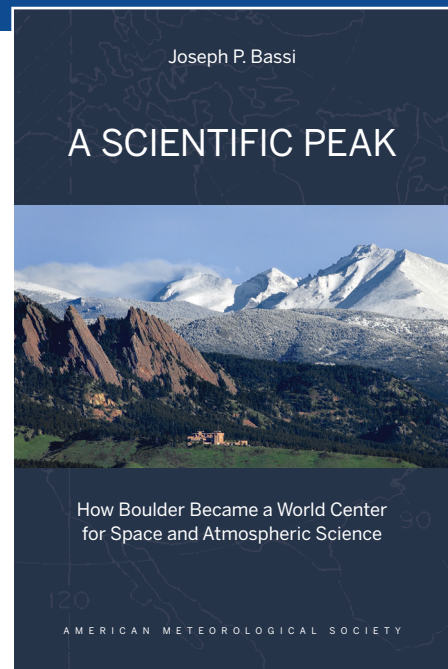
Joseph P. Bassi

Once a Wild West city tucked between the Rocky Mountains and the Great Plains, Boulder is now home to some of the biggest names in science, including NCAR, NOAA, and NIST.

Why did big science come to Boulder? How did Boulder become the research mecca it is today?

A Scientific Peak is a fascinating history that introduces us to a wide variety of characters, such as Walter Orr Roberts, and the serendipitous brew of politics, passion, and sheer luck that, during the post-WWII and Cold War eras, transformed this “scientific Siberia” into one of America’s smartest cities.

© 2015, 264 pages, paperback
 print ISBN: 978-1-935704-85-0 eISBN: 978-1-940033-89-1
 List price: \$35 AMS Member price: \$25



AMS BOOKS

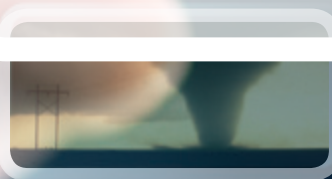
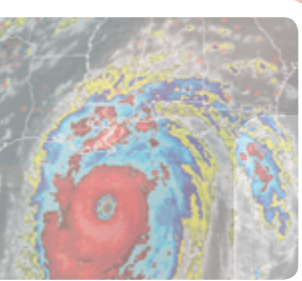
RESEARCH APPLICATIONS HISTORY

> bookstore.ametsoc.org

Science at Your Fingertips



AMS Journals are now optimized for viewing on your mobile device.

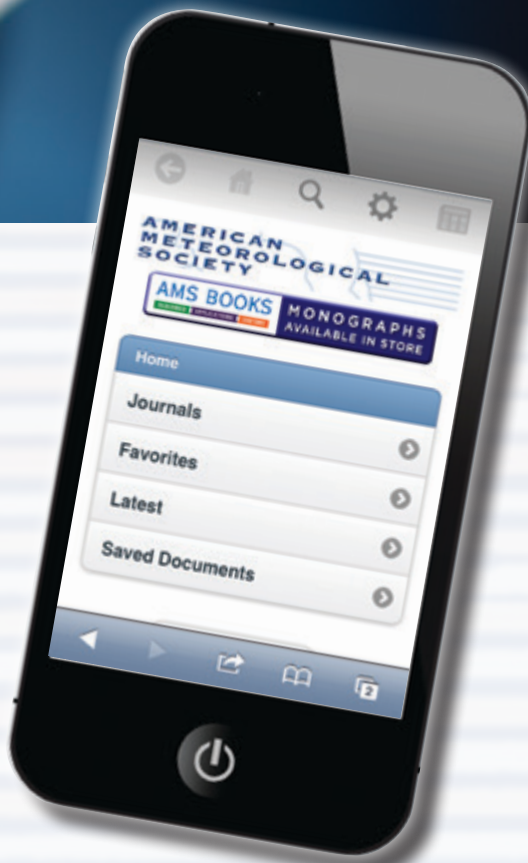


Access journal articles, monograph titles, and BAMS content using your iOS, Android, or Blackberry phone, or tablet.

Features include:

- Saving articles for offline reading
- Sharing of article links via email and social networks
- Searching across journals, authors, and keywords

And much more...



Scan code to connect to journals.ametsoc.org

AMERICAN METEOROLOGICAL SOCIETY

CALENDAR OF MEETINGS

The Call for Papers and Calendar sections list conferences, symposia, and workshops that are of potential interest to AMS members. **Complete information about events listed in the calendar can be found on the meetings page of the AMS website, www.ametsoc.org. New additions to the calendar are highlighted.**

To list an event in the calendar, please submit the event name, dates, location, and deadlines for abstracts, manuscripts, and preregistration to amsmtgs@ametsoc.org. For a submission to appear in a given issue, it must be submitted at least eight weeks prior to the month of publication (that is, to appear in the March *Bulletin*, the submission must be received by 1 January).

AMS MEETINGS

2016

MARCH

Forum on Observing the Environment from the Ground Up, 8–9 March, Washington, D.C.

Preregistration deadline: 1 February 2016
Initial announcement published: Jan. 2016

APRIL

2016 Washington Forum, 12–14 April, Washington, D.C.

Preregistration deadline: 10 March 2016
Initial announcement published: Jan. 2016

32nd Conference on Hurricanes and Tropical Meteorology, 17–22 April, San Juan, Puerto Rico

Abstract deadline: 20 November 2015
Preregistration deadline: 13 March 2016
Manuscript deadline: 17 May 2016
Initial announcement published: Sept. 2015

JUNE

***44th Conference on Broadcast Meteorology, 15–17 June, Austin, Texas**

Abstract deadline: 3 February 2016
Preregistration deadline: 4 May 2016
Initial announcement published: Sept. 2015

The 32nd Conference on Agricultural and Forest Meteorology, 20–24 June, Salt Lake City, Utah

Abstract deadline: 8 February 2016
Preregistration deadline: 9 May 2016
Manuscript deadline: 22 July 2016
Initial announcement published: Oct. 2015

22nd Symposium on Boundary Layers and Turbulence, 20–24 June, Salt Lake City, Utah

Abstract deadline: 8 February 2016
Preregistration deadline: 9 May 2016
Manuscript deadline: 22 July 2016
Initial announcement published: Oct. 2015

Third Conference on Atmospheric Biogeosciences, 20–24 June, Salt Lake City, Utah

Abstract deadline: 8 February 2016
Preregistration deadline: 9 May 2016
Manuscript deadline: 22 July 2016
Initial announcement published: Nov. 2015

17th Conf. on Mountain Meteorology, 27 June–1 July, Burlington, Vermont

Abstract deadline: 29 February 2016
Preregistration deadline: 31 May 2016
Manuscript deadline: 1 August 2016
Initial announcement published: July 2015

AUGUST

Joint 21st American Meteorological Society (AMS) Satellite Meteorology, Oceanography and Climatology Conference and 20th AMS Conference on Air–Sea Interaction, 15–19 August, Madison, Wisconsin

Abstract deadline: 1 April 2016
Preregistration deadline: 1 July 2016
Manuscript deadline: 19 September 2016
Initial announcement published: June 2015

NOVEMBER

28th Conference on Severe Local Storms, 7–11 November, Portland, Oregon

Abstract deadline: 7 July 2016
Preregistration deadline: 1 October 2016
Manuscript deadline: 7 December 2016
Initial announcement published: Jan. 2016

2017

JANUARY

16th Annual AMS Student Conference, 21–22 January, Seattle, Washington

Abstract deadline: 3 October 2016
Preregistration deadline: 15 December 2016
Initial announcement published: Feb. 2016

Fifth Annual AMS Conference for Early Career Professionals, 22 January, Seattle, Washington

Preregistration deadline: 15 December 2016
Initial announcement published: TBD

*An exhibit program will be held at this meeting.

***17th Presidential Forum, 22–26 January, Seattle, Washington**

Preregistration deadline: 1 December 2016
Initial announcement published: TBD

***Observational Symposium, 22–26 January, Seattle, Washington**

Preregistration deadline: 1 December 2016
Initial announcement published: TBD

***Social Science Symposium, 22–26 January, Seattle, Washington**

Preregistration deadline: 1 December 2016
Initial announcement published: TBD

***Lance Bosart Symposium, 22–26 January, Seattle, Washington**

Abstract deadline: 1 August 2016
Preregistration deadline: 1 December 2016
Manuscript deadline: 27 February 2017
Initial announcement published: TBD

***Robert Houze Symposium, 22–26 January, Seattle, Washington**

Abstract deadline: 1 August 2016
Preregistration deadline: 1 December 2016
Manuscript deadline: 27 February 2017
Initial announcement published: Feb. 2016

***33rd Conference on Environmental Information Processing Technologies, 22–26 January, Seattle, Washington**

Abstract deadline: 1 August 2016
Preregistration deadline: 1 December 2016
Manuscript deadline: 27 February 2017
Initial announcement published: Feb. 2016

***31st Conference on Hydrology, 22–26 January, Seattle, Washington**

Abstract deadline: 1 August 2016
Preregistration deadline: 1 December 2016
Manuscript deadline: 27 February 2017
Initial announcement published: TBD

***29th Conference on Climate Variability and Change, 22–26 January, Seattle, Washington**

Abstract deadline: 1 August 2016
Preregistration deadline: 1 December 2016
Manuscript deadline: 27 February 2017
Initial announcement published: TBD

***28th Conference on Weather Analysis and Forecasting / 24th Conference on Numerical Weather Prediction, 22–26 January, Seattle, Washington**

Abstract deadline: 1 August 2016
Preregistration deadline: 1 December 2016
Manuscript deadline: 27 February 2017
Initial announcement published: Feb. 2016

***26th Symposium on Education, 22–26 January, Seattle, Washington**

Abstract deadline: 1 August 2016
Preregistration deadline: 1 December 2016
Manuscript deadline: 27 February 2017
Initial announcement published: Feb. 2016

21st Conference on Integrated Observing and Assimilation Systems for Atmosphere, Oceans, and Land Surface (IOAS-AOLS), 22–26 January, Seattle, Washington

Abstract deadline: 1 August 2016
Preregistration deadline: 1 December 2016
Manuscript deadline: 27 February 2017
Initial announcement published: Feb. 2016

***20th Conference of Atmospheric Science Librarians International, 22–26 January, Seattle, Washington**

Abstract deadline: 1 August 2016
Preregistration deadline: 1 December 2016
Initial announcement published: Feb. 2016

***19th Conference on Atmospheric Chemistry, 22–26 January, Seattle, Washington**

Abstract deadline: 1 August 2016
Preregistration deadline: 1 December 2016
Manuscript deadline: 27 February 2017
Initial announcement published: TBD

* An exhibit program will be held at this meeting.

STUDENT TRAVEL GRANTS

Student Travel Grants are available for senior undergraduate and graduate students to attend AMS meetings held in the United States and Canada. The travel grants are available only to members, including student members, of the AMS.

AMS recognizes the considerable benefit that students can gain from attending conferences even if they are not presenting a paper there, and AMS wants to encourage interactions between students and other conference attendees. To this end, travel grants will be awarded to a student who is not presenting a paper at the conference.

Students who are presenting papers and potentially in need of travel support should inquire of the program chair whether any funds will be available for this purpose.

For more information and to complete an application form, please visit the AMS website at www.ametsoc.org.

***18th Conference on Aviation, Range, and Aerospace Meteorology, 22–26 January 2017, Seattle, Washington**

Abstract deadline: 1 August 2016
Preregistration deadline: 1 December 2016
Manuscript deadline: 27 February 2017
Initial announcement published: March 2016

***18th Conference on Aviation, Range, and Aerospace Meteorology, 22–26 January, Seattle, Washington**

Abstract deadline: 1 August 2016
Preregistration deadline: 1 December 2016
Manuscript deadline: 27 February 2017
Initial announcement published: TBD

***15th Conference on Artificial and Computational Intelligence and its Applications to the Environmental Sciences, 22–26 January, Seattle, Washington**

Abstract deadline: 1 August 2016
Preregistration deadline: 1 December 2016
Manuscript deadline: 27 February 2017
Initial announcement published: TBD

***15th History Symposium, 22–26 January, Seattle, Washington**

Abstract deadline: 1 August 2016
Preregistration deadline: 1 December 2016
Manuscript deadline: 27 February 2017
Initial announcement published: Feb. 2016

***15th Symposium on the Coastal Environment, 22–26 January, Seattle, Washington**

Abstract deadline: 1 August 2016
Preregistration deadline: 1 December 2016
Manuscript deadline: 27 February 2017
Initial announcement published: Feb. 2016

***14th Conference on Polar Meteorology and Oceanography, 22–26 January, Seattle, Washington**

Abstract deadline: 1 August 2016
Preregistration deadline: 1 December 2016
Manuscript deadline: 27 February 2017
Initial announcement published: TBD

***14th Conference on Space Weather, 22–26 January, Seattle, Washington**

Abstract deadline: 1 August 2016
Preregistration deadline: 1 December 2016
Manuscript deadline: 27 February 2017
Initial announcement published: TBD

***13th Annual Symposium on New Generation Operational Environmental Satellite Systems, 22–26 January, Seattle, Washington**

Abstract deadline: 1 August 2016
Preregistration deadline: 1 December 2016
Manuscript deadline: 27 February 2017
Initial announcement published: Feb. 2016

***13IMPACTS: Major Weather Events and Societal Impacts of 2015, 22–26 January, Seattle, Washington**

Abstract deadline: 1 August 2016
Preregistration deadline: 1 December 2016
Manuscript deadline: 27 February 2017
Initial announcement published: Feb. 2016

***12th Symposium on Societal Applications: Policy, Research and Practice, 22–26 January, Seattle, Washington**

Abstract deadline: 1 August 2016
Preregistration deadline: 1 December 2016
Manuscript deadline: 27 February 2017
Initial announcement published: Feb. 2016

***10th Annual CCM Forum, 22–26 January, Seattle, Washington**

Abstract deadline: 1 August 2016
Preregistration deadline: 1 December 2016
Manuscript deadline: 27 February 2017
Initial announcement published: TBD

***Ninth Symposium on Aerosol–Cloud–Climate Interactions, 22–26 January, Seattle, Washington**

Abstract deadline: 1 August 2016
Preregistration deadline: 1 December 2016
Manuscript deadline: 27 February 2017
Initial announcement published: TBD

***Eighth Conference on Environment and Health, 22–26 January, Seattle, Washington**

Abstract deadline: 1 August 2016
Preregistration deadline: 1 December 2016
Manuscript deadline: 27 February 2017
Initial announcement published: Feb. 2016

***Eighth Conference on Weather, Climate, and the New Energy Economy, 22–26 January, Seattle, Washington**

Abstract deadline: 1 August 2016
Preregistration deadline: 1 December 2016
Manuscript deadline: 27 February 2017
Initial announcement published: Feb. 2016

***Seventh Conference on Transition of Research to Operations, 22–26 January, Seattle, Washington**

Abstract deadline: 1 August 2016
Preregistration deadline: 1 December 2016
Manuscript deadline: 27 February 2017
Initial announcement published: TBD

***Seventh Symposium on Advances in Modeling and Analysis Using Python, 22–26 January, Seattle, Washington**

Abstract deadline: 1 August 2016
Preregistration deadline: 1 December 2016
Manuscript deadline: 27 February 2017
Initial announcement published: Feb. 2016

***Fifth Annual Symposium on the Weather, Water, and Climate Enterprise, 22–26 January, Seattle, Washington**

Abstract deadline: 1 August 2016
Preregistration deadline: 1 December 2016
Manuscript deadline: 27 February 2017
Initial announcement published: TBD

*An exhibit program will be held at this meeting.

***Fifth Symposium on Building a Weather-Ready Nation: Enhancing Our Nation's Readiness, Responsiveness, and Resilience to High Impact Weather Events, 22–26 January, Seattle, Washington**

Abstract deadline: 1 August 2016
Preregistration deadline: 1 December 2016
Manuscript deadline: 27 February 2017
Initial announcement published: Feb. 2016

***Fifth Symposium on Prediction of the Madden–Julian Oscillation: Processes, Prediction, and Impact, 22–26 January, Seattle, Washington**

Abstract deadline: 1 August 2016
Preregistration deadline: 1 December 2016
Manuscript deadline: 27 February 2017
Initial announcement published: Feb. 2016

***Third Symposium on High Performance Computing for Weather, Water, and Climate, 22–26 January, Seattle, Washington**

Abstract deadline: 1 August 2016
Preregistration deadline: 1 December 2016
Manuscript deadline: 27 February 2017
Initial announcement published: Feb. 2016

***Second Symposium on US-International Partnerships, 22–26 January, Seattle, Washington**

Abstract deadline: 1 August 2016
Preregistration deadline: 1 December 2016
Manuscript deadline: 27 February 2017
Initial announcement published: Feb. 2016

MEETINGS OF INTEREST

2016

APRIL

A&WMA Guideline on Air Quality Models: The New Path, 12–14 April, Chapel Hill, North Carolina

EGU—Aviation Meteorology: Observations, Modeling, and Operations, 17–21 April, Vienna, Austria

International Radiation Symposium 2016, 17–22 April, Auckland, New Zealand

JUNE

13th International Meeting on Statistical Climatology, 6–10 June, Canmore, Alberta, Canada

JULY

17th International Conference on Clouds and Precipitation, 25–29 July, Manchester, Wales, United Kingdom

SEPTEMBER

The Geological Society of America Annual Meeting, 25–28 September 2016, Denver, Colorado

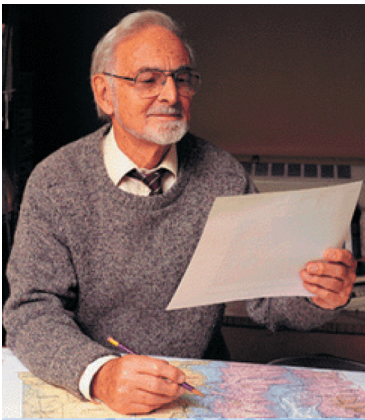
OCTOBER

Eighth EGU Leonardo Conference: From Evaporation to Precipitation—The Atmospheric Moisture Transport, 22–27 October, Ourense, Spain

NOVEMBER

Northeast Regional Operational Workshop, 2–3 November 2016, Albany, New York

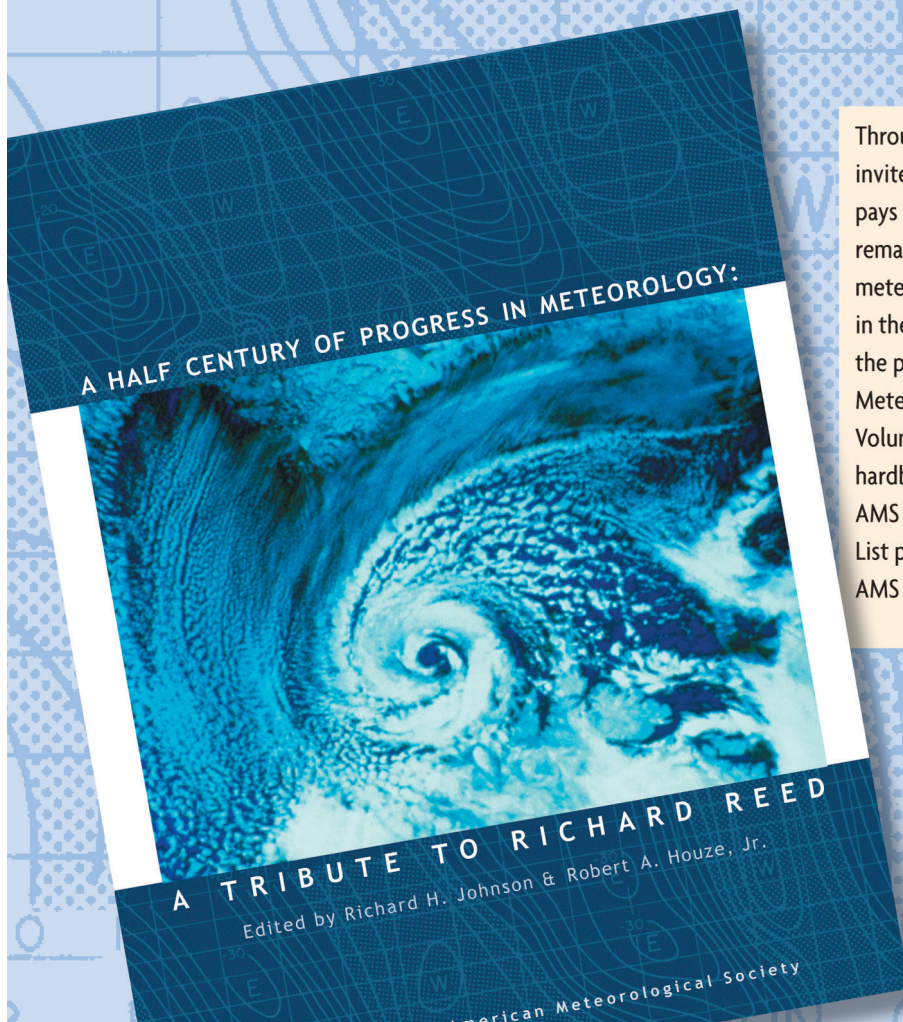
*An exhibit program will be held at this meeting.



A Half Century of Progress in Meteorology: A Tribute to Richard Reed

edited by **Richard H. Johnson and Robert A. Houze Jr.**

with selections by: **Lance F. Bosart Robert W. Burpee Anthony Hollingsworth
James R. Holton Brian J. Hoskins Richard S. Lindzen John S. Perry Erik A. Rasmussen
Adrian Simmons Pedro Viterbo**



Through a series of reviews by invited experts, this monograph pays tribute to Richard Reed's remarkable contributions to meteorology and his leadership in the science community over the past 50 years. 2003.

Meteorological Monograph Series, Volume 31, Number 53; 139 pages, hardbound; ISBN 1-878220-58-6; AMS Code MM53.

List price: \$80.00

AMS Member price: \$60.00

ORDER ONLINE: bookstore.ametsoc.org or see the order form at the back of this issue

CALL FOR PAPERS

CALL FOR PAPERS

18th Conference on Aviation, Range, and Aerospace Meteorology, 22–26 January 2017, Seattle, Washington

The 16th Annual AMS Student Conference, sponsored by the American Meteorological Society, and organized by the Aviation, Range, and Aerospace Meteorology Committee, will be held 22–26 January 2017, as part of the 97th AMS Annual Meeting in Seattle, Washington. The theme for the 2017 AMS Annual Meeting is “Observations Lead the Way.” For the full description of the theme, please visit the AMS 2017 Annual Meeting webpage: <http://annual.ametsoc.org/2017/>. See this website for preliminary programs, registration, hotel, and general information, which will be posted in late September 2016.

Papers for this conference are solicited on

- weather impacts to aviation, range and aerospace operations (convection, icing, space weather, turbulence, volcanic ash, wake vortices, wind shear, winter weather)
- weather information integrated into DSTs on the ground and in the air [ATM–weather

integration, decision support tools, weather technology in the cockpit (WTIC)]

- traditional and nontraditional nonaircraft sensors and observation capabilities (sensors and observation capabilities, satellites, radar, lightning)
- traditional and nontraditional aircraft sensors and observation capabilities (aircraft-based observations)
- advances in numerical weather prediction, ensemble modeling and the use of artificial intelligence techniques in support of aviation, range and aerospace operations (NWP, ensemble modeling, AI)
- what weather is worth to aviation, range and aerospace decision makers (benefits assessment)
- outside the (aviation) box: impacts of weather on range, aerospace, commercial spaceport and UAS operations (range, aerospace, commercial spaceport and UAS)
- the framework we rely on: NextGen and international programmatic, policy, and regulatory updates (NextGen, international, PP&R)
- the little guys: most vulnerable to weather impacts (GA Operations)

Please contact the program chairpersons (contact information noted below) by 2 May 2016 if you would like to propose a session topic for this conference.

Please submit your abstract electronically via the web by 1 August 2016 (refer to the AMS webpage at www.ametsoc.org/meet/online_submit.html). An abstract fee of \$95 (payable by credit card or purchase order) is charged at the time of submission (refundable only if abstract is not accepted) and includes the submission of your abstract, the posting of your extended abstract, and the uploading and recording of your presentation, which will be archived on the AMS website.

Authors of accepted presentations will be notified via e-mail by late September 2016. All extended abstracts are to be submitted electronically and will be available online. Instructions for formatting extended abstracts will be posted on the AMS website. Authors have the option to submit manuscripts (up to 10 MB) electronically by 27 February 2017. All abstracts, extended abstracts and presentations will be available on the AMS website at no cost.

For additional information, please contact the program chairperson, Matt Fronzak (email: mfronzak@mitre.org). (3/16)

A gift for every season.

(PLUS FREE SHIPPING!)



Fleece Scarf \$17

COLOR: Charcoal with AMS emblem



Ceramic Mug \$7

COLORS: Navy with white AMS seal
White with navy AMS seal



Umbrella with weather symbols \$14

COLOR: Navy with white symbols



Silk Tie with weather symbols \$17

COLORS: Navy with white symbols and Burgundy with gold symbols



Cotton T-Shirt

Adult: S, M, L, XL, XXL \$12
Child: S, M, L \$10

COLORS: Navy with white AMS seal
White with navy AMS seal



Travel Mug \$8

COLOR: Blue stainless steel with white AMS seal



Membership Lapel Pins \$10

COLOR: Gold



Soft Briefcase \$27

COLOR: Black with white AMS seal
DIMENSIONS: 16"L, 12.5"H, 3.75"W
(expands to 5")



Silk Scarf with weather symbols \$17

COLORS: Navy with white symbols
Burgundy with gold symbols



Long Sleeve T-Shirt

Mens: S, M, L, XL, XXL \$15

COLOR: Navy with white AMS seal

Womens: S, M, L, XL \$15

COLORS: Gray with blue AMS seal



12 Pocket CD Case \$9

COLOR: Blue with white AMS seal

ORDER TODAY! Prepay by check/money order, Visa, MC, or AMEX

CALL 617-226-3998 FAX 617-742-8718

MAIL AMS, 45 Beacon Street, Boston, MA 02108-3693

FOR MORE GIFT IDEAS check out the new AMS Online Bookstore (weather books, biographies, histories, monographs and more) at www.ametsoc.org/amsbookstore.



NOMINATION SUBMISSIONS

The Council of the American Meteorological Society invites members of the AMS to submit nominations for the Society Awards, Lecturers, Named Symposia, Fellows, Honorary members, and nominees for elective Officers and Councilors of the Society.

Information regarding awards, including award descriptions, listings of previous recipients, and the process for submitting nominations are on the AMS website www.ametsoc.org/awards.

Note: Deadlines differ and some nominations must be submitted on a specific form vs. electronic submission which is available on the AMS website or by request from Headquarters.

2016 AWARDS COMMITTEES

Each committee or commission listed below has the responsibility to select and submit to the Council the names of individuals nominated for the Society's awards listed. The name(s) of individual(s) nominated, a two-page cv, a bibliography of no more than three pages, and three supporting letters should be electronically submitted before **1 May 2016** for the awards that follow, unless stated otherwise. The nominees for awards remain on the committee's active list for three years.

ATMOSPHERIC RESEARCH AWARDS COMMITTEE

The Carl-Gustaf Rossby Research Medal
The Jule G. Charney Award
The Verner E. Suomi Award*
The Remote Sensing Prize (biennial)
The Clarence Leroy Meisinger Award
The Henry G. Houghton Award

OCEANOGRAPHIC RESEARCH AWARDS COMMITTEE

The Sverdrup Gold Medal
The Henry Stommel Research Award
The Verner E. Suomi Award*
The Nicholas P. Fofonoff Award

HYDROLOGIC RESEARCH AWARDS COMMITTEE

Hydrologic Sciences Medal

AWARDS OVERSIGHT COMMITTEE

The Charles Franklin Brooks Award for Outstanding Services to the Society
The Cleveland Abbe Award for Distinguished Service to the Atmospheric Sciences by an Individual
The Joanne Simpson Mentorship Award
The Award for Outstanding Services to Meteorology by a Corporation
Special Awards

EDUCATION AND HUMAN RESOURCES COMMISSION

The Louis J. Battan Author's Award (Adult and K-12)
The Charles E. Anderson Award
The Edward N. Lorenz Teaching Excellence Award
Distinguished Science Journalism in the Atmospheric and Related Sciences

PROFESSIONAL AFFAIRS COMMISSION

Outstanding Contribution to the Advance of Applied Meteorology Award for Broadcast Meteorology
Award for Excellence in Science Reporting by a Broadcast Meteorologist
The Henry T. Harrison Award for Outstanding Contributions by a Consulting Meteorologist

WEATHER AND CLIMATE ENTERPRISE COMMISSION

The Kenneth C. Spengler Award

LOCAL CHAPTER AFFAIRS COMMITTEE

Local Chapter of the Year Award
(nomination form available online at www.ametsoc.org/amschaps/index.html.)

* Recommended by the Atmospheric Research Awards Committee in even-numbered years and by the Oceanographic Research Awards Committee in odd-numbered years.

2016 AWARDS COMMITTEES

SCIENTIFIC AND TECHNOLOGICAL ACTIVITIES COMMISSION

The Charles L. Mitchell Award
The Award for Exceptional Specific Prediction
The Francis W. Reichelderfer Award
The Helmut E. Landsberg Award
The Award for Outstanding Achievement in Biometeorology

• LECTURERS

Robert E. Horton Lecturer in Hydrology
Bernhard Haurwitz Memorial Lecturer
Walter Orr Roberts Lecturer

• PAPER

Banner I. Miller

• STUDENT PAPERS

Robert Leviton Student Prize
Max A. Eaton Student Prize
Spiros G. Geotis Student Prize
Peter V. Hobbs Student Prize

• NAMED SYMPOSIA

Section E, of the Policy, Guidelines, and Procedures for Awards and Lectureships provides the Policy on Named Conferences/Symposia and Special Issues of AMS Journals (*full policy description available at www.ametsoc.org/awards*):

Recognition of scientists in the fields served by the AMS, living or deceased, in the form of a named conference or symposium or a named special issue of one of the Society's journals is an honor reserved for only the most outstanding of our colleagues. It should be awarded only to those individuals who are completing a career, or who have recently died having completed a career, of significant achievements in their field and whose contributions would make them worthy of consideration for Honorary Member of the AMS...

2016 FELLOWS COMMITTEE

The Committee's function is to submit to the Council the names of individuals for election to Fellow.

Article III, Section 6, of the AMS Constitution provides that those eligible for election to Fellow shall have made outstanding contributions to the atmospheric or related oceanic or hydrologic sciences or their applications during a substantial period of years. The nominees for Fellow must be a member of the Society and remain on the committee's active list for three years.

A nomination letter and three supporting letters should be electronically submitted before 1 May 2016. A list of Fellows and the process for submitting nominations are on the AMS website (www.ametsoc.org/awards).

NOMINATING COMMITTEE

The Committee's function is to submit to the Council the names of individuals for 1) the office of President-Elect for a term of one year starting at the close of the Annual Meeting and 2) four positions on the Council for a term of three years starting at the close of the Annual Meeting.

As per Article VI of the AMS Constitution, formal nominations by petition may be submitted to the Secretary-Treasurer by 1 July. In addition, the AMS Nominating Committee welcomes recommendations from the membership of candidates for office, which will be considered as the slate is prepared. Such recommendations will be most helpful if they are sent to the Nominating Committee nominating-committee@ametsoc.org by the end of December and are in the form of a 1-page letter describing the proposed candidate's background and qualifications. Questions about the nomination process should also be addressed to the Nominating Committee.

HONORARY MEMBERS

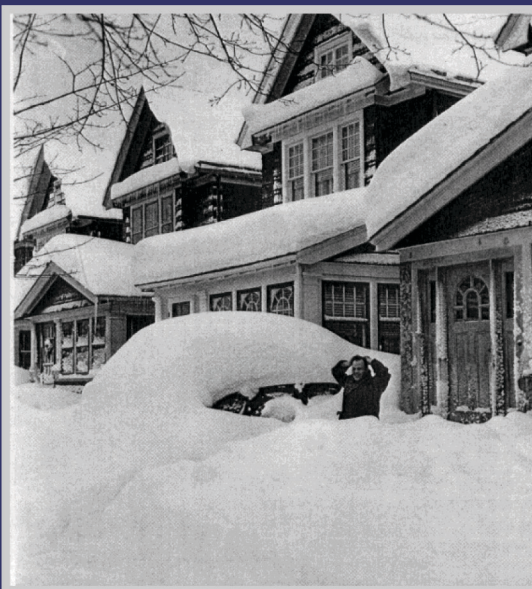
Article III, Section 5, of the AMS Constitution provides that Honorary Members shall be persons of acknowledged preeminence in the atmospheric or related oceanic or hydrologic sciences, either through their own contributions to the sciences or their application or through furtherance of the advance of those sciences in some other way. They shall be exempt from all dues and assessments. The nominees for Honorary member remain on an active list for three years.

Deadline: 1 June 2016; a form and list of Honorary Members is available at www.ametsoc.org/awards.



NORTHEAST SNOWSTORMS

Volume I: Overview



PAUL J. KOCIN & LOUIS W. UCCELLINI
Published by the American Meteorological Society



NORTHEAST SNOWSTORMS

Volume I: Overview
Volume II: The Cases

Paul J. Kocin and Louis W. Uccellini

Northeast Snowstorms offers the most comprehensive treatment on winter storms ever compiled: more than 50 years of professional experience in the form of a two-volume compendium of insights, examples, photographs, over 200 color figures, and a DVD of added material.

American Meteorological Society; 818 pages, hardbound;
AMS code MM54

Price: \$100.00 list/\$80.00 member/ \$60.00 student member

ORDER ONLINE!

www.ametsoc.org/amsbookstore
or see the order form at the back of this issue.



CORPORATION AND INSTITUTIONAL MEMBERS

SUSTAINING MEMBERS

Ball Aerospace & Technologies Corporation
Harris Corporation
Lockheed Martin Corporation
Northrop Grumman Corporation
The Boeing Company
The Weather Channel
University Corporation for Atmospheric Research
Vaisala, Inc.

REGULAR MEMBERS

AccuWeather, Inc.
Advances in Atmospheric Sciences
Aerospace & Marine International Corporation
All Weather, Inc.
Atmospheric and Environmental Research, Inc.
Atmospheric Technology Services Company, LLC
Baron Services, Inc.
Belfort Instrument Company
Botswana Meteorological Services
Campbell Scientific, Inc.
CLS America, Inc.
Coastal Environmental Systems
CSIRO Marine and Atmospheric Research
Davis Instruments Corporation
Earth Networks
EKO Instruments Company, Ltd.
Enterprise Electronics Corporation
Environmental Systems Research, Inc.
ERT, Inc.
Global Science & Technology, Inc.
Global Weather Corporation
I. M. Systems Group
Johns Hopkins University, Applied Physics Laboratory
Kipp & Zonen USA Inc.
Meteorological Technology International
Murray & Trettel, Inc.
National Centre for Medium Range Weather Forecasting
Orbital ATK, Inc.
Panasonic Weather Solutions
Pelmorex Media Inc.
ProSensing, Inc.
Radiometrics Corporation
Raytheon Company
R. M. Young Company
Riverside Technology, inc.

Royal Netherlands Meteorological Institute
Schneider Electric Weather
Science Applications International Corporation
Science Systems and Applications, Inc.
Scintec AG
SeaSpace Corporation
SGT, Inc.
Sonalysts, Inc.
SpectraSensors, Inc.
Sutron Corporation
The Aerospace Corporation
U.S. Department of Energy, Office of Science
Unisys Corporation
University of Alabama in Huntsville, Earth System Science Ctr
University of Illinois, Department of Atmospheric Sciences
University of Wisconsin—Madison, SSEC
Vieux, Inc.
Weather Decision Technologies
Weather Modification, Inc.
Weather Services International, Inc.

SMALL BUSINESS MEMBERS

Climadata Corporation
EWR Weather Radar Systems
Geonor, Inc.
Hwind Scientific, LLC
National Council of Industrial Meteorologists
National Weather Service Employees Organization
PCE Americas, Inc.
Remtech, Inc.
Tempus Global Data, Inc.
WeatherSTEM, Inc.
www.WeatherVideoHD.TV
Yankee Environment Systems, Inc.

PUBLICATIONS MEMBERS

Abdus Salam International Centre for Theoretical Physics
Air Force Weather Agency
ARPA FVG, Osservatorio Meteorologico Regionale
Bureau of Meteorology
Civil Aeronautics Administration, MOTC
Colorado State University Libraries
Columbia University, Lamont-Doherty Geological Observatory
Creighton University Reinert/Alumni Memorial Library
Dartmouth College Baker Library
Desert Research Institute

For questions relating to corporation and institutional membership, please contact Maria Sarantopoulos at AMS Headquarters—telephone: 617-227-2426, x3912; fax: 617-742-8718; e-mail: msarantopoulos@ametsoc.org; or write to American Meteorological Society, Attn: Maria Sarantopoulos, 45 Beacon St., Boston, MA 02108-3693.

CORPORATION AND INSTITUTIONAL MEMBERS

Membership in the American Meteorological Society does not imply AMS endorsement of an organization's products or services.

Deutscher Wetterdienst
Embry Riddle Aeronautical University
Environment Canada Library, Downsview
EUMETSAT Library
Finnish Meteorological Institute
Florida International University Library
Florida State University, Department of EOAS
Geophysical Institute/International Arctic Research Center
Harvard University, Gordon McKay and Blue Hill Libraries
Hong Kong Observatory Library
India Meteorological Department
Indian Institute of Technology Bhubaneswar
Indian Institute of Tropical Meteorology
Indiana University Library
Instytut Meteorologii i Gospodarki Wodnej
Irish Meteorological Service
Japan Weather Association
Joint Typhoon Warning Center
Los Alamos National Laboratory
Lyndon State College, Samuel Read Hall Library
MBL/WHOI Library
Meteo-France
Meteorological Service of New Zealand Ltd.
MeteoSwiss
Meteorologisk institutt
Millersville University, Department of Earth Sciences
MIT, Lincoln Laboratory
National Centers for Environmental Information
National Environment Agency
National Weather Center Library
Naval Postgraduate School, Dudley Knox Library
New York University
NIWA Wellington Library
NOAA - GLERL Library
NOAA AOML Library
NOAA Central Library
NOAA Seattle Library
North Carolina State University Hunt Library
Pennsylvania State University, Paterno Library
Purdue University Libraries
Republic of Korea Air Force, Headquarters
South African Weather Service
St. Louis University, Dept. of Earth & Atmospheric Sciences
Swedish Meteorological & Hydrological Institute
U.K. National Meteorological Library
U.S. Army Corps of Engineers, Library - ERDC
U.S. Department of Commerce, Boulder Labs Library
U.S. EPA Main Library
Universitätsbibliothek Innsbruck
Universitätsbibliothek Trier
University of Colorado Libraries
University of Copenhagen, Niels Bohr Institute Library
University of Delaware Library
University of Frankfurt Library
University of Hawaii at Manoa, Library
University of Maryland, McKeldin Library
University of Melbourne, Baillieu Library
University of New South Wales Library
University of North Carolina, Ramsey Library
University of North Dakota, Chester Fritz Library
University of Northern Colorado, Michener Library
University of Oklahoma, School of Meteorology
University of Washington Libraries
WeatherPredict Consulting Inc.
Weizmann Institute of Science
Yale University, Geology Library
Zentralanstalt für Meteorologie und Geodynamik

Color indicates new or reinstated member

FELLOWSHIP AND SCHOLARSHIP SPONSORS

FELLOWSHIPS

AMS Giving Program
DOE, Atmospheric System Research
Lockheed Martin Corporation*
NASA Earth Science
NOAA's Climate Program Office
NOAA's National Weather Service

FRESHMAN AND UNDERGRADUATE SCHOLARSHIPS

Baron Services Inc.
Earth Networks
CLS America, Inc.
Harris Corporation
Lockheed Martin MS2
Naval Weather Service Association
Raytheon Company
R. M. Young Company
SAIC, Center for Atmospheric Physics
Science and Technology Corporation
Stinger Ghaffarian Technologies
Vaisala, Inc.
Jerome Namias Memorial Endowed Scholarship
Edgar J. Saltsman Endowed Scholarship
Bernard Vonnegut and Vincent Schaefer Endowed Scholarship
Percival D. Wark and Clara B. (Mackey) Wark Endowed
Scholarship

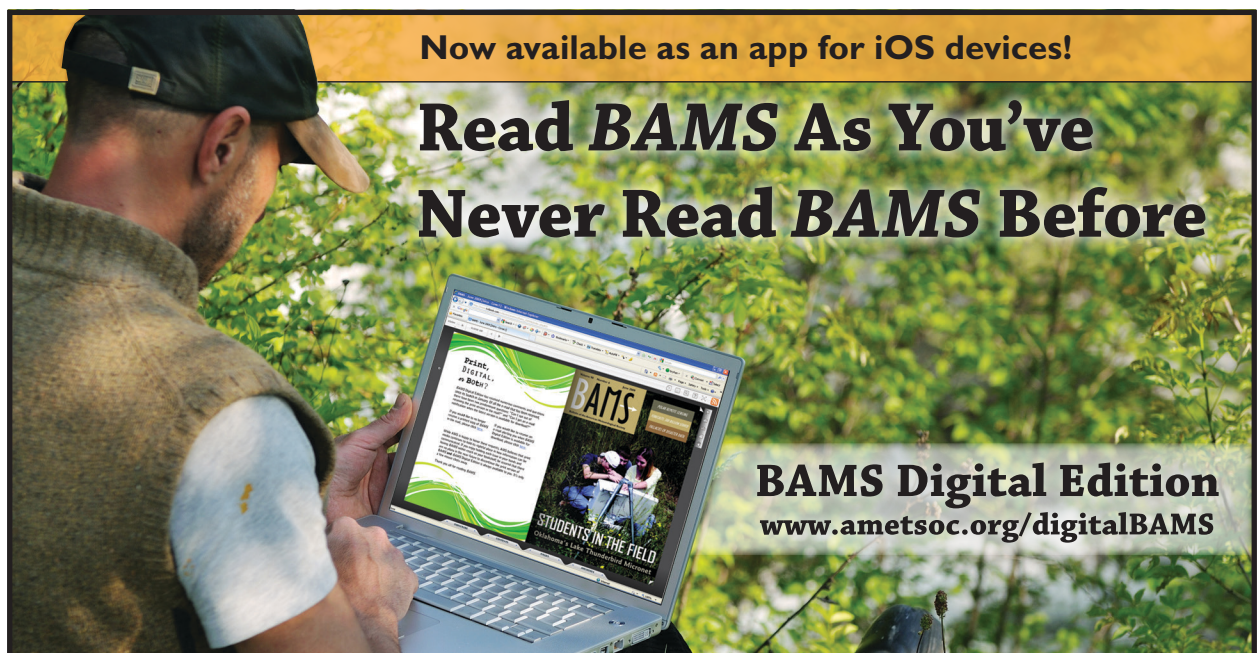
*Corporate Patron

MINORITY SCHOLARSHIPS

AMS Giving Program

SENIOR SCHOLARSHIPS

AMS 75th Anniversary Endowed Scholarship
Bhanwar Lal Bahethi Scholarship
Om and Saraswati Bahethi Scholarship
Saraswati (Sara) Bahethi Scholarship
Werner A. Baum Undergraduate Endowed Scholarship
Loren W. Crow Memorial Scholarship
The Dr. Robert Fraser Scholarship
Karen Hauschild Friday Endowed Scholarship
Bob Glahn Endowed Scholarship in Statistical Meteorology
The Jerry C. Glover Scholarship
Dr. Pedro Grau Undergraduate Scholarship
Richard and Helen Hagemeyer Scholarship
John R. Hope Endowed Scholarship in Atmospheric Sciences
David S. Johnson Endowed Scholarship
Larry R. Johnson Scholarship
Dr. Yoram Kaufman Scholarship
Carl W. Kreitzberg Endowed Scholarship
Ethan and Allan Murphy Endowed Memorial Scholarship
The Naval Weather Service Association Scholarship Award
K. Vic Ooyama Endowed Scholarship
The Orville Family Endowed Scholarship in Meteorology
The Ken Reeves Scholarship
Michael J. Roberts, Jr. Scholarship
Guillermo Salazar Rodriguez Undergraduate Scholarship
Mark J. Schroeder Endowed Scholarship in Meteorology



Now available as an app for iOS devices!

Read *BAMS* As You've Never Read *BAMS* Before

BAMS Digital Edition
www.ametsoc.org/digitalBAMS

LOOKING FOR AN EXPERT?

LOOK TO AMS!

AMS announces the launch of our new online directory of **Weather and Climate Service Providers.**

This new online directory replaces the former BAMS Professional Directory and lists an array of weather and climate service providers. You can find the new directory under the **“Find an Expert”** link from the AMS home page.

It’s easier than ever for the weather, water, and climate community and the general public to search for organizations and individuals offering these important services.

Learn more at www.ametsoc.org



NEW!

**Weather & Climate Service
Providers Directory**



AMS
American Meteorological Society

www.ametsoc.org

INDEX TO ADVERTISERS

Belfort Instruments	c4
Distromet Ltd.	321
Environmental Research Services	328
Geonor Inc.	336
Kipp & Zonen (USA) Inc.	c2
R. M. Young Company	326
Washington Forum	c3
Yankee Environmental Systems, Inc.	317

AMS PUBLICATIONS, PREPRINTS, ETC.

<i>Adaptive Governance and Climate Change</i>	466
AMS Books	454, 468–469
AMS eBooks	366
AMS Journals—Mobile Editions	492
AMS Merchandise Catalog	499
BAMS Digital Edition	505
<i>Eyewitness: Evolution of the Atmospheric Sciences</i>	424
<i>A Half Century of Progress in Meteorology:</i> <i>A Tribute to Richard Reed, MM No. 53</i>	497
<i>Living on the Real World: How Thinking and Acting</i> <i>Like Meteorologists Will Help Save the Planet</i>	344
<i>Midlatitude Synoptic Meteorology</i>	485
<i>Northeast Snowstorms, MM No. 54</i>	502
Online Career Center	507
Online Glossary of Meteorology	396
<i>Radar and Atmospheric Science: A Collection</i> <i>of Essays in Honor of David Atlas, MM No. 52</i>	467
<i>A Scientific Peak: How Boulder Became a World</i> <i>Center for Space and Atmospheric Science</i>	491
<i>Taken by Storm, 1938: The Societal and Meteorological</i> <i>History of the Great New England Hurricane</i>	324
<i>The Thinking Person's Guide to Climate Change</i>	453
Weather and Climate Service Providers Directory	506
<i>Weatherwise</i>	470



ONLINE CAREER CENTER

The AMS Online Career Center may be accessed through the AMS Web site at www.ametsoc.org/careercenter/index.html. In addition to posting positions, advertisers may search and view job seekers' résumés.

JOB POSTING RATES:

\$375 (30-day posting)

\$1593.75 (5 pack of jobs) Usable for 30-day job postings. Buy 5 job posting credits at a 15% discounted rate. These credits may be used at anytime during the next 12 months.

\$3000 (10 pack of jobs) Usable for 30-day job postings. Buy 10 job-posting credits at a 20% discounted rate. These credits may be used at anytime during the next 12 months.

\$3375 (12 pack of jobs) Usable for 30-day job postings or a continual 12-month posting. Buy 12 job-posting credits at a 25% discounted rate. These credits may be used at anytime during the next 12 months.

Advertisers may upload a company logo free of charge.

RÉSUMÉS: View complete resumes for free! If you find any candidates you are interested in, submit your interest to them. If the candidate is interested in your opportunity, we connect you for just \$20.00. If the candidate is not interested, you pay nothing!

AMS CORPORATION MEMBER DISCOUNTS: Active AMS Corporation Members (small business, regular, or sustaining) receive a 25% discount when posting a position. Contact Kelly G. Savoie (ksavoie@ametsoc.org) to receive a coupon code. To receive the discount, the code must be entered when you post a position. The discount code is non-transferable.

AMS MEMBER BENEFIT: AMS Members will be given 14-days advance access to a job listing. A member-only symbol will appear next to the posting. After 14 days, the job posting is open to all.

SUBMISSION OF ADS: Advertisers must create an online account and submit ad text through the AMS Career Center site. Ad text may be entered at any time.

PAYMENT INFORMATION: Prepayment is required by credit card or valid purchase order.

CONTACT INFORMATION: If you have questions, please contact Customer Service at 888-575-WORK (9675) (inside U.S.) or 860-440-0635 (outside U.S.).

ADVERTISING POLICY

The AMS will accept tasteful and accurate advertisements for products and services of professional interest to AMS members from organizations that are actively involved in the atmospheric and related sciences. The AMS also accepts advertising from organizations that have an interest in the atmospheric and related sciences and services, but are not actively involved in them. These organizations may promote their contributions to AMS activities and other good works, but may not directly promote products or services. The AMS reserves the right to refuse advertising that does not meet these criteria. Acceptance of advertising does not constitute the Society's endorsement of the product or service being advertised.

ORDER FORM

FOR AMS PUBLICATIONS ADVERTISED IN THIS ISSUE

Name: _____

Member (# _____)

Address: _____

Nonmember

City, State: _____ ZIP: _____

Province: _____ Country: _____

	Qty.	Member Price*	Nonmember Price*	Total
		(Please circle appropriate price)		
<i>Adaptive Governance and Climate Change</i> (p. 466)		\$22.00	\$35.00	
<i>Eyewitness: Evolution of the Atmospheric Sciences</i> (p. 424)		\$55.00	\$75.00	
<i>A Half Century of Progress in Meteorology:</i>				
<i>A Tribute to Richard Reed, MM No. 53</i> (p. 497)		\$60.00	\$80.00	
<i>Living on the Real World: How Thinking and Acting</i>				
<i>Like Meteorologists Will Help Save the Planet</i> (p. 344)		\$22.00	\$30.00	
<i>Midlatitude Synoptic Meteorology</i> (p. 485)		\$75.00	\$100.00	
Student member price:		\$65.00		
<i>Midlatitude Synoptic Meteorology Teaching CD</i> (p. 485)		\$75.00	\$100.00	
<i>Northeast Snowstorms, MM No. 54</i> (p. 502)		\$80.00	\$100.00	
Student member price:		\$60.00		
<i>Radar and Atmospheric Science: A Collection of Essays</i>				
<i>in Honor of David Atlas</i> (p. 467)		\$80.00	\$100.00	
<i>A Scientific Peak: How Boulder Became a World Center for</i>				
<i>Space and Atmospheric Science</i> (p. 491)	\$25.00	\$35.00		
<i>Taken by Storm, 1938: A Societal and Meteorological History</i>				
<i>of the Great New England Hurricane</i> (p. 324)		\$30.00	\$40.00	
<i>The Thinking Person's Guide to Climate Change</i> (p. 453)		\$20.00	\$30.00	
* Shipping and handling: Please add \$8 PER ORDER for delivery within the U.S. and \$15 PER ITEM for deliveries outside the U.S. There is no shipping and handling charge on DVDs or CD-ROMs for either U.S. or foreign orders. Shipping prices subject to change.		SHIPPING		
		TOTAL		

I am paying by: Check/money order

Credit Card No. _____

Exp. date: _____

Visa Mastercard American Express

Name on Card: _____

Billing address: _____

Signature: _____

Please include an AMS membership application with my order.

Please send prepaid orders to Order Department, American Meteorological Society, 45 Beacon St., Boston, MA 02108-3693

2016 AMS Washington Forum

Leveraging Environmental Intelligence to Enhance Risk Management



April 12-14, 2016 • Washington, DC

The 2016 AMS Washington Forum

The 2016 AMS Washington Forum is a must-attend meeting for anyone interested in learning more about how weather, water, and climate information can help support risk management across the public and private sectors. This includes agencies and companies whose operations and planning are reliant on environmental factors.

***Join other private
and public sector
thought-leaders.***

2016 Themed sessions include:

- Congressional and Executive Staffers
- Federal Agency Leads
- Space Weather
- NOAA Big Data
- Environmental Security
- Renewable Energy
- Water Resources
- Impacts of COP21
- Challenge.gov Program

Guest Speaker

*This year, AMS is honored to welcome **Dr. DJ Patil**, Chief Data Scientist at the White House Office of Science and Technology Policy*



Learn more at ametsoc.org/WashForum



AMS
American Meteorological Society

ASK BELFORT ENGINEERING

Questions regarding this product, contact us at:
ASKBELFORT@belfortinstrument.com



**All
Environment
Digital
Aerovane®**

**Model
AEDA
140A**

A NAME YOU CAN TRUST AT A PRICE YOU CAN AFFORD

Belfort's All Environment Digital Aerovane® is designed to operate in the toughest environments where reliable and accurate wind speed and direction measurements are essential. The large size aerodynamic design assures low starting torque, directional stability, minimal impact from ice and snow, and large sample size. Magnetic sensors and totally encapsulated electronics assure operation in

the presence of moisture, sand and dust. Durable and rugged this weather instrument is made of high impact thermoplastic and machined aluminum. The new Digital Aerovane will provide RS485 digital output or analog voltage/pulse output to an accuracy of 1° and 1 knot, unlike other wind instruments that fail to achieve this degree of precision. Contact Belfort today for more information.

BELFORT INSTRUMENT
The Standard of Measurement

www.belfortinstrument.com